Chapter1
Introduction

1.1 Fiber Optic Based Communication Technology

In 2009, Charles Koa won a Nobel Prize for his invention in the generation of low loss optical fiber which was as low as 20dB/km that aimed for transmitting the information using light along glass fiber. The big contribution indicates that the optical fiber give a high contribution for the communication industry after 45 years of its creation. This new finding, leads to the research development by the scientists in reducing the loss in the optical fiber. As a result, the optical fiber with the optical loss as low as 0.3dB/km has been designed. The research development is also supported by the extension and commercialization of optical light sources and photodiodes. Thus, the combination of the three key components which are of fiber optics, light source and photodiode proves to be the necessary jump start for fiber optic communications.

1.2 Wavelength Division Multiplexing (WDM)

Traditionally, optical fiber communications systems were based on the concept of a single channel to receive data and another channel to transmit data, due to the relative infancy of the technology. This makes optical fiber technology not commercially attractive, as many fibers have to be laid in order to increase the number of channels. However, increasing demands for bandwidth promotes research into increasing the data transmission capacities of the optical fiber to allow it to transmit data at higher rates over single fiber, resulting in the development of Wavelength Division Multiplexing

(WDM) technologies. WDM technology can increase a single fiber's carrying capacity by a hundred or perhaps a thousand times more. WDM technology is the basic technology for full optical fiber communication network system [1] and it is a suitable candidate to compliment the current system based on the Time Division Multiplexing (TDM) which multiplex many signals of the same type together electrically before they are put on a single wavelength. Before WDM technology is used, TDM technology is the only for multiplexing techniques, typically interleaving the lower-speed signals as to obtain a higher data stream speed. This however requires electronic devices with higher speed, putting a restraint on the implementation cost. This is proved by the present technology levels which do not allow electronic TDM systems to be used in excess of 10 Gb/s [2]. In order to overcome this problem, the Optical Time Domain Division Multiplexing (OTDM) system is introduced with reports indicating the system successfully able to dimultiplexing a 320 Gb/s OTDM to several 10 Gb/s using nonlinear optical loop mirror [3]. However, demand of technology for higher speeds and capacities continued to grow. As such, WDM can be seen to be complement to replace the TDM system. WDM systems operate by taking multiple optical signals, mapping them into individual wavelengths and multiplexing the wavelengths over a single fiber with approximately 30THz corresponding to the low loss region in single mode fiber. WDM can also carry multiple protocols without a common signal format**.** Beginning in the late 1980s, early WDM research began with two widely spaced wavelengths in the 1310 nm and 1550 nm region. This region was also known as the wideband WDM region. Subsequently, the early 1990s revealed the development of a second generation of WDMs known as narrowband WDMs which contained 2 to 8 channels spacing at an intervals of about 400 GHz in the 1550 nm window [4]

1.3 Dense WDM System

As the demand for data bandwidth increases, which is driven by the phenomenal growth of the internet, the move from electrical networking to optical networking is the focus of new technologies. Today, Dense WDM (DWDM) technology continues to be developed. DWDMs can be categorized as a WDM system that has over 20 wavelengths. DWDM uses temperature-stabilized lasers to fix the center wavelength and narrow band filters, giving many densely spaced channels. The typical frequency channel spacing is 100 GHz, corresponding to a channel spacing of approximately 0.8 nm. The wavelengths used are specified by the International Telecommunication Union (ITU) and the technology is well proven. The limits of this spacing are not precisely known and have probably not been reached, though systems are already available since mid-2000 with a capacity of 128 wavelengths on one fiber [5]. Systems with fewer active wavelengths are classed as coarse WDM (CWDM). CWDM systems give a coarse channel spacing of 20 nm (2500 GHz) between channels from wavelengths of 1310 nm to 1610 nm. In the CWDM system the laser diode does not require a precisely controlled temperature like the laser diode in the DWDM system, allowing the CWDM system to use un-cooled DFB laser diodes. Due to the characteristic of this laser diode the CWDM is able to have a spacing of 20 nm. Although CWDM systems cover a longer bandwidth as compared to DWDM systems and thus reducing the cost of the transponder, the wavelengths are relatively far apart. Apart from that, the DWDM systems also offer the advantages of a much higher number of wavelengths and also greater capacity.

1.4 Optical Amplifier an a Key Component in WDM System

The DWDM network system will experience losses after travelling a long distance such as 100km or more. The drop of the signal will affect the operation of the system. To overcome this problem, an optical amplifier is very necessary in order to ensure a proper operation in the network

Previously, this problem is solved by using problem an electronic repeater every 30 to 50 km. The electronic repeater is a device used to increase or boost the signal by converting the light signal to an electrical signal and subsequently re-clocking and re-transmitting the signal by converting the signal from an electronic form back into its optical form again. However this system requires a large number of digital electronic devices for the purpose of the electronic repeater installation in every 30 to 50 km and the regenerated signal is combined using TDM systems and presented to the optical transmission system as a single data stream. The installation of electronic repeaters faces a major issue in trying to increases the speed and quality of data streams due to a fundamental law of electronics, whereby any electronic signal is changed by the conditions it encounters along its path and thus it gets more complicated. There is need to have an all optical amplifier that is independent of bit rate and able also to cover a wider wavelength range.

This requirement finds birth to the invention of the Erbium Doped Fiber Amplifier (EDFA) making in the 3rd window of optical communication network which is 1550 nm Basically EDFAs is introduced by D. N. Payne in 1987 [6], as a potential solution to the limitations of the electronic repeater was thus made available. EDFAs have the advantage of allowing the signal amplification at 1550 nm to be combined with a 980

nm laser diode as a pump and a WDMto launch the coupled signals into the erbium doped fiber. EDFAs have lower noise figures than the repeater and also require less maintenance as they have fewer electronic components. Since 1987, EDFAs have been researched on, and EDFA technology has since then matured and successfully been commercialized. By 1995, most optical communication links have replaced the electronic repeater with the optical amplifier. The benefits of the optical amplifier are evident, with the optical amplifiers having a better installation span of 150 to 200 km compared to the electronic repeater with the span installation of only 30 to 50 km and at the same time the optical amplifier provides lower noise in optical communication links The use of EDFAs in optical communication links complements the change of the optical communications operation wavelength which is from 1310 nm to 1550 nm, as the 1550 nm signals happen to fall within the low-loss region of the EDFA. This new operation wavelength is designated as the Conventional or C-band. The use of the optical amplifier provides significant cost savings and a better performance through lower noise and furthermore it allows multiple data streams to be amplified in one optical fiber by sending more wavelength channel using a technique known as WDM. WDM is the basic technology for full optical fiber communication network system

1.5 Bandwidth Demand in Optical Communication System

The explosive growth of internet traffic has placed severe demands on our communications networks. Early fiber optic networks uses the optical wavelengths at 800 nm as a center wavelength, while later systems uses optical wavelengths at either the 1310 nm window to take advantage of zero-dispersion or the 1500 nm window for it low-loss characteristics. The 1550 nm systems also take advantage of the now

matured EDFA technology in the 1528 to 1563 nm C-band. But with bandwidth demands doubling at least every two years, the available 35 nm window will soon be insufficient. Even with the capacity increasing technologies, this window will eventually become insufficient to cope with the increasing demand. Thus it is inevitable that a new operating window must be found to accommodate the increasing demand for bandwidth. There are to two methods to solve this issue which by increasing the spectra efficiency of WDM in existing transmission band and are also increasing the optical bandwidth to get larger low-loss window in silica fiber than the presently supported on WDM systems [7]. The increasing spectra efficiency of WDM can be done through the modulation and coding technique. For the second approach, the technique can be used if the extension of gain of the C-band EDFA can be developed the second approach is to further expand the existing C-band towards the Long-Band (L-band) region covering 1560 nm-1620 nm. Currently, there have been many activities done out in expending the existing band region into the shorter region that is the Short-Band (S-band) covering from 1460 nm to 1520 nm. This thesis will focus on the various methods of archiving optical amplification in this S-band region

1.6 S-band Optical Amplifier

The S-band operates at a wavelength between 1460-1520 nm with a window bandwidth of approximately 60 nm. The research on a silica-based gain medium for amplification in the S-band region is important for the combination of the S-band amplifier with conventional optical amplifiers for the C- and L- bands in WDM systems. However, amplification in the S-band region by conventional EDFAs is limited due to same issues such as the incomplete inversion of the active erbium ions and amplified spontaneous emissions (ASE) and also the lasing from the high peak at wavelengths near 1530 nm

[8]. Therefore, thus based on this problem, there is still an need to investigate various approaches in obtaining amplification within the S-band region.

In this thesis, various methods to construct the amplifier in the S-band region will be investigated and highlight their advantages and disadvantages. Since Albore [8,9] demonstrated the silica based S-Band optical amplifier by using Depressed Cladding-Erbium Doped Fiber Amplifier (DC-EDFA) for WDM transmissions between the wavelengths of 1488 and 1508 nm giving the possibility of the opening of a new window by using silica based optical amplifier in the short wavelength region or S-Band region to overcome the limitation of bandwidth in the C- and L-band WDM system. These findings lead to new interest in the research of S-band optical amplifier. A lot of research and techniques have been done in improving the noise figure and the gain of characteristics of the DC-EDFA. One of the drawbacks of the DC-EDFA is that, it has a slightly higher noise figure compared to the conventional EDFA.

Raman Amplifier (RA) can be an interesting approach towards amplification in the S-band. The RA has provides gain which depends on the pump power and the wavelength. The amplification of RA is achieved by the interaction between non-linear effect of the fiber, signal and pump laser (Raman pump). The RA can divided into two types. They are the distributed RA and lumped RA. The different between them is the distributed RA is one in which uses the transmission fiber as the gain medium by combining pump wavelength with signal wavelength, while a lumped RA uses a shorter length of fiber to provide amplification. The main drawback for RA is that needs higher pump power (Raman pump) compared to the pump power in EDFA. However the RA has advantages in term of gain bandwidth because it depends on the pump wavelength

Apart from EDFA, DC-EDFA, and RA that can generate gain in S-band, Semiconductors Optical Amplifiers (SOA) can be a candidate for an S-band optical

amplifier. SOAs are compact devices designed to amplify passing optical transmissions, much like EDFA and DC-EDFAs or other doped fiber amplifiers. Although both the SOA and doped fiber amplifiers operate on the same principle of stimulated emission, the manner in which they achieve the gain is different. In doped fiber amplifiers, rare-earth ions such as Erbium (Er^{3+}) pumped by their corresponding wavelengths provide the amplification, while in SOAs an active semiconductor material that has been injected with an external current source provides the gain. In this manner, SOAs are essentially laser diodes with no optical feedback [10]. Besides optical amplifier operating in the S-band, there are also needs of having source which meets this region of interest.

1.7 Light Source in WDM

The study of the optical amplifier has given a significant influence on the WDM system [11-13]. With the discovery of the EDFA, an alternative source to replace the distributed feedback (DFB) laser array has been thoroughly researched, with such achievements as the Erbium Doped Fiber laser (EDFL) and the Brilloiun Doped Fiber Laser (BEFL). EDFLs that can generate power up to hundred of miliwatts [14] with a coupling efficiency of more than 99% using single mode fiber have been reported. The EDFL has many advantages such as a wide range of operating wavelengths, broad tunability, high quantum efficiency, larger output power and high compatibility with fiber devices [15, 16].

In order to ensure that the WDM or DWDM system is cost effective, it is thus imperative that the component-per-wavelength cost is reduced. In this manner, one possible approach is to have devices with similar functionality integrated into arrays such as laser arrays [17-19]. A successful result of this integration can be seen in the

form of multi-wavelength DFB lasers arrays which have been demonstrated in the 1550 nm wavelength region. These multi-wavelength DFB lasers are capable of generating up to 21 wavelengths [20]. For application purposes however, it is necessary to combine all the channels with different wavelengths into one single mode fiber for signal transmission or distribution. Thus, to use a multi-wavelength laser source in a real system, its wavelength spacing has to match the network specifications within the tolerance given by the optical bandwidths of the other wavelength selective device such as the filters, multiplexer and demultiplexers Many different approaches to generate a multiple wavelength EDFL at room temperature such as by using a technique of polarization or spatial hole burning [21-25], by using an independent gain media [26,27],by generating frequency shift [28], and by using a phase modulator [29] have also been reported, with a spacing of 0.9 nm achieved. Narrower line spacing requires the cooling of the EDF to reduce the homogeneous linewidth of the gain medium and to prevent mode competition between adjacent laser lines [30].As mentioned earlier, the need of alternative laser source is required to meet the current demand. Fiber based tunable laser has found application in the system network as replacement part for current laser diode in WDM system. There have been many investigations on the C-band and L-band fiber laser source. In this thesis the S-band based fiber laser source is demonstrated based on the amplification medium as discussed earlier. The S-band light source with a possibility to find the application in an optical network is discussed below

1.8 S-band Light Source in DWDM

Another approach to generate multi-wavelength laser sources is by introducing the stimulated Brillouin scattering (SBS) effect in an single mode fiber (SMF) with a combination of an EDFA as linear gain medium which can support a multi-wavelength comb by cascading the stokes shifting processes at room temperature. This combination

is called a Brillouin Erbium Fiber Laser (BEFL) and can be used in DWDM applications, sensors and gyroscopes [31]. 10 GHz and 20 GHz laser combs have been generated efficiently through the BEFL and as such the BEFL is the most definitely an attractive source for DWDM applications [32, 33]. Furthermore, its design allows the resonator to be constructed to support a multi-wavelength line with a narrow line spacing of 10 GHz or 0.08 nm at room temperature, thus making it suitable with the high bit rate of DWDM systems. Additional lines in the BEFL can also be obtained using a cascade technique. In regard to this, numerous studies on cascaded BEFL techniques have been conducted [32] by improving the EDFA setup [34] or by adding an additional EDFA in the BEFL sub loop [35].

The first reported S-band BEFL was by Harun et. al, which was reported at this laboratory (Photonics Laboratory, Physics Department, University of Malaya) using a depressed-cladding erbium doped fiber (DC-EDF) as the linear gain medium [36] to generate 7 Brillouin Stokes. Although the S-band BEFL can overcome the dense line spacing and provide a broad bandwidth, current S-band BEFL developments have been delayed due to some difficulties encountered as shown in Figure 1.1[36], which shows only a few output spectrums of the BEFL. These laser spectrums currently prevent the S-band BEFL from being used as a laser transmitter source for DWDM application systems.

Figure 1.1 shows fewer Brillouin wavelengths generated in the S-band region which in turn reduces the number of transmitted channels and also causes too much degradation due to the large DWDM multiplexing loss. Additionally, the wavelength tuning range of the S-band BEFL has a limitation due to the ASE of DC-EDFA which limits the bandwidth for positive gain in the S-band region as opposed to the bandwidth for positive gain in the C- and L-band regions. Hence, the BEFL will not experience

sufficient gain to allow lasing to occur and as such it causes the cascaded generation of multiple Stokes to cease.

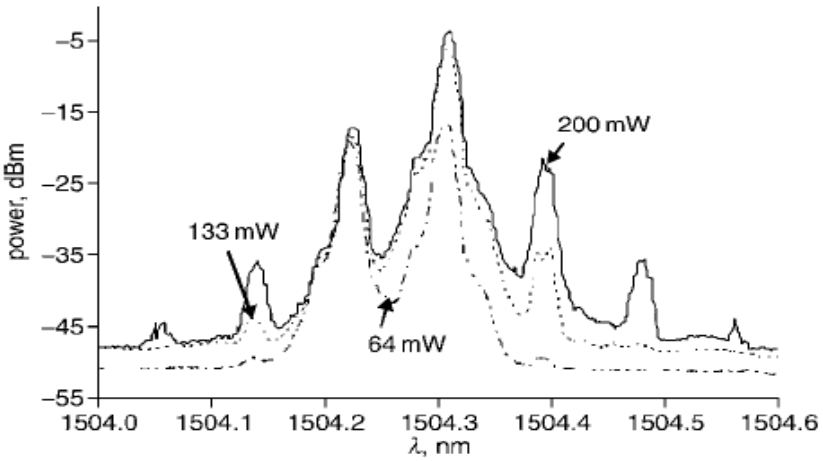

Figure 1.1: Brillouin wavelength generated in the S-band region [36]

The broad tuning range however does allow for the robust operation of the BEFL as the Brillouin pump (BP) already does not need to be matched accurately to the lasing wavelength region, provided that the BP can generate sufficient Brillouin gain. Therefore, the determination of the ASE bandwidth in the DC-EDFA where gain may be observed is crucial in the study of the S-band BEFL to obtain the maximum number of Stokes. Another limitation encountered with the S-band BEFL is the lack of gain in the DC-EDFA to generate more Stokes channels in the cavity system. However, this limitation can be overcome by adding a DC-EDFA in the linear cavity to increase the gain of the system as demonstrated by S.W. Harun [37]. There has been improvement in generating more line as demonstrated in this thesis

1.9 Thesis Objective

The main motivation of this thesis is to undertake a nearly comprehensive study of S-band optical amplifiers based on different media to provide a thorough comparison of the different gain media in terms of their advantages and shortcomings. The media of interest in this work are the standard EDF, DC-EDFs, RAs and SOAs. Comparisons of their gain, gain bandwidth and noise figure are discussed in depth in this thesis. From these measurements, the relevant gain media are used to generate the required fiber laser, and weaknesses such as the gain value, gain bandwidth and noise figure are addressed. This is presented in detail in Chapter 3.

The second objective of this thesis is to generate fiber lasers based on this gain media as a tunable, single output source. The proposed fiber laser will be characterized for its output power, tunability and stability, and combined in this thesis as a possible source for DWDM replacement parts. The results from this study are also important as a reference source for the development of the fiber lasers, especially in the optical communication systems. The results obtained are discussed in Chapter 4.

The third objective of this thesis is to further develop the results obtained in the gain medium measurement and also those from the fiber laser to generate multi-wavelength sources. The technique employed to achieve this multi-wavelength generation is based on the Brillouin effect. Combining the benefit as obtained in Chapter 3 and 4, the proposed design in the multi-wavelength Brillouin fiber laser in the S-band region has been studied well and has been reported for the first time as in the published papers listed in Appendix 1. The main characteristics such as the number of lasing Stokes wavelengths, flatness of the lasing spectrum and its operating range are detailed in Chapter 5. The research undertaken in this thesis can be a very interesting source for S-band amplifiers, S-band tunable fiber lasers and also multi-wavelength output in the S-

band region. The information presented here can help to design S-band amplifiers and sources that can find applications in WDM and DWDM systems.

1.10 Thesis Arrangement

Before any experiments are started, a literature review and understanding of operating principles of the EDFA, DC-EDFA, RA and SOA are undertaken. After the review is completed, the characterization experiment of EDFA, DC-EDFA, RA and SOA is being done. The main feature such as gain, gain bandwidth, gain saturation and NF are characterized. The result is than compared with one to another to see the difference between all of the S-band amplifiers.

The next process is to optimize the proposed designs and characterize the amplifiers for their laser applications. There have been 3 publications on S-band amplifiers as a result from this work which listed in Appendix 1. There have also been 2 publications on S-band fiber lasers, which are also listed in the same Appendix. On top of this, there are also 5 publications on multi-wavelength S-band fiber lasers which are taken from this thesis. The design of multi-wavelength Brillouin fiber laser is done by using all the information gathered from the S-band amplifier as a linear gain medium. The features such as number of Brillouin Stokes, 3dB flatness, tuning range and output power will be compared for each gain medium. Many techniques developed in this thesis have also been applied such as the use of the Arrayed Waveguide Grating as a tuning device has been used by other members in the research group in the area of C- and L-band regions and also in the O-band region which listed in Appendix 2.

The research approach is described as in Figure 1.2 below.

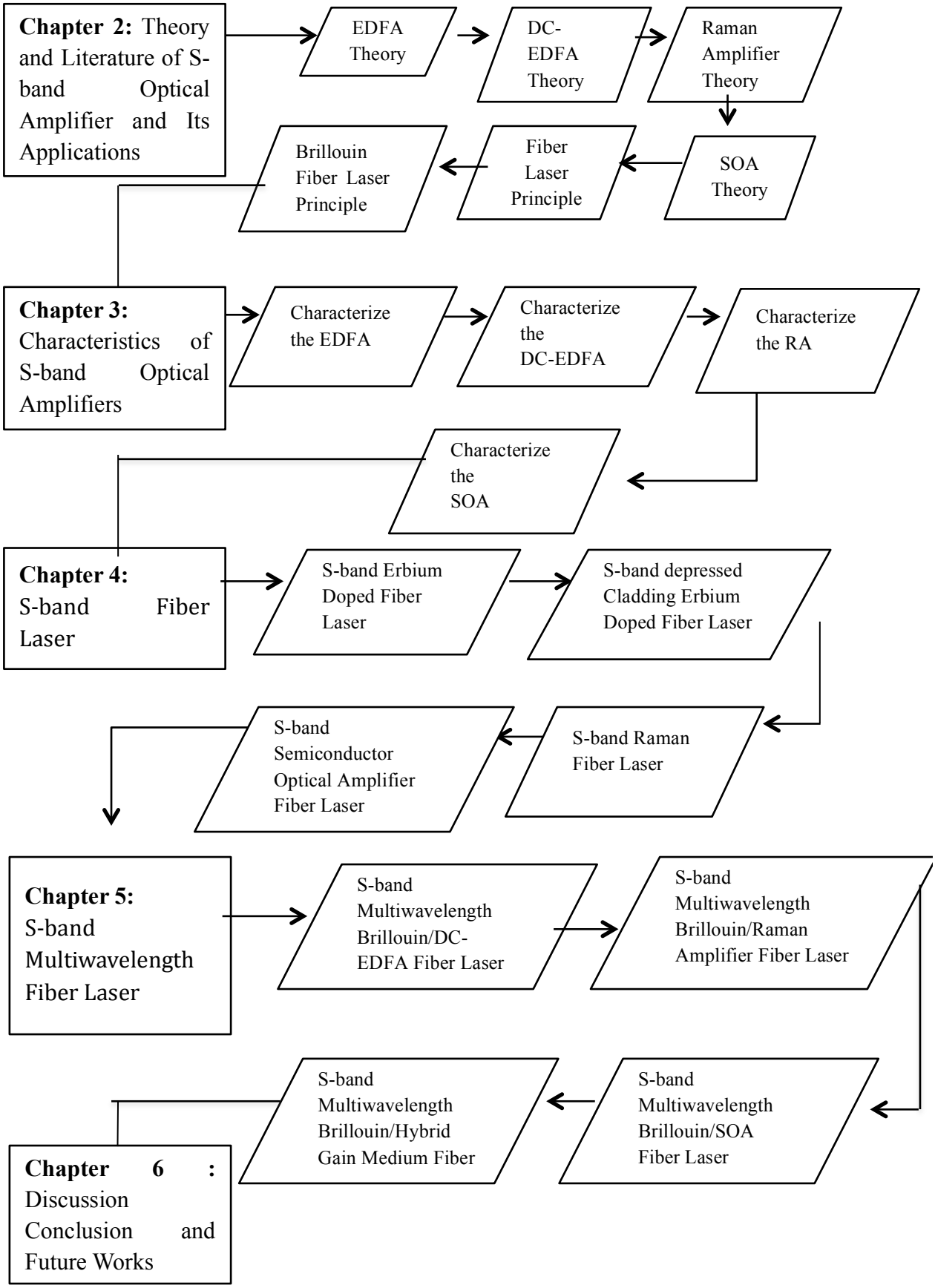

Figure 1.2 Research methodologies for the thesis

Reference

[1] Harry J. R. Dutton, "Understanding Optical Communications" International Business Machines Corporation 1998.

[2] Cheng Xiau San "Enhanced Brillouin Erbium Fiber Laser For DWDM System" Master Thesis, University of Malaya, 2003.

[3] A.T Clausen, A.I Siahlo, J.Seoane, L.K Oxenlowe, P. Jeppesen,"320 to10 Gbit/s Demultiplexing using a NOLM based on commercially available component" Electronic Letters, pp 265- 266 vol 41,2005.

[4] Dennis Derickson, "Fiber optic Test and Measurement" Prentice Hall Inc 1998.

[5] Kartalopoulos, Stamatios V "Introduction to DWDM Technology: Data in a Rainbow" IEEE Press, New York 1999.

[6] R.J. Mears, L. Reekie, I.M. Jauncey and D.N. Payne,"Low-noise Erbium-doped fiber amplifier at 1.54pm", Electron Letter, vol 23, pp.1026-1028, 1987.

[7] Mohammad N Islam, "Raman Amplifiers for Telecommunications 1, Sub-Systems and Systems, Springer-Verlag, pp 301 , 2004.

[8] M.A.Arbore, "Communication System Using S-band Er- Doped Fiber Amplifier With Depressed Cladding" United States Patent, Patent No 6903865.

[9] M.A. Arbore, Y Zhou, G. Keaton, T. Kane,"34dB gain at 1500 nm in S-band EDFA with distributed ASE suppression", Optical Communication, 2002. ECOC 2002. 28th European Conference on, vol 1, pp 1-2, 2002.

[10] K. Zhou, D. Zhou, F. Dong, and N. Q. Ngo,"Room-temperature multiwavelength erbium-doped fiber ring laser employing sinusoidal phasemodulation feedback," Optics. Letters, vol. 28,no 11, pp. 893–895, 2003.

[11] C.Y. Chen, M.M Choy, M J Andrejco, M. A Saifi and Chinlon Lin , " A Widely Tunable Doped Fiber Laser pumped at 532 nm" IEEE Photonics Technology Letters, vol.2, no 1, pp 18-20, 1990.

[12] P. Urquhart, "Review of rare earth doped fiber laser and amplifier" Optoelectronics, IEE Proceedings J Optoelectronik , vol.135, no.6, pp.385-407, 1988.

[13] M. C. Faries, R.I. Laming, P.R.Morkel, T.A.Birks, D.N.Payne and E.J Tarbox "Efficient high-gain erbium-doped fiber amplifier pumped with a frequency-double Nd-YAG laser" in OFC 89 Houston, TX, 1989 paper TUG5.

[14] M. S. O'Sullivan, J.Chrostowski, E. Desurvire, and J. R. Simpson, "High power narrow linewidth Er^{3+} doped fiber laser" Optics Letters, , vol. 14, issue 9, pp 438-440,1989.

[15] P. W France, "Optical Fiber Laser and Amplifier" CRC Press, Inc Boca Raton, Florida 2000.

[16] X.P Dong, S. Li, K.S Chiang, M.N Ng, B.C.B Chu, B.C.B. "Multiwavelength erbium-doped fiber laser with a high-birefringence fiber loop mirror" Electronics Letters, vol 36 no 19, pp 1609-1610, 2000.

[17] T.P Lee, Current Trends In Integrated Optoelectronic", World Scientific Publishing, August 1994.

[18] A.A.M. Staring, L.H. Spiekman, J.J.M. Binsma, E.J. Jansen,T.Van Dongen, P.J.A,Thijs, M.K Smit,B.H. Verbeek "A compact nine-channel multiwavelength laser", IEEE Photonics Technology Letters, vol 8, issue 9, pp 1139-1141, 1996.

[19] C.E Zah, F.J Favire, B. Pathak, R.Bhat, C. Caneau, P.S.D. Lin, A.S Gozdz, N.C Andreadakis, M.A Koza, T.P Lee,"Monolithic integration of multiwavelength compressive-strained multi quantum-well distributed-feedback laser array with

star coupler and optical amplifiers" Electronics Letters vol 28, issue: 25 pp 2361-2362, 1992.

[20] C. E. Zah, J. Gamelin, B. Pathak, F. Favire, P. S. D. Lin, N. C. Andreadakis, R. Bhat, C. Caneau, L. Curtis, D. D. Mahoney, W. C. Young, and T. P. Lee, "Multiwavelength light source with integrated DFB laser array and star coupler for WDM lightwave communications," Int. J. High Speed Electron. Syst, vol. 5, no. 1, pp. 91–109, 1994.

[21] X.F.Yang, X.Y Dong, S.M Zhang, F.Y Lu, X.Q. Zhou, C.Lu, "Multiwavelength erbium-doped fiber laser with 0.8 nm spacing using sampled Bragg grating and photonic crystal fiber" IEEE Photonics Technology Letters,vol 17, Issue 12, pp 2538- 2540, 2005.

[22] O. Graydon, W. H. Loh, R. I. Laming, and L. Dong, "Triple-frequency operation of an Er-doped twincore fiber loop laser," IEEE Photonics. Technology. Letters., vol. 8, no. 1, pp 63–65, 1996.

[23] G. Das and J. W. Y. Lit, "L-band multiwavelength fiber laser using an elliptical fiber", IEEE Photonics Technology Letters, vol. 14, no. 5, pp. 606–608, May 2002.

[24] C. L. Zhao, X. Yang, C. Lu, J. H. Ng, X. Guo, P. R. Chaudhuri, and X. Dong, "Switchable multi-wavelength erbium-doped fiber lasers by using cascaded fiber Bragg gratings written in high birefringence fiber Optics Communications, vol. 230, pp. 313–317, 2004.

[25] A. J. Poustie, N. Finlayson, and P. Harper, "Multiwavelength fiber laser using a spatial mode beating filter",Optics Letters, vol. 19, pp. 716–718, 1994.

[26] R. Slavik, I. Castonguay, S. LaRochelle, and S. Doucet, "Short multiwavelength fiber laser made of a large-band distributed Fabry–Pérot structure", IEEE Photonics. Technology Letters, vol. 16, no. 4, pp.1017–1019,2004.

[27] Q. Mao and J. W. Y. Lit, "Switchable multiwavelength erbium-doped fiber laser with cascaded fiber grating cavities," IEEE Photonics Technology Letters,vol. 14, no. 5, pp. 612–614, May 2002.

[28] A. Bellemare, M. Karasek, M. Rochette, S. LaRochelle and M. Tetu, "Room temperature multifrequency erbium-doped fiber lasers anchored on the ITU frequency grid", Jounal of Lightwave Technology, vol. 18, no. 6, pp. 825–831, 2000.

[29] K. Zhou, D. Zhou, F. Dong, and N. Q. Ngo, "Room-temperature multiwavelength erbium-doped fiber ring laser employing sinusoidal phase modulation feedback", Optics Letters, vol. 28, pp. 893–895, 2003.

[30] G.J Cowie, D. Yu, T.C Yew, "Brillouin/Erbium fiber lasers" Journal of Lightwave Technology, Volume 15, Issue 7, pp 1198 – 1204, July 1997.

[31] S. P. Smith, F. Zarinetchi, and S. Ezekiel, "Narrow-linewidth stimulated brillouin fiber laser and applications," Optics. Letters, vol. 16, pp. 393–395, 1991.

[32] G.J Cowle, D.Y Stepanov, "Hybrid Brillouin/erbium fiber laser", Optics Letters, vol 21, issue 16, pp.1250-1252,1996.

[33] D.Y Stepanov, G.J Cowle,"Properties of Brillouin/erbium fiber lasers" IEEE Journal of Selected Topics in Quantum Electronics, vol 3, issue 4, pp 1049-1057 1997.

[34] N. S Kim, "Multiwavelength operation of EDFA enhanced Brillouin/erbium fiber lasers", Electronics Letters, vol. 34, no 7, 1998.

[35] X.S Cheng, H. Ahmad and S.W. Harun, "Additional EDFA Induced Flatness of Brillouin Stokes Peak Power" ECTI Transaction on Electrical Eng Electronic and Communications, vol 3, no 2, pp 189-191, 2005.

[36] S.W. Harun, X.S. Cheng, N.K. Saat and H. Ahmad, "S-band Brillouin Erbium Fiber Laser" , Electronic Letters, vol. 41, no. 4, pp 174- 176, 2005.

[37] S.W. Harun, X.S. Cheng, and H. Ahmad, " An efficient S-band brillouin erbium fiber laser with additional EDFA" Optics & Laser Technology, vol 39, Issue 3, pp 616-618, 2007.

Chapter 2
Theory and Literature of S-band Optical Amplifier and Its Applications

2.1 Introduction

The extension of the existing C-band into the new regions of the L-band and S-band region was necessary in order to overcome the limited bandwidths of DWDM systems at the time. Of particular interest is the S-band region, ranging from 1460 nm to 1520 nm with a bandwidth of about 60 nm. Optical amplification in the S-band is of crucial importance in allowing for S-band operation, and can be achieved through many different approaches such as Erbium Doped Fiber Amplifiers (EDFAs), Depressed Cladding Erbium Doped Fiber Amplifier (DC-EDFAs), Raman Amplifier (RAs) and also Semiconductor Optical Amplifier (SOAs).

In this chapter, the basic principles that define the behavior and operation of S-band optical amplifiers are discussed. This chapter will also describe the operation of the S-band optical amplifier and its applications in fiber lasers, such as the Brillouin fiber laser.

2.2 Erbium Doped Fiber Amplifiers (EDFAs)

The amplification of optical signals is a key factor in allowing for the deployment of the long-range, high capacity communications systems of the modern world. The most common method for optical amplification is the rare-earth doped fiber amplifier, specifically the Erbium Doped Fiber Amplifier (EDFA). EDFAs have become the main choice for amplification in optical communications networks, replacing the traditionally used electronic regenerator. Furthermore, EDFAs have also recently found many new

and novel uses, such as in the development fiber lasers

The versatility of the EDFA arises from the use of the erbium ions (Er^{3+}). When exposed to incident light at 980 nm, the Er^{3+} ions are excited to higher energy levels. However, this high energy condition is not stable, and the ion quickly relaxes towards a lower energy level, in the process emitting a photon at a longer wavelength[1] and the As the ions relax towards a lower energy state, they emit photons at a wavelength of 1550 nm. This coincidently falls within the third window of optical communications where the attenuation in silica fibers is the lowest, thus making the EDFA the most suitable choice for amplification. Furthermore, because the amplification process does not require the incoming optical signal to first be translated into a corresponding electronic signal (as is the case with electronic regenerators), EDFAs (and for that matter any type of optical amplifier) also possesses significant advantages such as transparency to signal bit rates and modulation, the ability to amplify multiple signals simultaneously as well as high temperature stability. Another key advantage of the EDFA is that it can be coupled easily to conventional transmission fibers, thereby reducing the insertion loss and improving the overall performance of the system.

The next section will detail the fundamental principals that define the operation of the EDFA, examining the excitation and relaxation process and also the generation on an incoherent optical flux known as the amplified spontaneous emission (ASE) in the fluorescence band around the signal wavelength [1].

2.2.1 Atomic Rate Equation

In order to understand the excitation and relaxation processes that occur within an excited erbium ion, the simplest approach would be to describe the ion as three atomic

[1] This proses is known as down-conversion, as the photons emitted are at a longer wavelength and therefore have lower photon energies. Up-conversion on the other hand occurs when the emitted photon is at a shorter wavelength, indicating that the photon energies are higher. This occurs when the excitation mechanisms involve more than one photon absorbed for each emitted photon.

levels. These atomic levels are the ground level, which has a population density of N_1, the metastable level, which has a population density of N_2 and the pump level, which has a population density of N_3. The atomic levels of the erbium ions are shown in Figure 2.1.

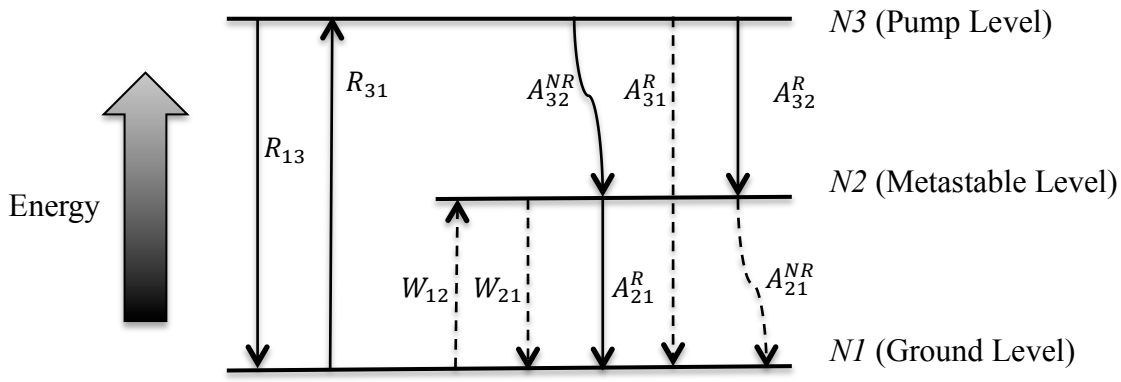

Figure 2.1: Erbium Atomic Levels

These population densities at each level can be described by the following equations [2]:

$$\frac{\partial N_1}{\partial_t} = A_{21}N_2 + W_{21}N_2 - W_{12}N_1 - RN_1 + R'N_3 \quad (2.1)$$

$$\frac{\partial N_2}{\partial_t} = A_{32}N_3 - A_{21}N_2 - W_{21}N_2 + W_{12}N_1 \quad (2.2)$$

$$\frac{\partial N_3}{\partial_t} = -A_{32}N_3 + RN_1 + R'N_3 \quad (2.3)$$

$$N_1 + N_2 + N_3 = N_T \quad (2.4)$$

Equations 2.1, 2.2 and 2.3 provide the rate equations for the pump, signal and ASE intensities, with W_{12} and W_{21} being the stimulated emission coefficients of the signal and pump respectively, R_{31} and R_{13} are the absorption transitions rates of the signal and the pump. A_{32}^{R} , A_{21}^{R}, A_{32}^{NR}, A_{21}^{NR} are the spontaneous transitions between the ground,

metastable and pump levels, with the subscripts *R* and *NR* referring to radiative and non-radiate transitions. The fourth equation provides the total dopant concentration, N_T.

When the erbium ion is exposed to incident light at 980 nm, multiple transitions take place between the three levels, making the model very complex. However, as transitions from the ${}^4 I_{11/2}$ to ${}^4 I_{13/2}$ levels are predominately non-radiative, while transitions between the ${}^4 I_{13/2}$ and ${}^4 I_{15/2}$ levels are radiative in nature, equations (2.1) to (2.4) can now be simplified into just two equations:

$$A_{32}^{NR} \gg A_{32}^{R} + A_{31}^{R} \tag{2.5}$$

$$A_{21}^{R} \gg A_{21}^{NR} \tag{2.6}$$

As A_{32}^{R} is a very fast non-radiative transition, it can be assumed that the transition rate of A_{32}^{R} is much higher than the pump rate or stimulated emission rates, such that $A_{32}^{R} \gg R_{13,31}$. Therefore, the complex three-level system can now be represented by a simpler two-level model.

2.2.2 Amplified Spontaneous Emission (ASE)

ASE occurs when a rare-earth doped fiber (in this case the EDF) is pumped by light at a specific wavelength, but not exposed to external signals from the 1550 nm region. ASE is defined as a process where spontaneously emitted radiation (luminescence[2]) from a pumped rare-earth-doped fiber is amplified to high power levels.

ASE is usually an unwanted effect as it has the tendency to limit the gain that can be achieved, typically in the order of 40–50 dB. Furthermore, ASE can also prevent lasing at extreme wavelengths in certain laser designs, thereby limiting their operational

2 ASE differs from luminescence in the sense that ASE is luminescence that has been amplified by the EDF. Furthermore, ASE is highly directional, occurring in the same direction as the propagating singal in the EDF. Luminescence on the other hand is not directional and can be observed in all directions from the EDF.

capabilities. Most importantly, ASE is a key factor of the noise figure of a system, which is a measure of the excess noise introduced by the EDFA into a transmission. However, in the case of fiber lasers, ASE is a desired effect and is used in conjunction with feedback and tuning mechanisms to form a laser resonator for a specific wavelength.

As the ASE is the amplified luminesce of a fiber being pumped, therefore a gain threshold is necessary in order for the fiber to exhibit the ASE effect. The estimated gain required for the generation of ASE in an EDF is derived as in Equation 2.7

$$h\nu\Delta\nu_e G = \mathrm{A}I_{sat} \tag{2.7}$$

where A is the fiber core area, I_{sat} is the saturation intensity, G is the single pass gain required and $\Delta\nu_e$ is the emission bandwidth of the ASE spectrum. The ASE spectrum can be observed in both the co-propagating (moving in the same direction with the pump signal) and counter-propagating (moving in the opposite direction of the pump signal) directions of the EDF.

2.2.3 Erbium Doped Fiber Amplifier in the S-band Region

As demands for capacity continue to increase, the bandwidths offered by the C- and L-bands are quickly reaching their limits. Although methods such as wavelength and time division multiplexing are able to cope with the current demands for traffic capacity, these methods will not provide a long-term solution. It is with this fact in mind that researchers are now increasing their efforts towards extending the telecommunications bandwidth into the short wavelength of the third communications window, also known as the S-band. The S-band operates from between 1460 to 1520 nm, with a window bandwidth of approximately 60 nm. This new band, when combined with the existing

bandwidth of 70 nm from the C- and L-bands would give a total channel bandwidth of 130 nm. This large bandwidth will undoubtedly be able to cater to any demands for capacity for a significant period of time in the future.

In reality however, the utilization of the S-band region is currently limited and cannot be fully exploited. The primary reason for this is the availability of amplification in this region. EDFA technology in the S-band region is currently plagued by a number of issues, among which include the incomplete inversion of the active erbium ions in the EDFA at the S-band region, thereby limiting the amplification in this region. Another key issue is the generation of ASE spectra with lasing at the 1530 nm region, which in turn suppresses the amplification of signals in the S-band region.

Recently, a new technique has made it possible to obtain S-band amplification from erbium ions using a special type of EDF known as a Depressed Cladding Erbium Doped Fiber (DC-EDF). This type of fiber differs from normal fibers such that it has two cladding layers instead of one, with the outer cladding layer having a lower refraction index than the inner cladding layer. The key characteristic of this fiber is that it has a cut-off wavelength of 1525 nm, which is below the 1530 nm ASE peak in normal EDFs and therefore is able to prevent the lasing at this region. The distributed loss for wavelengths above 1525 nm in a DC-EDF is more than 200 dB, but in the S-band region this loss is far less than the fiber's gain, with a 5 dB/km background loss measured at a wavelength of 1300 nm [4]. These types of fibers are manufactured using standard Modified Chemical Vapor Deposition (MCVD) methods [5] with a standard solution doping technique to add fluorine into the depressed cladding in order to create the refraction index variation and also aluminum and erbium ions into the core for amplification.

2.3 Depressed Cladding Fiber Erbium Doped Fiber

The most common fiber design is the matched cladding single mode fiber whereby relative index difference, △= 0.2 ~ 0.3 percent with a core diameter of 9-10 μm. These parameters are set in order to achieve the desired cut-off wavelength, λ_c for a low loss and zero dispersion wavelength λ_0 near 1300 nm [6].

However, matched cladding single mode fibers were found to be sensitive to microbending loss, especially in the longer wavelengths [6]. Initial efforts to reduce microbending loss found little success, with the most successful approach being to reduce core radius *r* and increase relative index difference △ to reduce the microbending sensitivity [7]. However, this created a problem as it moved λ_0 unacceptably long wavelength, as by reducing △ the sensitivity of the fiber to curvature loss was enhanced in higher wavelengths due to the poorer mode confinement that results from the dependence of the modal spot size ω_o on λ and △, as given in equation 2.8:

$$\omega \approx \frac{\lambda}{\sqrt{\Delta,}} \tag{2.8}$$

In order to overcome the problem of microbending sensitivity in matched-cladding fibers, an alternative fiber design is proposed, that is the depressed cladding fiber. The depressed cladding design concept overcomes the problems associated with the reduction in core radius *r* and increase of △ by allowing the core and cladding index to be varied independently from each other, as well as allowing the core diameter to be varied. By doing so, the core diameter of a could be kept as small as possible in order to reduce the sensitivity of the fiber to microbending loss, while still allowing △ to remain

large enough so as to reduce the sensitivity if the fiber to curvature induced losses at the higher wavelengths [7].

Unlike standard optical fiber (SMF-28), depressed cladding fiber (also known as W-profile fiber because the shape of the index distribution resembles the letter W) are surrounded by a secondary cladding. Within the depressed cladding fiber, the core, depressed cladding and secondary cladding all have a circular cross-section as show on the Figure 2.2. At region I associated with core radius *r*, extends from $0 \leq r \leq r_0$, while the depressed cladding and secondary cladding radius occupy the regions of II, III which lies between $0 \leq r \leq r_1$and $r \geq r_1$. The core has an index refraction number n_0, while the depressed cladding has an index of refraction of n_1 and the secondary cladding has an index of refraction of n_2. Figure 2.3 shows the refractive-index profile of a single-mode fiber with depressed inner cladding. In addition to the propagations of guided modes in the core, discrete modes are also able to propagate in the outer cladding. Substantial power can be transferred from the core-guided mode to the outer cladding modes when the phase velocities of the modes are identical.

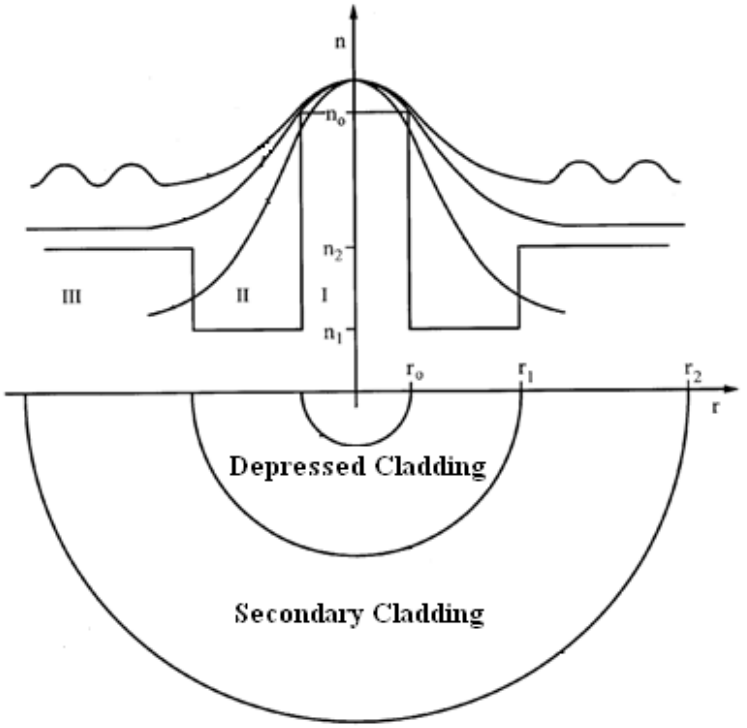

Figure 2.2: Depressed cladding fibre cross-sectional view[8]

Figure 2.3 illustrates the W-profile as obtained during normal manufacturing techniques. It is sufficient that the indices of the depressed cladding and secondary cladding average out to the values of n_1 and n_2 [9].

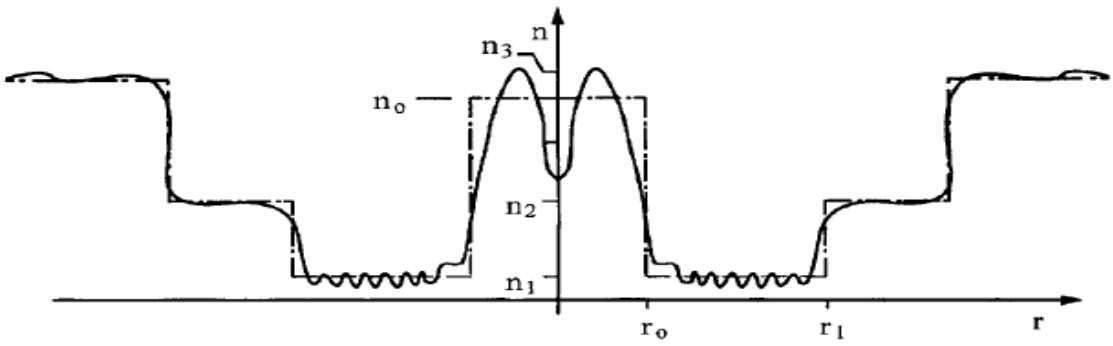

Figure 2.3: W-Profile of Single Mode fibre [9]

The average index number of the core must be significantly higher than the index n_1 of depressed cladding and the index n_2 of secondary cladding. A selection of appropriative value for the indices n_0, n_1, n_2 and radii r_0, r_1, r_2 must be determined beforehand to have the desire fundamental cut-off wavelength.

2.3.1 Characteristics of Depressed Cladding Fiber

This section discusses the characteristics of the depressed cladding fiber that ensure low loss, especially in the longer wavelengths that are essential for telecommunications networks [10-12]. This is because in matched clad fiber the light guiding properties are fundamentally different from the properties of the depressed cladding fiber [13].

2.3.1.1 Cutoff Characteristics of Depressed Cladding Fiber

In 1982 Leonard G. Cohen in his paper title "Radiating Leaky-Mode Losses in Single-Mode Light guides with Depressed-Index Claddings" [13] describes in the matched clad fiber the fundamental of HE_{11} mode step index fiber is not cut-off due to *LP01* mode is always guided [14]. Compared with the depressed cladding fiber the HE_{11} mode would become cut-off if *LP01* mode may be leaky as shown in Figure 2.4 below. The comparisons of matched clad and depressed cladding refractive index profile at long wavelength in even in a perfect light guide and if the effective modal phase-index becomes smaller than the index of the outer cladding the fundamental cut-off becomes $k = 2\pi/\lambda$ dependent on the ratio of modal propagation constants β to propagation constant $k = 2\pi/\lambda$ of plane in free space, β/k .

Figure 2.4 shows when $\beta/k > n_0$ as is the case in which there are no leakage losses and if the propagation constant is smaller $\beta/k < n_0$ the cutoff condition occurs due to power radiating through the outer cladding.

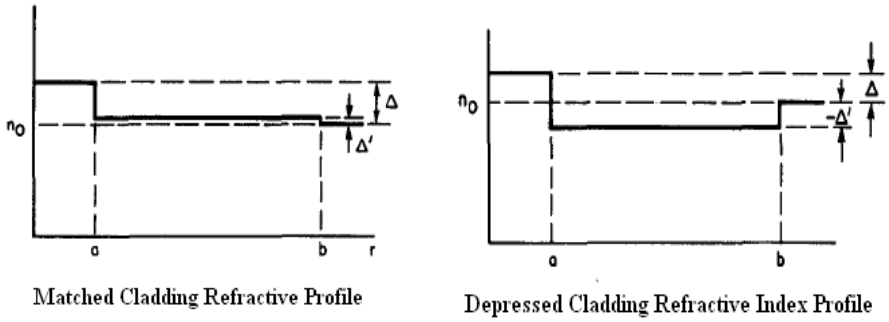

Figure 2.4 Matched Cladding and Depressed Cladding Refractive Index profile [13] where $\Delta = n_1 - n_2$ and $\Delta' = n_2 - n_0$

2.3.1.2 Microbending Loss in Depressed Cladding Fiber

Generally, the cladding in single mode fibers is found to be sensitive to microbending loss, especially in the longer wavelengths in this section we derive how to estimated microbending loss in depressed cladding fiber. A microbending lightguide can be represented by an equivalent straight lightguide whose effective-index profile n_{eff} is deformed as indicated below [15]:

$$n_{eff} = n(r)\left[1 + \frac{r}{R}\cos\emptyset\right] \tag{2.9}$$

where R is the radius of curvature of the bent fiber axis, $n(r)$ is the refractive index of the straight fiber, and r and $\emptyset$ are the radial and azimuthal coordinates of a cylindrical

polar coordinate system with $\emptyset = 0$ in the plane of the curved fiber. The worst case occurs in the plane of curvature where:

$$n_{eff} = n(r)\left[1 + \frac{r}{R}\right] \tag{2.10}$$

The radius of curvature that makes $n_{eff} = \beta/k$ at r = b is given by:

$$R = \frac{bn_0}{\beta/k - n_0} \tag{2.11}$$

If, for example, $(\beta/k - n_0)/n_0 = 0.1$ percent in a straight fiber, the guided mode field would turn into a radiating field at r = b when the radius of curvature reaches the value $R = b \times 10^3$ which could be on the order of 50-100 mm. Thus, even if $\beta/k > n_o$ in the straight fiber as shown in Figure 2.5 (a) a bend can deform the refractive index profile so that $\beta/k < n_{eff}$ as shown in Figure 2.5 (b). For this reason it is desirable to make b/a large enough to ensure tolerable leakage losses even if $\triangle = 0$ because this case may arise unintentionally when the fiber is bent.

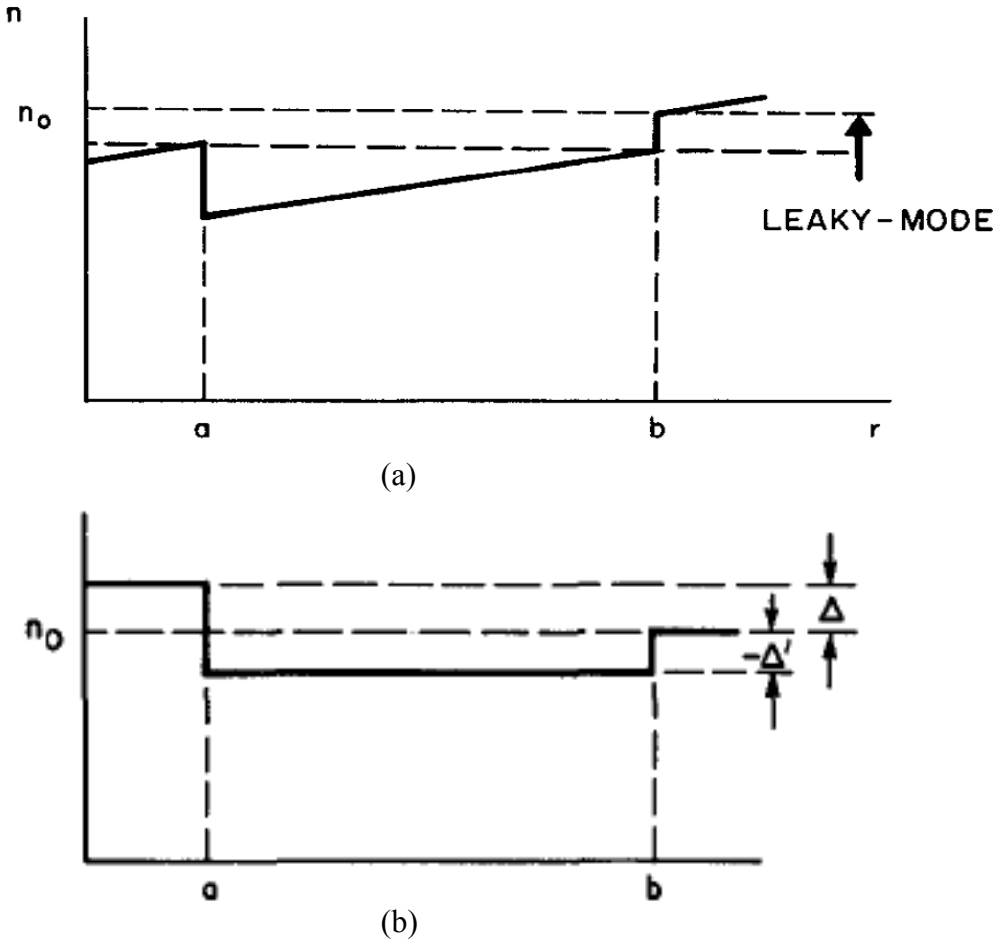

Figure 2.5 (a) The effective refractive index profile, in the plane of curvature of a bent fiber,(b) shows how an actual profile would be distorted by a bend [13].

2.4 Characteristics of Erbium Doped Fiber Amplifier

2.4.1 Gain of Erbium Doped Fiber Amplifier

The gain of the EDFA and DC-EDFA is defined as the ratio of the output signal power to the input signal power as in the equation 2.12 below and is limited by the fact that there are a limited number of Erbium ions in the core.

$$G = \frac{P_{S,Out}}{P_{S,In}} \tag{2.12}$$

whereby the output signal power is defined as $P_{s,out}$ and input signal power is defined as $P_{s,In}$

2.4.2 Small Signal and Saturation Gain of Erbium Doped Fiber

The small signal gain can be defined when the gain is independent to the input signal and also corresponds to the input power levels where signal amplification does not reduce [16] The small signal gain EDFA gain is given by the expression

$$G(\infty) = exp\{[1 - \eta_p/\eta_s)/1 + \eta_p)]\rho_o\, \sigma_e L'\} \tag{2.13}$$

where η_p and η_s, is ratio of emission to absorption cross section at pump and signal wavelength, ρ_o , σ_e, is peak dopant density, total emission cross section, where $L' = \Gamma_s L$ is reduce effective length accounting for the *RE* mode overlap effect. In ideal case where complete inversion can be achieved, the highest unsaturated gain of EDFA is

$$G(\infty) = \exp\,(\rho_o\, \sigma_e L') \tag{2.14}$$

The gain in unsaturated region with different input signal power is linear. The saturation gain of EDFA is usually occur when operated at high power input signal. The gain in an ASE-free model can be written implicitly as function of the ration of the output power, P_{out} to the saturation power, P_{sat} [16,17]

$$G = G_0 exp\left[-\frac{G-1}{G}\frac{P_{out}}{P_{sat}}\right] \tag{2.15}$$

where G_0 is the small signal gain. The saturation power P_{sat} at a specific wavelength is the power required to invert the EDF sufficiently to obtain optical transparency in other words zero gain. P_{sat} is written as

$$P_{sat} = \frac{A_{mf} h\nu}{\sigma_a \tau_{sp}} \quad (2.16)$$

where A_{mf}, σ_a, τ_{sp} is the mode field area, absorbtion coefficient and spontaneous life time of the ion in the metastable state

2.4.3 Gain Bandwidth

Gain bandwidth can define as the width of the gain over the input signal wavelength. Ideal gain bandwidth of optical amplifier is can cover widest bandwidth by using only single piece of device for example by using very short length of Bismuth/Erbium doped fiber amplifier (Bi-EDFA) which is can produce a wide band gain bandwidth which is can cover over C- and L-band. In S-band optical amplifier, the finding to extend the bandwidth to the S+-band is still on progressing, Apart from Raman Amplifier, they have some research is demonstrated the EDF with special filter to get the S+-band amplification[18,19].

2.4.4 Amplified Spontaneous Emission and Noise Figure

When the EDFA was pumped its create the ASE and combine with spontaneous emission produced by the signal source. As the ions have a finite excited state lifetime ($\tau = 10ms$), some of the ions spontaneously return to the ground state and these photons have no coherence charecteristics with respect to the incoming signal light, as opposed to a photon generated by stimulated emission [20]. This spontaneously emitted photon can be amplified as it travels down the fiber and stimulates the emission of more photons from excited ions, photons that belong to the same mode of the electromagnetic field as the original spontaneous photon. This parasite process occurs at any frequency

within the fluorescence spectrum of the amplified transition. This reduces the gain from the amplifier. It takes away photons that would otherwise participate in stimulated emission with the signal photons. This background noise is usually referred to as ASE. Ultimately, the ASE limits the total amount of gain available from the amplifier

The generated ASE power propagates in both direction along the fiber, forward and backward propagation with the pump power. In the unsaturated region, the output ASE in a given bandwidth Δv of an amplifier with gain *G* can be expressed as:

$$P_{ASE}^{\pm} = n_{sp}^{\pm} h v_s (G-1) = n_{eq}^{\pm} h v_s \Delta v G \tag{2.17}$$

where $n_{sp}^{\pm}$ and $n_{eq}^{\pm}$ are the spontaneous emission factor and the equivalent input noise, respectively corresponding to the forward and bacward direction. Because the output spectrum contain spontaneous emission from both the source and EDFA under test, the EDFA ASE cannot be determined directly from the output spectrum measurement. The calculation of EDFA noise figure (NF) required that the portion of the output ASE level that generated by EDFA is known. This is calculated as the different between the output spontaneous emission power and the equivalent source spontaneous emission power at the amplifier output

The NF is a measure of how much noise the amplifier adds to the signal. The definition is:

$$NF = \frac{SNR_{in}}{SNR_{out}} \tag{2.18}$$

where SNR is the signal-to-noise ratio. Due to ASE, the SNR_{out} at the amplifier output is less than that at the input, SNR_{in}. If the signal is much stronger than the noise, the NF can be written as [21]:

$$NF = (1 + \frac{2P_{ASE}}{h\nu\Delta\nu_{sp}})\frac{1}{G} \quad (2.19)$$

where P_{ASE} is the ASE noise power, h is Planck's constant, ν is the frequency of the light and $\Delta\nu_{sp}$is the bandwidth of the noise (i.e. the bandwidth of the EDFA).

2.5 S-band Raman Amplifier

2.5.1 Principle of Raman Amplifier

One type of optical amplifier which produces amplification in the S-band is Raman amplifier. Raman amplifier is based on the Raman effect principle which uses the external pump to have eneregy tranfer inparting the incoming signal. To get the Raman gain, the relocation or transfer of power from one optical beam to another will cause the frequency to be downshifted by energy of an optical phonon. Figure 2.6 shows the Raman gain spectrum of SMF, the Raman gain bandwidth of the SMF is about 40 THz and the higest gain is obtained at 13.2 THz from the pump wavelength of 1500 nm. The main advantage of the Raman amplifier is the tunable gain bandwidth. The gain bandwidth can be set by using different Raman pump wavelength. The selected pump wavelength is normaly 100 nm below the need gain spectrum. The detailed interaction between Raman pump and signal is governed by following equations [24]

$$\frac{\delta P_s}{\delta_z} = \frac{g_R}{A_{eff}} P_p P_s - \alpha_s P_s \quad (2.20)$$

$$\frac{\delta P_p}{\delta_z} = \frac{\omega_p}{\omega_s} . \frac{g_R}{A_{eff}} P_p P_s - \alpha_p P_p \quad (2.21)$$

where the absorption coefficients α_s and α_p account for the fiber loss at the signal and pump wavelengths respectively, assuming the pump and signal are co-polarized, and neglecting the first term on the right-hand side of equation 2.21 that is responsible for pump depletion.

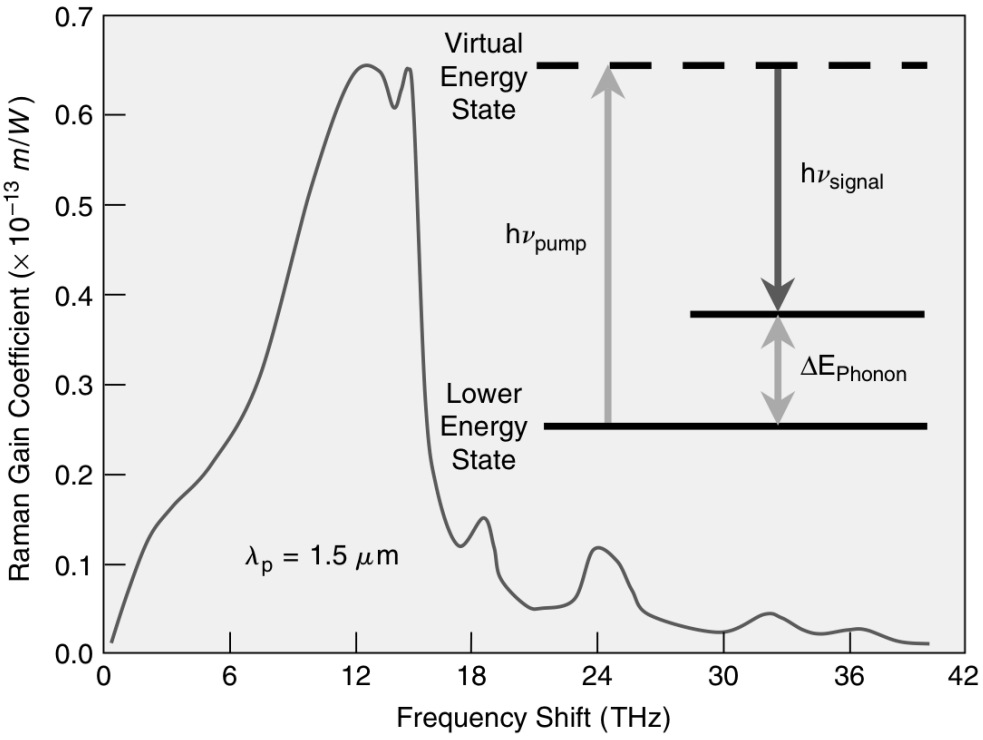

Figure 2.6 Raman gain spectrum with Raman pump at 1500 nm in fused silica. Inset shows an energy level diagram representative of the Raman process. [22-24]

In the case of the signal power, the equation can be simplified by following equation.

$$P_s(z) = P_s(0)e^{((g_R/A_{eff})P_p z_{eff} - \alpha S z} \tag{2.22}$$

where $z_{eff} = (1 - e^{\alpha p z})/\alpha_p$ is the efective fiber length, $\frac{g_R}{A_{eff}}$ is the Raman gain efficiency, with g_R the Raman gain coefficient, A_{eff} is the effective core area of the pump, $P_P(z)$ is the power of the pump and $P_S(0)$ is the power of the signal.

From equation 2.22 to increase the Raman gain efficiency the higher Raman gain

efficiency $g_R$and a smaller effective core area A_{eff} are need. The SMF fiber has A_{eff} of about $72\mu m^2$. The A_{eff} of different types of fiber is shown in Table 2.1. From the table the smallest A_{eff} is Dispersion Compensating Fiber (DCF) with A_{eff} is about 20 μm^2 and this is the reason we used the DCF for our experiment.

Table 2.1 The effective area of different fiber types

Fiber Type	Effective Area μm^2 at 1550 nm
Single Mode Fiber	72-80
Non Zero Dispersion Shifted Fiber	55-72
Dispersion Shifted Fiber	45-50
Dispersion Compensating Fiber	20-35

2.5.2. Noise Figure of a Raman Amplifier

There are several sources of noise in Raman amplifier such as Double Rayleigh Scattering (DRS), noise arising from the short upper-state lifetime from Raman amplification, ASE and phonon-stimulated optical noise. However, the primary source of noise in the Raman Amplifier is still the ASE, which can be defined by Equation 2.23 below:

$$NF = \frac{1}{G}\left(\frac{2S_{ASE}(v)}{hv+1}\right) \tag{2.23}$$

where

$$S_{ase}(v) = (G-1)hv\left(\frac{N_2}{N_2-N_1}\right) \tag{2.24}$$

N_2 is the upper state population and N_1 is the lower state population. For Raman amplifiers the $(\frac{N_2}{N_2-N_1})$ term is always equal to one, whereas in EDFAs it is usually greater than one [25]. For the case of EDFA, this term is only equal to one for an amplifier fully inverted through the entire length of the gain fiber. Furthermore, the small fraction of passive loss of gain fiber also needs to be added to the noise figure due to Raman amplifier which uses a longer fiber length.

2.6 S-band Semiconductor Optical Amplifier

The Semiconductor Optical Amplifier (SOA) is compact optoelectronic device designed to amplify light signals. Unlike the EDFA, the SOA is driven electronically, requiring and external current injection to provide the gain of the signal. The main advantage of the SOA is its compact size; it's gain characteristics are comparable to that of an EDFA, but in a compact package almost half the size.

In the SOA, the optical input signal carrying original data enters into the semiconductor active region through coupling. The coupling is required because the mode field diameter of a single mode beam is 9.3 μm while the size of active region is less than the order of tenth of micrometers [26]. The coupling carries the noise at the output of SOA. This additive noise is produced by the amplification process itself and so cannot be entirely avoided. The amplifier facets are reflective causing ripples in the gain spectrum [27].

There are two types of SOAs Fabry-Perot SOA (FP-SOA) and Traveling Wave SOA (TW-SOA). The basic principle of the FP-SOA is the same as with the Fabry Perot laser with multiple reflections of light passing trough the active region via the reflected cleaved faced and a portion of the light power leaves the cavity. Unlike FP-SOA, the TW-SOA is an amplifier without reflective facet and the signal is amplified in a single

pass. The difference between these this two types of SOAs is the ASE spectrum, where the FP-SOA produces an ASE spectrum produces multiple peaks due to the reflection from the ends of faces whilst the TW-SOA has a smooth ASE spectrum. The different spectra generated are shown in Figure 2.7.

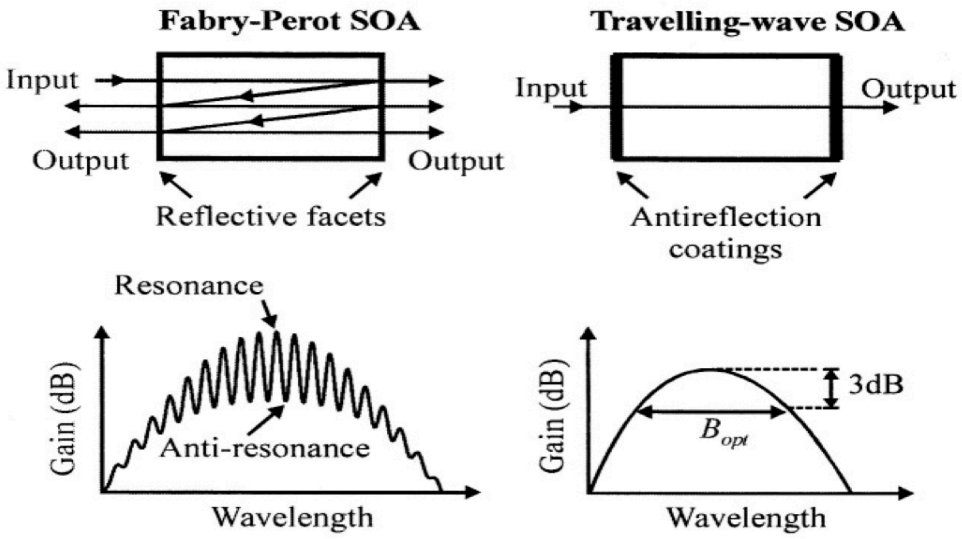

Figure 2.7 The different of the FP-SOA and TW-SOA [27]

2.6.1 Principle of SOA

In this thesis, the TW-SOA is used for all the experiments. The TW-SOA carries electrons. These electrons need an external injection current in the active region to energize carriers and occupy energy states in the conduction band (CB) of the active region material, leaving holes in the valence band (VB). Three radiative mechanisms are possible in the semiconductor [27]. These are shown in Figure 2.8 for a material with an energy band structure consisting of two discrete energy levels.

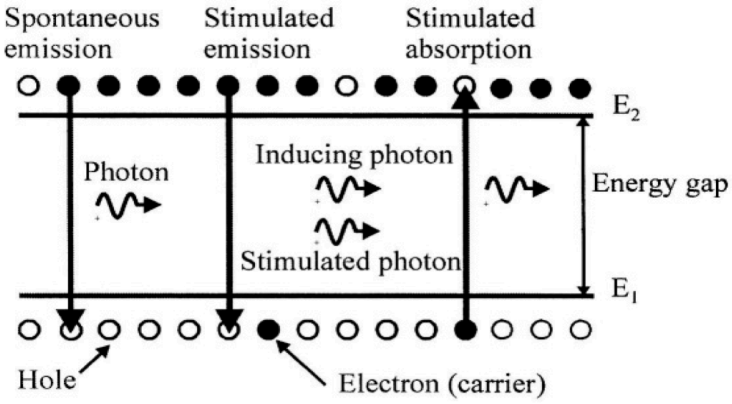

Figure 2.8 Energy level of SOA[27]

In an SOA, amplification is achieved through the emission of photons as a result of the recombination of electron-hole pairs. Electron-hole pair recombination takes place when excited electrons residing in the higher energy Conduction Band (CB) decay and in the process recombine with the holes that reside in the lower energy Valance Band (VB) [27-29]. This process is accompanied by the release of energy in the form of a photon, and it is this energy release that is utilized to impart gain in a passing optical signal.

In this two-level system, high-energy electrons (or more commonly carriers) injected from an external current source into the SOA active region will move to occupy the CB, resulting in the creation of holes in the VB, creating electron-holes pairs. The transitions of the electrons between the CB and VB can be defined by three processes; stimulated absorption, stimulated emission and spontaneous emission.

Stimulated absorption occurs when an incident photon with sufficient energy stimulates a carrier in the VB to move to the CB. In the process, the photon is eliminated, making the process a loss process. However, a photon of suitable energy can stimulate the recombination of a CB carrier with a VB hole while the photon itself continues to travel through the active region (the use of the term ‘suitable energy’ is used in the case of

stimulated emission to differentiate from a photon with 'sufficient energy' as in the case of stimulated absorption [27-29]). The process of stimulated emission is of the most importance to the SOA, as this will give rise to optical gain. During the process of recombination, the CB carrier loses its energy in the form of a coherent photon that has an identical phase, frequency and direction of that of the incident photon. Both the original photon and the stimulated photon will continue to travel trough the gain medium to promote more stimulated transitions. If there is enough current to create a population inversion, where the carrier population in the CB significantly exceeds that of the VB, the probability of stimulated emission is much greater than that of stimulated absorption and thus the SOA will exhibit optical gain. In addition to stimulated absorption and stimulated recombination processes, spontaneous emission also occurs in the gain medium of the SOA due to the non-zero probability per unit time that a CB carrier will spontaneously recombine with a VB hole, resulting in a photon that has a random phase, frequency and direction. This is a detrimental process that not only contributes noise to the amplified signal, but also reduces the population inversion that is available for optical gain. However, due to the nature of semiconductors spontaneous emissions will occur during the amplification process and cannot be avoided. These emissions are independent of the intensity of the inducing signal, unlike stimulated processes that are dependent on the intensity. The transitions of the electrons between the CB and the VB are the fundamental factors that contribute to the SOA operation. These factors arise specifically from the material used to form the SOA gain medium

2.6.2 Small Signal Gain

The most important operation of the SOA is its ability to amplify incoming light signals. This ability of the SOA is known as the gain of the SOA and can be typically

given as either its intrinsic gain or its fiber-to-fiber gain [27]. The intrinsic gain, G is simply the ratio of the power of the signal at the input facet to the power of the signal at the output facet. The fiber-to-fiber gain on the other hand includes the input and output coupling losses of the SOA. The fiber-to-fiber gain can be calculated as the ratio of the output signal P_{out}, to the input signal P_{in} so that:

$$G(v) = \frac{P_{out}}{P_{in}} \tag{2.25}$$

The amplification energy imparted to the propagating signal by the SOA originates from the bias current. As well as the gain coefficient and injection current, the SOA gain is also dependent on the wavelength of the passing signal. The small signal gain of an SOA at an optical frequency of f can be written as [30]:

$$G\ (f) = \frac{(1-R_1)\ (1-R_2)G_S}{(1-\sqrt{R_1R_2}G_S)^2+4\sqrt{R_1R_2}G_S sin^2[\frac{(f-f_0)L}{v}]} \tag{2.26}$$

where G_s is the single-pass amplifier gain, $R_1$and R_2 are the reflectivity of the input and output facets, f_0 is the centre frequency and v is the velocity of the light when travelling in the SOA gain medium (v can be obtained from the ratio of the speed of light in air, c ,to the refractive index of the material, n, so that $v = \frac{c}{n}$) [26]. Because the SOA gain medium and facets form a reflective cavity, giving rise to resonant and non-resonant frequencies which in turn will affect the gain of the SOA. Resonant frequencies occur when the sin^2 factor is 0, giving maximum gain, while anti-resonant frequencies occur when the sin^2 factor is 1, giving minimum gain. The single pass gain, G_s,can be measured in terms of the material gain coefficient, confinement factor Γ, absorption coefficient α and active region length L as [27-29]:

$$G_s = \exp[\Gamma g_m - \alpha)\, L \tag{2.27}$$

Equation 2.27 can be simplified by taking the reflectivities to be the same (as in the case of most SOA designs) so that $R_1 = R_2 = R$ .These yields:

$$G\,(f) = \frac{(1-R_2)^2 G_s}{(1-RG_s)^2 + 4RG_s sin^2[\frac{(f-f_0)L}{v}]} \tag{2.28}$$

Equation 2.28 is the general formula for calculating the small signal gain in an SOA and is applicable to the FP-SOA where the reflectivities are of concern. In a TW-SOA, the reflectivities have no discernible effect on the gain of the SOA and therefore, $R_1 = R_2 = R = 0$ and equation 2.28 can be reduced to $G(\omega) = G_s$

Another factor that can affect the SOA gain is the input signal power. This is because as the signal power increases, the gain of the SOA decreases due to gain saturation [26]. The relation between the input signal power dependent gain, $G(p)$ and the input signal power can be given as:

$$G(p) = G_0 \exp[\frac{(G-1)P_{out}}{GP_{sat}}] \tag{2.29}$$

G is given as in equation 2.25 and P_{sat} is obtained from the saturation power of the SOA.

Using these equations, we are thus able to predict the small signal gain for the SOA under varying drive currents, input wavelengths and input powers. However, these equations are only true for certain conditions [27]. Typically, SOAs can exhibit an unsaturated gain of between 8 dB to as high as 29 dB [31], but as the drive current and input signal power increase, these equations become invalid. In the case of the bias current, the gain increases as the bias current is increased only until before the

saturation current point, after which there is no longer any additional gain even though the drive current is increased [26, 31]. In the same manner, significant gain is imparted to low-power input signals, but the gain decreases as the input signal power increases until the point of the saturation power [26, 32 and 33]. Furthermore, the wavelength of the signal that the SOA can amplify is also limited to the SOA bandwidth [26, 27 and 33].

2.6.3 Saturation Current, Saturation Power and Bandwidth

The maximum gain an SOA can impart is limited by the maximum bias current that can be injected into the SOA active medium, and the input signal that can be amplified by the SOA is dependent on its power and wavelength. Above the saturation current, there is no longer any increase in the gain of the SOA even if the SOA current is increased. This occurs due to the semiconductor nature of the SOA; as the injection current is increased, more and more carriers are displaced from the VB to the CB [28,29]. However, as there are only a finite number of energy states in the CB for the carriers to occupy, thus only a certain amount of carriers can exist in the CB with the maximum number of carriers in turn determining the maximum gain that the SOA can impart. Above the saturation current, excess carriers can no longer flow through the semiconductor active medium, and are instead converted to heat which must be vented, less the SOA overheat and fail. The gain saturation parameter of an SOA determines the maximum amount of gain that an SOA can impart based on the power of the input signal. Although equations 2.26 and 2.27 indicate that a signal of any power will always be amplified, in reality the gain of the SOA is limited by the input signal saturation power. This is because the material gain coefficient is dependent on the signal frequency and power [27], such that:

$$g\,(f,P) = \frac{g\,(f)}{1+\frac{P}{P_{sat}}} \tag{2.30}$$

From equation 2.30 the material gain coefficient can be seen to be dependent on the input signal power. As the input power increases, the material gain coefficient begins to decrease until half the maximum material gain coefficient is obtained when the signal is fully saturated. The reason for this is the high number of photons in the input signal fully depleting the carriers in the CB through recombination with VB holes, leaving no more electrons to recombine even if the number of external photons increased [32]. From the material gain coefficient, the gain can be computed to be:

$$G_s = 1 + \left(\frac{P_{sat}}{P_{in}}\right) \ln \frac{G_s^{max}}{G_s} \tag{2.31}$$

where G_s^{max} is G_s at ω_0 and P_{sat} is the saturation power. Similar to EDFA, the saturation power of SOA is defined as the signal power at which the gain of the SOA is half (3 dB) the small-signal gain.

The usable wavelength range of the SOA is given by the bandwidth of the SOA. By definition, the bandwidth of the SOA is the frequency range at which the gain is half the maximum value, coinciding with the SOA saturation power. The bandwidth of the SOA can be obtained from equation 2.28 where reducing the gain by a factor of 2 [27] yields:

$$BW = \Delta f = (f - f_o) = \left(\frac{v}{L}\right) sin^{-1} \frac{(1-RG_S)}{[2\sqrt{RG_S}} \tag{2.32}$$

where v is the speed of the signal in the SOA cavity as given by $v = \frac{c}{n}$. Hence, the saturation current, saturation power and bandwidth can be combined to set the

operational limits of the SOA to provide a more realistic theoretical model.

2.6.4 Noise Figure and Amplified Spontaneous Emission (ASE)

As well as the gain and saturation limits, another important parameter in determining the performance of the SOA is its NF. As with the case of optical amplifiers, the NF of an SOA gives how much noise the SOA adds to a signal and therefore how badly a passing signal deteriorates. Therefore, an SOA with a high as possible gain and a low as possible noise figure is always sought after. The NF of SOA is defined as the input to output signal to noise ratio of an optical amplifier. This parameter is useful in quantifying the performance of an optical amplifier, and is generally given by [27]:

$$NF = \frac{\left(\frac{S}{N}\right)_i}{\left(\frac{S}{N}\right)_o} \tag{2.33}$$

where $\left(\frac{S}{N}\right)_i$ is the input signal-to-noise ratio and is$\left(\frac{S}{N}\right)_o$ is the output signal-to-noise ratio. In the case of the SOA, the NF can be expressed more specifically in terms of the SOA gain and ASE power as [34,35]:

$$NF = \frac{1}{G} + \frac{P_{ASE}}{Ghf\Delta f} \tag{2.34}$$

where h is Planck's constant and f is the signal frequency and Δf is the bandwidth. An important point to note from equation 2.34 is that the SOA NF is inversely proportional to the SOA gain, thus as the gain increases the NF will decrease. The ASE power, $P_{ASE}$is a result of carriers that spontaneously decay from the upper energy level to the lower energy level of the SOA, in the process releasing photons that have random

phases and directions. Although these photons fall within the same frequency range as the signal, their random phase and direction does not contribute to amplifying the passing signal, instead generating noise. The average peak ASE power can be obtained by the formula [27]:

$$P_{ASE} = 2n_{sp}hfG\Delta f \tag{2.35}$$

The factor 2 in equation 2.35 is due to the fact that the ASE will propagate equally in both the forward and backward directions, and thus the ASE power measured at either end of the SOA is only half of the total ASE power generated [36]. The spontaneous emission factor, n_{sp} of the SOA is a result of the ratio of carriers still in the upper level to the carriers that have already decayed spontaneously and is given by [27]:

$$n_{sp} = \frac{N_2}{N_2 - N_1} \tag{2.36}$$

In typical optical amplifier operations, the ASE is usually a detrimental effect. Forward or co-propagating ASE will generate noise in the receiver that will deteriorate the system performance [27], while backward or counter-propagating ASE will deplete the population inversion available for signal amplification, affecting the SOA's gain performance.

2.6.5 Polarization Sensitivity

In general, the gain of an SOA depends on the polarization state of the input signal. This dependency is due to a number of factors including the waveguide structure, the

polarization dependent nature of anti-reflection coatings and the gain material. Cascaded SOAs accentuate this polarization dependence. The amplifier waveguide is characterized by two mutually orthogonal polarization modes termed the Transverse Electric (TE) and Transverse Magnetic (TM) modes. The input signal polarization state usually lies somewhere between these two extremes. The gain $G_{TE/TM}$ polarization sensitivity of an SOA is defined as the magnitude of the difference between the TE mode gain G_{TE} and TM mode gain G_{TM}.

$$G_{TE/TM} = |G_{TE} - G_{TM}| \text{ (dB)} \tag{2.37}$$

2.7 Applications of S-band Optical Amplifiers

2.7.1 S-band Fiber laser

An optical amplifier is a key component of many applications. One of them is fiber laser. Fiber laser is an important part in optical network systems such as WDM and DWDM. The advantages of the fiber laser are they have narrow linewidth, high power, compactness, low threshold and wide tunability. Fiber laser can be formed into two types namely linear cavity of ring cavity and Fabry Perot cavity or linear cavity fiber laser. This is illustrated in Figure 2.9. Both of these cavities use optical amplifier as the laser gain medium. For the ring cavity fiber laser as shown in Figure 2.9 (a), the input and output gain medium are connected to become a ring cavity. The optical fused coupler is normally used to tap out the output power of the laser. In the linear cavity fiber laser, the optical amplifier is placed between two mirrors to covert fiber amplifier to the laser. In fiber laser system the mirror is typically replaced by Fiber Bragg Grating (FBG) as shown in Figure 2.9(b). There are two types of FBG in linear cavity fiber laser, namely the front FBG that usually has higher reflectivity and the back FBG that

normally has a lower reflectivity. The back FBG is normally used as the output for the laser power as shown in Figure 2.9 (b)

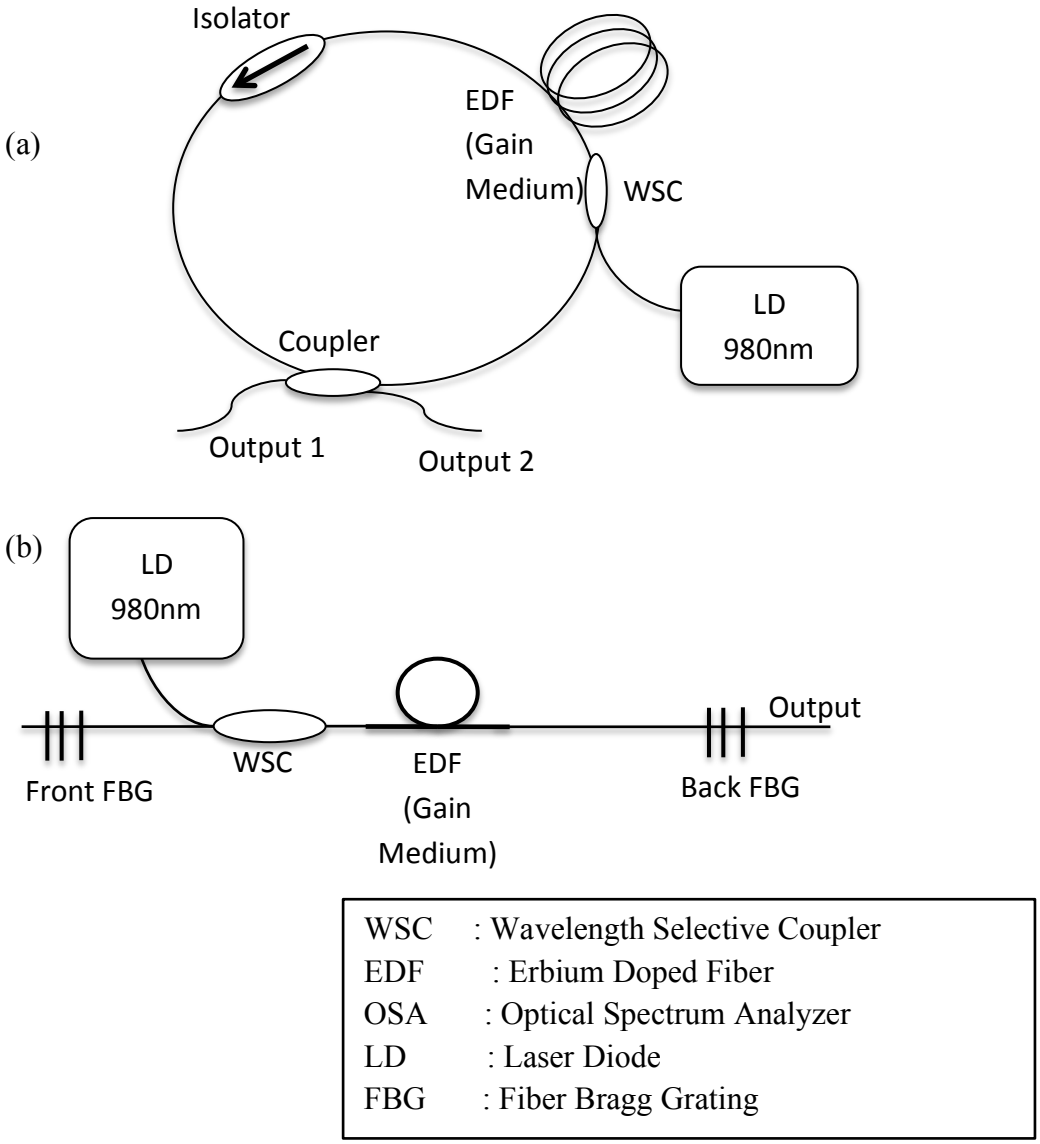

Figure 2.9: Types of cavities of the fiber laser (a) Ring Cavity (b) Linear Cavity

2.7.1.1 Wavelength Tunable Operation of Fiber Laser

One of the advantages of the fiber laser is its ability to select or tune a single channel from a multi-wavelength comb or the wide ASE [37] and its generally stable output with narrow linewidth emission line which is compatible with existing optical network

systems. Besides its application in the telecommunication, the tunable fiber laser can be a source for spectroscopy and for use in the fiber sensor. This flexibility spurs intense research in developing a stable switchable wavelength that can have a wide tuning range. There are various methods of realizing switchable outputs such as that based on polarization dependent device in the cavity [38], the use of high birefringence fiber loop mirror (HiBi-FLM), cascaded FBG cavities and cavities with birefringence FBG or cascaded Birefringence FBGs [39–42]. The development of the tunable fiber laser using Sagnac loop mirrors (SLM) [43] and compression strain FBG for tunable wavelength has also been demonstrated [44,45].

2.7.1.2 Output Power of Fiber Laser

Fiber laser has many advantages compared to the bulk glass laser in terms of heat distribution management. The efficiency heat management distribution will allow a laser to operate in logger life span and also will produce high efficiency of output power. The efficiency of output power of fiber laser can be defined as the ratio of the pump power to the output power of the laser.

2.7.1.3 Side Mode Suppression Ratio

The Side Mode Suppression Ratio (SMSR) is one of the fiber laser characteristics is studied in this thesis. The SMSR can be defined as the ratio of the signal peak power to the next highest mode. The highest SMSR of fiber laser is important in determining the quality of fiber laser system. In this thesis the Optical Spectrum Analyzer (OSA) is used to measure the SMSR by fixing the mask range to ±1 nm.

2.7.2 S-band Multiwavelength Brillouin/ Fiber Laser

2.7.2.1 Non-Linear Effects in Single Mode Fibre

One of the problems in fiber optics communication system is the effect of non-linear phenomenon within the optical fiber. This affects the power level of the transmission and occurs when intense laser light propagates through the fiber.The non-linear effect arises due to the an harmonic motion of bounded electron under the influence of the applied electromagnetic field. Subsequently, the polarization *P* from the electric dipoles is not linear with the electric field *E* which is given by:

$$P = \varepsilon_o[x^{(1)}.E^{(2)}:EE+x^{(3)}:EEE+L] \tag{2.38}$$

where ε_o is the vacuum permittivity and $x^{(1)}$ (j+1,2,3,…) is the j^{th} order susceptibility. The linear susceptibility of $x^{(1)}$ is the dominant contribution to P, while the 2nd order susceptibility $x^{(2)}$ represents the second harmonic and sum-frequency generation. The final nonlinear order in the equation, $x^{(3)}$, is responsible for third harmonic generation, four-wave mixing and nonlinear refractions. The non-linearities in silica-based fiber can be categorized into two groups, namely non-linear refraction [46] and stimulated scattering [47]. Non-linear refraction refers to the intensity dependence of the refractive index that results in a number of interesting non-linear effects, such as self-phase modulation (SPM) and cross-phase modulation (XPM). SPM refers to the self-induced phase shift and spectral broadening experienced by the optical field as the light propagates through the fiber, while XPM is the nonlinear phase shift of the optical field induced by a co-propagating field of a different wavelength. Another interesting nonlinear phenomenon is four wave mixing (FWM) which occurs when three

electromagnetic waves co-propagating through a fiber generate a fourth electromagnetic wave.

The second category of nonlinear effects is stimulated scattering effects in which there is a transfer of energy from the optical field to the SMF. The two scattering effects which are of important are stimulated Raman scattering (SRS) and stimulated Brillouin scattering (SBS) which are a result of the vibrational excitation modes of silica. The primary difference between SRS and SBS is that in SRS the phonons are optical in nature, while in SBS the phonons are acoustic in nature. Another critical characteristic that differentiates SRS and SBS is that SRS occurs in the forward directions, while SBS occurs only in the backward directions. In this thesis, the SBS becomes a focus of interest as although it is detrimental in optical communications systems, SBS has been found to be a valuable tool in applications such as in Brillouin lasers, amplifiers and BEFLs. The principles of SBS are discussed in the following section.

2.7.2.2 Principles of Stimulated Brillouin Scattering

SBS in a single mode fiber arises from the interaction between pump wave, backscattered Brillouin wave and an acoustic wave. When a narrow linewidth and high-powered signal propagates through the optical fiber, it will begin to generate acoustic waves that travel in the same direction as the pump wave. The acoustic wave has a wavelength approximately half of the optical wavelength and travels at the speed of sound in the fiber. Simply put, the SBS effect can be described as a moving Bragg grating which reflects pump light in the backward direction, with the reflected light being Doppler-shifted to a slightly lower optical frequency. This is shown in Figure 2.10:

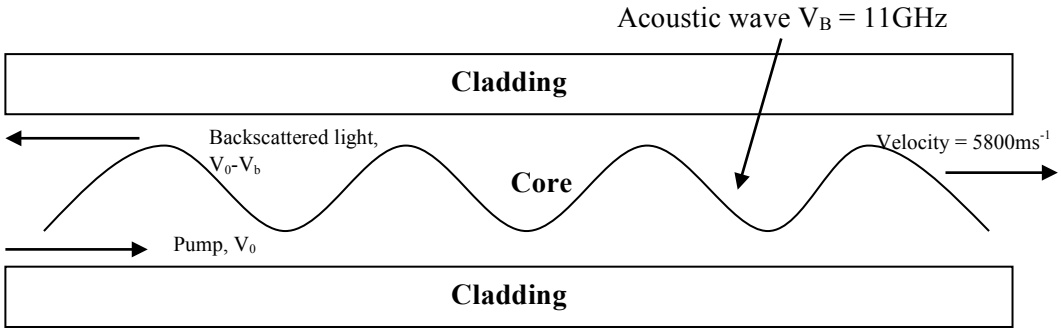

Figure 2.10: Stimulated Brillouin Scattering Effect

For a wavelength of 1550 nm travelling in a silica based fiber, the acoustic wave velocity gives a Brillouin frequency shift of approximately 11 GHz. SBS has certain interesting traits, such as low threshold and large Brillouin gain.

2.7.2.3 Brillouin Frequency Shift

The SBS process can be understood by viewing it as the Bragg reflection of light as it propagates through a crystal and experiences a frequency shift due to the Doppler effect.

The Brillouin frequency shift can be described by the following process; the pump wave will generate an acoustic wave due to electrostriction, which in turn causes the periodic modulation of the reflective index. The acoustic wave will travel at a velocity of V_a corresponding to a wavelength λ_a with a refractive index grating period. The pump wavelength λ_p (with the wave number k_p) will experience a Bragg reflection by the grating and be strongly diffracted in a specific direction θ with the wavelength λ_s. The frequency of the scattered wave and acoustic wave (represented by w_a and w_s with the wave numbers k_a and k_s) are related by:

$$w_s = w_p - w_a \tag{2.39}$$

$$k_s = k_p - k_a \tag{2.40}$$

The frequency w_s and wave number k_a of the acoustic wave satisfy the dispersion relation in the Doppler effect as the Brillouin frequency shift is given by:

$$w_p - w_s = w_a = k_a V_a = 2V_a k_p sin(\theta/2) \tag{2.41}$$

As described by equation above, the Brillouin frequency shift depends on a scattering angle which has a maximum value when $\theta = \pi$ which indicates backward scattering and a minimum value when $\theta = 0$, which indicates forward scattering due to the *sin (θ /2)* parameter in the equation. When then medium used is a SMF, only backward scattering is produced, therefore $\theta = \pi$ and $k_p = 2\pi n/\lambda_p$ in equation 2.41. This gives a Brillouin frequency shift v_B of:

$$v_B = \frac{w_a}{2\pi} = \frac{2nV_a}{\lambda_p} \tag{2.42}$$

whereby *n* is the refractive index of the medium. Using $c = v\lambda$, the Brillouin frequency shift can be given as a Brillouin wavelength shift by:

$$\Delta\lambda_B = \frac{(\lambda_p)^2}{c}\Delta v_B \tag{2.43}$$

where c is the speed of light in vacuum. In a silica-based fiber, the main component is SiO_2, and therefore V_a = 5.96 km/s, n=1.45, and λ_p=1550 nm, then from equation 2.42

$$\Delta v_B = 11.2 \text{ GHz} \tag{2.44}$$

Substituting into 2.43 and 2.44 gives

$$\Delta\lambda_B = 0.09 \text{ nm} \tag{2.45}$$

which is the Brillouin wavelength shift of:

$$\Delta\lambda_B \approx 0.09\, nm \tag{2.46}$$

2.7.2.4 Brillouin Gain Coefficient

The Brillouin Gain coefficient determines the growth of the Brillouin Stokes wave which has a peak value at $v = v_B$. The spectra of Δv_B of the Brillouin gain is small (approximately 10 MHz ~ 5 THz) and is related to the damping time of the acoustic waves or the phonon lifetime T_B. The acoustic waves are assumed to decay as *exp(-t/T_B)* with a Lorentzian spectra profile given as

$$g_B(') = \frac{(\Delta v_B/2)^2}{(v - v_B)^2 + (\Delta v_B/2)^2}\, g_B\,(v_B) \tag{2.47}$$

where Δv_B is the full width at half maximum and is related to the phonon lifetime by $\Delta v_B = (\pi T_B)^{-1}$ .The peak value of the Brillouin gain coefficient is given as:

$$g_B(v_B) = \frac{2\pi n^7 {p_{12}}^2}{c{\lambda_p}^2 \rho_0 v_a \Delta v_B} \quad (2.48)$$

where p_{12} is the longitudinal elasto-optic coefficient, ρ_0 is the material density and λ is the pump wavelength. From equation 2.42, v_B varies inversely with λp, and as such Δv_B is also expected to vary inversely with $\lambda p2$. The narrowing of the Brillouin gain –profile with an increase in λp cancels the decrease in the gain as shown in 2.48, and as such the gain coefficient is nearly independent of the pump wavelength.

For a continuous wave (CW), the Brillouin gain is considerably reduced if the spectral width exceeds. This happens when a multimode pump and a single mode pump whose phase varies rapidly on the time scale is shorter than the photon lifetime. When pump coherence length, $L_{coh} << L_{int}$, where L_{int} is the pump interaction length defined as the distance over which the Stokes amplitude varies appreciably, then the Brillouin gain is significantly reduced.

2.7.2.5 Brillouin Threshold

The Brillouin Stokes light is continuously amplified by the interaction of fiber with the pump wave propagation and grows exponentially in the backward direction as:

$$I_s(0) = I_s(L) exp\left(g_B \frac{P_0 L_{eff}}{A_{eff}} - \alpha L\right) \quad (2.49)$$

where $I_s(0)$ is the incident pump intensity at fiber position z=0, P_0 is the input power and A is the effective core area. The effective interaction is given as equation 2.38 shows how a Brillouin Stokes signal at z=*L* will grow in the backward direction.

The Brillouin threshold is defined as the critical pump power at which the Brillouin Stokes power is equivalent to the input light power at z=0 as is given by:

$$P_{th} \cong \frac{21A_{eff}}{g_B L_{eff}} \tag{2.50}$$

This happens when the Brillouin Stokes increases rapidly as the pump power increases and when the pump power exceeds the critical value it is converted into Stokes light, which in turn sets the limit for the maximum pump power. In equation 2.50 the numerical factor of 21 is only given as an approximate as the value must in fact be determined by the exact value of the Brillouin-gain linewidth and whether the pump Stokes waves maintains their polarization along the fiber. Typically the values for the parameters of A_{eff}, L_{eff} and g_B are 50 μm^2, 20 km and 5x10-11 m/W for a fiber used in standard 1550 nm optical communication systems and will give the value of P_{th} = 1mW. Thus the low Brillouin threshold makes SBS a dominant nonlinear process in the optical fiber.

2.7.2.6 Hybrid Brillouin/Erbium Doped Fiber Laser

The Brillouin Erbium Fibre Laser (BEFL) operates on the combined actions of two gain media, namely from the non-linear effects of the SMF and the gain from the EDF. When the SMF is pumped with a narrow-linewidth laser source, also known as a Brillouin Pump (BP). this generates a Stokes-shifted wave in the reverse direction

which is then amplified by the EDF. The potential for this type of laser is that the wavelength of the resulting laser can be determined very accurately due to the known frequency shift from the pump signal. By pumping the EDF with a 980 nm laser diode (in most cases) gain can be produced to overcome the resonator loss. When the BP wavelength is set close to the maximum gain produced by the EDF, lasing will occur at the Stokes-shifted wavelength. The broad-band gain with the maximum peak wavelength of x is generated by the EDF, while narrow-band gain is generated from the SBS process in the SMS at a wavelength of y. If the total gain of wavelength y is greater than that of wavelength x and is equal to the threshold gain of g_{th}, then lasing actions will commence due to the combination of the two gain media. However, if the peak is not near the wavelength x, but instead at a different wavelength z as shown in Figure 2.11, then the lasing will occur at wavelength x nonetheless, but will only be generated by the gain of the EDF.

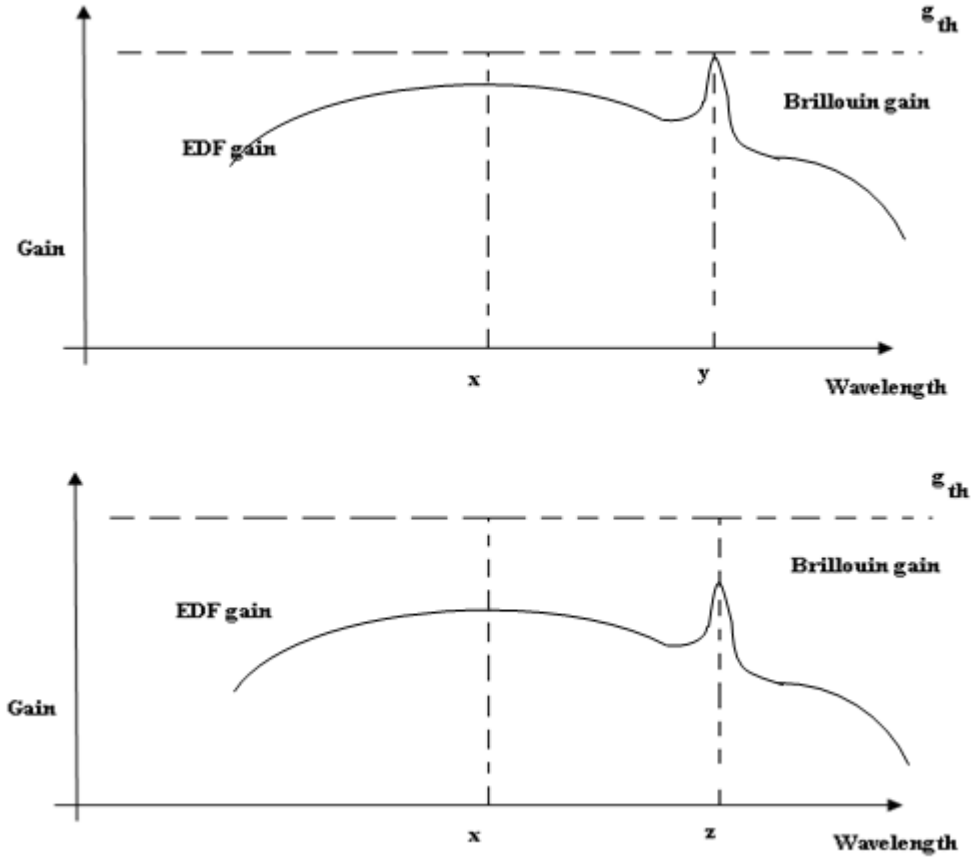

Figure 2.11 Schematics of BEFL Operation

The conversion efficiency of the laser can be determined by the amount of pump power that is converted to output. As the BEFL comprises of two gain media, each gain media will contribute to the pump power and the overall conversion efficiency can be written as [48]:

$$\eta\,(I_E\,I_B) = \frac{I_{out}}{(I_E + I_B)} \tag{2.51}$$

where I_{out}, I_E , and I_B are the laser output, EDF pump and BP intensities respectively. The output intensity depends on the pumping level of the EDF and SMF and can be written as follows:

$$I_{out} = \eta_E I_E + \eta_B I_B + \eta_{EB} I_E I_B + I_{sat} \ln(1 - R) \quad (2.52)$$

I_{sat} is the saturation intensity, R is the coupler ratio, $\eta_{E,}\eta_B$ are erbium and Brillouin efficiencies and η_{EB} the cross efficiency of Brillouin/Erbium.

2.8 Summary

This chapter discusses the theory of S-band optical amplifier and its applications, covering the fundamental operating principals and also its operation.

The EDF has three main advantages over the conventional approach of electronic regeneration. It is transparent to signal bit rates and modulation techniques and is able to amplify multiple signals simultaneously on WDM transmissions while also having high temperature stability. In order to understand the amplification process, the atomic rate equation of EDF is presented at the beginning of this chapter. The generation of the ASE in EDFAs is also discussed in this chapter. The chapter then discusses the current limitation of EDFAs in generating amplification in the S-band region, including the incomplete inversion of the active erbium ions in the EDFA for S-band amplification (which does not provide sufficient amplification for S-band signals) and also the occurrence of ASE or lasing from the high peak at wavelengths near 1530 nm, which again suppresses the amplification of S-band signals.

The following section of this chapter described the DC-EDF, a specialty fiber designed to overcome the limitations of current EDFAs in amplifying S-band signals. The reflective index profile of the DC-EDF is described in detail, as it is a key factor in understanding the sensitivity of the DC-EDF to bending. The sensitivity of the DC-EDF itself is used to tune the cut-off wavelength of the DC-EDF, which allows for the

suppression of the 1530 nm peak in the generated ASE. This aspect of the DC-EDF is discussed theoretically, followed by a theoretical discussion on the optical amplifier's gain, small signal gain, gain saturation, gain bandwidth and NF.

In addition to the EDFA and DC-EDFA, Raman amplification is another viable option for the amplification of signals in the S-band region. This chapter describes the fundamental principles of the RA, as well as sources of noise that arise from the RA. The theoretical aspect of Raman amplification is discussed, with a specific focus on the fiber effective core area, A_{eff}. It can be discerned that the smaller the A_{eff}, the higher the gain that can be obtained. A comparison of A_{eff} of the different fiber types is examined in this chapter. This chapter also examines the SOA as an amplification mechanism for S-band signals. The SOA differs from rare-earth doped fibers in that it is pumped electronically (as opposed to rare-earth doped fibers, which are pumped with incident light). As such, the characteristics of the SOA differ from rare-earth doped fibers, with different small signal gains, saturation currents, saturation powers and gain bandwidths.

The final section of this chapter details the possible applications of the S-band optical amplifier. In this work, the focus is on only two applications; S-band fiber lasers and S-band Brillouin fiber lasers. The S-band fiber laser is analyzed by the two common designs employed, namely the ring and linear cavity configurations. This chapter analyses the main characteristics of the S-band fiber laser such as tunable wavelength operation, output power and SMSR. The development of S-band Brillouin fiber lasers is also discussed in this chapter, covering the fundamental operating principals as well as key characteristics such as the Brillouin Gain Coefficient and the Brillouin threshold. The final section of this chapter discusses the principle of the Hybrid Brillouin and EDFfiber laser, which will be the focus of the later parts of this work.

Reference

[1] Gerd Keiser, Optical Fiber Communication, 3rd edition McGraw-Hill International Edition, pp 91-133,chapter 3, 2000.

[2] Emmanuel Desurvire. "Erbium –Doped Fiber Amplifier", Wiley-Interscience Publication, pp 6, 1994.

[3] P.W France, "Optical fiber laser and Amplifier", Blankie, pp 177, 1991.

[4] Nor Kamilah Saat, "Investigation of S-Band Erbium Doped Fiber Amplifier" Master Thesis, Unversity of Malaya, 2006.

[5] S. W. Harun, K. Dimyati, K. K. Jayapalan, H. Ahmad "An overview on S-band erbium-doped fiber amplifiers", Laser Physics Letter, vol 4, issue 1 , pp 10-15, 2006.

[6] P. D Lazay and A. D Pearson, "Development in single mode fiber design , material and performance at Bell Laboratories" IEEE Journal of Quantum Electron, vol QE-18, pp 504-510,1982.

[7] S.R Nagel, "Review of the depressed cladding single-mode fiber design and performance for the SL undersea system application" Journal of Lightwave Technology, vol. 2, pp 792-801, 1984.

[8] M.A. Arbore and G. L. Keaton,"Fiber amplifiers with depressed cladding and their uses in Er-doped fiber amplifiers", US Patent Issued on 2005.

[9] M A. Arbore, "Communication system using S-band Er-doped fiber amplifiers with depressed cladding" US Patent Issued on 2005.

[10] B. J. Ainslie, K. J. Beales, C. R. Day, and J. D. Rush, Interplay off design parameters and fabrication conditions on the performance of monomode fibers made by MCVD," IEEE Journal of Quantum Electronic, vol. QE-17, pp. 854-857, June 1981.

[11] A. D. Pearson, P. D. Lazay and W. A. Reed, "Fabrication and properties of sine mode optical fiber exhibiting low dispersion low loss, and tight mode confinement simultaneously," Journal of Bell System Technology, vol. 61, no. 2, pp. 262-266, 1982.

[12] J. Irven, K. C. Byron, and G. J. Cannell, "Dispersion characteristics of practical single mode fibers," in Tech Dig., 7th Europe Conference on Optical. Communication (ECOC), Copenhagen, Denmark, Sept.8-11, 1981.

[13] L. G.Cohen, D. Marcuse and W. L. Mammel, "Radiating Leaky-Mode Losses in Single-Mode Light guides with Depressed-Index Claddings",IEEE Transactions on Microwave Theory and Techniques, vol. Mtt-30, no 10, 1982.

[14] M. Monerie, "Propagation in doubly clad single-mode fibers", IEEE Journal of Quantum Electronics, volume 18, issue 4, pp 535-542,1982.

[15] K. Petermann, "Microbending loss in monomode fibers," Electronics Letters, vol. 12, pp. 107-109, 1976.

[16] D. Derickson, Fiber optic test and measurement, Hewlett-Packard professional books, Prentice Hall PTR, Upper Saddle River, New Jersey, 1998

[17] X.Zhang and A. Mitchell, "A simple black box model for erbium-doped fiber amplifiers" IEEE Photonics Technology Letters, vol.12, no.1, pp.28-30, 2000.

[18] J.B. Rosolem, A.A Juriollo, "S Band EDFA Using Standard Erbium Doped Fiber, 1450 nm Pumping and Single Stage ASE Filtering," Optical Fiber communication/National Fiber Optic Engineers Conference, 2008. OFC/NFOEC 2008 Conference on, vol., no., pp.1-3, 2008.

[19] C. Kakkar and K. Thyagarajan, "Extending S-band of EDFA to 1450 nm," in Conference on Lasers and Electro-Optics/Quantum Electronics and Laser Science Conference and Photonic Applications Systems Technologies, OSA Technical Digest (CD), paper JTuA72, 2007.

[20] Sulaiman Wadi Harun, "Design of Enhanced L-band Erbium-Doped Fiber Amplifier", PhD Thesis, University of Malaya, 2004

[21] J.Bromage, H.J Thiele and L.E Nelson,"Raman amplification in the S-band," Optical Fiber Communication Conference and Exhibit, 2002. OFC 2002 , vol., no., pp. 383- 385, 2002.

[22] Mohammad N Islam, "Raman Amplifiers for Telecommunications 1", Springer Series in Optical Sciences, Vol. 90/1, 2004.

[23] R. H. Stolen and E. P. Ippen, "Raman gain in glass optical waveguides. Applied. Physics. Letter", vol22, issue 6, 1973.

[24] G. P. Agrawal, Nonlinear Fiber Optics, 2nd ed., New York: Academic, 1995.

[25] M.N. Islam, "Raman amplifiers for telecommunications", IEEE Journal of Selected Topics in Quantum Electronics, vol.8, no.3, pp 548-559, 2002.

[26] D.H. Mynbaev and L.L. Scheiner , "Fiber-optic communications technology," Pearson, Education, 4th Ed., pp. 546-547, 2004.

[27] M. J. Connelly, "Semiconductor Optical Amplifiers", Springer, Verlag, 2002.

[28] M. Quillec, "Materials for Optoelectronics", Springer, 1996.

[29] S. Ritchie, "Semiconductor Optoelectronic Materials", Optoelectronic Materials, IEEE Colloquium on, pp. 411-413, 1990.

[30] Y. Yamamoto, "Characteristics of AlGaAs Fabry-Perot Cavity Type Laser Amplifiers", Quantum Electron., vol. 16, no. 10, pp. 1047-1052, 1980.

[31] A. E. Kelly, I. F. Lealman, L. J. Rivers, S. D. Perrin and M. Silver, "Low Noise Figure (7.2dB) and High Gain (29dB) Semiconductor Optical Amplifier with a Single Layer AR Coating", Electronics. Letters, vol. 33, no. 6, pp 536-537, 1997.

[32] E. Conforti, C. M. Gallep, S. H. Ho, A. C. Bordonalli and S. M. Kang, "Carrier Reuse with Gain Compression and Feed-Forward Semiconductor Optical Amplifiers,"IEEE Transaction Microwave Theory and Technology., vol. 50, pp. 77–81, 2002.

[33] N. K. Dutta and Q. Wang, "Semiconductor Optical Amplifiers", World Scientific Publishing, Singapore, 2006.

[34] S. W. Harun, P. Poopalan and H. Ahmad, "Gain Enhancement in L-Band EDFA through a Double-Pass Technique", Photonics Technology Letter, vol. 14, no. 3, pp. 296-297, 2002

[35] Product Note 71452-1, EDFA Testing with Interpolation Technique", Agilent Technologies, U.S.A, 2000.

[36] D. Marcuse, "Principles of Optical Fibre Measurements", Academic Press, New York, 1981.

[37] S.Feng , O.Xu, S. Lu, T.Ning and S Jian, "Switchable multi-wavelength erbium-doped fiber ring laser based on cascaded polarization maintaining fiber Bragg gratings in a Sagnac loop interferometer", Optics Communications, vol 281, issue 24, pp 6006-6010 , 2008.

[38] Y.W. Lee and B. Lee, "Wavelength-switchable erbium-doped fiber ring laser using spectral polarization-dependent loss element" IEEE Photonics Technology Letters, vol.15, no.6, pp.795-797, 2003.

[39] S. Hu, L. Zhan, Y.J. Song, W. Li, S.Y. Luo, and Y.X. Xia, “Switchable multiwavelength erbium-doped fiber ring laser with a multisection high-birefringence fiber loop mirror”, IEEE Photonics Technology Letters, , vol.17, no.7, pp.1387-1389, 2005.

[40] Q. Mao and J.W.Y Lit, “Switchable multiwavelength erbium-doped fiber laser with cascaded fiber grating cavities”, IEEE Photonics Technology Letters, vol.14, no.5, pp.612-614, 2002.

[41] Z.C. Liu,Y Xiufeng, L.Chao, N.J. Hong, G Xin, P.R. Chaudhuri, D Xinyong, “Switchable multi-wavelength erbium-doped fiber lasers by using cascaded fiber Bragg gratings written in high birefringence fiber”, Optics Communications, vol 230, issues 4-6, pp 313-317, 2004.

[42] T.V.A Tran, K Lee, S.Bae Lee, and Y.G.Han, "Switchable multiwavelength erbium doped fiber laser based on a nonlinear optical loop mirror incorporating multiple fiber Bragg gratings," Optics Express, vol 16, pp1460-1465, 2008.

[43] G. Das and J.W.Y. Lit; “Wavelength switching of a fiber laser with a Sagnac loop reflector”, IEEE Photonics Technology Letters, vol.16, no.1, pp.60-62, 2004.

[44] C.S. Goh; M.R. Mokhtar; S.A. Butler; S.Y. Set; K. Kikuchi and M. Ibsen; “Wavelength tuning of fiber Bragg gratings over 90 nm using a simple tuning package”, IEEE Photonics Technology Letters, vol.15, no.4, pp.557-559, 2003.

[45] S.K Liaw, K.L Hung, Y.T. Lin, C.C. Chiang and C.S. Shin, “C-band continuously tunable lasers using tunable fiber Bragg gratings” Optics & Laser Technology, vol 39, issue 6, pp 1214-1217, 2007.

[46] C.C Lee and S. Chi, "Measurement of stimulated-Brillouin-scattering threshold for various types of fibers using Brillouin optical-time-domain reflectometer" IEEE Photonics Technology Letters,vol 12, issue 6, pp 672-674, 2000.

[47] Mohd Kamil Abdul Rahman "Multiwavelength Fiber Laser for DWDM System" PhD Thesis, University of Malaya, 2001.

[48] D.Y Stepanov and G.J Cowle "Properties Brilloiun/Erbium Fiber Laser" IEEE Quantum Electron, vol 3 no 4, pp 1049-1057, 1997.

Chapter 3
Characteristics of S-band Optical Amplifiers

3.1 Introduction

One of the key factors in enabling the deployment of long-range optical communications networks is the availability of amplification. In-line fiber amplifiers fulfill this role excellently, amplifying multiple signals simultaneously while being transparent to bit-rates, modulation techniques and other detrimental effects such as cross-talking. EDFs (or for that matter any in-line optical amplifier) also form the backbone of a variety of other fiber optic technologies, including fiber lasers and optical fiber sensors.

In optical communications systems, such as Dense Wavelength Division Multiplexing (DWDM) systems, the bandwidth limitations currently faced by the existing conventional-band (C-band) (1530 nm to 1560 nm) requires the exploration of other bandwidths that will be capable supporting the future demands for capacity. In this regard, researchers are now looking towards new bandwidths in the long-wavelength band region (L-band), stretching from 1560 nm to 1640 nm and also, of more interest in this work, the short-wavelength band region (S-band) of 1460 nm to 1520 nm. The L-band region is actively being explored and utilized, and while still a far way from reaching its limits, current usage trends indicate that it would be only a short-time before the L-band region can no longer sustain the demands for data capacity. As such, researchers are now looking towards the S-band region in order to sustain future demands for capacity.

In this chapter, the various types of S-band optical amplifiers are discussed and demonstrated. The performance of these amplifiers in terms of their gain and NF under various conditions is studied so as to provide a clear understanding of the behavior of the optical amplifier in telecommunications networks. An understanding of the S-band amplifier's operation is crucial, as this will become the basis of the work carried out in the subsequent chapters. This chapter begins with a detailed analysis of S-band amplification in a conventional silica-based EDF. The gain and NF characteristics will be analyzed, and the optimum length for the conventional silica-based EDF will be simulated, and compared to experimental results.

The following section discusses S-band amplification by the more recent approach of using DC-EDFs. As with the conventional silica-based EDF, the gain, output power and NF are characterized under various conditions. In this section also the effect of the spooling diameter on the fiber is also discussed, as the DC-EDF has the unique ability of being able to control the cut-off wavelength of the fiber by adjusting its bending radius. A novel application of the DC-EDF is also discussed in this chapter, whereby a DC-EDF is used to obtain a flat spectrum. A hybrid setup of two different gain media as a method to improve the performance of the NF is also discussed in this section.

The subsequent section details the characterization of a Raman amplifier in the S-band region. The effect of the Raman Pump wavelength on the performance of the gain and NF bandwidth is demonstrated.The section is then concluded by a discussion of the sources of noise in a Raman Amplifier.

The last section of this chapter studies the characteristics of an S-band SOA, examining its gain bandwidth, output power, NF and polarization dependence gain (PDG).

3.2 S-band Operation in a Standard 3m of Erbium Doped Fiber

The EDFA is typically deployed in one of three different configurations, these being the forward, backward and bi-directional pumped configurations as shown in Figures 3.1 (a), (b) and (c). The forward pumped configuration, as shown in Figure 3.1 (a) has both the pump and signal wavelengths propagating in the same direction through the EDF (M-12, Fibercore Ltd). The backward pumped configuration, as shown in Figure 3.1 (b) on the other hand is constructed with the pump and signal light propagate in the opposite direction whereas bidirectional-pumping is defined as two pump laser at both ends of the EDF where the propagating signal encounters the pump light in both direction. The pump laser used can be either 980 nm or 1480 nm laser diode (LD) combined with signals by using wavelength selective coupler (WSC). The pump absorption throughout the EDF length results in a population inversion that varies with positions along the fiber, reaching a minimum value at the fiber end furthest from the pump laser (in the case of unidirectional pumping) or at the middle of the fiber (in the case of bidirectional pumping with equal pump powers). The optical isolator is placed to give a unidirectional travelling of the signal while blocking any light from the opposite direction. However in our experiment, the bi-directional pumping configuration is not being tested due to the issue of the 980 nm LD protection from reflected power of both directions of the LD.

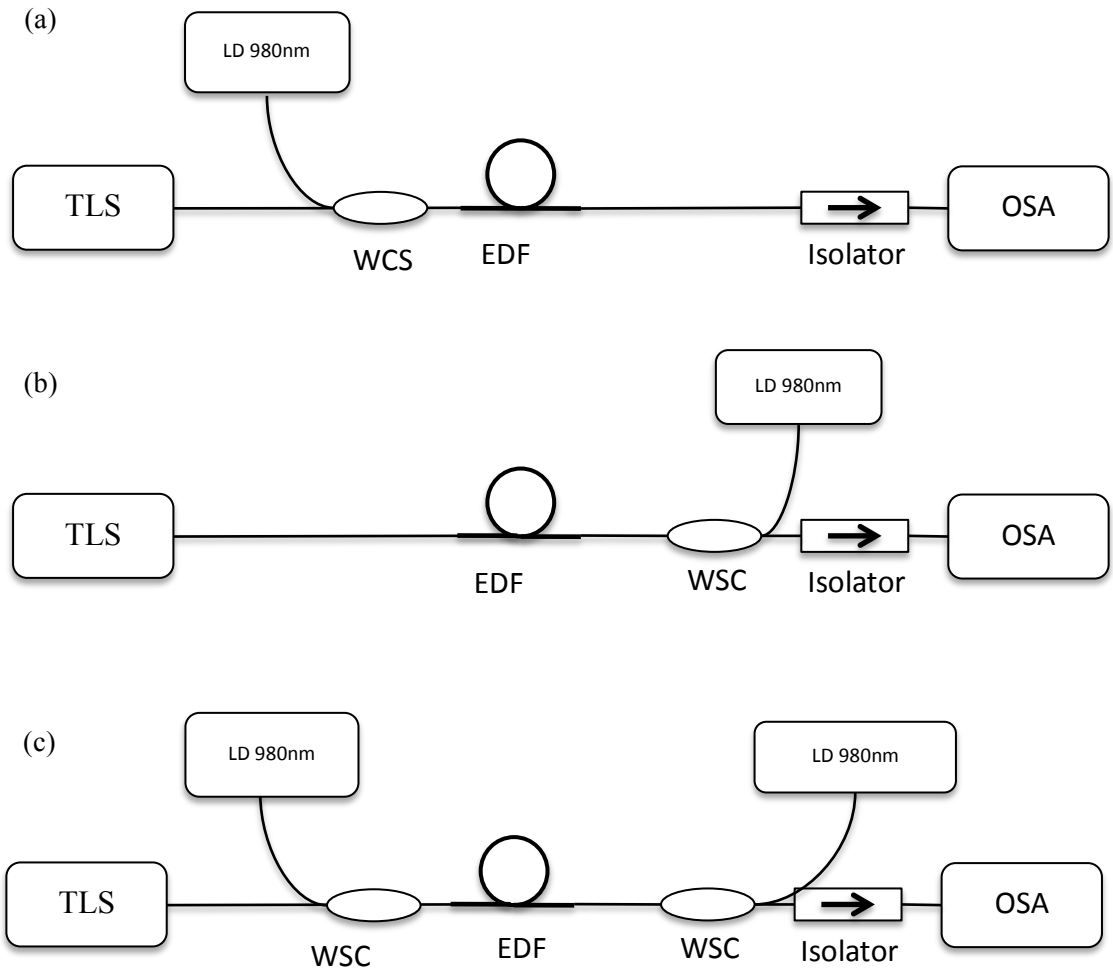

Figure 3.1: The pumping configuration of Erbium doped fiber amplifier (a) forward pumping (b) backward pumping (c) bi-directional pumping

3.2.1 Simulation of S-band Standard Silica Erbium Doped Fiber Amplifier.

To achieve gain in EDFA, inversion of $^4I_{3/2}$ level of Er^{3+} with respect to the $^4I_{15/2}$ level must be arising [1, 2]. By exciting the $^4I_{11/2}$ level with 980 nm pump absorption followed by relaxation to the $^4I_{3/2}$ level or by 1480nm pump absorption to obtain excitation of $^4I_{3/2}$ level to create the inversion, therefore subsequent emission from the $^4I_{3/2}$ level extends into the S-band at sufficiently high inversion rates.

Figure 3.2 shows the emission spectra of erbium-doped silica fiber at various inversion

rates [2, 3]. From the figure, the gain of S-band can only be obtained at the inversion rates of more than 0.7. However the strongest emission wavelength at 1530nm tends to saturate the amplification of S-band and limits the achievable S-band gain.

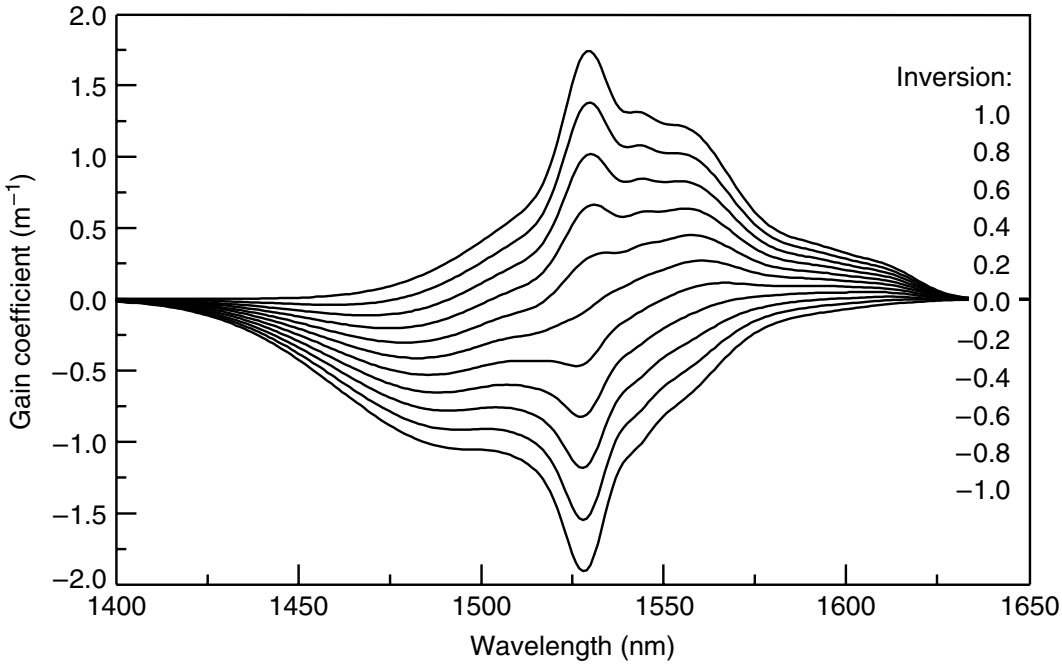

Figure 3.2 Representative gain spectra of erbium-doped silica fiber at various inversion levels [2]

In order to achieve inversion rate of more than 0.7, in obtaining S-band amplification, the simulation of EDFA with different length of EDF are being simulated. The simulation is done by using commercial EDFA simulation software GainMaster provide by Fibercore Ltd. The EDF parameters are being provided by Fibercore as shown in the Table 3.1

Table 3.1: The parameter of Metrogain EDF we use in this experiment (length of 3m)

Parameter	Specifications
Cut-off Wavelength	900 – 970 nm
Numerical Aperture	0.21 - 0.23
Absorption at Pump Wavelength	11 – 13dB/m at 980 nm
Absorption at Peak Wavelength (1530 nm)	18dB/m
Absorption at Peak Wavelength (1530 nm)	< 0.005dB/m

The screen shot of the setup is show in Figure 3.3.

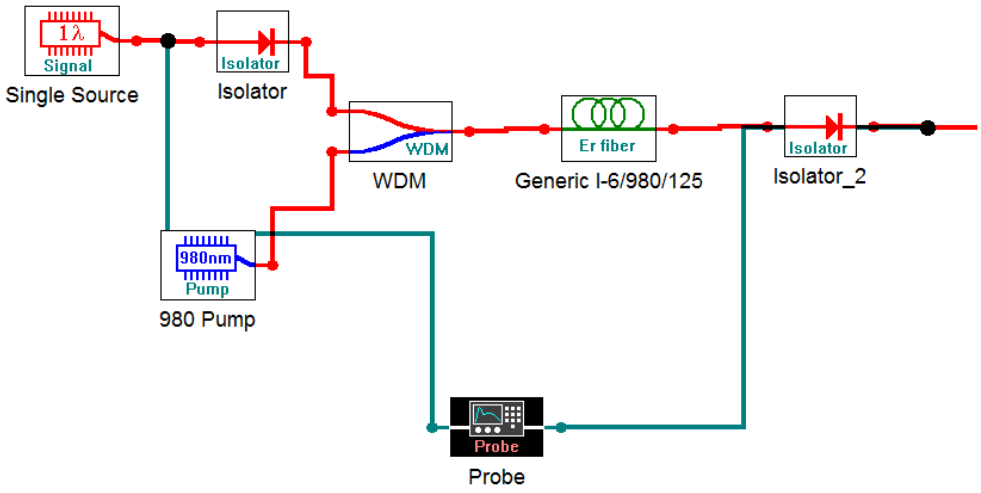

Figure 3.3: The screen shot of simulation configuration of GainMaster Software by Fibercore Ltd

Figure 3.4 shows the inversion rate at different position of the EDF length. The position is varied from 0 to 10 m. The input signals wavelength and pump wavelength is set to be 1500 nm and 980 nm and the signal power and pump power is set to be -30dBm and 300mW. The inversion rate for the EDF at 1500 nm wavelength is higher than 0.7 from 1.8 m to 3.8 m. It is also clearly shown that the highest inversion rate is at 3m length with the inversion rates about 0.89

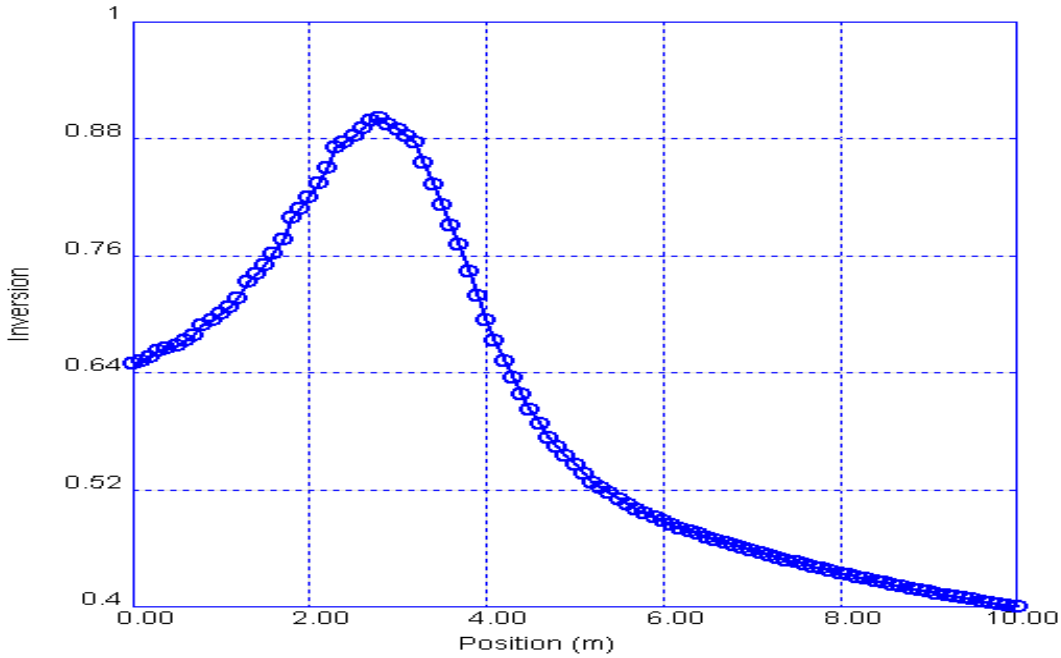

Figure 3.4: The inversion rates again the length of EDF

The gain with different pump power in the forward pumping setup at different length of EDF from 1 m to 9 m is shown in Figure 3.5 with input signal power and wavelength at -30 dBm and 1500 nm and Figure 3.6 is at input signal power and wavelength at 0dBm and 1500 nm. The gain profile follows the same profile of the inversion in Figure 3.4 with 3 m being the highest inversion. The maximum gain of 3 m EDF is about 9 dB and the gain saturated when the pump power is pumped over the 100 mW. The gain dropped when the length is increased with 9 m length of EDF showing no positive gain.

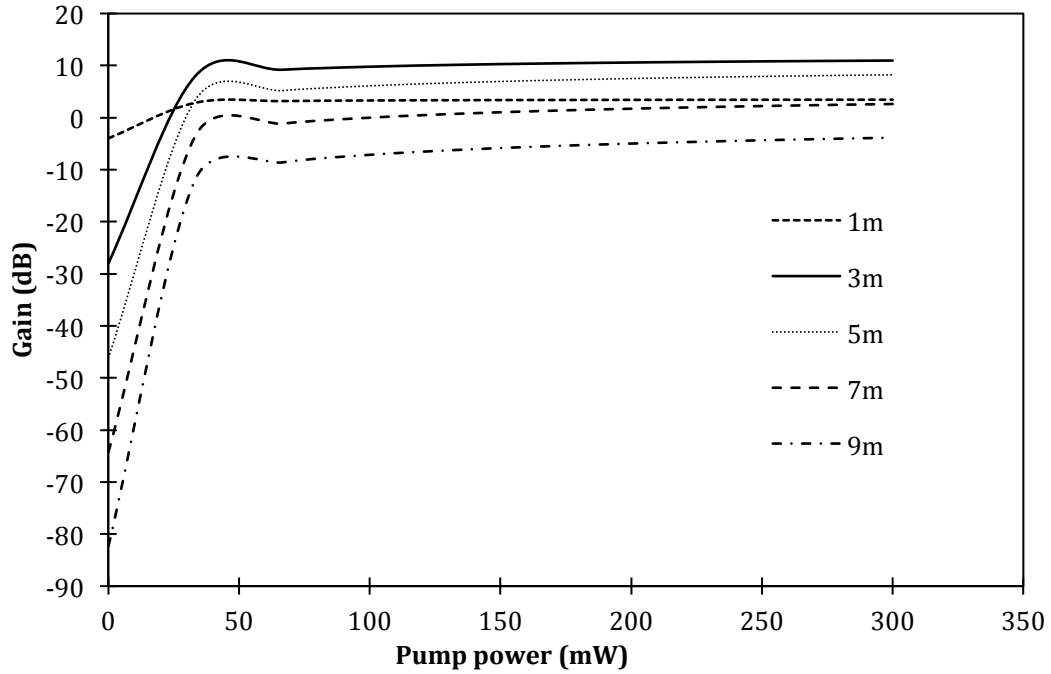

Figure 3.5: The gain performance for different EDF length against pump power of forward pumping setup with an input power of -30dBm. (Simulated Result)

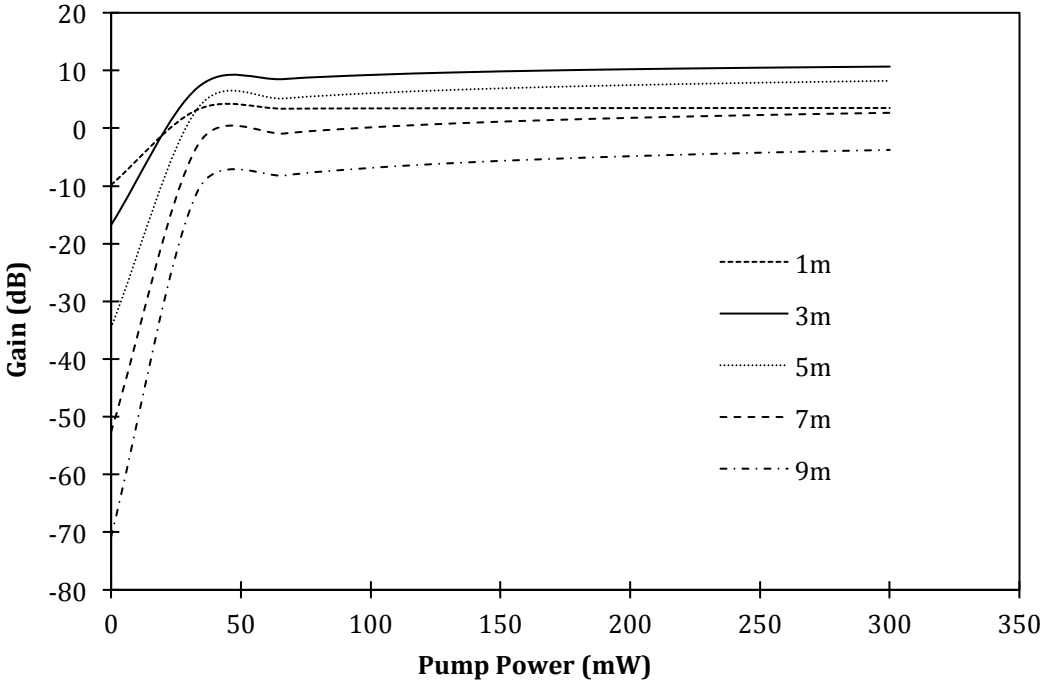

Figure 3.6: The gain performance for different EDF length against pump power of forward pumping setup with an input power of 0dBm. (Simulated Result)

The same gain profile is also shown in the backward pumping setup with an input signal power of -30dBm and 0dBm as shown in Figure 3.7 and 3.8. The 3m EDF also shows

higher gain compared to other length. The highlighted observation of this results is the optimum length L_{opt} of the EDF for S-band amplification. If the fiber length $L < L_{opt}$, high population inversion is growing and the signal amplification rate is in the saturated condition thus limited the amplification. If the $L > L_{opt}$, the signal is reabsorbed along the fiber due to an absence of population inversion in the fiber length. For this EDF type, the optimum length for S-band amplification is 3m.

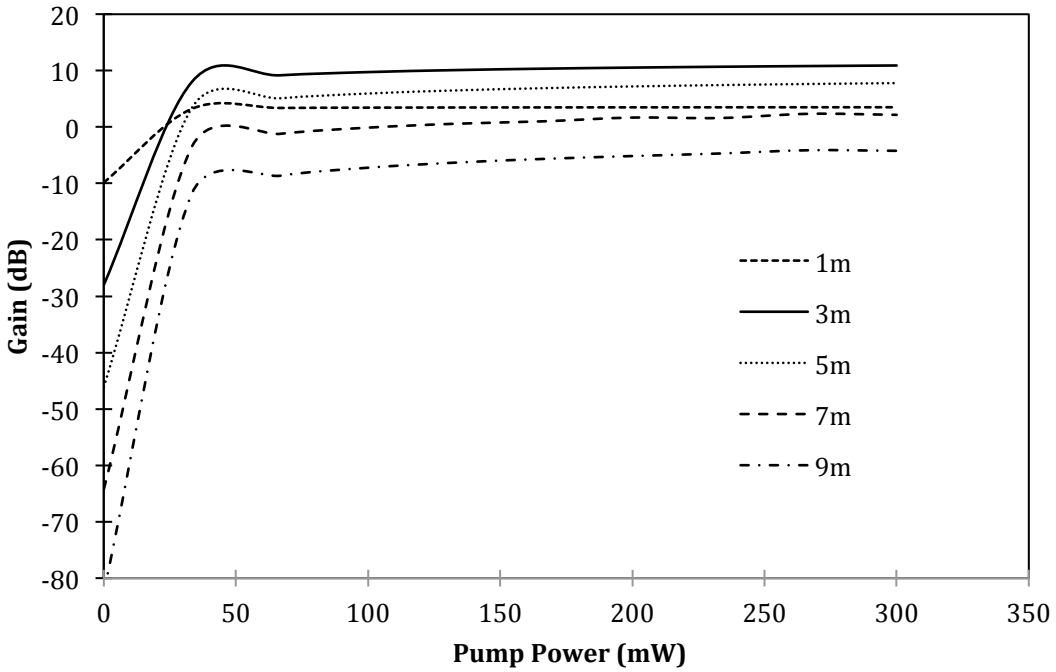

Figure 3.7: The gain performance for different EDF length against pump power of backward pumping setup with input power -30dBm.

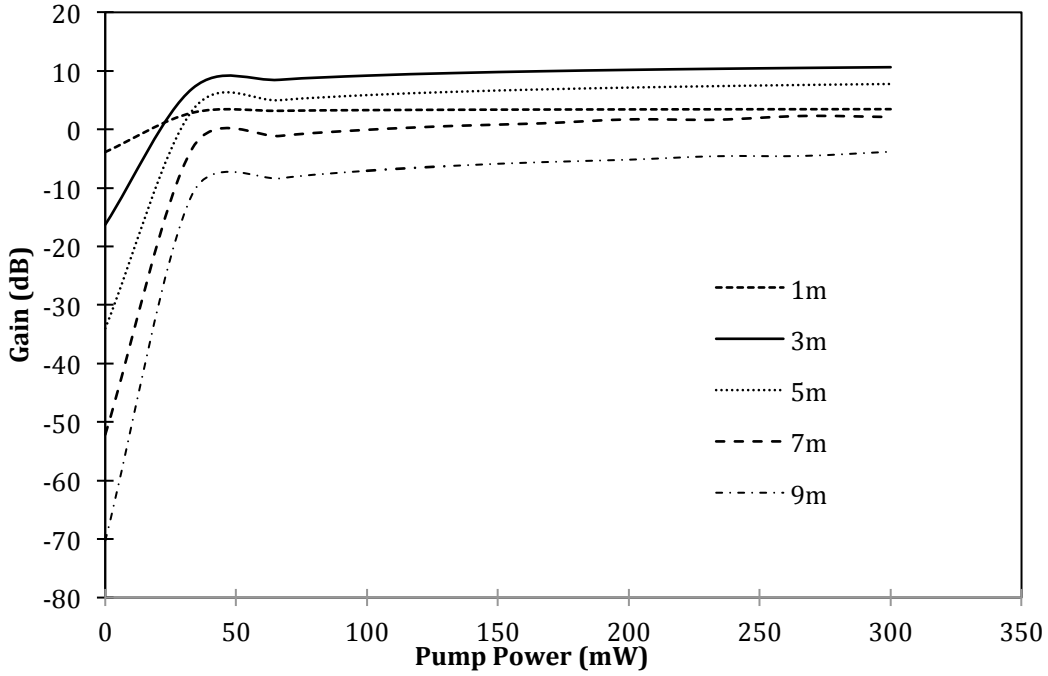

Figure 3.8: The gain performance for different EDF length against pump power of backward pumping setup with input power 0dBm. (Simulated Result)

The comparison of gain for 3m lengths of EDF for both pumping with input power of -30dBm and 0dBm is shown in Figure 3.9. The gain pattern for forward pumping and backward pumping setup show a similar pattern with the gain for input power of -30dBm is higher than the input power 0dBm, due to the excited ions are enough to provide amplification for this small signal power. The difference of the gain value is about 0.24dB for the input power -30dBm. The smallest difference is due to the condition of the uniform full inversion along the 3m EDF. Therefore the gain value for the forward pumping and backward pumping is about the same.

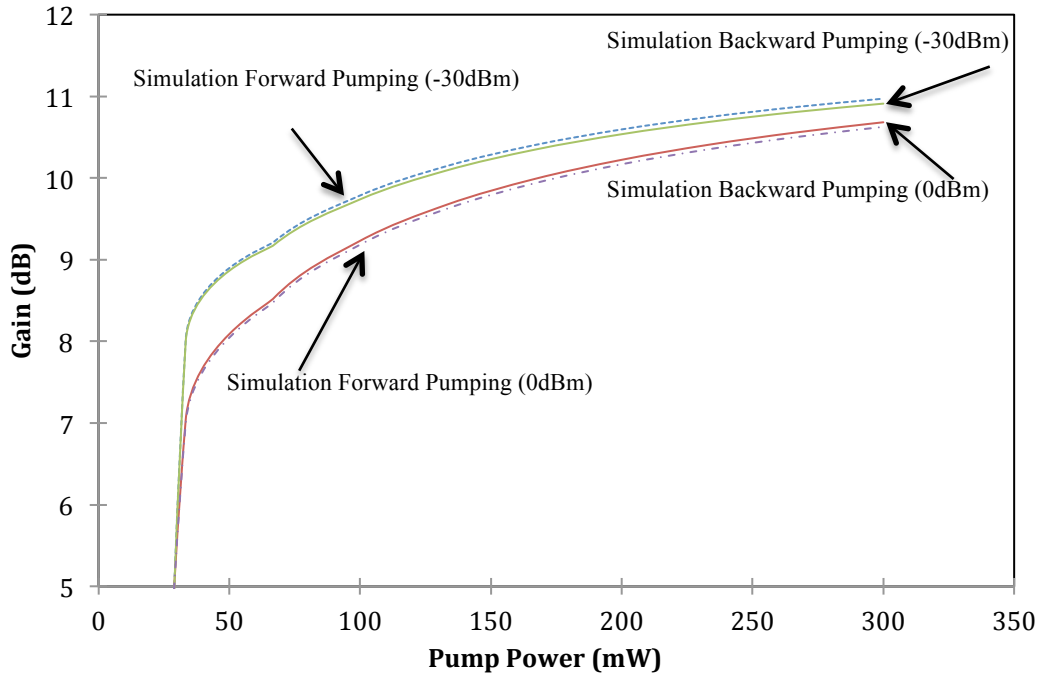

Figure 3.9: The gain comparison of 3m EDF for forward pumping and backward pumping setup with input signal -30dBm and 0dBm

In order to verify the simulation result, the result of the simulation is compared with the experimental result. The EDF manufactured by Fibercore Ltd and the parameter of the fiber are the same as shown in Table 3.1. The length of the EDF is cutted to about 3m. The comparison between the simulation result and experimental result is shown in Figure 3.10. The EDF is pumped with 90mW in the experimental setup. The input signal power and wavelength is set at -30dBm and 1500nm respectively. From the Figure, the forward and backward pumping setup of the experimental result shows the similar gain profile as the forward and backward pumping setup of the simulation result except that the gain value of the experimental setup is lower than 3dB. The difference of the gain value is due to the splicing loss in the experimental setup while simulation is in an ideal case, which has no splicing loss element.

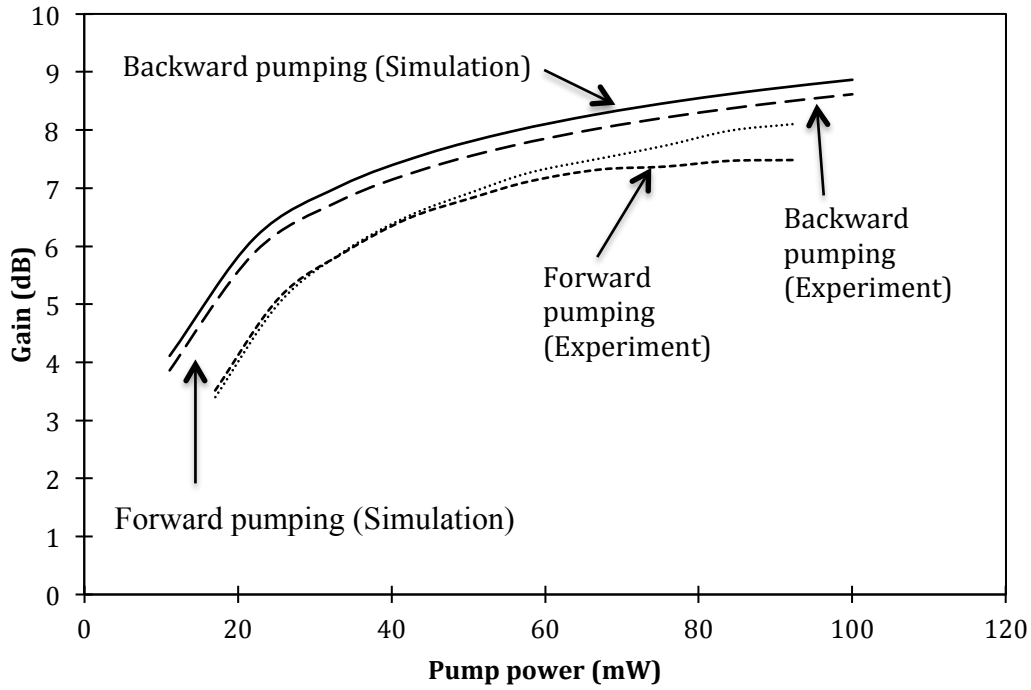

Figure 3.10: The comparison of gain between simulation and experimental result.

3.2.2 Experiment of S-band Standard Silica Erbium Doped Fiber Amplifier

3.2.2.1 Small –Signal and Saturation Gain

The small signal gain is defined simply as the gain obtained when a very weak signal is amplified. This means that no gain saturation can occur as the input power is too low. [4,5]. The small signal gain is also measured to simulate and test the performance of EDFA under its use as a pre-amplifier. As defined above the pre-amplifier is required for high gain at low input signal for optical communication network system. The small signal gain is also called an unsaturated regime, which is normally defined when the gain curves are linear.

A saturated gain is observed when the input signal into the amplifier is large and the EDFA characteristic departs from those linear relations [1,5]. A useful figure of merit is the input saturation power, defined as the input signal power required to reduce the net

amplifier gain by 3 dB, the gain G in this case is

$$G=G_{max}-3dB \tag{3.1}$$

where G_{max} is the maximum value of small-signal gain. The saturated gain measurement is important to characterize the power amplifier of the EDFA performance. The power amplifier requires a very high saturation gain. Figure 3.11 shows the saturation gain defined by changing the input signal power. Below saturated gain condition the gain decreases gradually.

The experimental of small signal gain and saturation gain for the 3m EDF with 1500 nm signal and different pumping setup is shown in Figure 3.11. The gain is measured by OSA with a resolution of 0.02 nm. The forward pumping setup shows a better gain performance compared to the backward pumping configuration. The difference between the two pumping configuration from input power -40 dBm to -10 dBm is almost constant with a difference of about 0.15 dB. The input signal saturation for both setups is about 1 dBm.

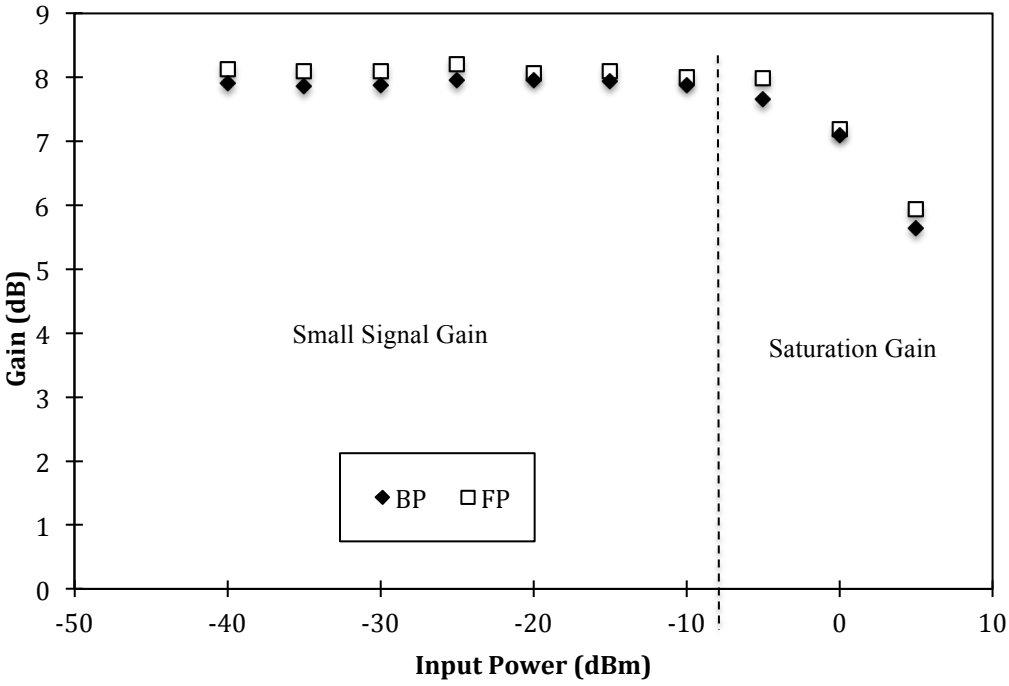

Figure 3.11: The gain performance for different input power

The saturation gain is also analyzed as shown in Figure 3.11. The average gain difference for the forward pumping and backward pumping in saturation region from -5dBm to 5dBm is about 0.34dB. The 3dB input saturation for forward pumping and backward pumping configuration is about 5dB respectively.

3.2.2.2 Gain Bandwidth

In an optical amplifier, an important characteristic is the gain bandwidth. Gain bandwidth is the gain of an optical amplifier over the bandwidth. For example, in the C-band, the gain covers from the 1530 nm to 1560 nm which is about 30 nm gain bandwidth. Another definition of gain bandwidth is the 3dB gain bandwidth. The 3 dB gain bandwidth is defined as the bandwidth of the gain when a 3dB drop from the maximum gain of the signal wavelength happens. For the case of low input power (-30 dBm) with pumping power of about 90 mW, the gain bandwidth in S-band covers

from 1480 nm to 1525 nm which is about 45 nm for both pumping setup as shown in the Figure 3.12. In the Figure 3.12 it is shown that the gain from 1480 nm increases exponentially to 1525 nm with the minimum gain at 1480 nm is only about 0.87 dB in backward pumping setup and the maximum gain at 1525 nm is about 13.93 dB in forward pumping setup. The exponential pattern is most likely due to the lower signal power thus failing to suppress the ASE which results in the gain pattern follow the ASE curve as shown in inset of the Figure 3.13. From the figure, it is also shown the gain of forward pumping setup is at the highest gain compared to the gain of backward pumping configuration with the average difference about 1.58 dB. Figure 3.13 shows the ASE spectrum with injected signal 1500 nm with input power -30 dBm and 0 dBm and without signal. As shown in the figure the exponential curve is more obvious when no signal is injected and the exponential curve is reduced when high power signal (0dBm) is injected. The ASE curves are related to the gain bandwidth pattern as shown in the Figure 3.12 and Figure 3.14 below.

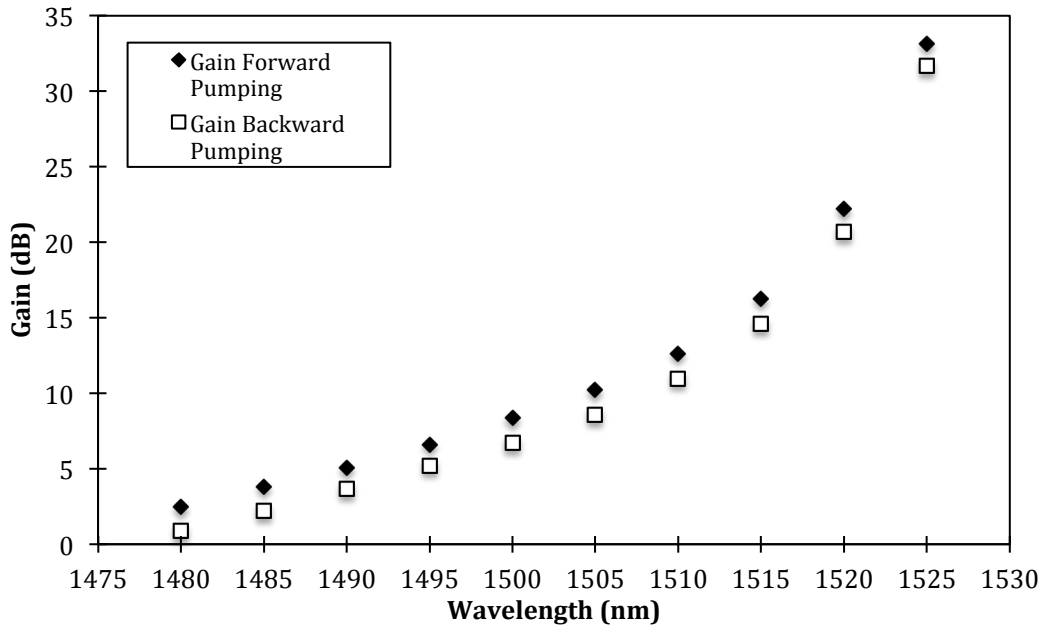

Figure 3.12: The gain performance with different input signal wavelength with input power -30dBm

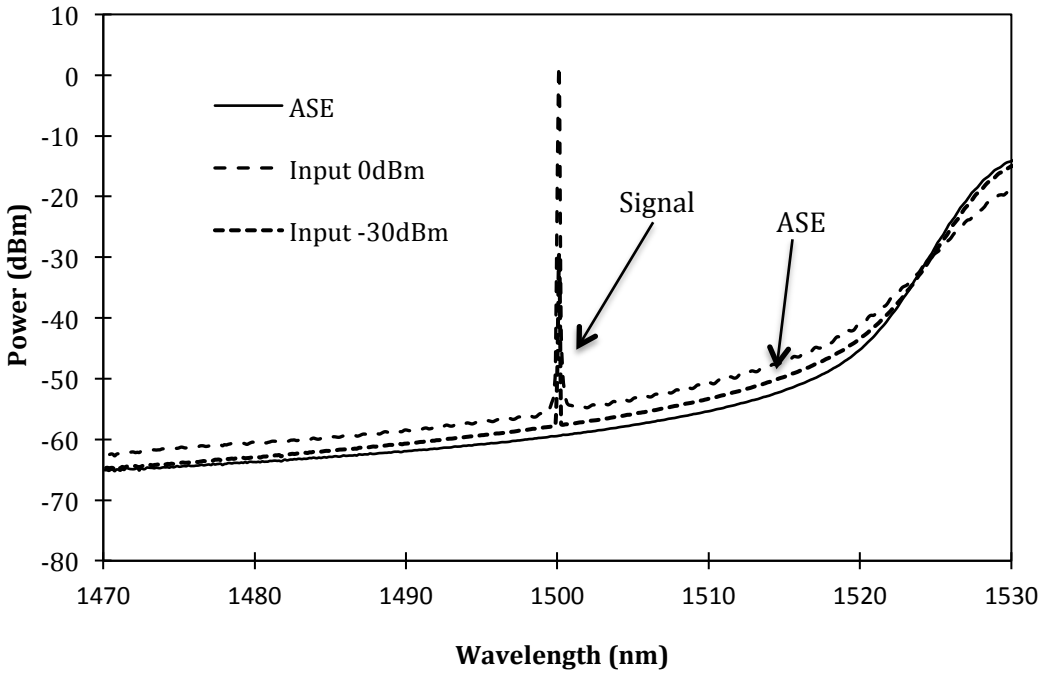

Figure 3.13: The ASE spectrum of EDF with pumping power 90mW

For the case of high input signal power (0dBm) the bandwidth pattern is different from the case of lower input signal. Figure 3.14 shows the gain of forward pumping and backward pumping setup with different signal wavelengths and fixed input power of 0dBm. The gain is increases linearly when the wavelength signal goes towards longer wavelength. The minimum gain is about 0.7dB with backward pumping setup and the maximum gain is about 14dB for forward pumping. Figure 3.14 also shows the gain difference become smaller when the signal wavelength is close to the C- band. The biggest difference between the two setups is at the wavelength 1480 nm with the difference is about 1.32 dB.

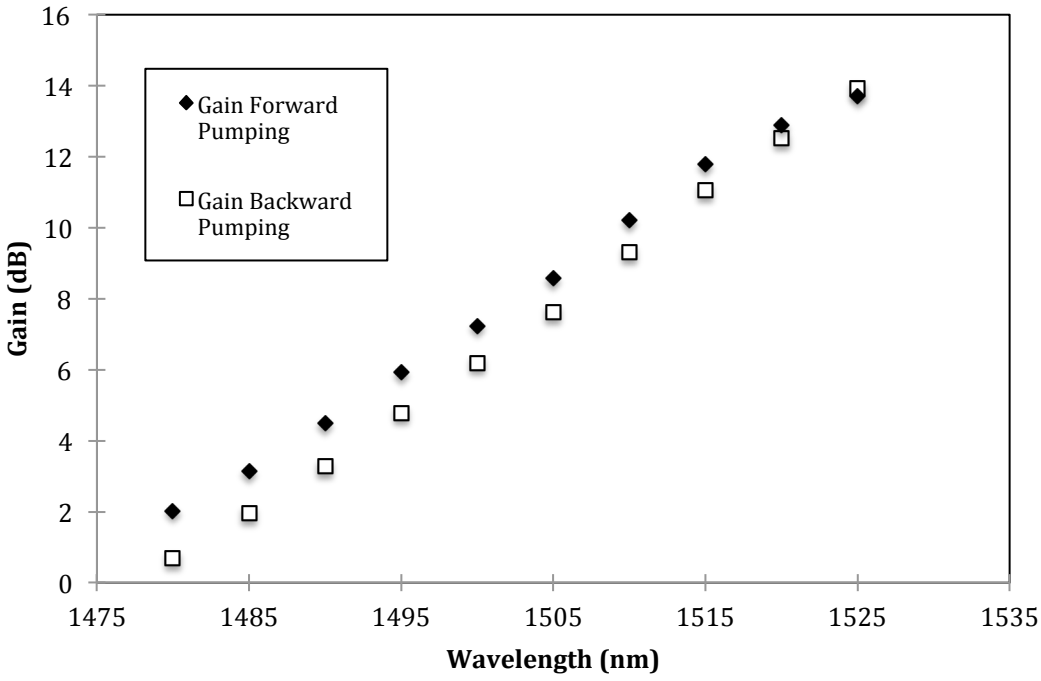

Figure 3.14 The gain performance with different input signal wavelength with input power 0dBm

3.2.2.3 Amplified Spontaneous Emissions and Noise Figure Characteristic in S-band

The NF is also one of the key parameter of optical amplifier. The good performance of optical amplifier must have high gain, wide bandwidth and low NF. As discussed in Chapter 2, the NF can be defined by the ratio of the input signal to noise ratio (SNR_i) and Output signal to noise ratio (SNR_o). Furthermore the NF only can be defined when the coherent input signal is used as a signal source. In our experiment the NF is measured by using OSA with ASE interpolating technique method. In the ASE interpolation technique, measurements are taken on either side of the signal wavelength. The level of the amplified spontaneous emission at the signal wavelength is then interpolated from these measurements and the resulting value is subtracted from the signal wavelength [8]. This technique is extremely useful in the measurement of a

single or a few EDFAs because it requires a linear ASE spectrum in a narrow wavelength (typically ±1 nm). [6]

The NF performance of the EDF in the S-band region is measured. The NF is thus likely to be sensitive to the fiber parameters and pump power, wavelength and direction. [7,8]. The NF with different pump power and fixed input power of -30 dBm and signal wavelength 1500 nm for forward pumping and backward pumping setup is shown in the Figure 3.15. As shown in the figure it is clearly stated that when the pump power is high, the NF level is reduced from 5.5 dB to 4.16 dB. This is due to the maximum population inversion created when the pump power is increased thus making the value of gain becomes higher and the NF becomes lower. The NF of backward pumping setup is slightly higher than the forward pumping setup due to high ASE power detected at the end of the length of EDF**.** The difference of NF between two setups at pump power of 92.2mW is about 0.18dB.

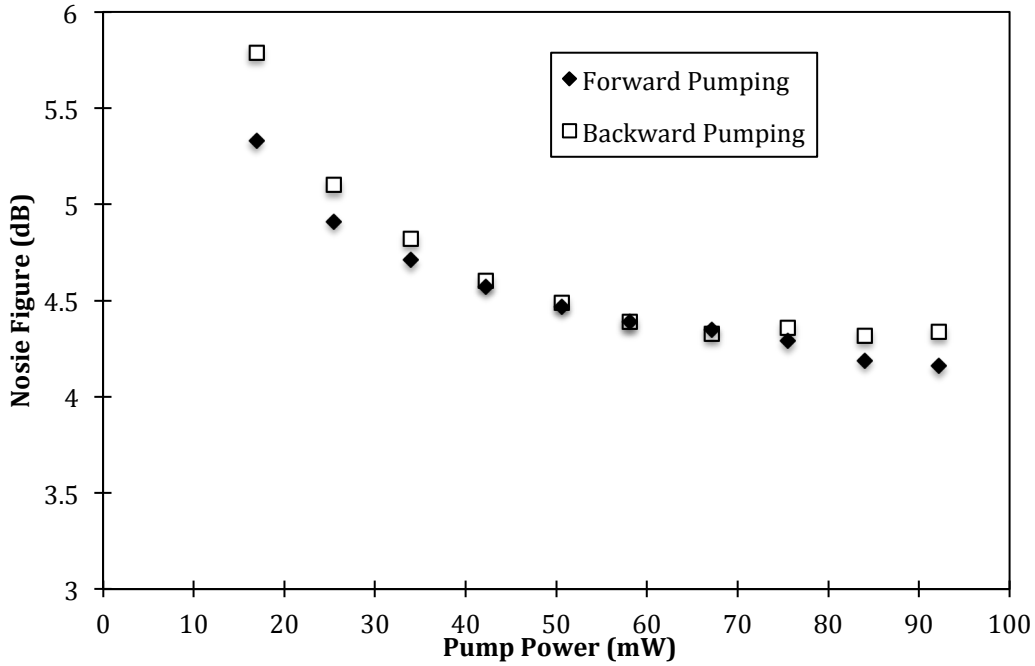

Figure 3.15: The NF of forward pumping and backward pumping setup as a function of 980 nm pump power at signal wavelength and power of 1500 nm and -30 dBm respectively

The NF of forward pumping and backward pumping setup with different input signal power with the signal wavelengths and pump power fixed at1500 nm and 92 mW is shown in the Figure 3.16. From Figure 3.16, the NF of the forward pumping setup at the lower input signal -40 dBm to -15 dBm is recorded with almost constant value which is about 4.04 dB with a difference of about 0.05 dB while NF of backward pumping setup is slightly higher compared to the forward pumping setup with a difference of about 0.39 dB. The NF value for forward pumping and backward pumping setup increases when the input signal is increased to a maximum value of 5dBm, with the highest NF value is 6.77dB for forward pumping and 6.36dB for backward pumping setup. These characteristics could be attributed to the mixture of the effect of self-induced saturation by the backward ASE and signal-induced saturation [1]. The two effects are connected to each other when signal-induce saturation occurs to change the distribution of ASE along the fiber. The power of signal-induced saturation significantly reduces the backward ASE near the fiber input end thus making higher medium inversion in this region. Finally when the medium inversion is higher at the input of EDFA the high NF is obtained at higher input signal

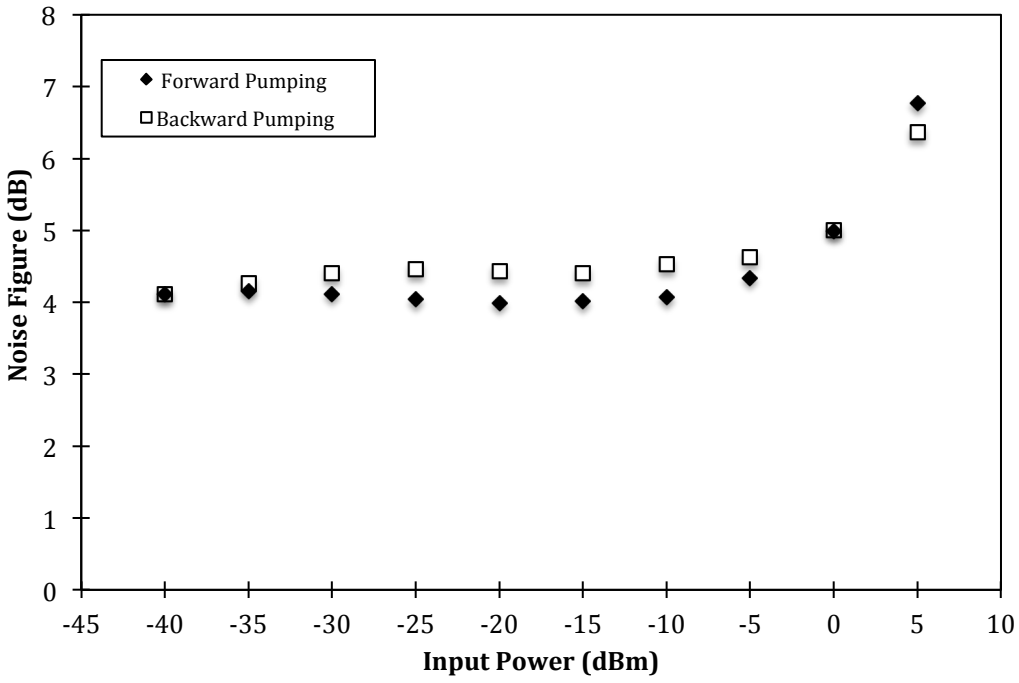

Figure 3.16: The NF characteristics with different input power at 1500nm signal wavelength

Figure 3.17 shows the performance of the NF between the forward pumping and backward pumping setup with different input signal wavelengths at an input power -30 dBm. The forward pumping setup shows lower NF compared to the backward pumping setup with an average NF of about 4.2 dB from 1480 nm to 1525 nm of the forward pumping setup and average NF for the backward pumping with the same wavelength range is about 5.79 dB. The same pattern of NF is observed at a high input signal of 0 dBm as shown in Figure 3.18. The NF of the backward pumping setup is higher than the NF of the forward pumping setup with an average difference of 1.09 dB between the signal wavelengths from 1480 nm to 1525 nm. The minimum NF is about 4.59 dB with forward pumping setup.

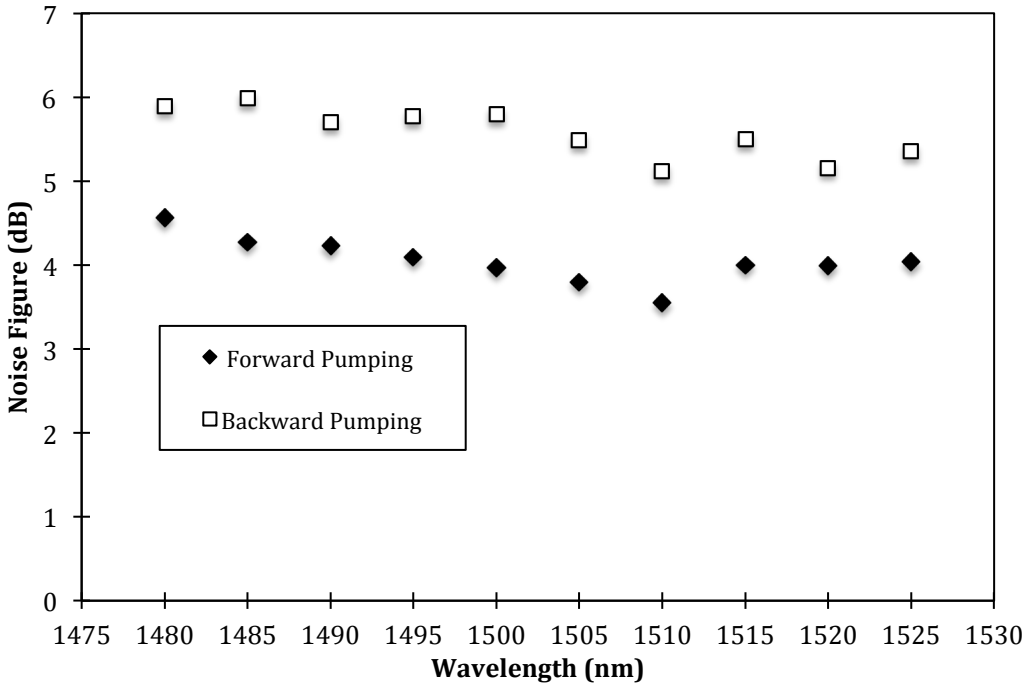

Figure 3.17: The NF with different signal wavelengths at input power of -30dBm (lower input signal)

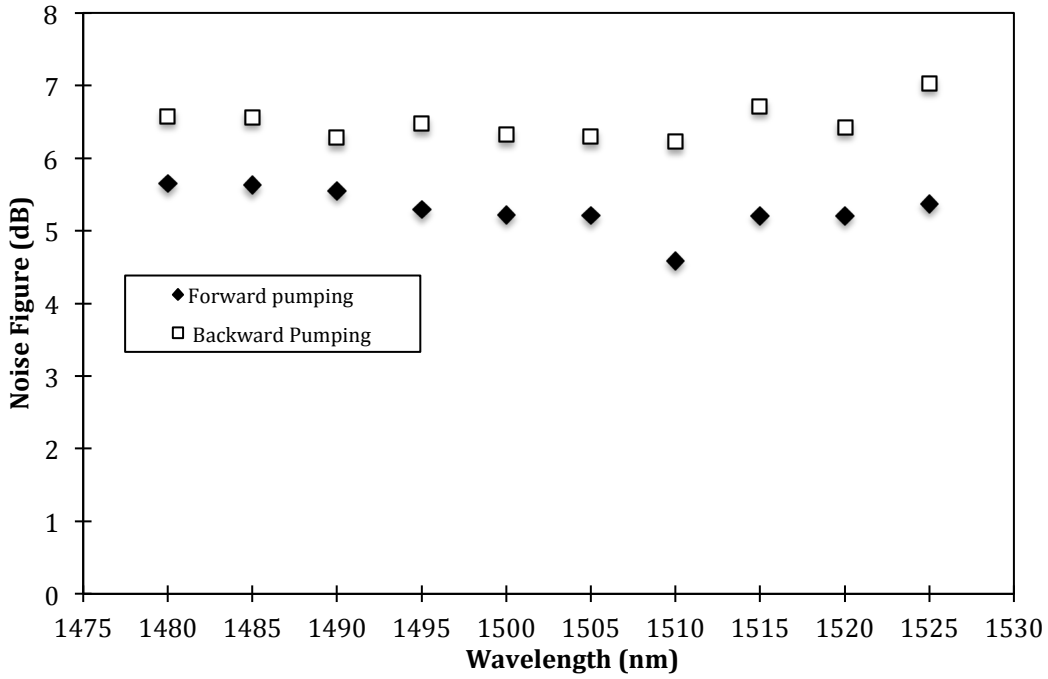

Figure 3.18: The NF with different signal wavelengths at input power of 0dBm. (Saturated input signal).

3.3 S-band Depressed Cladding Erbium Doped Fiber Amplifier

3.3.1 Depressed Cladding Erbium Doped Fiber

From the previous section, it can be seen that standard silica EDFs have a significant limitation, in that there is a significant population inversion and strong emission at a wavelength region of around 1530 nm. Solving this problem is simple enough; all that is needed is to filter out the strong emission at 1530 nm using optical filters. Researchers have looked towards many options to suppress the emissions at 1530 nm, but the most promising solution is the development of the DC-EDF, an EDF made to work like a filter [9]. The DC-EDF achieves this by having a unique structure which allows it to determine the cut-off wavelength for the fiber by changing the index profile of the fiber. The first demonstration of this fiber is done by Arbore [9,10].

The DC-EDF is fabricated using a standard modified chemical vapor deposition (MCVD) process with standard solution doping [11] with insertion of fluorine into the depressed cladding. The DC-EDF is surrounded by a secondary cladding and has a core with a circular-cross section. This circular cross-section is also present in the depressed cladding and secondary cladding with the depressed cladding cross-section larger than core cross section. In the DC-EDF ions of the rare earth erbium are doped into the core of the fiber. These erbium ions act as a lasing medium and exhibit high gain at the C- and L- band region. Figure 3.19 below shows the W-profile of the fiber [12]

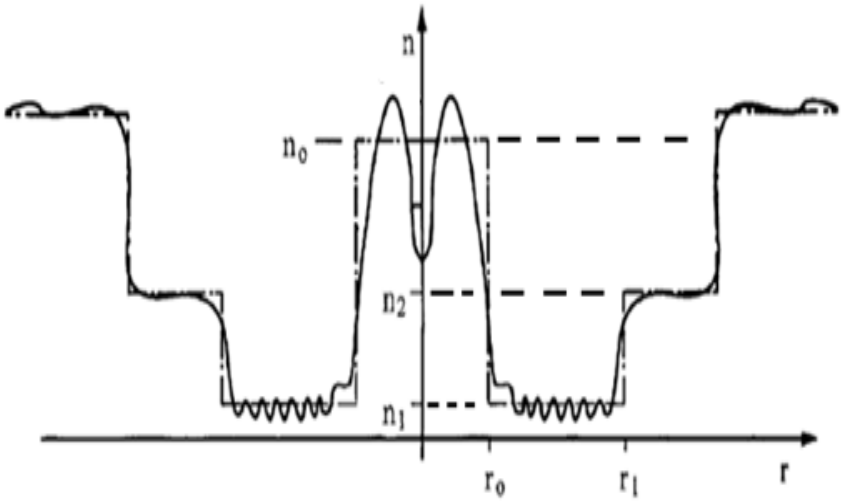

Figure 3.19: W-Profile of fiber [12]

In order to obtain the amplification at the S-band region by using the DC-EDF, the fundamental mode cutoff wavelength must be between the S-band and the long wavelength bands of the C- and L-band region. In particular the fundamental mode cutoff wavelength due to be S-band signal that remains in the core [13] is preferably set near 1530 nm [14, 15]. This desired fundamental mode cutoff wavelength can be produced by selecting the values of the indices n_0, n_1, n_2 and radii r_0, r_1, r_2 as shown in Figure 3.19 where n_0 is the reflective index of the core, n_1 is the reflective index of the depressed cladding and n_2 is the reflective index of the secondary cladding while r_0 is the radius size of the core, r_1 is radius size of the suppressed cladding and r_2 is radius size of the secondary cladding [12]. Figure 3.19 is also called the W-profile and can be obtained with normal manufacturing techniques. These values are fixed by the manufacturer of the depressed cladding fibers.

The fundamental mode cutoff can be determined by adjusting the cross section and refractive indices of core, depressed cladding and secondary cladding. The adjustment to the fundamental mode cut-off can also be made by adjusting the spooling diameter of

the DC-EDF. Thus, by using fiber spools of varying diameters, the effect of the spool diameter on the fundamental mode cutoff of the DC-EDF can be observed in the study of the S-band EDFA. As well as the fundamental mode cutoff, other important parameters of the depressed cladding EDFA related to the spooling diameter can also be observed, such as the attenuation of the fiber due to the bending loss and the variation in the gain and noise figure of the S-band EDFA. These factors are critical in the development of compact EDFAs, as the size of the EDFA must have no detrimental effect on the performance of the EDFA. With this in mind, the study of the DC-EDF fundamental mode cutoff under different spooling diameters will be discussed in the next section.

3.3.2 Tunable Fundamental Mode Cutoff DC-EDF by Spooling Effect.

In order to obtain the fundamental mode cutoff in DC-EDFs, an experiment is designed to study the effects of the spooling diameter in determining the desired cutoff wavelength. This is necessary to obtain the cutoff wavelength for optimum amplification in the S-band region.

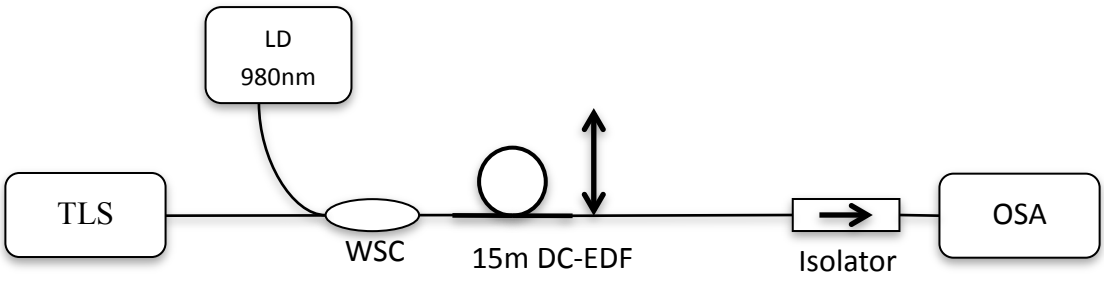

Figure 3.20: Experimental Setup for Spooling Effect on the Tunable Fundamental Mode Cutoff of a DC-EDF [6]

The studies of the spooling diameter effect to the fundamental cut-off wavelength of the DC-EDF uses a basic setup consisting of the erbium doped fiber amplifier (EDFA) as shown in Figure 3.20. The setup consists of a tunable laser source (TLS) which is used as a test signal / input signal and is set to operate at the S-Band region of 1460 nm to 1530 nm. Figure 3.20 also consists of a WSC which is optimized for C-band operation and is used to combine the 980 nm pump signal with the test signal with the loss of the WDM already known. The setup also consists of a 15 meter DC-EDF (OFS) with a background loss of less than 5 dB/km spooled into five spools with constant diameters ranging from 5-9 cm. The fiber is pumped by a 980nm laser diode using a forward pumping scheme with a pumped absorption rate of approximately 7dB/m. Finally, an OSA is used to analyze the output signal of the setup.

In Figure 3.21 the Amplified Spontaneous Emission (ASE) of EDFAs at a constant pump power of 100mW with different spooling diameters is shown. As shown in Figure 3.21, the effective cut off wavelength shifts to a value of 1520 nm and 1490 nm for spooling diameters of 9 cm and 5 cm respectively. This shift is caused by the effects of the mechanical strains due to the spooling effect of the DC-EDF, subsequently resulting in a shift in the effective refractive structure [16] as shown in Figure 3.22 and Figure 3.23 below. The Figures 3.22 show the effective refractive index of a straight fiber and Figure 3.23 show index structure for the fiber under mechanical stress due to the spooling of the fiber, whereby n_0 is the outer cladding, a is the core radius, b is the depressed cladding radius, Δ is refractive index of core and $-\Delta$ is the refractive index of the DC-EDF.

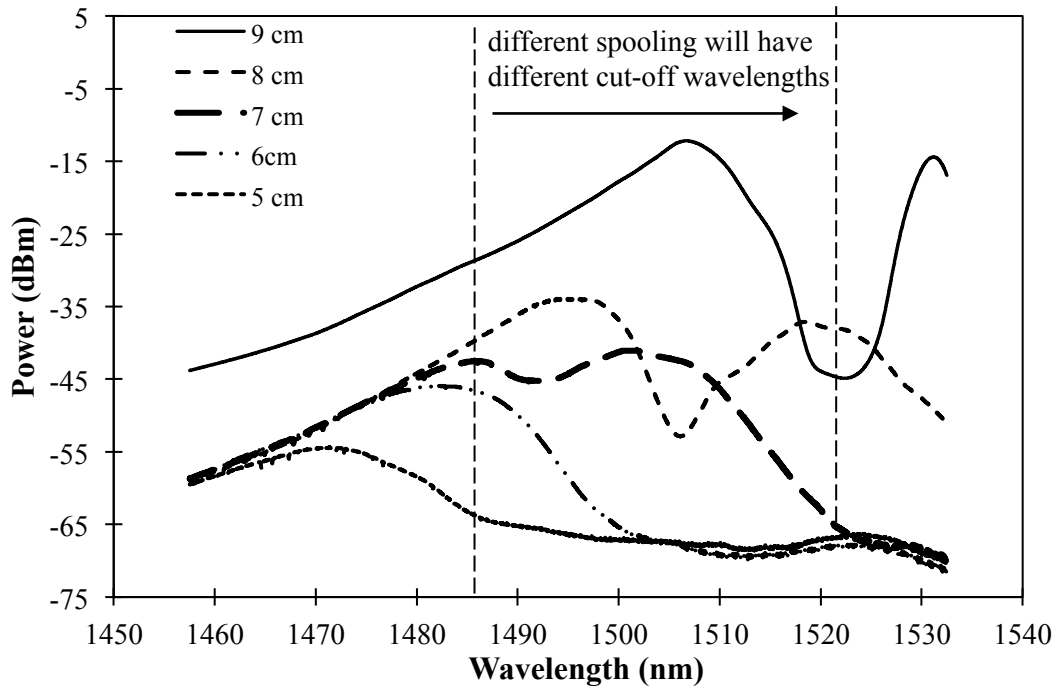

Figure 3.21: Amplified Spontaneous Emission (ASE) of DC-EDFAs with different spooling diameters [6]

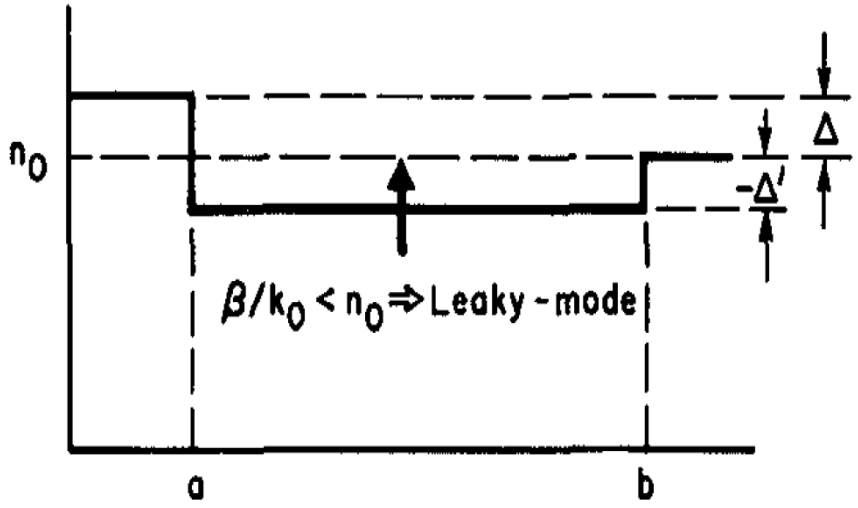

Figure 3.22: The effective refractive index profile in the straight fiber [16]

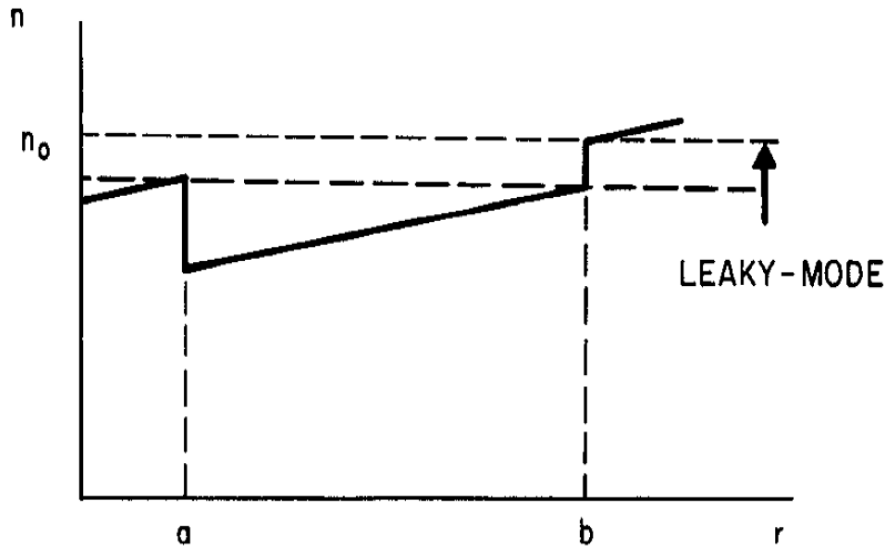

Figure 3.23: The effective refractive index profile in the plane of curvature of the bent fiber [16]

The effective refractive index is the ratio of free-space velocity to the velocity of propagation or guide velocity (v_{guide}) [17] and is given by the equation:

$$n_{eff} = c/v_{giude} \tag{3.2}$$

The effective refractive index in turn affects the cut-off wavelength of the DC-EDF as determined by the equation:

$$\lambda_c = \left[\frac{2\pi an}{v}\right]\sqrt{2\Delta} \tag{3.3}$$

At the cut-off wavelength $\lambda_c$the cladding index begins to leak out as a radiation mode [18]. Using this phenomenon, a signal whose wavelength is longer than cut-off

wavelength λ_c can be filtered out passively in the DC-EDF while signal wavelengths shorter than the cut-off wavelength λ_c will experience a negligible loss as shown in Figure 3.21 above, in which the ASE reduces as the spooling diameter becomes smaller.

From the results of the experiment as shown in Figure 3.21, it can be seen that the spooling diameter of 9 cm gives the highest ASE value, and a cut-off wavelength of 1520nm, which is the longest wavelength that can be guided along the core of the DC-EDF before leaking into the cladding. In addition, the ASE for the spooling diameter of 9 cm falls between the bandwidth required for S-band amplification, thus making the setup suitable for the study of the DC-EDFA

3.3.3 Small-signal and Saturation Gain of Depressed Cladding Erbium Doped Fiber Amplifier

The gain of DC-EDFA in this thesis is measured using 30m length of DC-EDF. The longer length of the gain medium needs more pump power to create the population inversion in the DC-EDF. Therefore in this experimental setup 300mW pump power is used to pump the DC-EDF. Except for the length, all the components remain the same as shown in the Figure 3.1. The gain and NF measurement for different input powers at the center wavelength of 1500 nm is shown in Figure 3.24. In the Figure, the gain values for backward pumping setup are observed to be higher compared to the forward pumping setup. A slightly difference in the gain of low input powers of -40 to -15 dBm, with the average gain of backward pumping is observed to be about 28.65 dB while the average gain of forward pumping is about 26.84 dB.

The gain difference increases with the increasing value of input signals from -15 dBm to 5 dBm. A large gain difference between the forward pumping and backward pumping can obviously be seen for the input powers of -5 to 5dBm by the value of 4.96 dB. The highest gain for 5dBm input signal of backward pumping recorded to be about 8.18 dB while the forward pumping gain is about 3.22dB. The large difference is most likely due to saturation gain effect. The saturation gain effect is different for different pumping setup. For the case of backward pumping the saturation gain is higher compared to the forward pumping. The saturation gain occurs when all pump power is consumed to generate full population inversion and saturates the ASE power. When the ASE power is saturated in DC-EDF input, any further gain is not able to be generated thus limit the gain at the high input signal region.

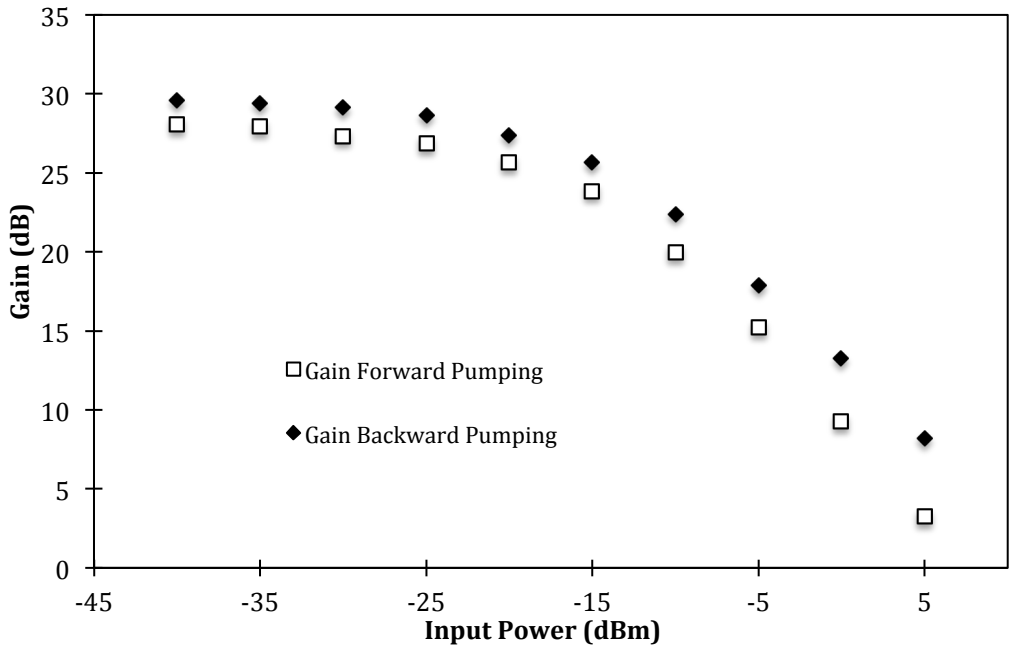

Figure 3.24: The gain of DC-EDFA with different input power at signal wavelength 1500 nm

The output power for forward pumping and backward pumping with different input powers is shown in the Figure 3.25 below. Obviously, the output powers for backward pumping shows a higher value than the forward pumping. The small output power difference between the forward pumping and backward pumping at a lower input powers ranging from -40 dBm to -15 dBm is observed to be about 2.5 dB, while a larger power difference at the higher input powers in the range of -10 dBm to 5 dBm is observed to be about 5.04 dB power. The figure shows that the backward pumping setup has a higher output powers compared to the forward pumping setup with the maximum output power of about 13.01 dBm. At input powers of more than -5dBm the output powers of the forward pumping setup plunge and this is significantly caused by the signal being absorbed at the end of the output of forward pumping setup while the signal of backward pumping setup is still being amplified due to the high pump energy at the end of the output of backward pumping.

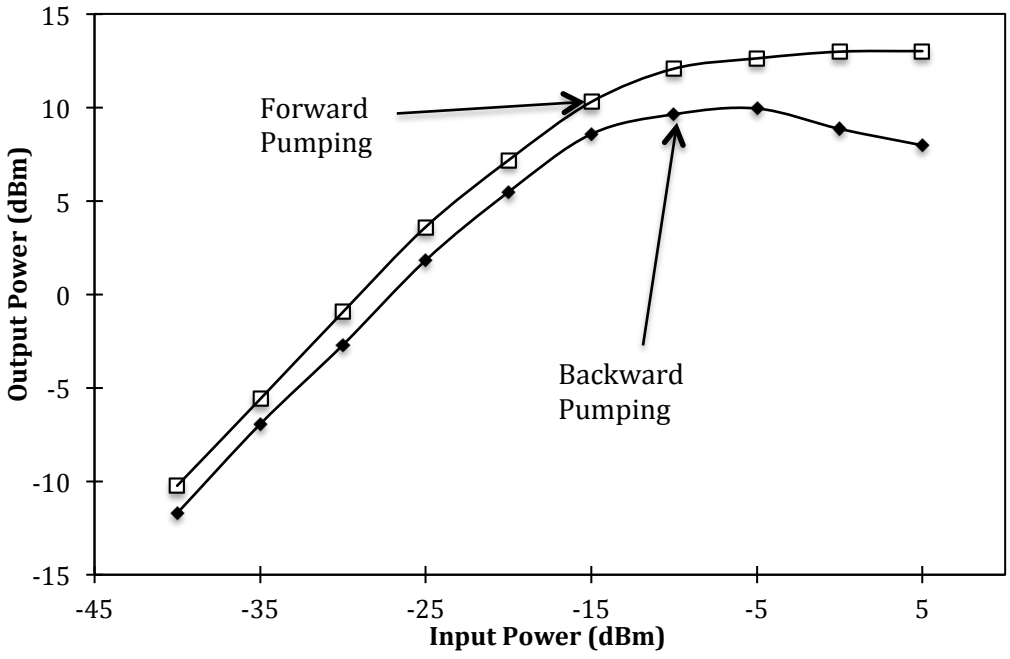

Figure 3.25: The output power performance with different input power

3.3.4 Gain Bandwidth of Depressed Cladding Erbium Doped Fiber Amplifier

The small signal input (-30 dBm) gain of multi-wavelength for forward pumping and backward pumping are shown in Figure 3.26. The gain bandwidth is about 55 nm for the forward pumping. The backward pumping are showing the same pattern in the gain bandwidth, ranging from 1470 nm to 1525 nm. The gain for the backward pumping is observed to be slightly higher than the forward pumping with less than 1.5 dB gain difference**.** It is contributed by the uniformity of full inversion along the 30 m DC-EDF which is caused by the amplification rate in forward pumping. The backward pumping is almost similar to the forward pumping. The gain at 1510 nm shows a dip due to the coupling effect between the guided mode in the core and the discrete cladding mode [10].

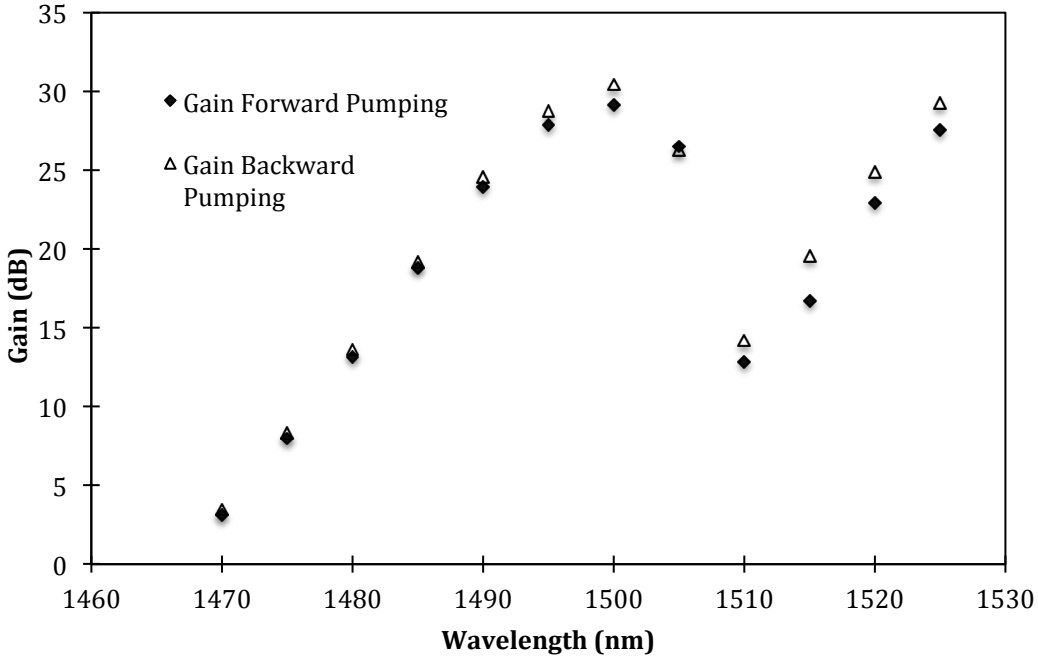

Figure 3.26: The gain and with different input wavelength and -30dBm input power

The gain and NF for the saturation input signal (0 dBm) with different input wavelength for forward pumping and backward pumping configuration are shown in Figure 3.27.

For a high saturation input power, the gain pattern for forward and backward pumping expose a linear pattern at a wavelength range of 1470 nm to 1485 nm. For longer wavelength starting from 1485 nm, they exhibit different gain values between the forward and backward pumping. The gain of backward pumping is higher compared to forward pumping for wavelengths of 1485 nm to 1525 nm. The gain difference at wavelength of 1500 nm for forward and backward pumping is about 3.53 dB. Starting from wavelength of 1490 nm and longer, the forward pumping shows a decreasing gain pattern due to the full saturation effect at a wavelength longer than 1490 nm while the backward pumping gain shows a different pattern. This means that the backward pumping experiences a high gain saturation at wavelength of 1495 nm and longer.

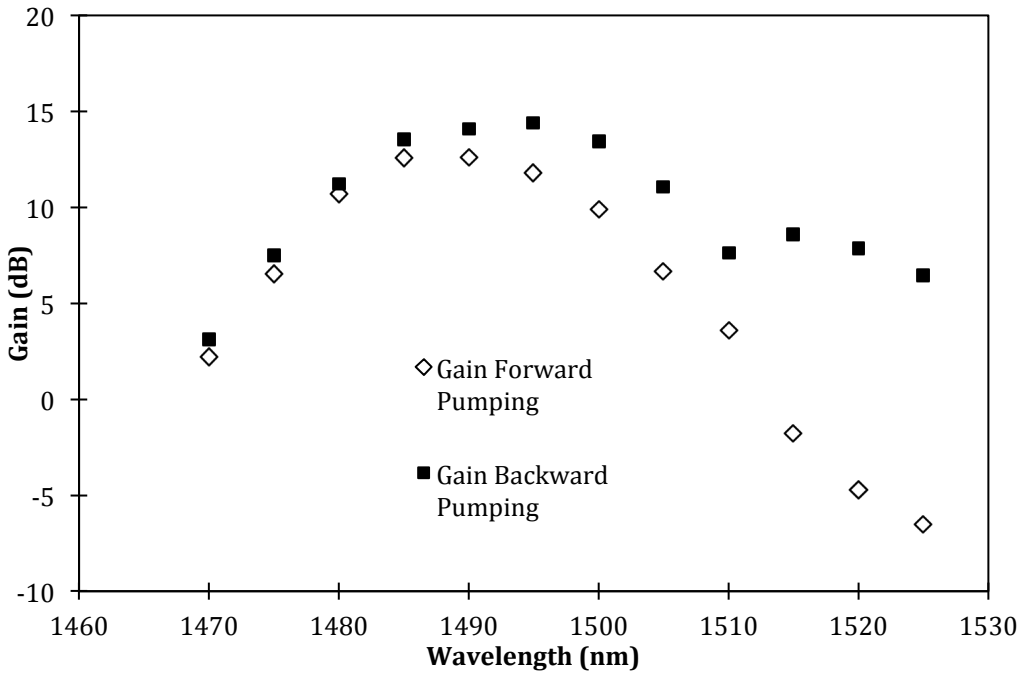

Figure 3.27: Gain with different input wavelengths and 0dBm input power

3.3.5 Noise Figure of Depressed Cladding Erbium Doped Fiber Amplifier

As shown in Figure 3.28 below, the NF for forward pumping and backward pumping of the DC-EDFA for several different input powers from -40 dBm to 5 dBm is plotted at a fixed wavelength of 1500 nm. From the figure, the NF is almost constant at 10.16dB and 11.7 dB for forward and backward pumping respectively for input powers of -40 dBm to -20 dBm. In the case of backward pumping, the NF increases when the input signal is changed from -15 dBm to 5 dBm. The maximum NF for backward pumping is about 15.17 dB at input signal 5dBm. This increment in the noise figure is due to that causes the gain to saturate at the EDF input end. This is also known as signal-induced saturation. The effect of signal-induced saturation is the change in the spontaneous emission factor n_{sp}. This occurs when the signal is high enough to significantly decrease the backward ASE near the fiber input end, causing a higher population inversion in this region. As this population inversion is higher at the EDFA input, a higher noise figure is thus seen. For the case of forward pumping, the NF is slightly reduced to 8.9 dB when input signal is increased from -15 dBm to -5 dBm before the NF increased to the 10.9 dB at input signal 5 dBm. The decreased of the NF is called dip effect and this occurs from signal saturation.

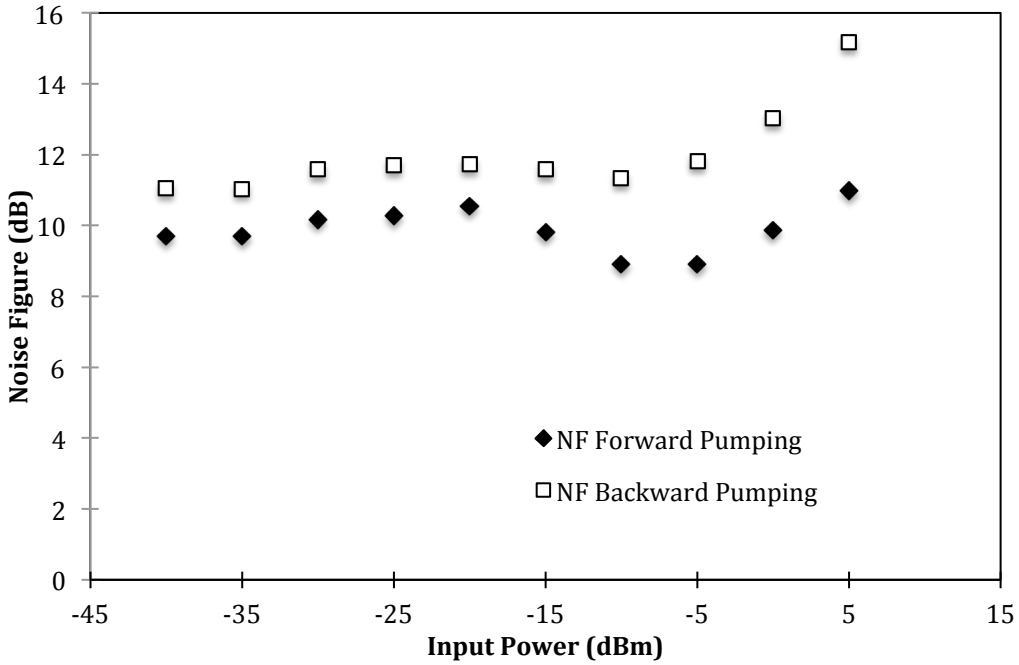

Figure 3.28: The NF performance with different input signal power at wavelength 1500nm

Figure 3.29 shows the NF at different wavelengths against a set of input power of -30 dBm. The wavelength is increased in 5 nm increments from 1450 nm to a final value of 1525 nm. The NF values for the backward pumping are measured to be higher compared to the forward pumping. This is prompted by the high saturation effect at the end of the setup in which it causes a higher value of NF. The average values of NF for forward pumping and backward pumping with different input wavelengths ranging from 1450 nm to 1525 nm with an input power -30 dBm are about 9.59 dB and 12.7 dB respectively. From the figure below it can be seen that the NF at input signal 1510 nm to 1525 nm is higher than the other wavelength. This is due to the distributed losses and also the fundamental mode cutoff which reduces the available output power,

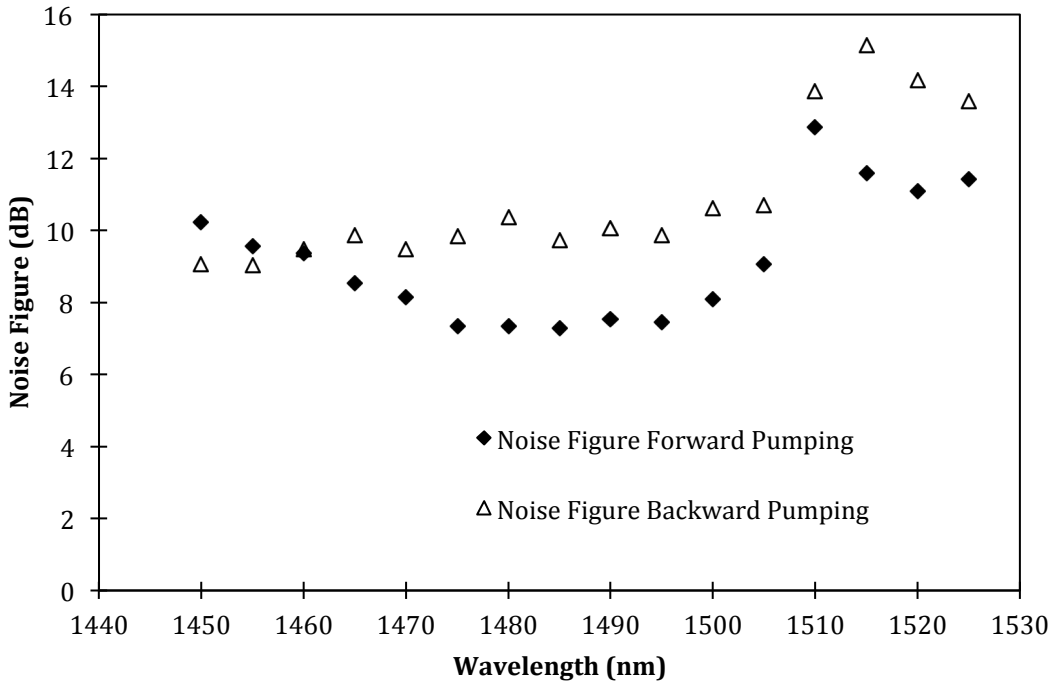

Figure 3.29 The NF performance with different input signal wavelength at input power -30 dBm

Figure 3.30 below shows the NF performance at different signal wavelengths and 0dBm input power for backward pumping and forward pumping setup of the DC-EDFA. The same behavior is shown in the figure which is the NF of the forward pumping setup is lower than the NF of the backward pumping setup. The NF of the forward pumping setup has significant drop at signal wavelength of 1475 nm to 1500 nm with an average NF at this region of about 8.4 dB while the NF of the backward pumping setup shown is almost flat NF from 1450 nm to 1495 nm with an average NF of about 11.27 dB. On average the NF of backward pumping setup is 3.69 times higher than the NF of the forward pumping setup

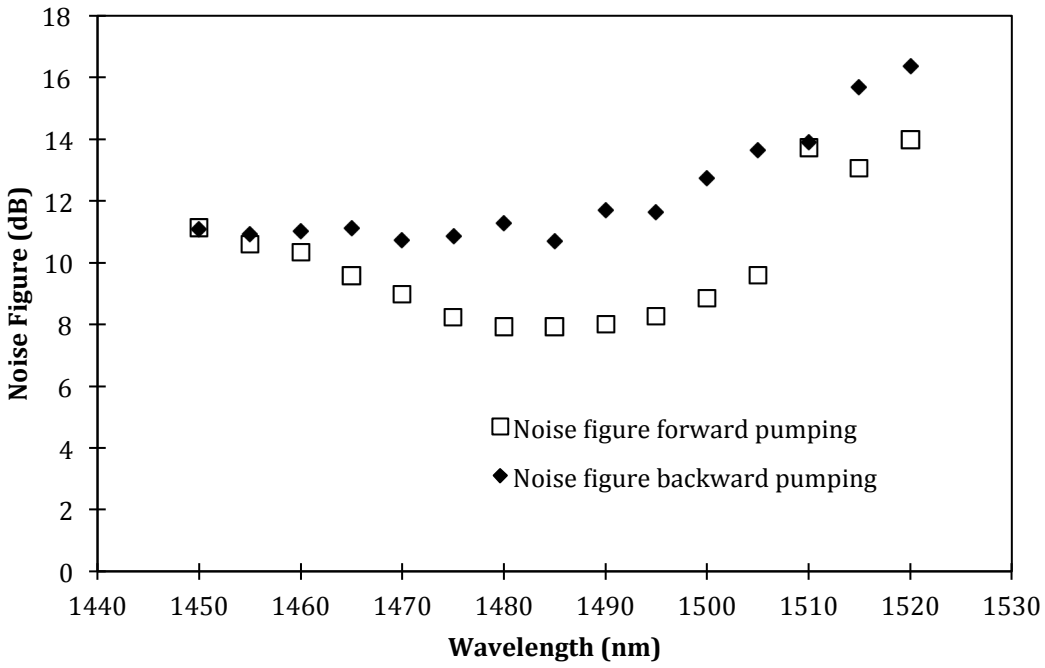

Figure 3.30 NF performance against different input signal wavelength at input power of 0 dBm

3.3.6 Flat bandwidth S-band Depressed Cladding Erbium Doped Fiber Amplifier

The other important characteristic of an optical amplifier is the flat gain of bandwidth. The WDM optical network system requires the same output power along the bandwidth, so the data rate is equal in the system. Normal approaches to get flat bandwidth of optical amplifier is by using gain flattening filter (GFF) normally made by FBG and also by ASE correction [19,20]. However, as shown in the Figure 3.21 the spectrum of the ASE of the DC-EDFA has to be designed by using the special GFF to flattened out the ASE. In our approach, we used the tunable Mach-Zehnder filter (TMZF) as a device to flatten the ASE. The TMZF has been chosen because this devise can adjust the wavelength spacing and the extinction ratio.

The experimental setup of the proposed S-band DC-EDFA with a TMZF is shown in Figure 3.31 below:

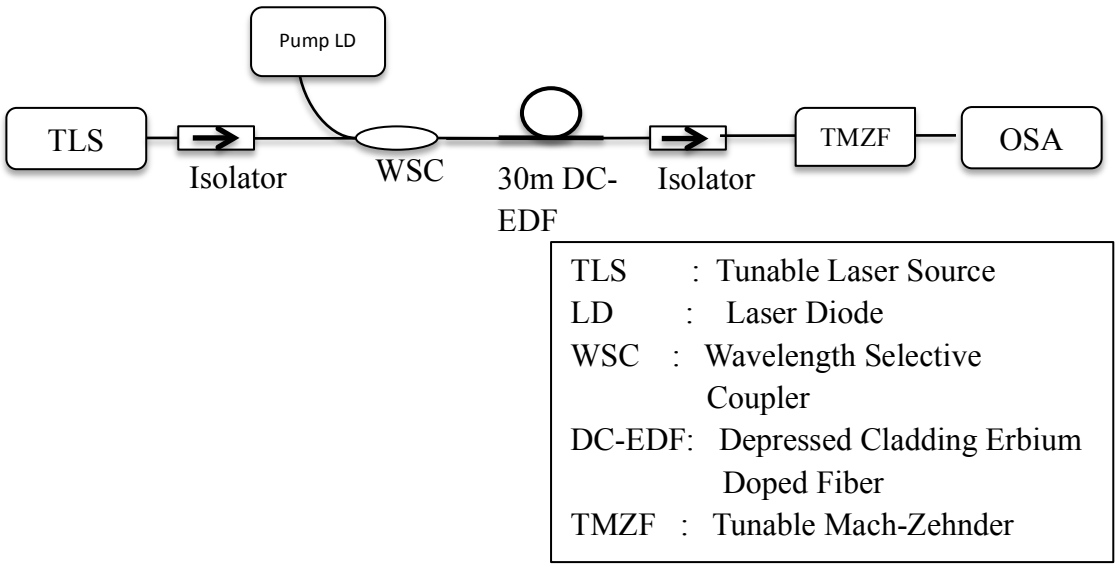

Figure 3.31 Experimental Setup of the Proposed S-band DC-EDFA with a TMZF

The experimental set-up comprises of a 30 m long DC-EDF with an absorption coefficient of 7.6 dBm/m at 980 nm. The DC-EDF is spooled into a ring of 8 cm diameter to optimize the ASE in the S-band region, which is manually adjusted to enhance the performance of the DC-EDFA in the 1480 nm to 1520 nm region. The pump source for the gain medium is a 980 nm laser diode operating at 300 mW spliced to the 980 nm port of a 980 / 1550 nm WSC (the 1550 nm port is spliced to the optical source that will act as the test signal). An optical isolator is used in the cavity to prevent back reflections and to also improve the noise figure. A TMZF is incorporated into the setup after the isolator to flatten the ASE output from the DC-EDF by inducing suitable loss in the C-band region. A TLS with a tuning range from 1460 nm to 1620 nm is used to generate the test signal that will be used to characterize the gain and noise figure of the proposed DC-EDFA, while an OSAwith a resolution of 0.02 nm is used to analyze the output of the proposed system. The system is automated to increase the efficiency and speed of the experiment as well as reducing possible errors that may arise due to manually obtained readings [21].

Figure 3.32 shows the gain and noise figure performance of the proposed system against different test signal wavelengths at an input power of -30 dBm.

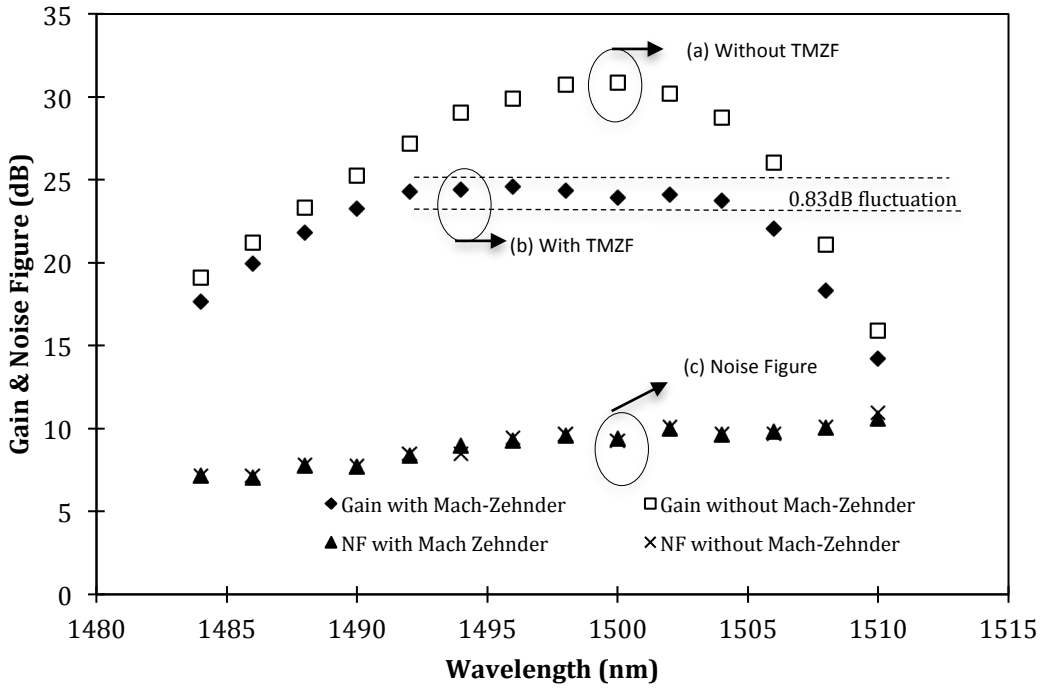

Figure 3.32 Gain and Noise Figure measurement at different input wavelength at input power of -30dBm (a) gain without TMZF (b) gain with TMZF (c) noise figure for both cases

From Figure 3.32 it can be clearly seen that the TMFZ is able to flatten the gain spectrum of the S-band DC-EDFA when it is tuned to the correct region of the ASE spectrum. A flat gain spectrum is achieved with an average gain of 24.21 dB over a wavelength region of 1492 nm to 1504 nm, with only minor gain fluctuations of approximately 0.83 dB and a 3 dB bandwidth of 18 nm. However, it is observed that the highest gain obtained by the system with the TMZF incorporated is 6.4 dB lower than the highest gain obtained by the system without the TMZF, as this is attributed by the loss factor of the TMZF in flattening the gain spectrum. The noise figure also does not vary much for both setups of the proposed system (i.e. with and without the TMZF). The measured noise figure is approximately 7.13 dB and increases to 10.94 dB as the input signal wavelength increases from 1484 nm to 1510 nm.

The insertion loss of the TMZF and the gain difference is shown in Figure 3.33.

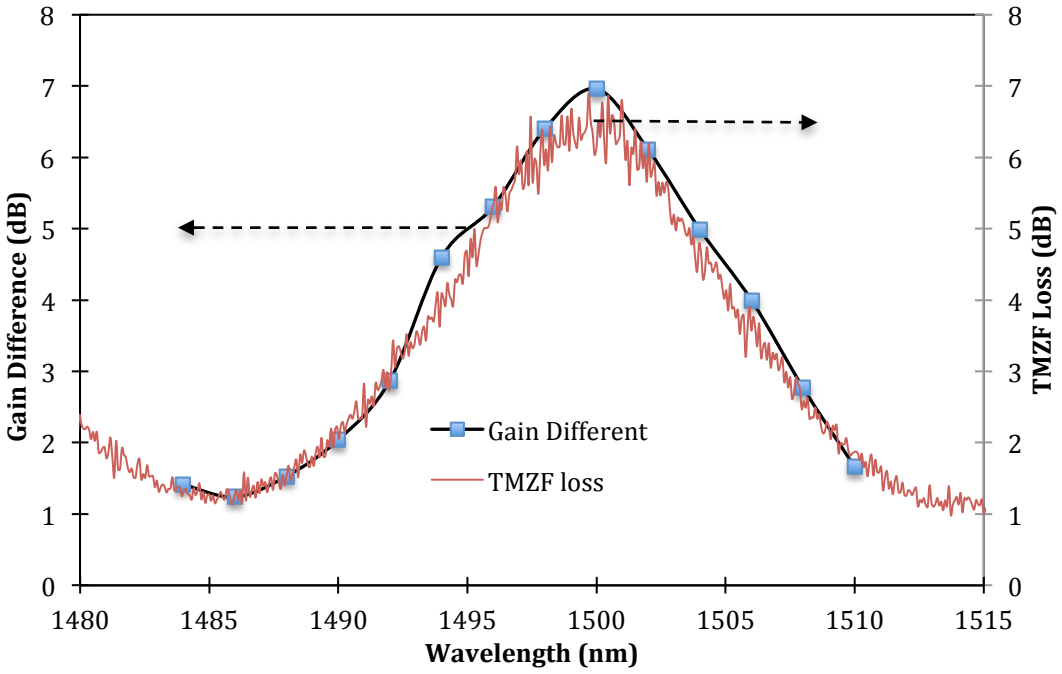

Figure 3.33 Loss measurement at different wavelength of TMZF and gain difference without and with TMZF

Figure 3.33 shows the characteristic behavior of the TMZF obtained using a white light source. It shows the loss spectrum of the proposed setup, and it can be seen that the gain difference spectrum closely matches that of the TMZF loss, thus inferring that the TMZF is the responsible component for flattening the gain of the proposed system

Figure 3.34 shows the actual testing of the S-band DC-EDF optical amplifier from input signal at λ_1 (1490 nm), λ_2 (1495 nm), λ_3 (1500 nm) and λ_4 (1505 nm) with in channel spacing of 5 nm. Figure 3.34 (a) shows the four channel input of the proposed setup, whilst Figure 3.34(b) shows the amplified riding on top of the ASE. It can be seen from Figure 3.34(b) that peaks of the signal wavelengths are not flat, and instead have values of λ_1 at -10.03 dBm, λ_2 at 8.97 dBm, λ_3 at -6.54 dBm and λ_4 at 9.89 dBm for the case without TMZF. In the case of the system with the TMZF, the amplifier provides a flat response with an average peak value of 10.5 dBm with peak variation of 0.082 dB. In

this regards, the proposed design will provide an efficient optical amplifier in the S-band region which has a flat response from 1490 nm to 1505 nm.

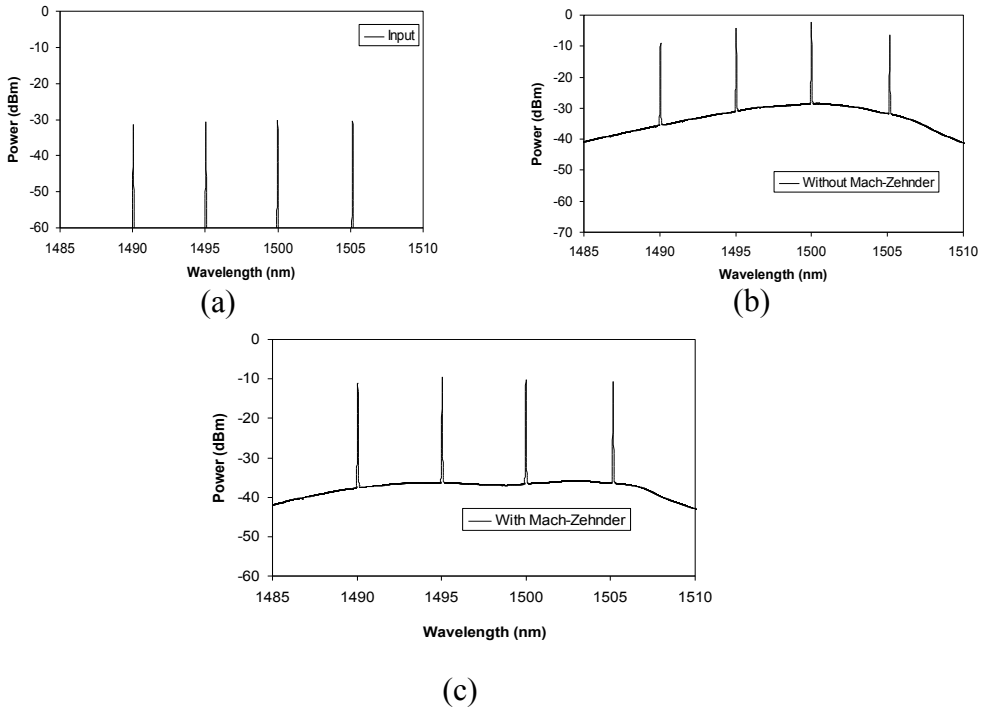

Figure 3.34: Multiple channels test on the amplification behavior of the S-band DC-EDF Optical Amplifier.

3.3.7 Low Noise Figure of S-band Amplifier with Cascading Depressed Cladding Erbium Doped Fiber Amplifier and Erbium Doped Fiber Amplifier

One of the disadvantages of the DC-EDFA is a higher NF, as reported by [22, 23]. To overcome this problem, a novel design has to be done to make S-band DC-EDFA with lower NF by cascading the gain medium which is DC-EDF and EDF. As discuss in EDFA section the S-band EDFA has lower gain but good quality of the NF discussed while the gain of DC-EDFA is higher but the quality of the NF is poor. From this issue we make a novel design to overcome this problem.

Figure 3.35 shows the experimental setup of the proposed low NF S-band amplifier. Figure 3.35(a) shows the S-band DC-EDFA with a 30m length of DC-EDF with about 7.6dB/m of absorption at 980 nm. The DC-EDF is pumped using a 980 nm Laser Diode (LD) at 300mW of output power. A high pump power is required to provide a full population inversion in the DC-EDF, due to the relatively long length of fiber being used. The LD output power is combined with the signal using a 980 nm/1500 nm WSC fused coupler. The S-band TLS with a tuning range of 1460 nm-1530 nm is used as an input signal for the amplifier. Optical isolators are used at the input and output of DC-EDF to give a unidirectional propagation of the signal and the ASE. Figure 3.35(b) shows the proposed setup of the low noise S-band amplifier. The proposed low noise S-band EDFA consists of additional 3m length EDF with an absorption of about 11dB/m at 980 nm. The high germanium co-doped EDF is composed of the erbium-doped fiber that is co-doped with germanium by 12% in molarity. The EDF is pumped using a 980 nm LD at 92 mW of output power and it is combined with a 1500 nm signal wavelength using a WDM. The proposed low noise S-band amplifier is generally a cascade or a hybrid of two different EDF. The first stage of the amplifier uses the highly germanium co doped EDF and the second stage the DC-EDF as the gain mediums. The gain and NF

for both setups are analyzed using an OSA, assisted by an automated measurement system for data accumulation [21].

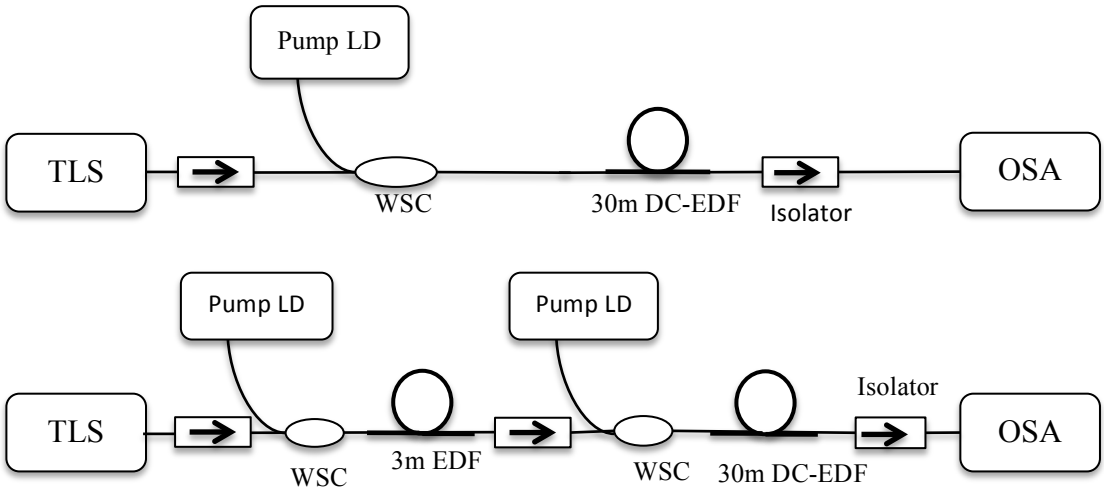

Figure 3.35 The experimental setup of (a) conventional DC-EDFA (b) hybrid S-band optical amplifier

The high germanium co-doped EDF is used as a pre-amplifier and it is connected to the DC-EDFA in a cascaded configuration, namely hybrid S-band EDFA. The performance of the gain and NF of hybrid S-band EDFA is shown in Figure 3.36. The gain and NF are than studied at variation of pump power of the pre-amplifier whilst the pump power of DC-EDFA is fixed. The gain increases linearly at the pump power between 0 to 10mW and then shows a flat profile after the pump power is further increased to 67.1mW while the NF is observed to be decreasing with the increasing pump power. The lowest NF recorded at the highest pump power is about 5.61dB. Figure 3.36 also shows that the gain signal finally reaches its saturation condition after 10mW of pump power is injected into the pre-amp. This is due to the DC-EDFA has been in its gain saturation condition. Note that only small amount of ASE power from the pre-amp that mainly causes the saturation of DC-EDFA

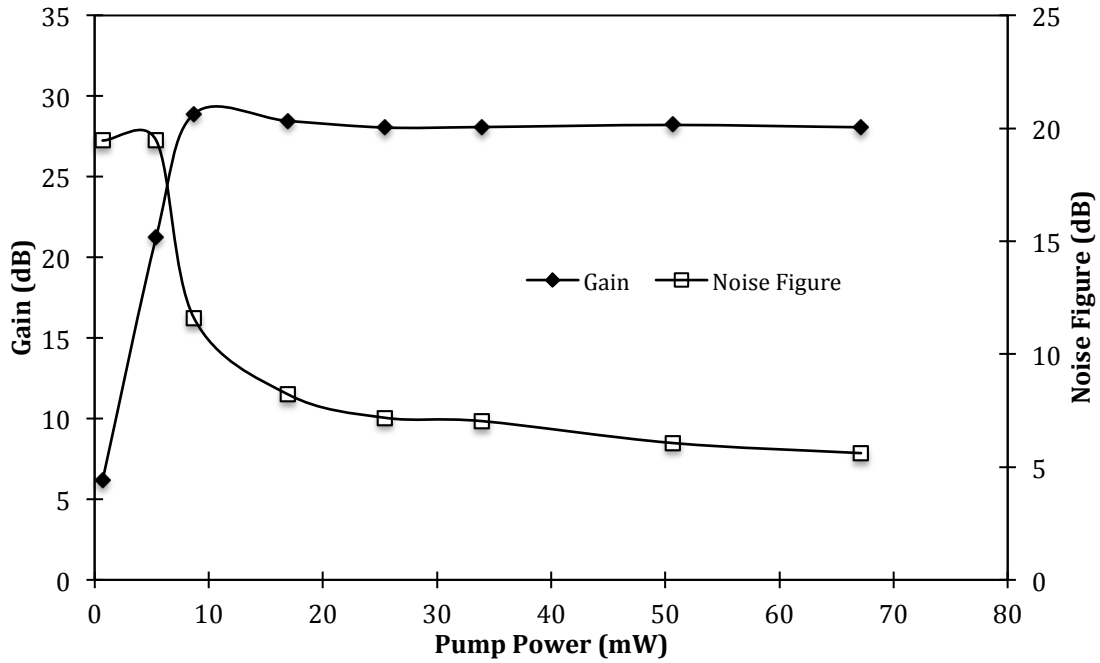

Figure 3.36 The gain and NF performance of Hybrid S-band EDFA with different pump power of pre-amplifier

Figure 3.37 shows the gain and NF performance of the hybrid S-band EDFA and the conventional S-band EDFA setup with different input powers at center wavelength of 1500nm. It is obvious that the saturation effect is the biggest influence of the gain profile of the hybrid S-band EDFA compared to the conventional S-band EDFA. The gain difference of hybrid S-band EDFA is less than 4 dB at the low input powers between -40 dBm to -15 dBm and the difference becomes smaller when the input power is higher than -15 dBm. The interesting observation is the NF performance of the hybrid S-EDFA. The NF of the hybrid S-EDFA is significantly lower than the conventional S-band EDFA. The NF of hybrid S-EDFA experiences a penalty of about 3.81 dB at low input signal. The improvement of NF in the hybrid configuration is attributed by the high quality of SNR signal that passes through the pre-amp and also due to the low NF design of high germanium co doped EDF. The combination of this effect then result inlow NF in the hybrid S-EDFA.

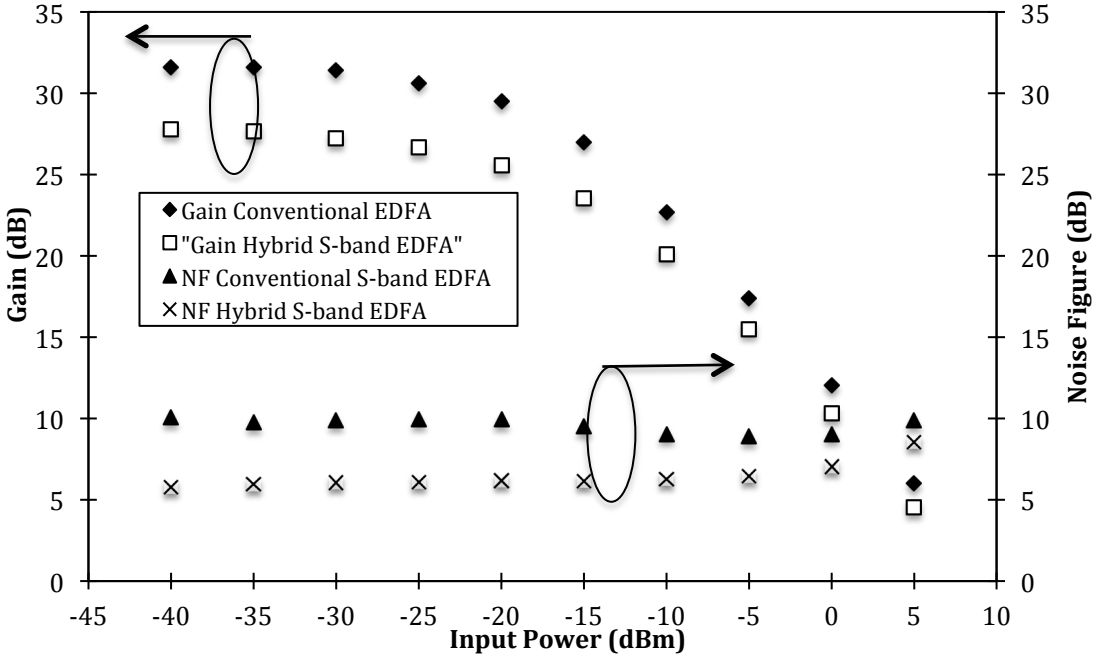

Figure 3.37 The performance of gain and NF between hybrid S-band EDFA and conventional S-band EDFA with different pump power at 1500 nm center wavelength

Figure 3.38 shows the performance of the gain and NF for both setups with different input wavelength at input power of -30 dBm. The setup of conventional S-band EDFA shows higher gain compared to hybrid S-band EDFA at wavelength range from 1480 nm to 1505 nm. The largest gain difference is calculated to be about 5.43 dB at 1485 nm. The largest difference in the shorter wavelength region is fairly large due to the pre-amplifier characteristic that is recorded to generate only small signal gain at shorter wavelength as discussed earlier. The NF for hybrid S-band EDFA is noted to be lower than the conventional S-band EDFA. The NF penalty is observed to be larger towards the longer wavelength due to the increased SNR of the high germanium co-doped EDF towards the C-band region.

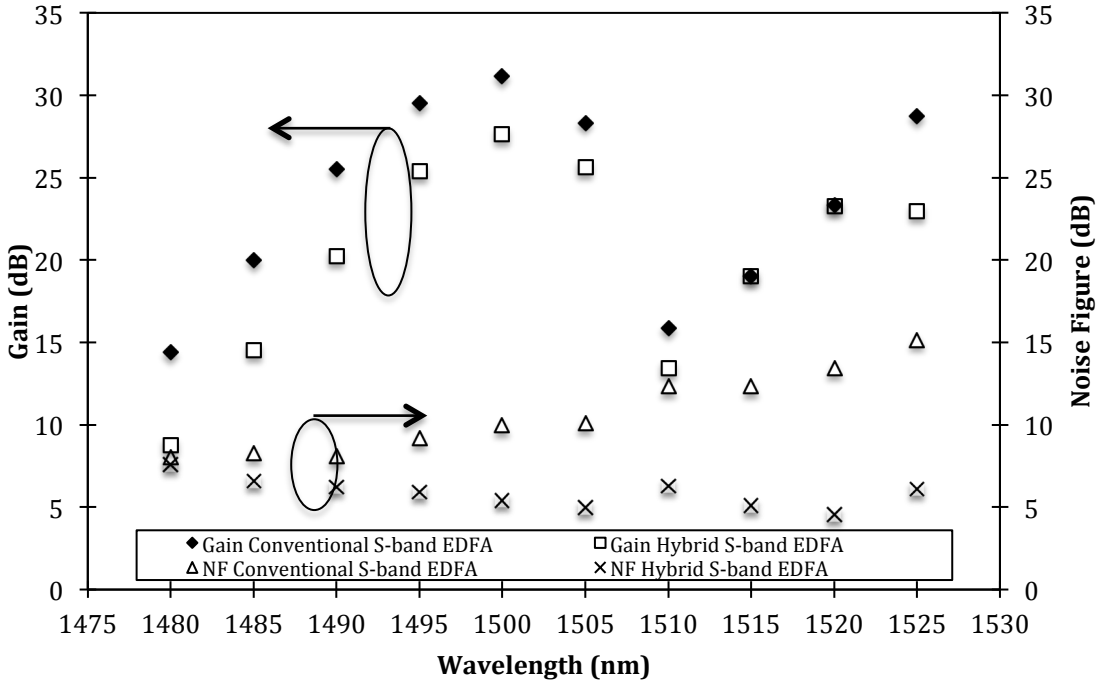

Figure 3.38 The gain and NF with different input wavelength at input power -30dBm

The performance of both setups is also studied at high input signal power of 0dBm. Figure 3.39 shows that the gain of the conventional S-band EDFA setup is also higher compared to the hybrid S-band EDFA. The highest gain recorded is about 14.82dB at 1485 nm for conventional setup and 13.41 dB at wavelength 1490 nm for hybrid S-band EDFA. At high input signal, wavelengths longer than 1505 nm experiences a high saturation effect that causes the signal to be reabsorbed at the DC-EDF and this maneuveres to a negative gain occurrence. This effect is experienced in both setups.

At high input signal power, the NF values between the two setups show only small differences at shorter wavelength. However, larger differences can be seen in the NF values observed towards longer signal wavelengths starting from 1495 nm with the largest difference at 1505 nm. Because of the negative gain, the NF is also showing a higher value for both setups at wavelengths longer than 1510 nm with an average NF is about 17 dB.

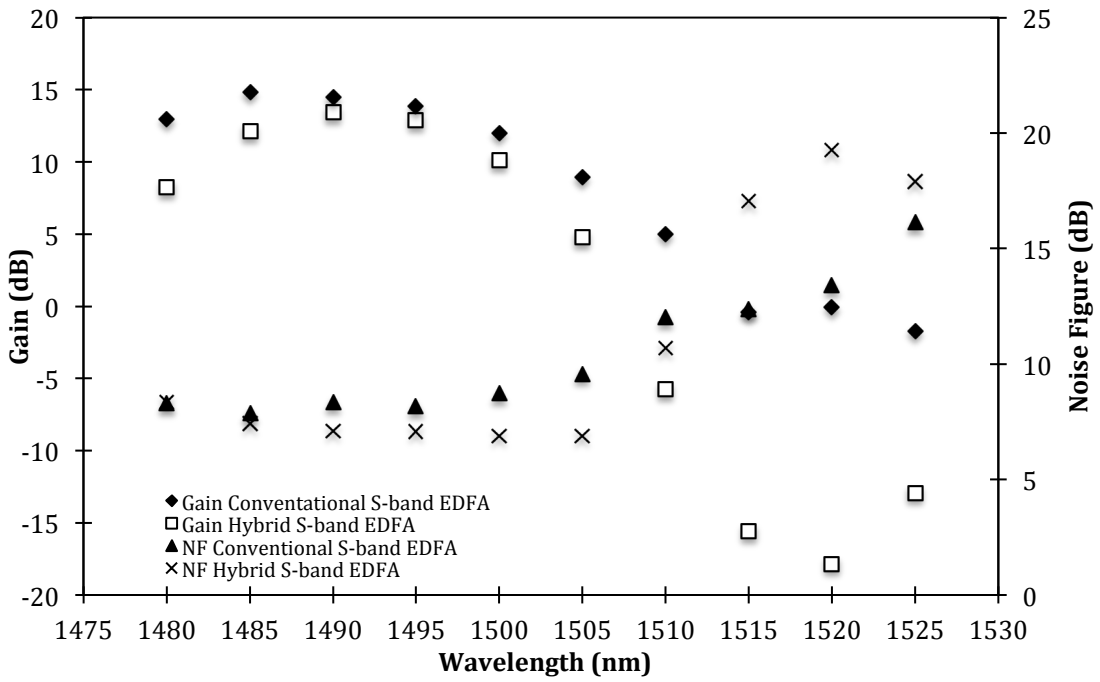

Figure 3.39 Gain and NF performance with different input wavelength in the high input signal (0dBm)

3.4 S-Band Raman Amplifier

3.4.1 Type of Raman Amplifier

Raman Amplifier (RA) is one type of optical amplifier which can provide amplification in the S-band region. The advantage of RA is that it can amplify the signal in any band depending largely on the Raman Pump (RP) wavelength. RA can be categorized into three categories, distributed, discrete or lumped and also hybrid RA

3.4.1.1 Distribute Raman Amplifier

The Distribute Raman Amplifier (DRA) is an amplifier where the pump power extends into the transmission line fiber [24]. The DRA normally uses the transmission optical fiber network as a gain medium. Figure 3.40 shows the setup of the DRA.

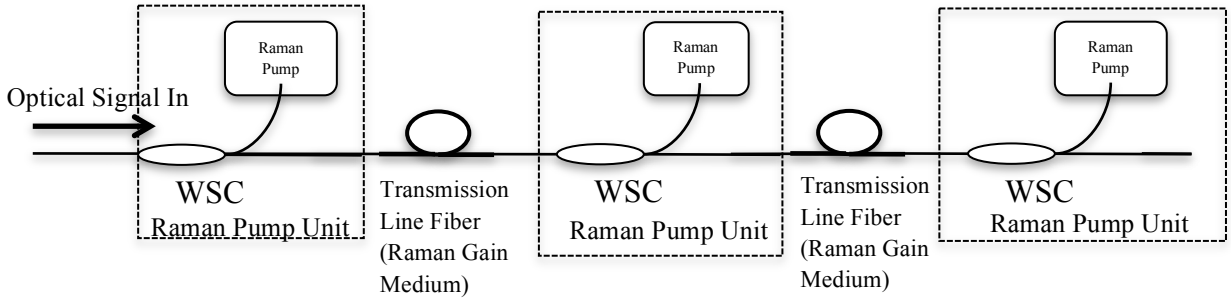

Figure 3.40 The Distribute Raman Amplifier configuration in optical network system

There are many advantages of DRA in literature [25]. One of the advantages of DRA is that can achieve longer span [26,27] or higher bit rate due to its advantages in the improvement of the SNR. However the DRA is not covered in this thesis because all of the S-band Optical amplifier were discussed are basically using their own gain medium and provide black box gain.

3.4.1.2 Discrete Raman Amplifier

Discrete Raman amplifier can be defined as lumped element that is inserted into the transmission line to provide gain, like EDFA and SOA Discrete Raman amplifier has input and output terminal as shown in the Figure 3.41. In our experiment, the Raman Gain Fiber that is used in this setup is the Dispersion Compensated Fiber (DCF) from

Corning Incorporated as this fiber can provide higher gain of RA. The result and discussion are discussed in section 3.5.2

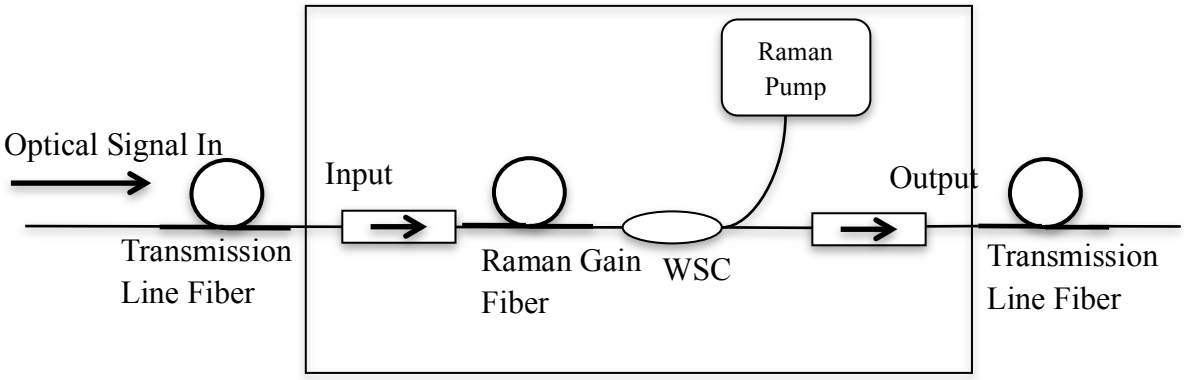

Figure 3.41 The configuration setup of a Discrete Raman Amplifier

3.4.1.3 Hybrid Raman Amplifier

Other type of Raman amplifier is the hybrid Raman amplifier (HRA). HRA is an amplifier which combines two gain medium such as combining EDFA and SOA together. Figure 3.42 shows the example of HRA. The advantage of Hybrid Raman Amplifier is that it can provide high gain and it is also able to overcome the drawback of an EDFA or an SOA

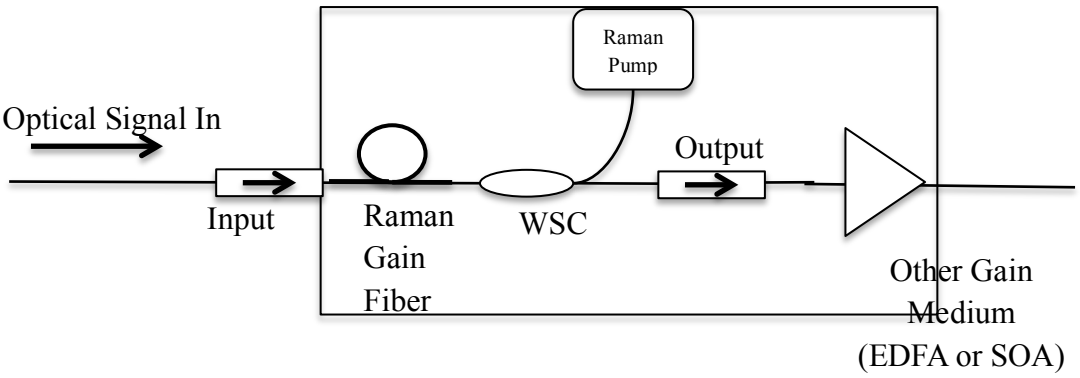

Figure 3.42 The Hybrid Raman amplifier setup.

3.4.2 Characteristics of S-band Discrete Raman Amplifier

Figure 3.43 shows the setup of S-band Discrete Raman Amplifier which consists of a TLS, two Raman pumps with both having pump wavelength of 1425 nm and with total power of 390mW, WSC (WSC1 and WSC2) to combine and split the power of the signal and Raman pump. As for the amplifier medium, the dispersion compensated fiber (DCF) as nonlinear media with an effective core area of 55μm^2 and a length of 7.7km is used. The Raman amplifier is built from this setup by injecting Raman pump laser into the amplifier medium through WSC1. The signal that comes from the TLS will be amplified due to the Raman scattering effect along the amplifier medium. The spectrum is analysed by an OSA.

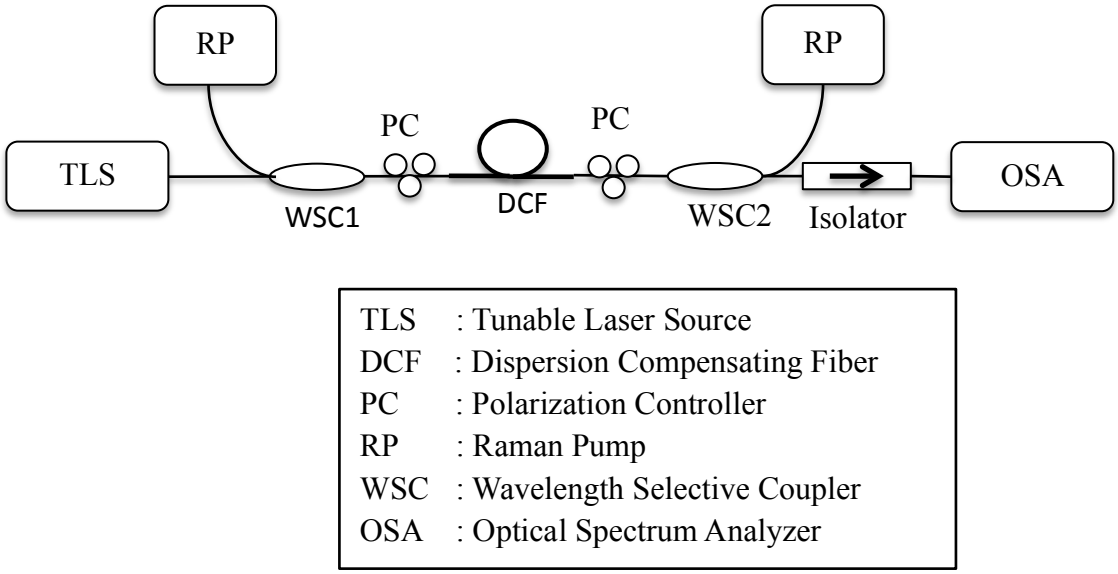

Figure 3.43 The experimental setup of S-band Discrete Raman Amplifier

3.4.2.1 Pump Efficiency of S-band Discrete Raman Amplifier

Figure 3.44 shows the gain of the Discrete Raman Amplifier at signal wavelength of 1500 nm and input signal power of -30 dBm and 0 dBm. The gain for both input signal power shows linear response with the increased of Raman pump power. The positive gain only starts when Raman pump power exceeds 250 mW for both input signal power. Due to the lack of Raman pump power the maximum gain we can achieve is about 4.8 dB for both input signal power with the Raman pump power is about 390 mW. We believe the gain of Discrete Raman Amplifier can be obtained higher if we pump with higher Raman pump power. From the experiment, the gain over Raman pump power is found to be 0.04 dB/mW.

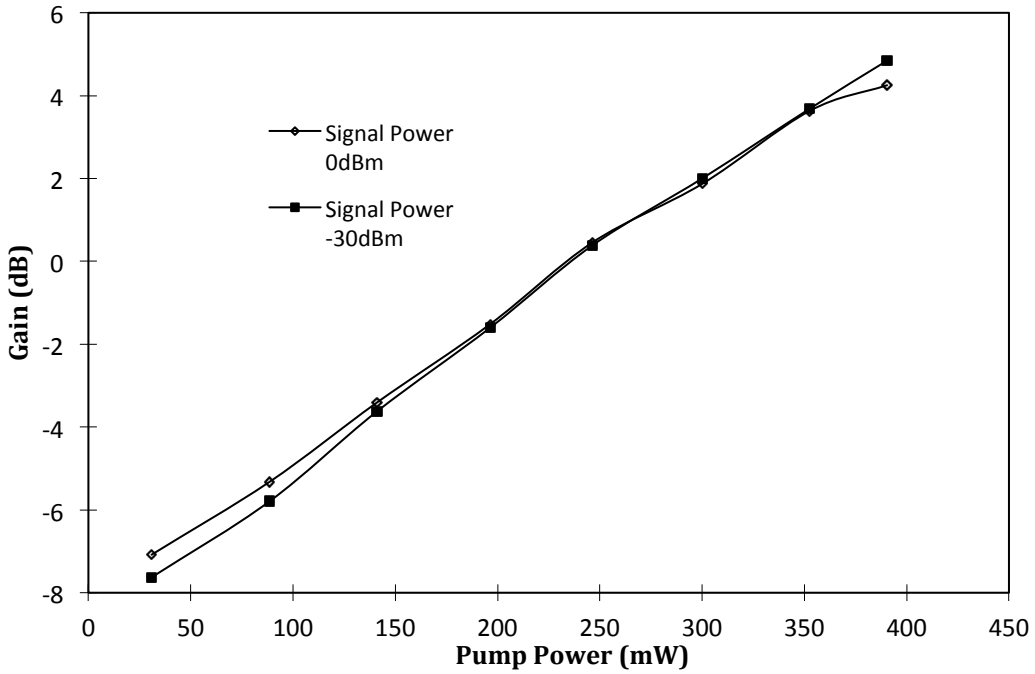

Figure 3.44 The gain of S-band Discrete Raman Amplifier with different Raman Pump Power at signal wavelength 1500 nm and input signal power -30 dBm and 0 dBm

3.4.2.2 Small – Signal and Saturation Gain of Discrete Raman Amplifier

Figure 3.45 shows the gain of Discrete Raman Amplifier at different input signal power and the signal wavelength is 1500 nm. The gain at low signal power shows constant value of about 5.48dB from input signal power of -45 dBm to -5 dBm. Compared to the EDFA and SOA, the 3 dB saturation input signal gain of Raman amplifier is higher, which is about -2 dBm and this makes the Raman amplifier having an advantage for the use in high power fiber laser setup. Figure 3.45 also shows the gain at higher input signal from 0 to 5dBm drops due to saturation effect and proved the limitation of Raman pump power to produce enough ASE at higher signal gain regime.

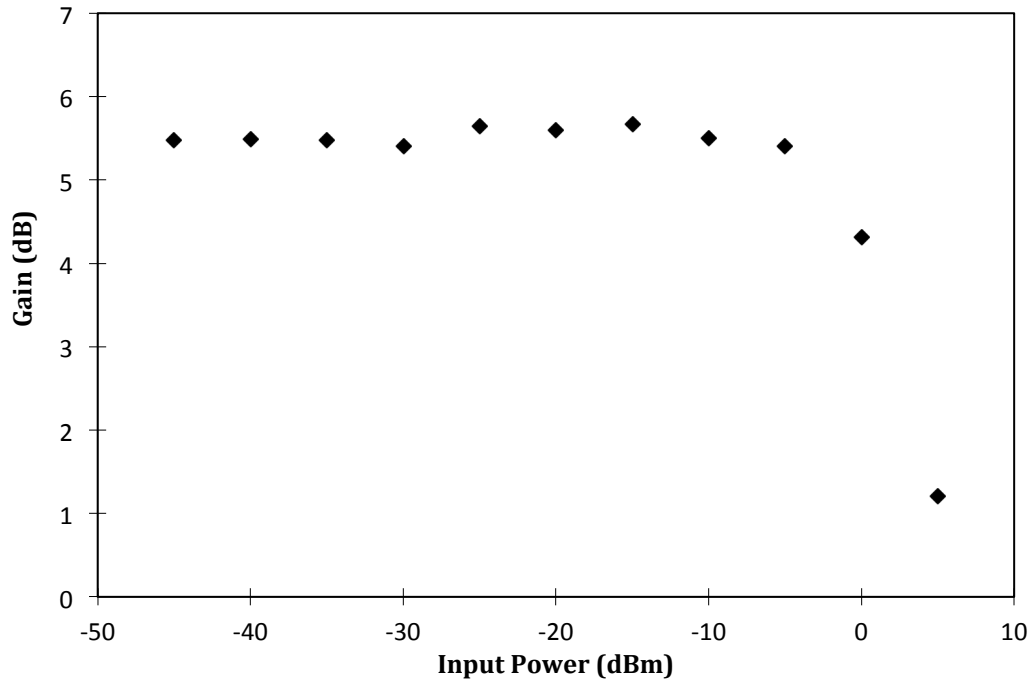

Figure 3.45 The gain of S-band Discrete Raman Amplifier with different input signal power and signal wavelength 1500 nm

3.4.2.3 Gain Bandwidth of S-band Discrete Raman Amplifier

From the literature the good features of Raman amplifier is able to provide a wide bandwidth. The Raman amplifier bandwidth can be chosen and it depends on the wavelength of the Raman pump. Figure 3.46 shows the gain of S-band Discrete Raman Amplifier at different input signal wavelengths at input signal of -30 dBm and 0 dBm, only using Raman pump wavelength of 1425 nm. The gain bandwidth covered is 30 nm from 1500 nm to 1530 nm with the highest gain obtained at input signal of 1510 nm which is about 6.17 dB. The small fluctuation of the gain can be adjusted by controlling the polarization effect of the setup.

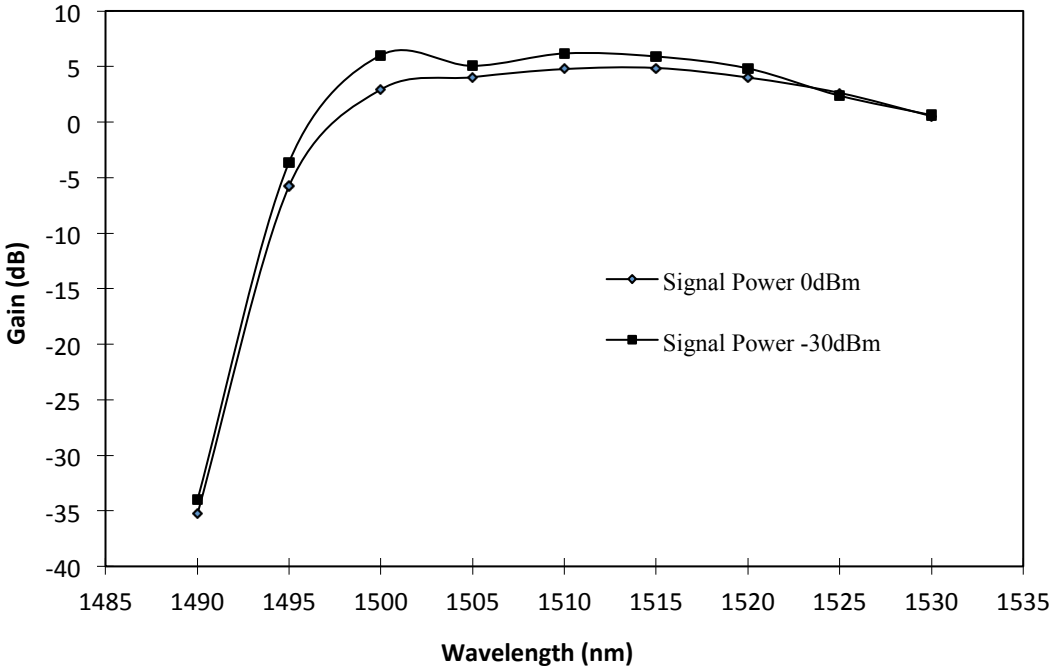

Figure 3.46 The gain of S-band Discrete Raman Amplifier at different input signal wavelengths with input signal of -30 dBm and 0 dBm

To demonstrate the effect of the pump wavelength, one of the 1425 nm Raman pump from the Raman amplifier setup as show in the Figure 3.43 is changed to 1420 nm Raman pump with the same pump power. The S-band Discrete Raman amplifier has now two different Raman pumps wavelength 1420 nm and 1425 nm respectively. Figure 3.47 shows the comparison of the gain by using the same and different wavelength of Raman pump. As explained in the literature, when the wavelength of the Raman pump is changed, the gain bandwidth increases. The gain bandwidth increases 5nm when the Raman fiber is pumped by using the 1420 nm and 1425 nm Raman Pump .The bandwidth is extended from 1490 nm to 1530 nm and the smallest gain is recorded at input wavelength of 1490 nm which is about 0.7 dB for both input signal power.

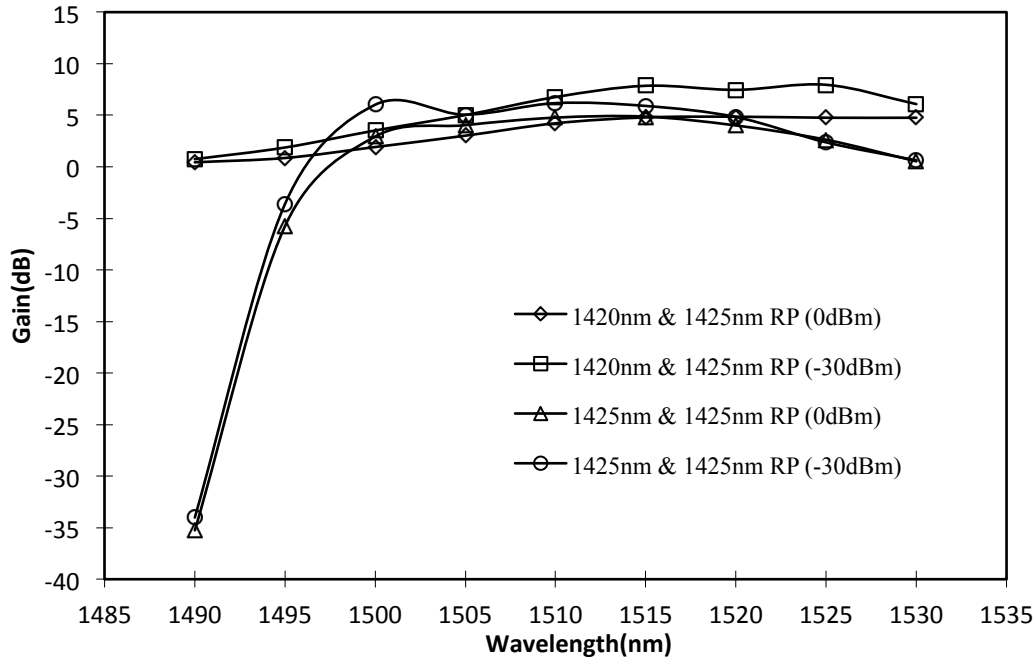

Figure 3.47 The comparison of gain by using same wavelength of Raman pump and different wavelength of Raman pump

3.4.2.4 Noise Figure in S-band Discrete Raman Amplifier

The NF of S-band Raman amplifier measured for different Raman pump power and different input signal power -30 dBm and 0 dBm is shown in the Figure 3.48. The NF value for input signal -30 dBm reduce from 7.8 dB to 5.3 dB when the Raman pump power is increased from 30.7 mW to 390.4mW. For the case high input signal, the NF value also increases when the Raman pump power is increased but slightly fluctuating at from 300 mW to 390 mW. This is due to polarization sensitive of the S-band Raman amplifier.

The measurement of NF is also taken with different input signal at 1500 nm wavelength. With the same pattern obtained by using S-band EDFA, DC-EDFA and

SOA, the S-band Raman amplifier also has higher value of NF with 8.0 dB at higher input signal and 4.3 dB at lower input signal as show in the Figure 3.49.

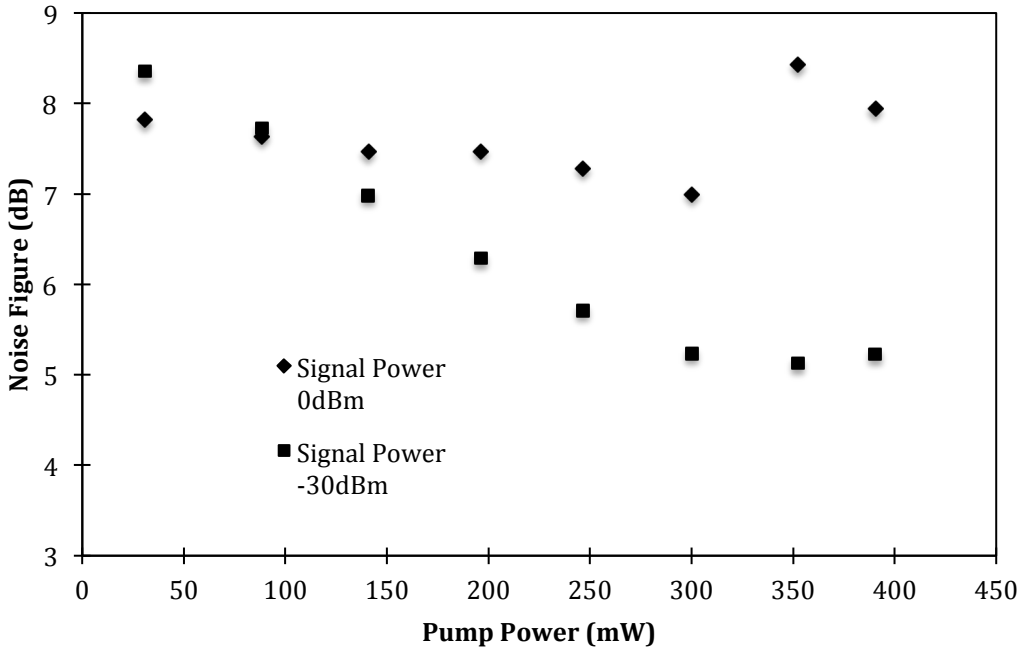

Figure 3.48 The performance of NF of Raman Amplifier with different Raman Pump and input power at 1500 nm input wavelength

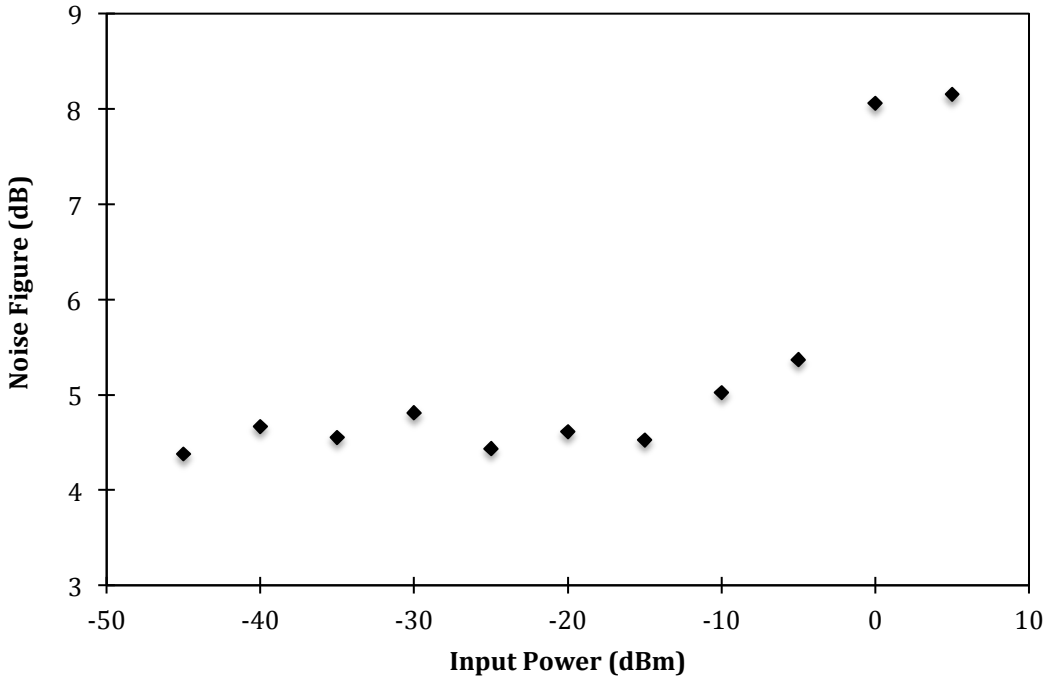

Figure 3.49 The performance of NF of Raman Amplifier with different input signal power at wavelength of 1500 nm.

Figure 3.50 shows the NF value at different input wavelength with fix input power values of -30dBm and 0dBm. The NF is about 4.8dB at input signal – of 30dBm and slightly higher at input signal 0dBm which is 6.9dB. Contradict with the gain value of different input wavelength, the high NF is measured when the input wavelength is not in the region of the gain bandwidth.

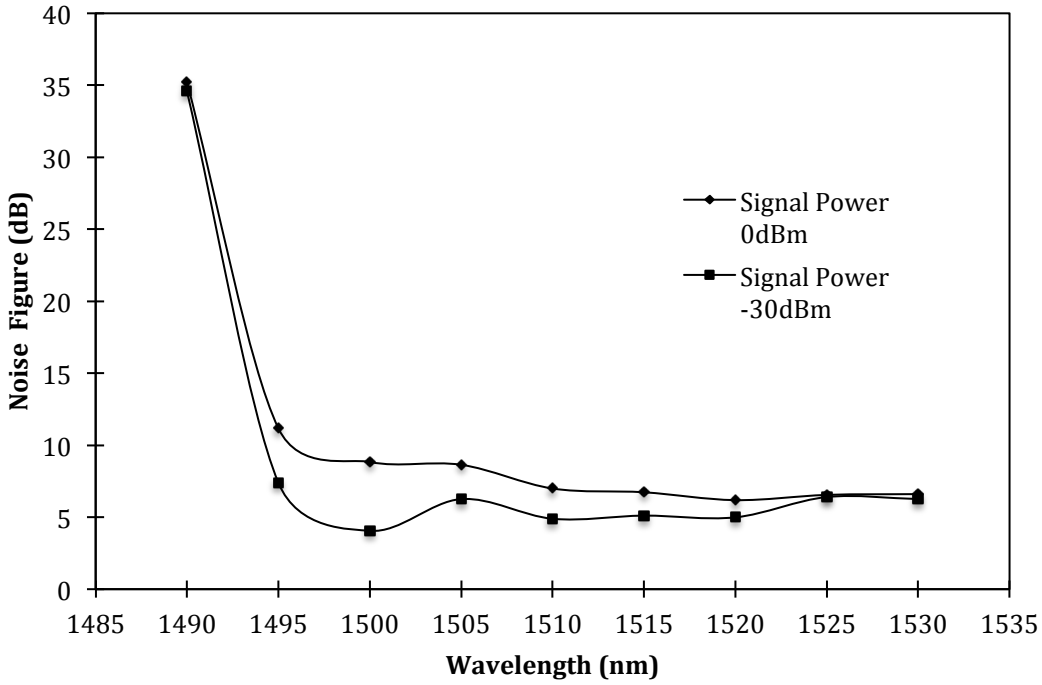

Figure 3.50 The performance of NF of Raman Amplifier with different input signal wavelength at input power of 0dBm and -30dBm

3.5 Semiconductor Optical Amplifier

Semiconductor Optical Amplifier is a device which has more compactness of the packaging compared to EDFA besides being pumped electrically [28]. Most of the SOA is fabricated to operate in the 1310 nm and 1550 nm range. SOA also has many advantages, especially in non-linear applications such as, four-wave mixing (FWM),

wavelength converter and optical switch [29-34]. In this section, we characterize the performance of SOA in the amplification of S-band in terms of gain, NF and polarization dependence gain and also its ability to produce ultra wide band amplifier which also supports the gain at C-band (1530 nm to 1560 nm) and L-band (1561 nm-1620 nm).

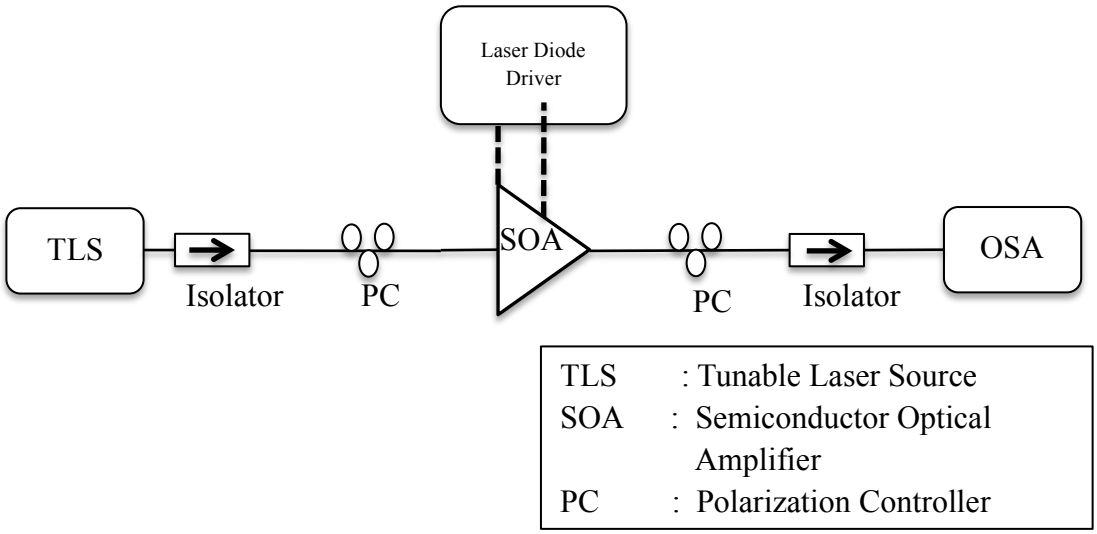

Figure 3.51 Experimental setup of an SOA as S-band amplifier

The experimental setup is shown in Figure 3.51, which consists of the SOA (Alphion) as the gain medium in the amplifier configuration. The SOA is fabricated by utilizing the quantum dot technology in order to provide a wide band ASE. The SOA is driven at input current of 460 mA. A wide band TLS with a tunability range of 1440 nm to 1600 nm is used to provide the signal input. A pair of C-band optical isolators with 1.5 dB insertion loss in the S-band and 0.9 dB insertion loss in the L-band region has been utilized in the configuration to create a uni-directional propagating signal. The isolators are placed before and after SOA. To minimize the effect of polarization dependent gain

(PDG) in the output spectrum, two polarization controllers (PCs) are located at the input and at the output of the SOA. An OSA with a resolution of 0.02 nm has been used to analyze the gain and noise figure of the output spectrum.

3.5.1 Amplified Spontaneous Emissions of Semiconductor Optical Amplifier

As shown in the Figure 3.52 below, the ASE spectrum of the SOA covers the whole wavelength range from 1420 nm until 1620 nm, with a bandwidth of about 200 nm. As noted, the ASE spectrum covers the three detrimental transmission regions of communication which include the S-band (1460 nm-1530 nm), C-band (1530 nm-1560 nm) and L-band (1565 nm-1625 nm). The ASE spectrum reading is taken through several drive current variations of 70 mA, 110 mA, 190 mA, 230 mA and 390 mA. The maximum drive current of 390 mA is observed to attain the widest bandwidth and highest level of ASE spectrum compared to the rest of the drive currents.

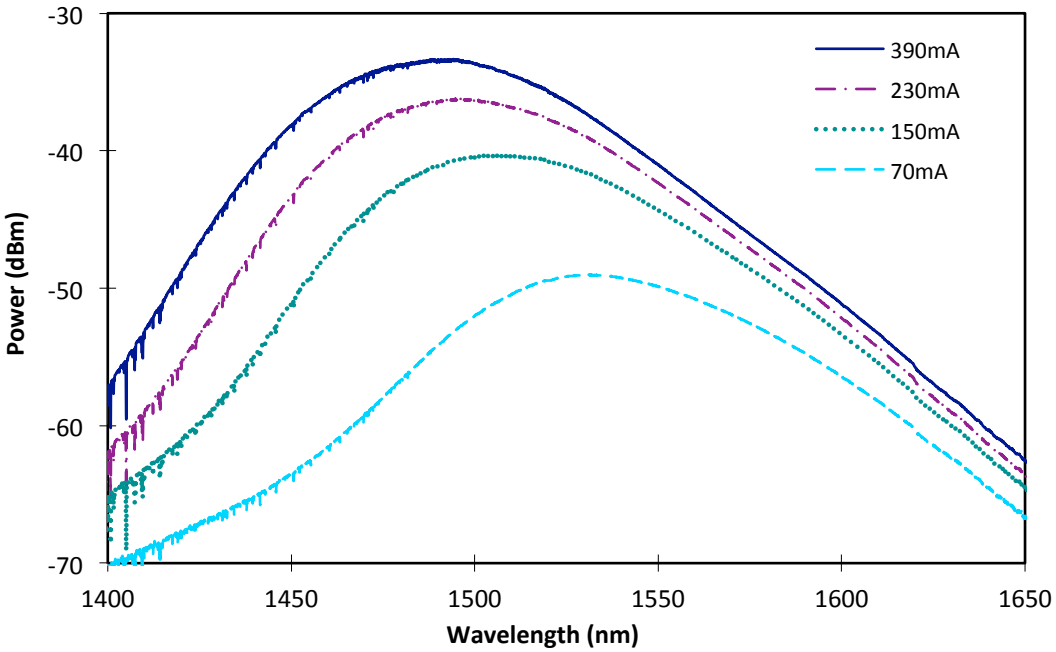

Figure 3.52 Amplified Spontaneous Emission (ASE) of injection current variations.

3.5.2 Gain Bandwidth of Semiconductor Optical Amplifier

Figure 3.53(a) shows the graph of the gain at different wavelengths from 1440 nm to 1600 nm at input signal power of -30 dBm. The gain bandwidth at low input power is about 160nm wide. In the S+ band region (1440 nm to 1480 nm) the gain increases linearly from 9.88 dB to 23.57 dB. However, at wavelength of 1472 nm, the gain drops to 21.2 dB due to the PDG effect. The PDG effect will be discussed in section 3.6.5. The gain in S-band shows a nearly flat pattern from 1485 nm-1525 nm. This gain profile is more advantageous compared to wide band gain silica erbium doped fiber that has been reported earlier to show a decrease in the gain in this region [35]. At the C-band and L-band region the gain shows a linear decrement from 23.1dB at 1530nm to 8.5 dB at 1600 nm.

Figure 3.53 (b) below shows the gain results at wavelengths variation for 0 dBm signal input power. It can be observed that the gain pattern increase linearly in the short wavelength region of 1440 nm to 1480 nm. The gain pattern also shows a slower increment within the wavelength range of 1480 nm to 1530 nm, giving a nearly flat gain profile. Compared to the previous graph of the -30 dBm input power, it can be seen that higher input power 0dBm input signal produced nearly equal gain value for each transmission wavelengths while lower input power (-30 dBm input signal) creats a gain pattern that follows the ASE pattern mainly due to the saturation gain of input signal. The saturation gain will be characterized and discussed in the next section.

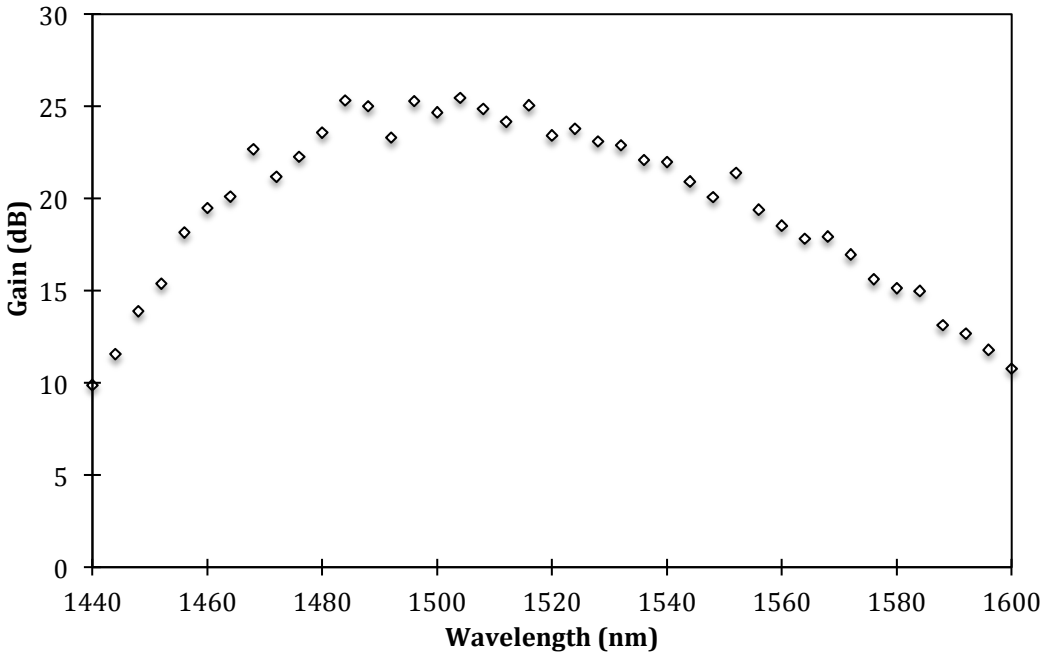

(a)

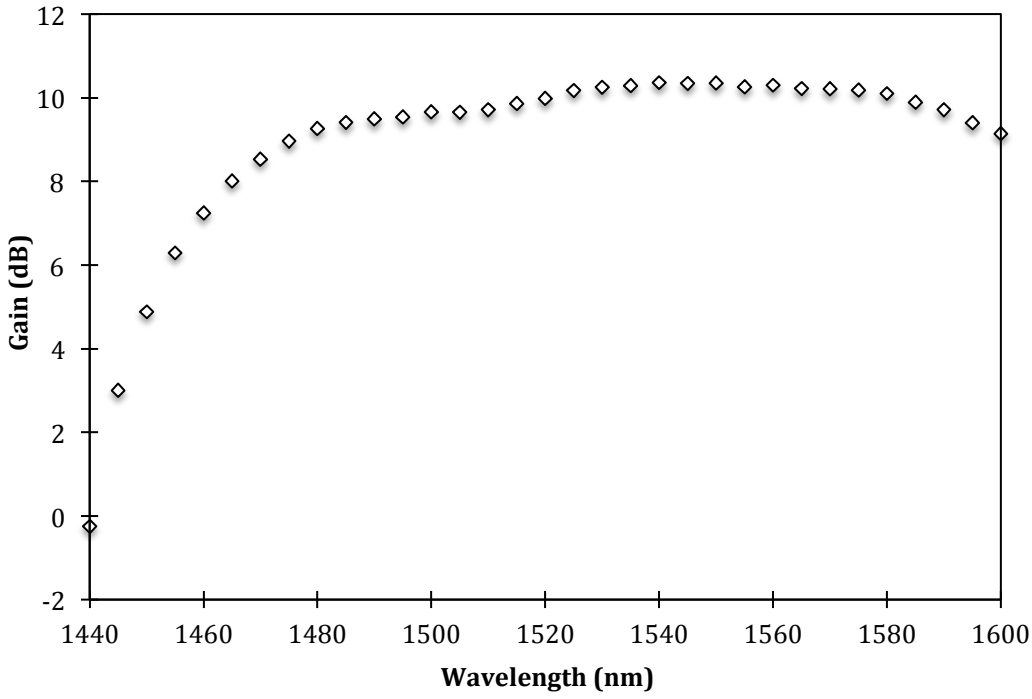

(b)

Figure 3.53 Gain performances for different input wavelengths with fixed input power (a) -30dBm (b) 0dBm

3.5.3 Small-signal Gain and Gain Saturation

In the Figure 3.54 below, the tabulated series of graph shows the gain for three different wavelengths at variation of input power of -40dBm to 5dBm. It can be observed that at signal wavelength of 1500 nm, the gain is the highest, having a value of 24.47dB at input power of -35dBm. The gain value then decreases with an increasing input power to a value of 6.12 dB at 5 dBm input power. At 1550 nm, it can be seen that there is almost a flat pattern of the gain at -40 dBm input power until the input power of -15 dBm, before a negative slope occurs as the input power is increased to 5 dBm. For the case of 1580 nm input signal, similar gain pattern is also observed. However the gain value for 1580 nm input signal is lower compared to the gain at 1500 nm and 1550 nm input signal. The average gain at lower input signal (-40 dBm to -10 dBm is about 10.2 dB with difference from the 1500 nm and 1550 nm signal are about 13.5 dB and 6.9 dB respectively. The lower gain at 1580 nm signal is due to limitation of ASE in an SOA. The 3 dB saturation input powers are given by -18.5 dBm for wavelength of 1500 nm, -7.5 dBm for wavelength of 1550 nm and -3.5 dBm for wavelength of 1580 nm. It can be seen that the 3dB saturation input powers increase with longer wavelength.

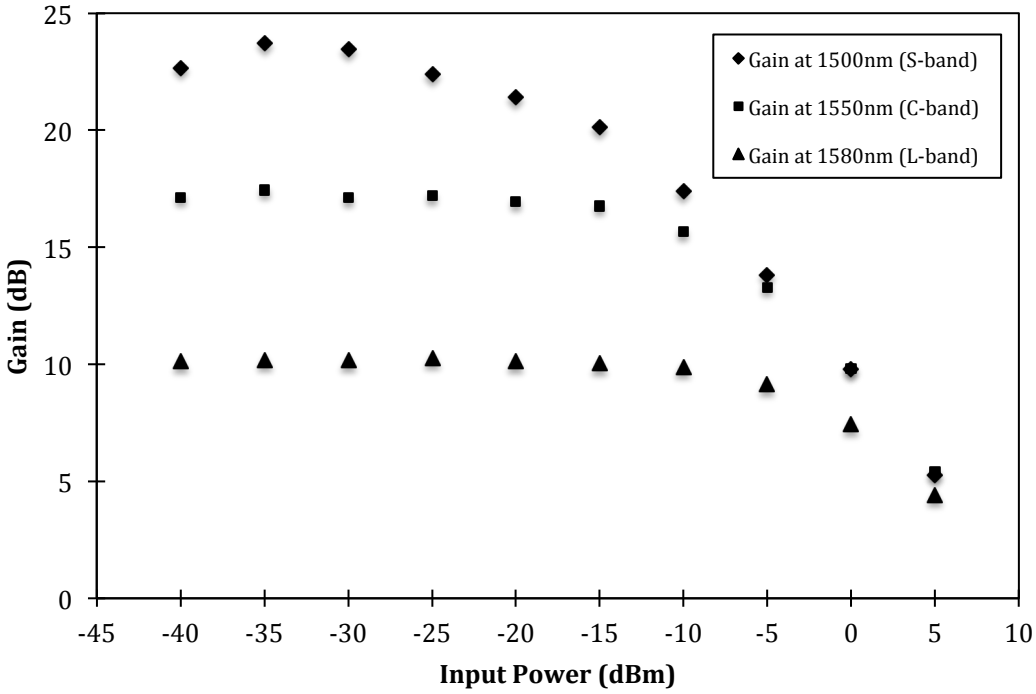

Figure 3.54 Gain with input power variations for three different wavelengths.

3.5.4 Noise Figure of Semiconductor Optical Amplifier

The NF performance of SOA at different signal input wavelengths with input power level of -30dBm is shown in Figure 4.55. The NF values from the S+ to S band (1440 nm to 1500 nm) show a fluctuation due to the PDG effect of the SOA. The maximum extinction ratio of the NF obtained is about 4.27 dB while the noise figure from C-band to L-band shows a flat pattern with an average value of 6.44 dB.

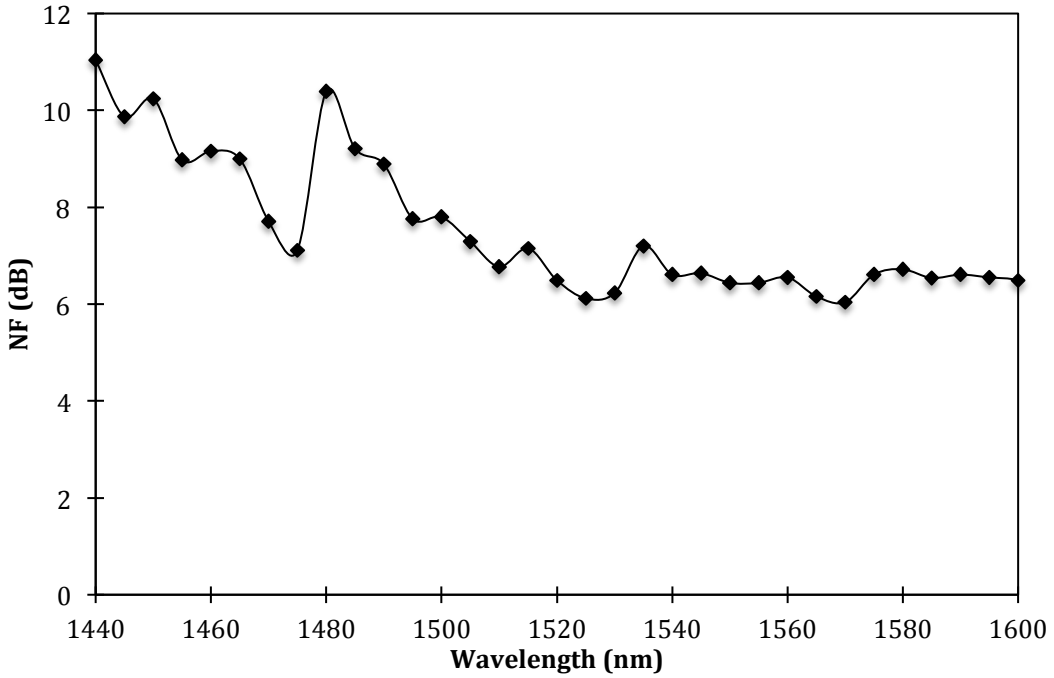

Figure 3.55 The NF performance of SOA at different input wavelengths with the input power of -30dBm.

Figure 3.56 shows the NF at high input signal power level of 0dBm with a maximum and minimum value of 12.52dB and 6.33dB respectively. The PDG effect is lower compared to that of the low signal

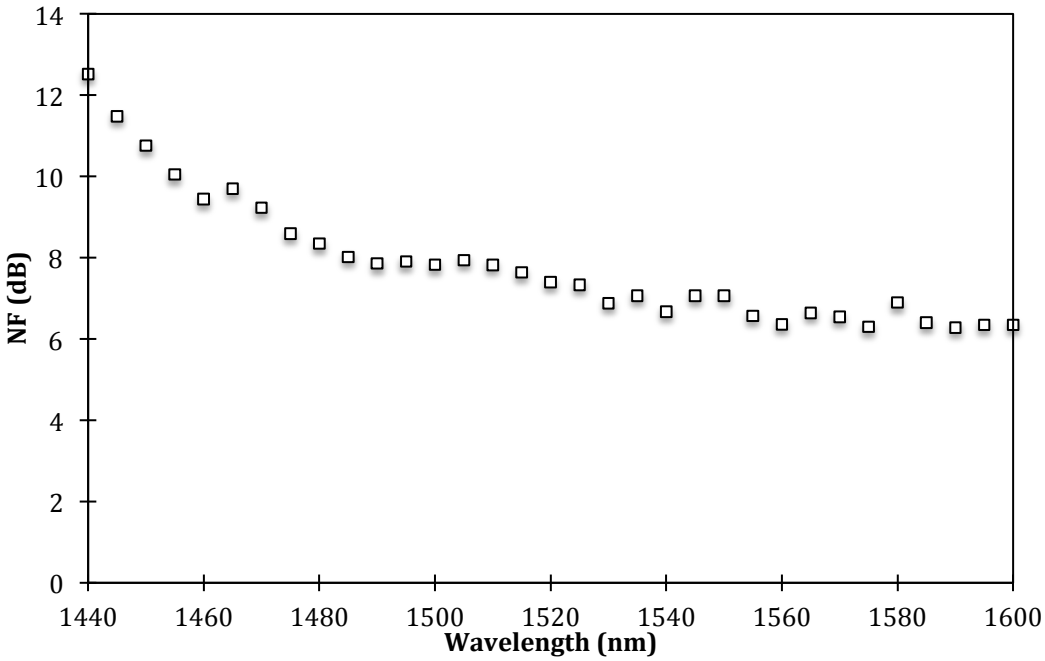

Figure 3.56 The NF performance of SOA with different input wavelength at input power level of 0dBm.

Figure 3.57 shows the performance of NF at different input signal power level which is varied from -40dBm to 5dBm. The signal wavelength is also varied by the center wavelength of 1500 nm for S-band, 1550 nm for C-band and 1580 nm for L-band. At wavelength of 1500 nm, the NF shows fluctuation values of 9.48 dB to 6.63 dB, 8.55 dB to 6.40 dB for wavelength 1550 nm and 8.55 dB to 6.80 dB for wavelength of 1580 nm. The fluctuations are due to the PDG effect which play an important role in most semiconductor optical amplifiers.

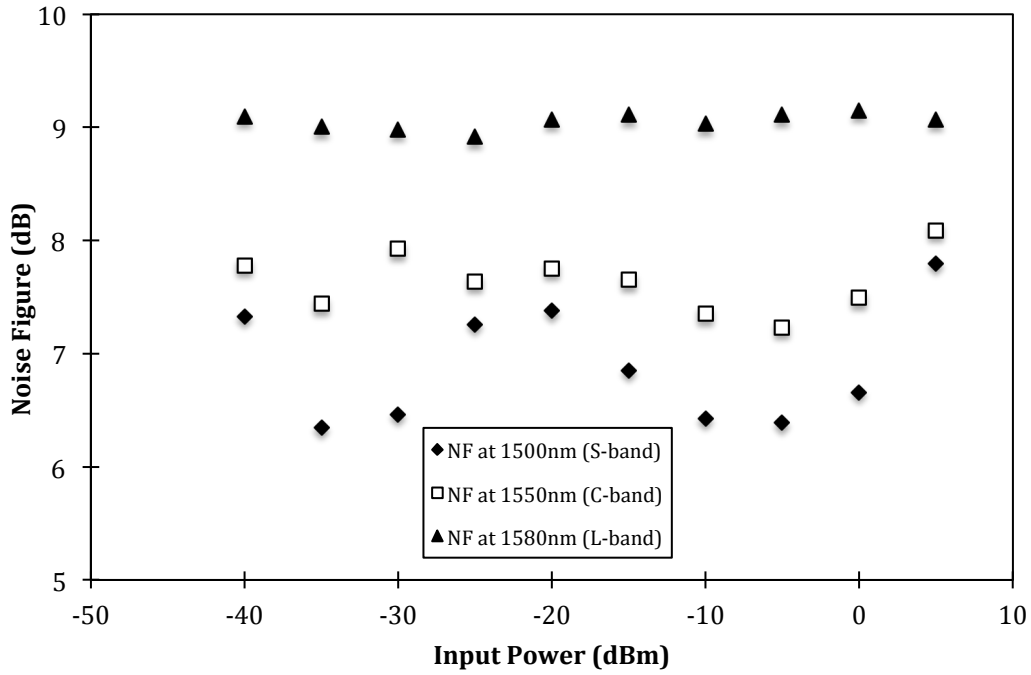

Figure 3.57 The NF performance at different input signal power level with different signal wavelength such as 1500 nm, 1550 nm and 1580 nm.

3.5.5 Polarization Dependence Gain of Semiconductor Optical Amplifier

The third part of the SOA characterization is the polarization dependent gain (PDG) effect. Since most SOAs are very sensitive to the input signal polarization state, this particular characterization is vital to observe the effect of polarization on the gain of an SOA. This experiment is done by adjusting the Polarization Controllers (PCs) that are attached at the input and output of SOA to their maximum and minimum achievable

output powers. The maximum and the minimum values attained are then subtracted from each other, to obtain the PDG value. Note that we only take the amplitude reading instead of considering the negative or positive symbols, as depicted in the expression below

$$PDG = \left|P_{o(max)} - P_{o(min)}\right| \tag{3.4}$$

Figure 3.59 shows the effect of PDG at different input signal wavelengths and at input signal power level of -30 dBm and 0 dBm. As shown in the figure, it can be seen that the maximum PDG value is 4.31 dB at wavelength of 1485 nm, for low input signal of -30dBm. For high input signal power level of 0dBm, the maximum value of PDG is 3.04 dB at signal wavelength of 1540 nm. The graph covers the whole three transmission band of S-, C- and L-band. From the figure, it also can be observed that the PDG at low input signal power level of -30 dBm fluctuates more compared to PDG at high input signal. This is due to the high ASE level at low input signal that can be sensitive to the polarization effect.

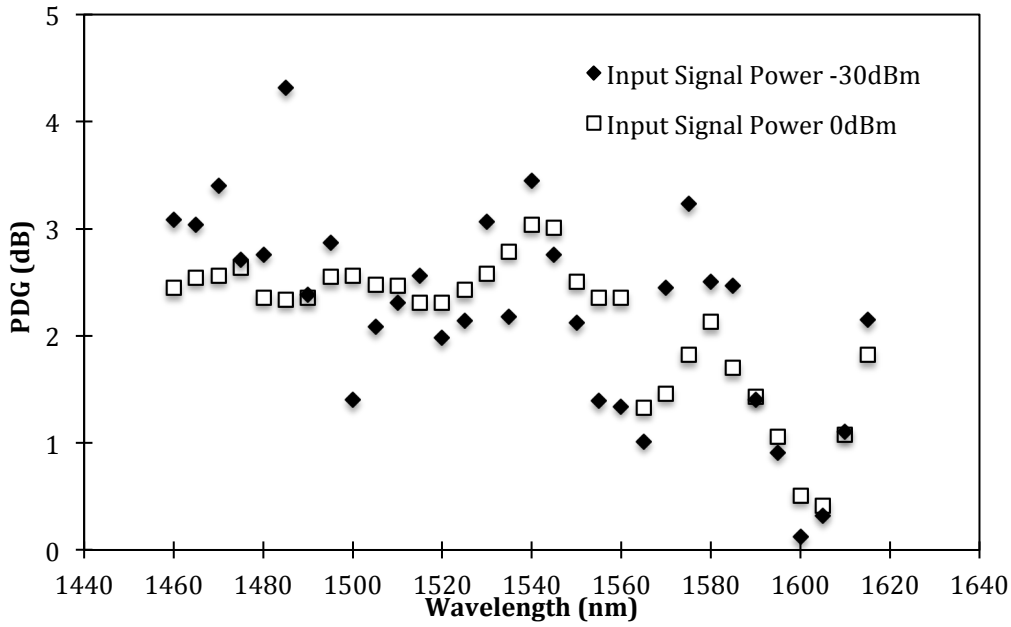

Figure 3.58 The PDG effect at different input signal wavelengths and input signal power level at -30dBm and 0dBm

Figure 3.59 shows the PDG results against input powers variation, at three center wavelengths of 1500 nm (for S-band), 1550 nm (for C-band) and 1580 nm (for L-band). The maximum PDG for signal wavelength of 1500 nm is observed to be about 3.4dB at the input signal power of -35 dBm. While the maximum PDG for signal wavelength of 1550 nm is about 2.92 dB at the input power of 5 dBm input power and the maximum PDG for signal wavelength of 1580 nm is about 2.9 dB at the input power of -40 dBm.

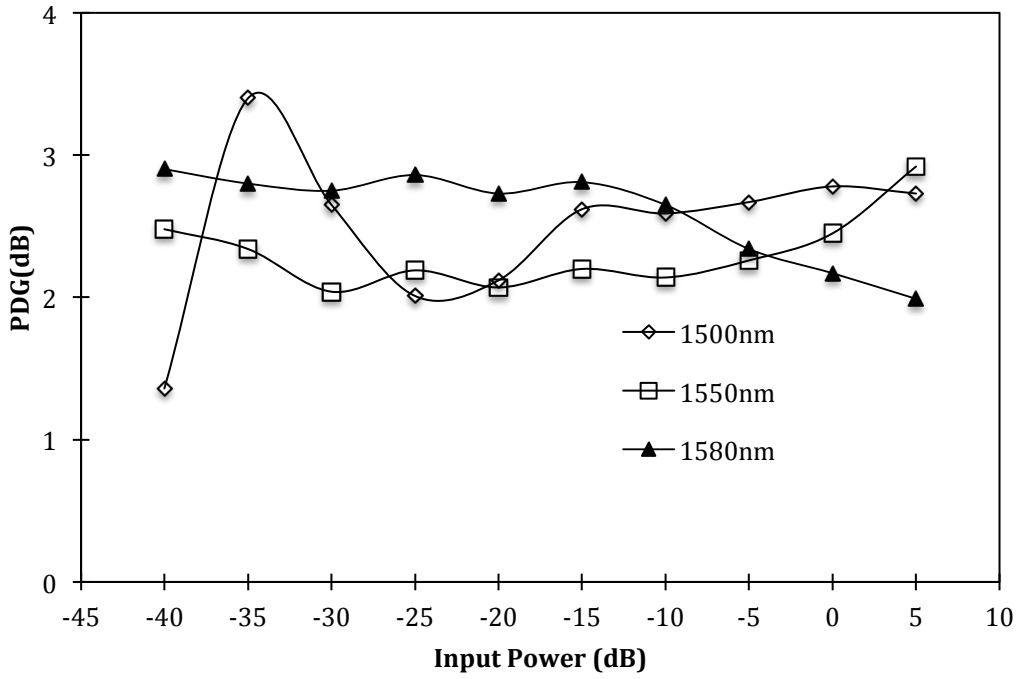

Figure 3.59 The PDG of signal wavelength 1500 nm, 1550 nm and 1580 nm against the input signal power

3.5.6 Improvement of the S-band Gain of Semiconductor Optical Amplifier with Double Pass Setup

The performance of the gain in the S-band is one of the main subject of this thesis, many reports and techniques have been made to improve the gain of the S-band. One of them is by using double pass technique. Double pass technique was first demonstrated by S.W Harun on 2002 [36]. It is of a simple idea to make double propagation in the

EDFA by using optical circulator. In this section the performance and characteristic of the gain and NF are investigated in order to improve the gain and NF in the S-band.

Figure 3.60 below shows the experimental setup of the high-gain S-band SOA in a double-pass configuration. It consists of an SOA (Alphion SAS28p) with an Amplified Spontaneous Emission (ASE) spectrum covering 1420 nm to 1600 nm as discussed earlier.

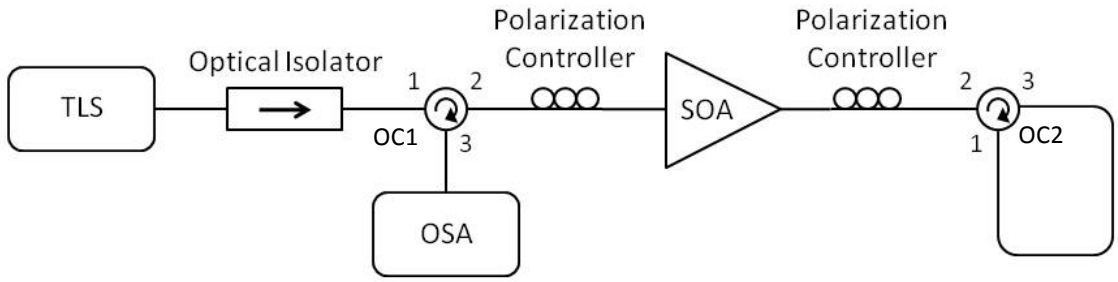

(a)

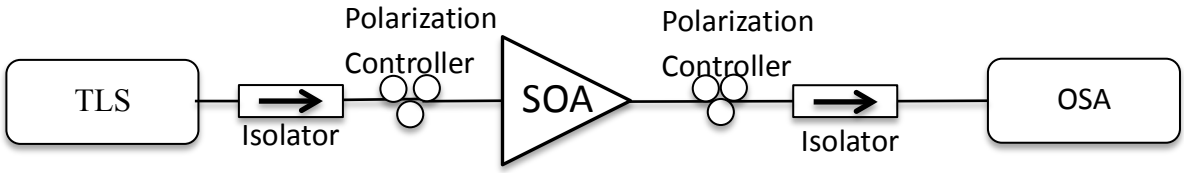

(b)

Figure 3.60 Experimental Setup of High Gain S-band SOA in (a) the Double Pass Configuration and (b) the conventional configuration.[37]

As discussed above the S-band band SOA is driven by an ILX Laser Diode Controller at a current of 460 mA, while a Yokogawa AQ2211 Tunable Laser Source (TLS) with a tunability range of 1440 nm to 1530 nm and a resolution of 0.001 nm is used to provide the S-band input signal. An optical isolator is placed after the TLS to force the signal to propagate in a unidirectional path and also to prevent any back-reflected signals that can cause damage to the TLS. The S-band signal generated from the TLS firstly travels to

Port 1 of the First Optical Circulator (OC1). It then propagates to Port 2 towards the polarization controller and onwards to the SOA. The use of the polarization controller is to provide a means of optimizing the gain.. The amplified signal will then exit the SOA and enter another polarization controller. After that, it enters the second Optical Circulator (OC2) where Ports 1 and 3 are connected, acting as a 'mirror'. This back-reflected amplified signal will then be re-amplified by the SOA and emitted through Port 3 of OC1 (entering OC1 through Port 2) and analyzed by an Optical Spectrum Analyzer (OSA) (Ando AQ6317C). For the case of single pass setup, there is no optical circulator that act as 'mirrors' as in the double-pass setup. Instead, the signal is measured directly after passing the SOA as shown in Figure 3.60(b). The setup of the single pass SOA is the same as discussed in the section 3.6. The characteristics of the double-pass SOA are discussed in the next section.

Figure 3.61 shows the comparison of ASE spectra of the SOA in the single- and double-pass setups. From Figure 3.61, the ASE power level of double pass is observed to be -24 dBm at a wavelength of 1500 nm when the SOA is driven at a current of 460 mA. At a similar condition the single pass setup only yields an ASE power of –32 dBm, 8 dB lower than that of the double-pass setup. However, the optimum ASE bandwidth for the double pass setup is observed to be limited to a wavelength range of 1440 nm to 1540 nm whilst the single pass setup ASE shows wider bandwidth coverage from 1400 nm until 1540 nm. As can be seen Figure 3.61, the ASE of the single pass and double-pass setup experience a very distinct difference in shape. The ASE for double pass setup is observed to be slightly concentrated at the longer transmission wavelength region that fits well in the S-band region; whilst the single-pass ASE disperses over a wider transmission wavelength range. The distinct difference in the ASE shape of the double-pass setup is influenced by the inhomogeneous broadening property of the SOA material gain, InGaAsP [13-17].

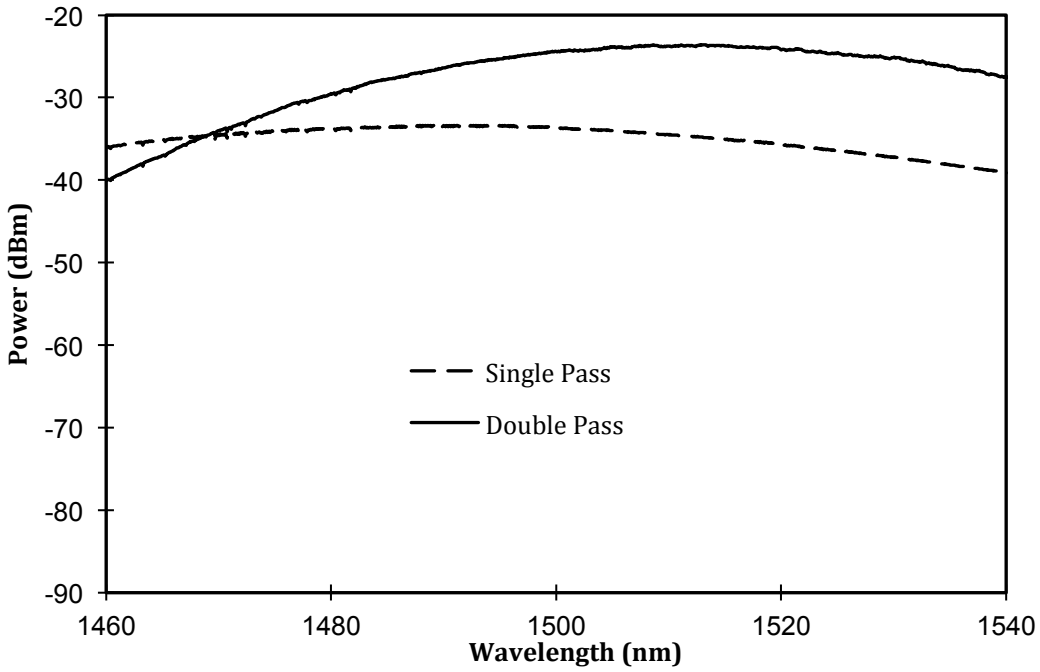

Figure 3.61 ASE Spectra at S-band comparison between single pass setup and double pass setup at a 460 mA injection current.

The gain and Noise Figure (NF) performance for both setups against different input wavelengths at signal input power -30 dBm is shown in Figure 3.62. As can be seen from Figure 3.62, the initial gain values of both the single- and double-pass setup are almost similar, with the difference between them producing a value of approximately 2 to 3 dB until an input wavelength of 1500 nm. However, at longer wavelengths the gain of the single-pass setup drops, whereas the gain of the double-pass setup continues to increase to a maximum value of 27.06 dB at the wavelength of 1516nm with an improvement of 6.01 dB over that of the single-pass setup. This gain performance can be explained by the ASE spectra of the two setups as given in Figure 3.61. The NF of the single-pass setup fares better from 1480 nm until 1520 nm compared to the double-pass setup that has a better NF from 1460 nm to 1480 nm. The NF for the single-pass setup at 1490 nm is about 11 dB and reduces to 8 dB around 1520 nm. Normally, the NF of an SOA is always high, and as such the values obtained can be considered as a

good achievement. The fluctuating NF of the double-pass system at the longer wavelength region is attributed to the Polarization Dependence Gain (PDG) effect in the SOA.

Besides above, the SOA characteristics of gain and NF at different signal input power levels from -40 dBm to -5 dBm (simulating low to high powered input signals) are also measured at a fixed wavelength, in this case 1500 nm. This is shown in Figure 3.62 whereby the double-pass setup shows a higher gain performance with respect to the single-pass setup, having a maximum gain of 31.07 dB at an input signal power of -40dBm. This is about 6.7 dB higher that the maximum gain of the single-pass setup at the same condition.

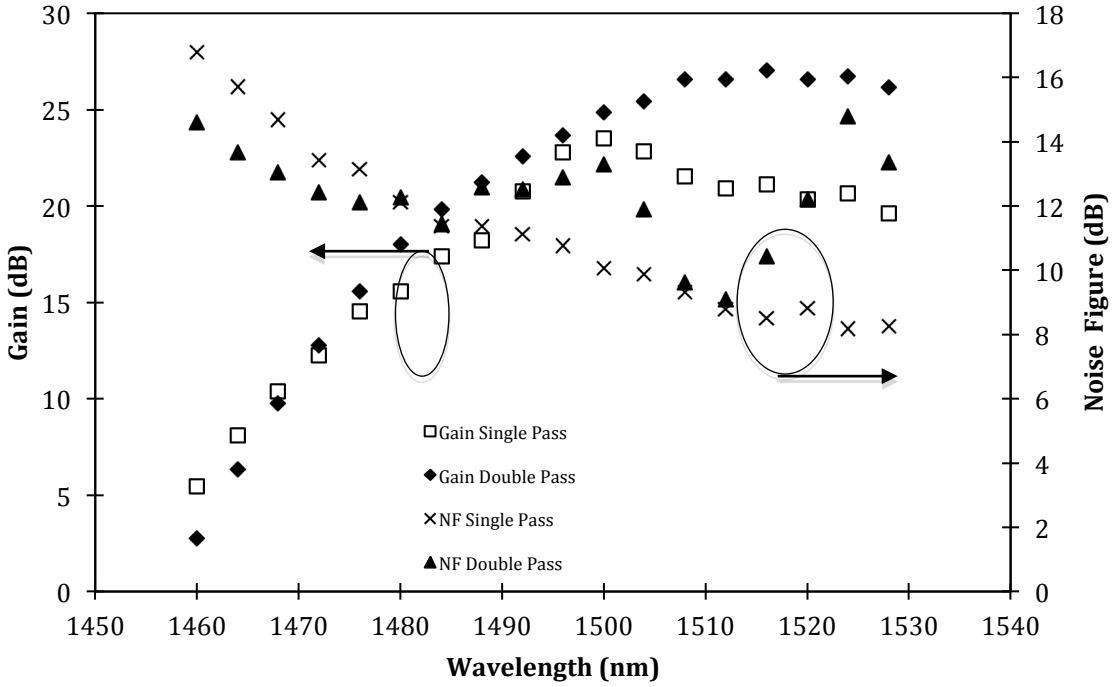

Figure 3.62 Gain and NF Performance with Different Input Wavelengths at Input power -30dBm.

As the signal power level increases, the gain of the double-pass is observed to exceed that of the single-pass setup, but at higher signal powers such as -5 dB, they tend to merge, which is largely due to saturation The measured NF at different power levels

averages out to 10 dB with a similar profile to that of the single-pass configuration, which has a slightly lower noise figure of between 8 dB to 9 dB (a difference of only 1 dB to 2 dB). In overall, this specific SOA can function as a good alternative for obtaining high gain amplification in the S-band region. As also observed in Figure 3.63, the gain difference measured at 1500 nm and taking a particular case of an input power of – 30dBm does not correspond well with that of Figure 3.62 where for the case of the input signal wavelength of 1500 nm and input signal power of -30dBm. This difference is largely due to the PDG of all types of SOAs. This can be avoided by the careful adjustment of the polarization controllers.

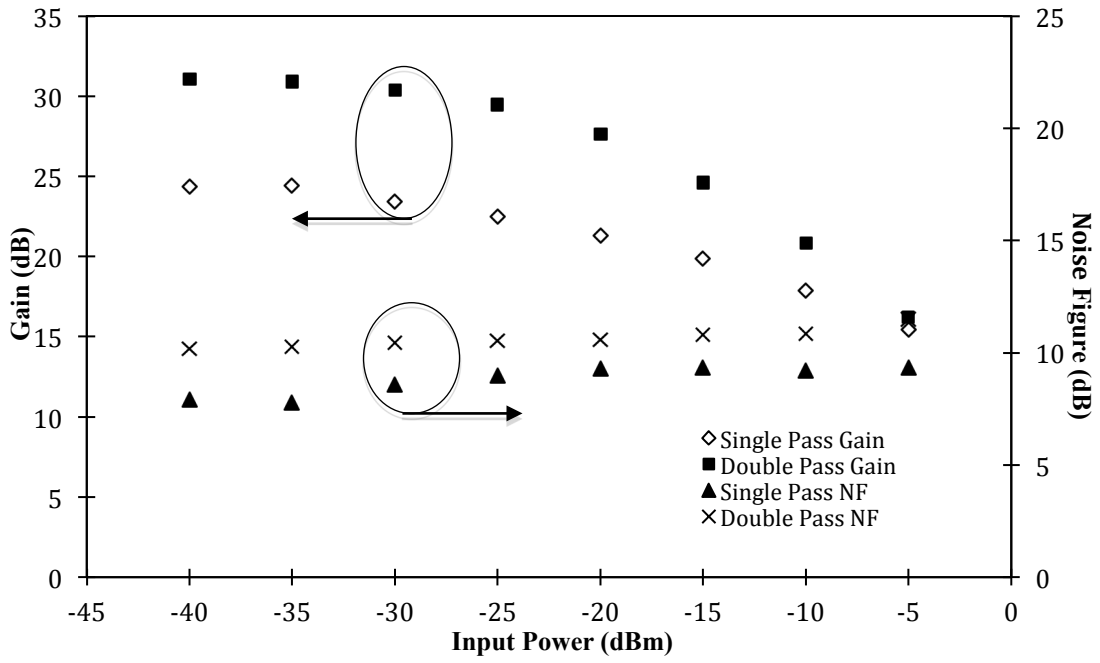

Figure 3.63 Gain and NF Performance against Different Input Powers at a Wavelength of 1500 nm

The PDG characteristics against the input signal power are shown in the Figure 3.64 by measuring the maximum and minimum gain of the SOA via the adjustment of the polarization controllers. The maximum and minimum gain are about 23.41 dB and 20.73 dB respectively, whilst the PDG is 2.68 dB, taken at a signal power of -30dBm

for the case of a single-pass SOA configuration. This value can be larger for a double-pass configuration.

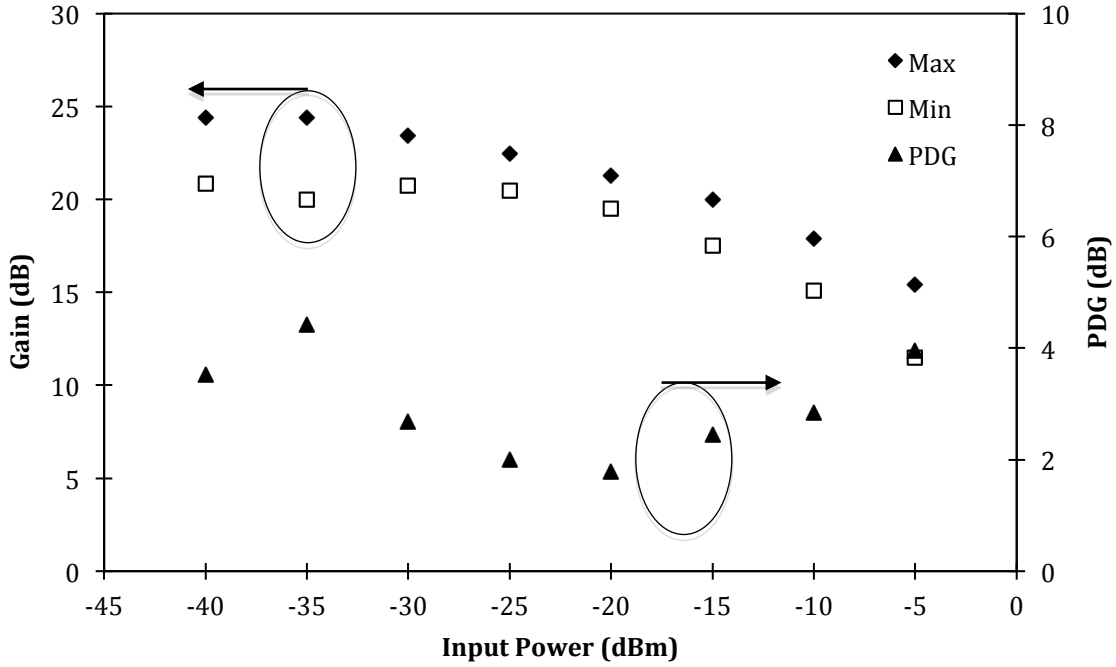

Figure 3.64 The maximum and minimum gain obtained by changing the polarization controller and also the PDG at different input powers

3.6 Summary

3.6.1 Erbium Doped Fiber Amplifier

S-band amplification by using a standard silica EDFA has been characterized in chapter 3 and the inversion rate of the Erbium Doped Fiber (EDF) was been simulated by using GainMaster software provided by Fibercore Ltd company to simulate the optimum length of EDF in obtaining a higher gain in the S-band region. The result of the simulation shows that the 3 m EDF is the best length to obtain the highest gain at S-band. The simulation work has been proved by the experimental work. From the experimental work, the highest gain obtained is about 8.1 dB at 1500 nm and pumping power is about 90 mW. The characteristics of gain are also covered with different pumping configuration which is forward pumping and backward pumping. The gain of forward pumping setup is showing a higher value compared to the gain of backward pumping setup. The gain of the forward pumping setup with different input signal power at 1500 nm and pump power of 90 mW is higher at low input signal between -40 dBm to -10 dBm with the average gain is about 8.0 dB. The gain drops when input signal reaches a higher value which is between -5 dBm to 5 dBm with 7.19 dB of average gain. Similar pattern is exhibited in the gain of backward pumping setup however the gain is about 0.3dB lower than forward pumping setup. The gain performance is also tested with different input signals wavelengths from 1480 nm to 1525 nm between -30 dBm and 0 dBm of input signal power. The gain of forward pumping is higher than that of the backward pumping setup with 1.65 dB of gain different. The Noise Figure (NF) is also characterized with difference input signal at 1500 nm and with different input wavelength at -30 dBm and 0 dBm input power. The average NF of forward pumping setup is about 3.97 dB lower 1.82 dB than that of the

backward pumping setup which is due to high gain produced by the forward pumping setup.

3.6.2 Depressed Cladding Erbium Doped Fiber Amplifier

The Depressed Cladding Erbium Doped Fiber (DC-EDF) is a fiber that is designed to overcome the limitation of EDF in S-band amplification. It is designed with different index profile and this is called W-shape index profile. To get amplification on S-band, the DC-EDF needs to be spooled with different spool diameter. The significant of doing this is to tune the cut off wavelength of this fiber in order to filter out the C-band ASE thus getting amplification only in the S-band. The experimental work of the spooling effect to tune the cut off wavelength has been done with diameter variation of 5cm to 9cm. The peak of Amplifier Spontaneous Emission (ASE) of DC-EDF is shifted to the shorter wavelength from 1510 nm to the 1470 nm for the smaller spooling diameter However the spools cannot be too tight to prevent loss inside the DC-EDF fiber. The optimum spooled diameter which provides the highest ASE power in the S-band region is about 9cm. The same characteristics such as gain, NF and output power are measured with different pumping setup which consist forward and backward pumping configuration. The gain shows a slightly different value between the two pumping setup with the backward pumping setup produces a higher gain compared to the forward pumping configuration. The gain with different power of input signal between -40dBm to 5dBm is also characterized on DC-EDFA for both backward pumping and forward pumping configuration. At small input signal which is from -40dBm until -10dBm, the gain is about 27.9dB and it is 3.3 times higher compared to the gain of the S-band EDFA at the same condition. On the other hand, the gain of the backward pumping

configuration is 1.79dB higher than the forward pumping. The DC-EDFA also shows a higher gain at high input signal power of -5dBm to 5 dBm with 6.25dB of average gain. The gain of the backward pumping is higher than forward pumping is this condition. The backward pumping setup is more suitable for high power and high gain application. The DC-EDFA is also tested with different input wavelength at input power of -30dBm and 0dBm with different pumping setup (forward pumping and backward pumping). The gain bandwidth of the DC-EDFA is about 55 nm and the highest gain is 30.45 dB at wavelength 1500 nm.The gain bandwidth of S-band DC-EDFA is wider than the gain bandwidth of S-band EDFA. The NF of DC-EDFA has also been characterized for different input signal at wavelength 1500 nm and for different input wavelength with input power of -30 dBm and 0 dBm by using the two different pumping setup (forward pumping and backward pumping). As a conclusion, the NF of the DC-EDFA is higher than that of the EDFA with 10.28 dB gain is recorded at small input signal of -40 dBm to -10 dBm which increases to 11.0 dB at high input signal of -5 dBm to 5 dBm. The NF of backward pumping setup is higher than that of the forward pumping with 2.0 dB of NF difference. The NF at different input signal (at input power -30 dBm and 0 dBm) shows the highest value at wavelength 1514 nm for the input signal of -30 dBm and also at 1515 nm for the input signal of 0 dBm with the NF of backward pumping configuration is higher than that of the forward pumping design.

The improvement of DC-EDFA in term of its characteristic is also being studied. One of the importance parts for the optical amplifier is the flat gain bandwidth. The flat gain bandwidth for DC-EDFA is being demonstrated by using Tunable Mach-Zehnder Filter (TMZF). The TMZF can be tuned close to the highest part of the ASE power, thus can flatten the gain bandwidth. The flat gain 3 dB bandwidth is about 18 nm. The gain for the flattened DC-EDFA is about 24.21 dB and it is 6.4 dB lower compared to conventional DC-EDFA. The difference is due to the insertion loss of the TMZF which

has also been characterized in chapter 3. However the NF of the DC-EDFA with TMZF has almost similar value with the conventional DC-EDFA with the average NF is about 9.4dB.

Optimizing the quality of NF is also important for the optical amplifier before it is appliedto the real network system. At last section of the DC-EDFA, the proposed setup is used to reduce NF, which consists of DC-EDFA hybrid with the EDFA. The hybrid gain medium is demonstrated to take advantage of the low NF by using EDFA as discussed earlier. The NF of hybrid gain medium is reduced from 19.46dB to 5.41dB with the pump power of about 300mW and 90mW for DC-EDFA and EDFA respectively. However the gain of the proposed setup slightly decreased due to lower gain and absorption of S-band signal at the EDFA. The gain difference is about 4.2dB.

3.6.3 Raman Amplifier

S-band Raman amplifier can be categorized in two type of amplifier which are Distribute Raman Amplifier (DRA) and Discrete Raman Amplifier. The gain measurement of the discrete Raman amplifier is similar with the gain measurement for EDFA, DC-EDFA and SOA. Based on this reason the discrete Raman amplifier is chosen to be further characterized In this thesis the Discrete Raman Amplifier is characterized by observing the pump efficiency to the gain value. The higher Raman pump power needs to get more Raman gain in literature. The gain of the Raman amplifier is tested with different pump power from 30.7mW to 390mW for different input signal powers which are -30dBm and 0dBm. The gain only occurs when the

Raman pump power exceeds 250 mW and the maximum gain for 390 mW pump power is about 4.8dBm. The gain per Raman pump power is about 0.04 dB/mW.

The small signal and saturation gain of Raman Amplifier are also measured in Chapter 3. The maximum gain at small signal region is about 5.4 dB. The Raman amplifier has a high 3 dB saturation gain which is about 2.0 dB .The gain at high input signal 5dbm is about 1.2 dB. The gain is expected to be higher if more pump power is applied.

The gain bandwidth of Raman amplifier is measured by changing the input signal wavelength from 1490 nm to 1530 nm for input signal of -30 dBm and 0 dBm. The gain bandwidth is about 30 nm with 6.1dB of average gain from 1500 nm to 1530 nm. The gain bandwidth can be changed or expended by using different Raman pump wavelength. The gain bandwidth can be changed to 35 nm by using two different Raman pump wavelengths which are 1420 nm and 1425 nm.

3.6.4 Semiconductor Optical Amplifier

The Semiconductor Optical Amplifier (SOA) is one of the devices which can provide gain in S-band region. The SOA principle is different with the EDFA in the way that the photon is pumped by external laser diode with injection current to produce ASE. At the beginning of the SOA section, the ASE characteristics of the SOA with different current are characterized. The ASE of the SOA is shifted to the shorter wavelength when the current is increased from 0mA to 390mA thus the bandwidth of the ASE also becomes wider. The maximum current of 390mA can produce a wider ASE which can cover wide band range from S-, C- to L band. This is good a advantage for optical amplifier to have a wide ASE in a single chip. The characteristic of the gain begins with the

different input wavelength at input power of -30 dBm and 0 dBm which covers the gain at C-band and L-band. The gain bandwidth of SOA covers from 1440 nm to 1600 nm with the bandwidth of about 160 nm in the single chip. The gain is higher at the S-band region with a value of 25.29 dB at 1500 nm compared to C-and L-band region. This is due to the optimization of the cavity inside the SOA which is optimized at S-band. However the gain at C-band and L-band and also have merit gain with the maximum gain at the C-band region is about 21.38 dB at the wavelength of 1552 nm while for L-band region the maximum gain is about 14.98dB at the wavelength of 1584 nm for low input signal power -30 dBm. At high input signal power, the gain bandwidth also covers the same bandwidth as covered by the low input signal power but the gain is slightly flat from 1475 nm to 1600 nm due to the saturation effect of SOA. From both results, it can also be observed that the fluctuation of gain is higher at low input signal compared to the high input signal. This is due to the Polarization Dependence Gain (PDG) of SOA. The small signal gain and saturation gain is also characterized in the S-, C and L region. The range of the input signal power is from -40 dBm to 5 dBm with the wavelength 1500 nm for S-band, 1550 nm for C-band and 1580 nm for L-band. The gain at lower input signal for S-band is higher compared to the other bands which are about 23.71 dB at input power of -30 dBm. While the maximum gains at C- and L-band at lower signal power are about 17.4dB and 10.16dB respectively. At high input signal power the gain of the entire band show almost similar value with the maximum gain at S-, C- and L-band are about 5.27dB, 5.41 dB and 4.42 dB respectively.

The NF of SOA is also being characterized with different input wavelength from 1440 nm to 1600 nm at input power of -30 dBm and 0 dBm. The average NF value is about 7.15 dB at –input signal of -30 dBm and the NF pattern is shows that the NF is higher at shorter wavelength within 1440 nm to 1495 nm with the average of NF is about 9 dB and it also shows some the NF fluctuation a due to the PDG. Compared to the lower

input signal power, the NF at high signal power is more constant with average NF of 7.64 dB for input wavelength within 1440 nm to 1600 nm The NF for different input signal power has also been measured with 1500 nm, 1550 nm and 1580 nm to test the S-,C- and L band region. For lower input power, which is -40 dBm to -10 dBm the NF at S-, C- and L-band are about 6.85 dB, 7.35 dB and 9.07 dB respectively. The NF at S-band is showing NF fluctuations with the extinction ratio of about 0.95 dB.

The PDG effect has also been characterized in chapter 3.The experiment to study PDG effect is done by changing the polarization controller (PC) to get the maximum and minimum gain of the SOA with different parameters. For the case of different input wavelength and fix input power of -30 dBm and 0 dbm the PDG is strong at the lower input signal compared to the higher input signal. The average PDG for different input wavelength at input signal power of -30 dBm is about 3.07 dB whereas for the input signal powers of 0 dBm the average PDG is about 2.31dB. The PDG also been characterized with different input signal power and the wavelength is fix at 1500 nm, 1550 nm and 1580 nm for S-,C-and L-band. The highest fluctuation of PDG occurs at lower input signal of -40 dBm to -10 dBm at wavelength 1500 nm with average PDG of 2.62 dB . It is also shown that the PDG at 1580 nm wavelength is the highest compared to the other wavelength bands.

The improvement of the S-band gain is also demonstrated in this section. The improvement of the S-band gain is achieved by using with the double pass setup. The double pass setup is one of the techniques to get higher gain without extra active components. The proposed setup demonstrates a high gain amplifier covering the S-band region from 1480 to 1520 nm. Within this range, the gain of the double pass configuration obtained is higher than that of the single pass configuration, with a gain value of 31.07 dB at an input signal power level of -40 dBm and at the wavelength of 1500 nm. The NF of the double pass system also fares better from 1480 until 1520 nm

at 11 to 8 dB in comparison with the single pass system, although the single pass system has a better NF at wavelengths shorter than 1480 nm. This system provides a good alternative for a high gain and compact amplifier in the S-band region

3.6.5 Performance Comparison of the S-band Amplifiers

The performance parameters such as pump power, gain at lower and higher input signal, gain bandwidth, polarization sensitivity and NF are being compared. In term of pump power the S-band EDFA uses the lowest pump power compared to the other S-band amplifier such as DC-EDFA and Raman Amplifier. However the gain value of the S-band EDFA is lower compared to the DC-EDFA and SOA. The main advantage of S-band EDFA is that it has lower NF compared to other types of amplifier. The DC-EDFA is shows a good performance in terms of gain and gain bandwidth compared to the S-band EDFA. The gain of S-band DC-EDFA is three times higher than that of the S-band EDFA at low input signal and 3dB higher at high input signal. The bandwidth of DC-EDFA is wider compared to the bandwidth of S-band EDFA. The main drawback of S-band DC-EDFA is that it exhibits higher value of NF compared to other S-band amplifiers. The Raman amplifier has the advantage in term of the gain bandwidth. The bandwidth can be tuned and chosen by having the right wavelength of Raman pump. Other advantage of S-band Raman amplifier is that it has higher saturation gain characteristics as the Raman amplifier, can produce high gain if they have enough Raman pump power.

The performance of SOA also shows an excellent merit in term of the bandwidth. The SOA has widest bandwidth compared to other types of amplifiers. However, the SOA is

more polarization sensitive compared to the S-band EDFA, DC-EDFA and Raman amplifier.

As the conclusion, the performance of the S-band amplifier is shown in Table 6.1. The performance parameter such as pump power, gain at lower and higher input signal, gain bandwidth, polarization sensitivity and NF are compared. In term of pump power the S-band based on EDFA uses quite small amount of power compared to the others such as DC-EDFA and Raman Amplifier. Comparison in term of pump power between the SOA and EDFA, DC-EDFA and Raman Amplifier cannot be made due to their different principles of operation. However the gain value of the S-band EDFA is lower compared that of DC-EDFA and SOA. The main advantage of S-band EDFA is that it has a lower NF compared to other type of amplifiers. The DC-EDFA show a good performance in terms of gain and gain bandwidth compared to the S-band EDFA. The S-band DC-EDFA gain is three times higher than S-band EDFA gain at lower input signal and it is 3dB higher at high input signal. The bandwidth of DC-EDFA is wider compared to the bandwidth of S-band EDFA. The main drawback of S-band DC-EDFA is that it exhibits a higher value of NF as compared to other S-band amplifiers. The Raman amplifier has an advantage in term of the gain bandwidth. The bandwidth can be tuned and chosen by having the right wavelength of the Raman pump. Other advantage of S-band Raman amplifier is that it has a higher saturation gain characteristic, therefore providing a higher gain when it is pumped at high pump power. The performance of SOA as shown in the Table 3.2 has an excellent characteristic in term of its bandwidth. The SOA have the widest bandwidth as compared to other type of amplifiers. However the SOA has problem associated with PDG which does not exist in the case of using S-band EDFA, DC-EDFA and Raman amplifier.

The next chapter will be discussing about the S-band fiber laser by using all type of S-band amplifier as the gain medium. The discussion covers the characteristics of single

wavelength fiber laser such as tuning range, output power and Side Mode Suppression Ratio (SMSR) for every type of S-band fiber laser.

Table 3.2: Comparison of S-band Optical Amplifier

	EDFA	**DC-EDFA**	**SOA**	**RA**
Pump power	90 mW	300 mW	NA	390 mW
Gain at lower input signal	8.2 dB	29.3 dB	23.2 dB	5.47 dB
Gain at highest input signal	5.6 dB	8.1 dB	5.4 dB	1.2 dB
Gain bandwidth	45 nm	55 nm	160 nm	Depends on the pump wavelength
Polarization Sensitivity	No	No	3 dB	1 dB
Noise Figure	4 dB	10 dB	6 dB	4 dB

EDFA : Erbium Doped Fiber Amplifier
DC-EDFA : Depressed Cladding Erbium Doped Fiber Amplifier
SOA: Semiconductor Optical Amplifier
RA: Raman Amplifier
NA: Not Applicable

Reference

[1] E. Desurvire, Erbium-Doped Fiber Amplifiers Principles and Applications, New York: Wiley, 1994.

[2] Mohammad N Islam, “Raman Amplifiers for Telecommunications 2, Sub-Systems and Systems, Springer-Verlag, pp 307, 2004.

[3] Y. Sun, A. K. Srivastava, J. Zhou, and J.W. Sulhoff, “Optical fiber amplifiers for WDM optical networks Bell Labs Technical Journal, vol 4, issue 1, pages 187–206, 1999.

[4] Dennis Derickson, “Fiber Optic Test and Measurement”, Prentice Hall, vol 1 , pp 529, 1997.

[5] Adzir Mahdi, “Novel Broadband Erbium-Doped Fiber Amplifiers for WDM Transmission System, PhD Thesis, University Malaya, 2001.

[6] Mohd Zamani Zulkifli, “S-band Multiwavelength Fiber laser” Master of Science Thesis, University of Malaya, 2008.

[7] R.I Laming and D.N Payne, “Noise characteristics of erbium-doped fiber amplifier pumped at 980 nm”, IEEE Photonics Technology Letters, vol.2, no.6, pp.418-421, 1990.

[8] R.I. Laming, M.N. Zervas and D.N. Payne, “Erbium-doped fiber amplifier with 54 dB gain and 3.1 dB noise figures”, IEEE Photonics Technology Letters, vol.4, no.12, pp.1345-1347, 1992.

[9] M. A. Arbore, Y. Zhou, G. Keaton, and T. Kane, "36dB gain in S-band EDFA with distributed ASE suppression," in Optical Amplifiers and Their Applications, J. Nagel, S. Namiki, and L. Spiekman, eds., Vol. 77 of OSA Trends in Optics and Photonics Series (Optical Society of America, 2002), paper PD4.

[10] M. A. Arbore, Y. Zhou, H. Thiele, J. Bromage, and L. Nelson, "S-band Erbium-Doped Fiber Amplifiers for WDM Transmission Between 1488 and 1508 nm," in Optical Fiber Communication Conference, Technical Digest (Optical Society of America, 2003), paper WK2.

[11] S. W. Harun, K. Dimyati, K. K. Jayapalan, H. Ahmad, "An overview on S-band erbium-doped fiber amplifiers", Laser Physics Letters, vol 4, issue 1, pp 10–15, 2007.

[12] M.A. Arbore, "Suppression of Cladding Mode Loss in Fiber Amplifier with Distrbuted Suppression of Amplified Spontaneous Emission (ASE)", United States Patent, Patent No 6970, 631B2

[13] M. A. Arbore, "S-band light sources using erbium-doped fiber with depressed cladding" United States Patent, 6844962.

[14] M. Foroni, F. Poli, L. Ruggeri, S.Selleri, A. Cucinotta, P. Vavassori, "Bending influence on depressed-cladding EDFA gain spectrum", Transparent Optical Networks, 2005, Proceedings of 2005 7th International Conference , vol.2, no., pp. 351- 354 vol. 2, 2005.

[15] M. A. Arbore, " Application of Fundamental-Mode Cutoff for Novel Amplifiers and Lasers," in Optical Fiber Communication Conference and Exposition and The National Fiber Optic Engineers Conference, Technical Digest (CD) (Optical Society of America, 2005), paper OFB4.

[16] L.G Cohen, D. Marcuse, W.L Mammel, "Radiating Leaky-Mode Losses in Single-Mode Lightguides with Depressed-Index Claddings" IEEE Transactions on Microwave Theory and Techniques, vol.30, no.10, pp.1455-1460, 1982.

[17] Djafar K. Mynbaev, Lowell L. Scheiner, "Fiber Optic Communication Technology", Prentice Hall, 2001.

[18] S. Yoo, Y. Jung, J.Kim, J. W.Lee and K. Oh, "W-type fiber design for application in U-and S-band amplifiers by controlling the LP01 mode long wavelength cut-off", Optical Fiber Technology, vol 11, issue 4, pp. 332-345, 2005

[19] B.Bakhshi, M. Vaa, E.A Golovchenko, H. Li, G.T Harvey, "Impact of gain-flattening-filter ripple in long-haul WDM systems", Optical Communication, 2001. ECOC '01. 27th European Conference on , vol.3, no., pp. 448- 449 vol.3, 2001.

[20] L.J. Qiao and P.J. Vella, "ASE Analysis and Correction for EDFA Automatic Control", Jounal of Lightwave Technology, vol 25, pp 771-778, 2007.

[21] M. Z. Zulkifli, S.W Harun, K. Thambiratnam, H.Ahmad, "Self-Calibrating Automated Characterization System for Depressed Cladding EDFA Applications Using LabVIEW Software With GPIB", IEEE Transactions on Instrumentation and Measurement,vol.57, no.11, pp. 2677-2681, 2008.

[22] S W.Harun, N.K. Saat and H.Ahmad, "An efficient S-band erbium-doped fiber amplifier using double-pass configuration", IEICE Electronics Express, vol.2, no 6 pp. 182-185, 2005.

[23] S W.Harun and H.Ahmad, "Gain and noise figure improvements in double-pass S-band EDFA, Optics and laser Technology, vol 39, issue 5,pp 935-938, 2007.

[24] Mohammad N Islam, "Raman Amplifiers for Telecommunications 1, Sub-Systems and Systems, Springer-Verlag, pp 307, 2004.

[25] H.Kidorf, K Rottwitt, M Nissov, M Ma and E. Rabarijaona, "Pump interactions in a 100-nm bandwidth Raman amplifier", IEEE Photonics Technology Letters, vol.11, no.5, pp.530-532, 1999.

[26] Z.Tong; H.Wei and S. Jian, “Comparison of different Raman amplification schemes in long-span fiber transmission systems with double Rayleigh backscattering”, IEEE Photonics Technology Letters, vol.15, no.12, pp.1782-1784, 2003.

[27] V.E Perlin and H.G. Winful, “On Distributed Raman Amplification for Ultrabroad-Band Long-Haul WDM Systems” Journal of Lightwave Technology, vol. 20, no. 3, 2002.

[28] Z. Li and G.F Li; , “Ultrahigh-speed reconfigurable logic gates based on four-wave mixing in a semiconductor optical amplifier”, IEEE Photonics Technology Letters, vol.18, no.12, pp.1341-1343, 2006.

[29] C.F Zhang, L.Y Wang, and K Qiu, “Proposal for all-optical generation of multiple-frequency millimeter-wave signals for RoF system with multiple base stations using FWM in SOA”,Optics. Express, vol 19, pp 13957-13962, 2011.

[30] M.Matsuura and N Kishi, “High-Speed Wavelength Conversion of RZ-DPSK Signal Using FWM in a Quantum-Dot SOA”, IEEE Photonics Technology Letters, vol.23, no.10, pp.615-617, 2011.

[31] M.L.Nielsen, B.Lavigne and B.Dagens,“Polarity-preserving SOA-based wavelength conversion at 40 Gbit/s using bandpass filtering” Electronics Letters, vol.39, no.18, pp. 1334- 1335, 2003.

[32] M Spyropoulou, N. Pleros, K.Vyrsokinos, D. Apostolopoulos, M. Bougioukos, D. Petrantonakis, A. Miliou, and H. Avramopoulos, “40 Gb/s NRZ Wavelength Conversion Using a Differentially-Biased SOA-MZI: Theory and Experiment,” Jounal of Lightwave Technology, vol 29, pp 1489-1499, 2011.

[33] C.Meuer, C.Schmidt-Langhorst, R.Bonk, H.Schmeckebier, D.Arsenijević, G.Fiol, A.Galperin, J.Leuthold, C. Schubert, and D.Bimberg, “80 Gb/s

wavelength conversion using a quantum-dot semiconductor optical amplifier and optical filtering,"OpticsExpress, vol 19, 5134-5142, 2011.

[34] H. Ju, S. Zhang, D. Lenstra, H. de Waardt, E. Tangdiongga, G. Khoe, and H. Dorren, "SOA-based all-optical switch with subpicosecond full recovery", Optics. Express, vol 13, pp 942-947, 2005.

[35] C.H Yeh; C C. Lee and S. Chi, "120-nm bandwidth erbium-doped fiber amplifier in parallel configuration", Photonics Technology Letters, IEEE vol.16, no.7, pp.1637-1639, 2004.

[36] S.W.Harun, P. Poopalan, H. Ahmad, "Gain enhancement in L-band EDFA through a double-pass technique", IEEE Photonics Technology Letters, vol.14, no.3, pp.296-297, 2002.

[37] H.Ahmad, M.Z. Zulkifli; N.A Hassan, A.A Latif and S.W Harun, "High gain S-band semiconductors optical amplifier with double-pass configuration", Laser Physics, vol. 21, Issue: 7, pp 1208-1211, 2011.

.

Chapter 4
S-band Fiber Laser

4.1 Introduction

In optical network systems, the transmitter or signal source is among the three critical components that allow optical communications to be realized (the other two being the receiver and the transmission medium). Most modern optical communications systems use discrete wavelength semiconductor laser diodes as the signal source for a number of reasons, including good laser beam quality and stability. However, the advent of DWDM systems has rendered the semiconductor laser diode unsuitable for the task; with channel spacings of 100, 50 and most recently 12.5 GHz [1, 2], the cost and number of discrete wavelength sources that will be required to operate these systems would be too large to be feasible. As such, DWDM systems are rarely used to their full capacity, and therefore cannot be used to overcome the current capacity limitations being faced around the world.

Of late however, significant efforts have been placed on the research and development of fiber lasers. Fiber lasers have been seen as a viable alternative to the use of the distributed feedback (DFB) laser diode as a signal source due to a number of key advantages, including wavelength tunability and the ability to generate multiple output wavelengths from a single source, significantly reducing the cost per wavelength. Furthermore, fiber lasers can also be applied in many other fields of science, such as sensing [3, 4] and frequency generation [5 - 7].

In this work, the focus of the research is to develop an S-band fiber laser as an alternative to DFB laser diodes for operation in the S-band region. The primary

objective of this research is to design a fiber laser with the same characteristics as a DFB such as wavelength tunability, single longitudinal mode, high output power and compact size [8]. Another area of interest is the development of a multi-wavelength source for S-band DWDM applications. As the S-band fiber laser uses erbium ions as the active gain media, difficulties have been encountered in trying to generate a multi-wavelength output due to the effects of homogeneous broadening in the gain media. Many techniques have been put forward to solve this issue, such as cooling the gain media with liquid nitrogen at 77 K [9, 10], exploiting the polarization hole burning effect [11, 12], using a hybrid gain medium [13], and controlling the cavity loss of a multi-wavelength fiber laser [14 - 16]. However, these approaches are complex and not suitable for real-world applications. Alternatively, the use of inhomogeneously broadened gain media, such as S-band SOAs and non-linear gain media, such as Raman Amplifiers, have shown success in generating a stable, multi-wavelength output. The development of S-band fiber lasers and multi-wavelength lasers has become critical due to the increasing demand for bandwidth.

In this chapter, an Erbium Doped Fiber Laser (EDFL) in a ring cavity configuration is demonstrated and studied. Subsequently, a tunable multi-wavelength S-band fiber laser is designed and demonstrated, using the silica-based EDFA as the gain medium and a TBFG filter as a tuning element. SLM operation is and the design of the TBFG is also discussed. The following sections will then discuss the different techniques and aspects of wavelength tunability and multi-wavelength laser generation using a DC-EDFA, followed by an examination of the use of an AWG as a wavelength selection mechanism. In this chapter also S-band Raman Amplifiers will be studied and demonstrated, particularly its tunability and threshold powers. The final section of this chapter will discuss the development of SOA based S-band multi-wavelength fiber lasers.

4.2 Cavity Configurations of S-band Fiber Laser

There are two possible configurations for S-band fiber lasers, namely the Fabry Perot or linear cavity and the ring cavity designs. In the case of Fabry Perot or linear cavity fiber lasers, the gain medium is placed in between two reflectors, typically FBGs of the same wavelengths or optical circulators, such that the oscillating wavelength or wavelengths achieve lasing. The ring cavity configuration on the other hand does not uses reflectors, but rather loops the laser output from the gain medium back into itself, allowing the generated wavelength or wavelengths to pass the gain medium multiple times and achieve lasing. Fiber lasers have many potential applications as laser sources and also optical sensing and spectroscopy [23]. The output of fiber lasers has narrow linewidths, and can be used to generate multiple lasing wavelengths at very close spacings.

4.3 S-band Fiber Laser in Silica Erbium Doped Fiber

In this section we discuss the design, setup and characterization of an S-band fiber laser using conventional silica EDF as the active gain medium. In this section, and in all subsequent section except where mentioned, the fiber laser is operated in a Continuous Wave (CW) condition.

4.3.1 Cavity Design

In conventional EDFLs, lasing can easily occur in either the C- band or L-band regions. However, lasing wavelengths in the S-band region are very difficult to obtain due to high peak emission at 1530 nm. In order to obtain lasing wavelengths in the S-band region, a filtering device or mechanism needs to be employed, such as a Tunable Bandpass Filter (TBF) or a FBG.

In order to develop the S-band fiber laser using silica EDF as the gain medium, it is necessary to overcome the cavity losses in the S-band. Figure 4.1 shows the experimental setup of ring cavity silica EDFL. It consists of a 3 m EDF pumped by a 980 nm laser diode at 90 mW. The absorption of the EDF at 980 nm is about 11 dB/m and has the same fiber characteristics as the EDF discussed in Chapter 3. An optical isolator is placed inside the cavity to force the uni-directional propagation of light inside the cavity. The TBF used is optimized for operation in the C-band with a 3dB linewidth of about 1.0 nm. The analysis of the output spectrum is made using an Optical Spectrum Analyzer (OSA) with a resolution of 0.02 nm, with a 90/10 optical fused coupler used to tap 10% of the laser output for analysis.

Figure 4.2 shows the output spectrum of S-band EDFL. The wavelength is first tuned to detect the shortest wavelength that can be obtained within the tuning range. From the spectrum of Figure 4.2, the shortest wavelength in the S-band with a significant output power is 1515.62 nm. The TBF also can be tuned to wavelengths shorter than 1515.62 nm but as the laser power is very low, compared to the power of longer lasing wavelengths, thus the shortest wavelength is set at 1515.62 nm. The cause of this cold be either one of two possibilities; firstly, the high TBF insertion loss will introduce extra cavity loss, or secondly the limited population inversion at the S-band region in the EDF itself.

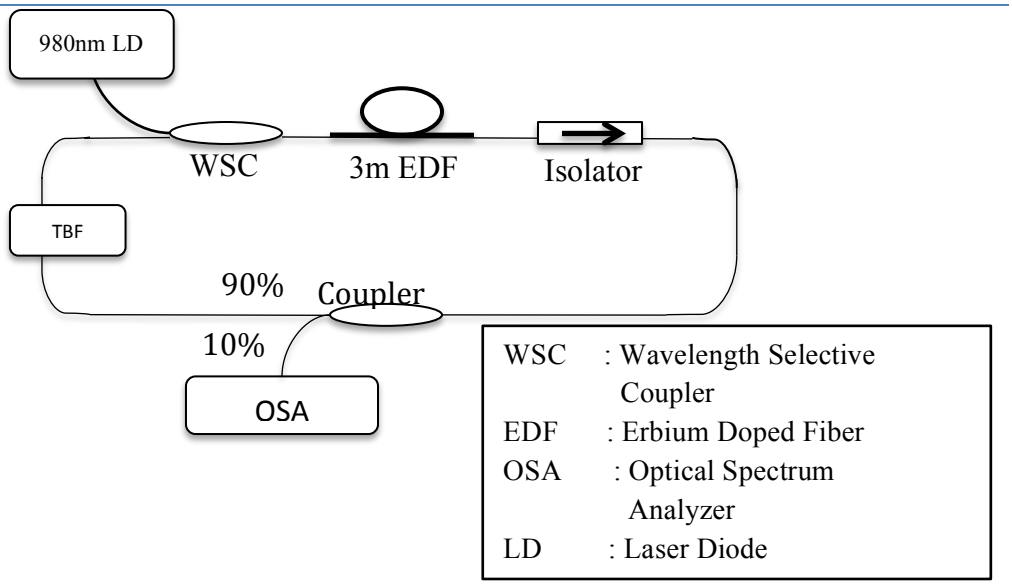

Figure 4.1: The setup of fiber ring laser by using TBF as a selective gain medium.

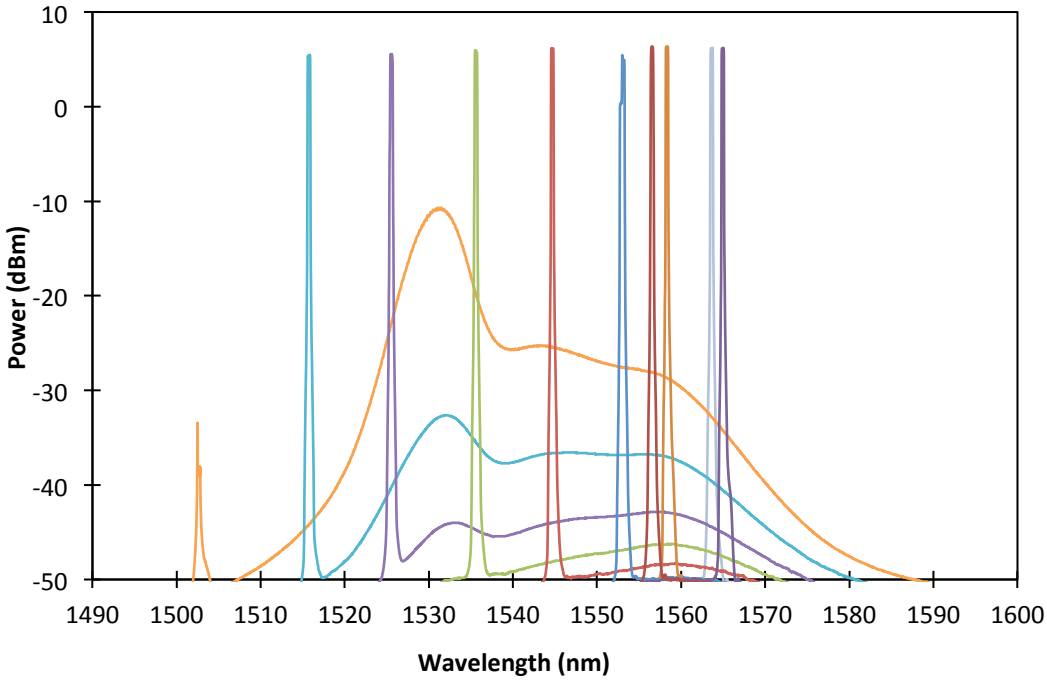

Figure 4.2: The output spectrums of S-band EDFL by using TBF which is tuned randomly.

One of the viable options in achieving lasing in the S-band region is the use of a 1500 nm FBG inside the laser cavity as a wavelength filter. The 1500 nm FBG has a reflectivity of 99%. In order to determine the effectiveness of this approach, the same setup as in Figure 4.1 is used, with the only difference being the addition of an optical

circulator within the ring cavity so as to be able to accommodate the 1500 nm FBG. Port 1 of the optical circulator is fusion spliced to the output of optical isolator and the 1500 nm FBG is fusion spliced to port 2 of optical circulator to provide the desired optical feedback. The length of the EDF is kept the same at 3 m, as is the power of the pump at 90 mW. The output laser is tapped using a 90/10 optical coupler, as shown in Figure 4.3.

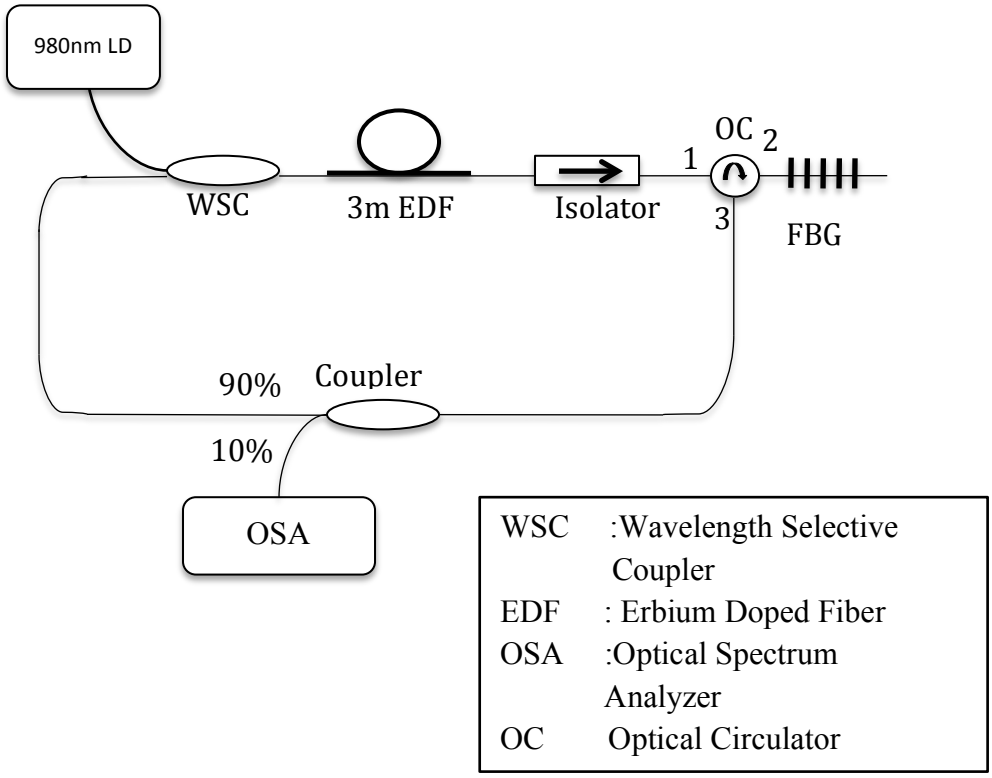

Figure 4.3: The experimental setup of S-band Erbium doped fiber laser using fiber Bragg grating

Figure 4.4 shows the output spectrum of the S-band EDFL. The figure shows that the dominant lasing wavelength occurs at 1500.07 nm, which is approximately the same with the FBG wavelength. However, lasing wavelengths can still be observed in the C-band region around 1530 nm due to the oscillation of the high Amplified Spontaneous Emission (ASE) oscillation as a result of 4% reflectivity from the end of the FBG. These unwanted lasing wavelengths can be eliminated by applying index matching gel

or by cleaving the end of the FBG at an angle so as to eliminate back-reflections. Figure 4.5 shows an enlarged view of the 1500.07 nm laser with output power at about - 4.76 dBm with a 3dB spectra width is about 0.04 nm.

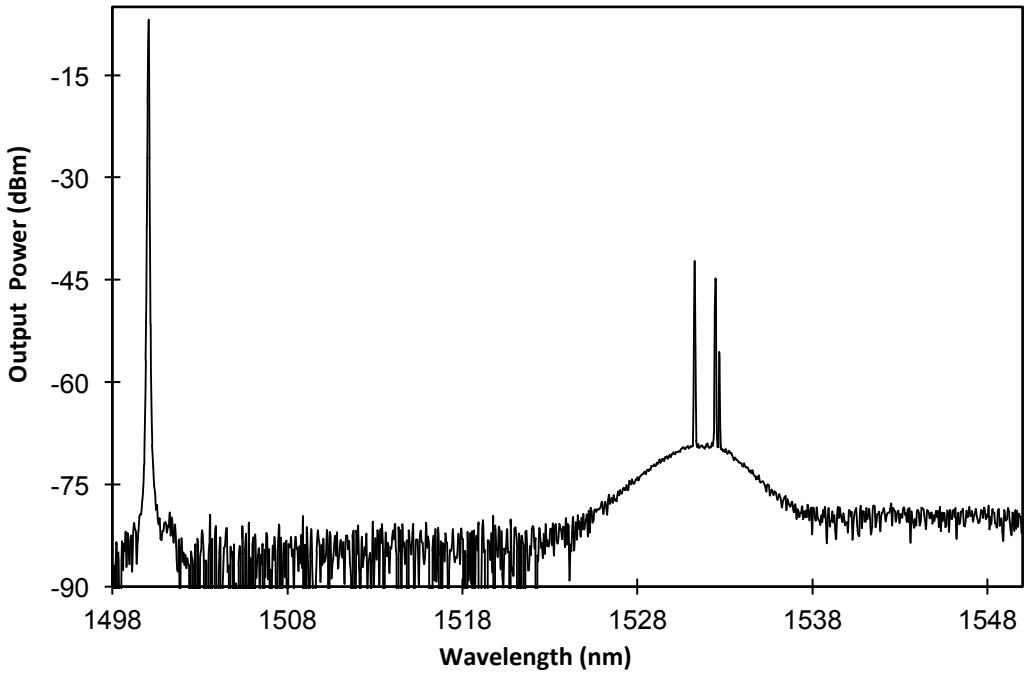

Figure 4.4: The output spectrum of the S-band EDFL using FBG with wide span

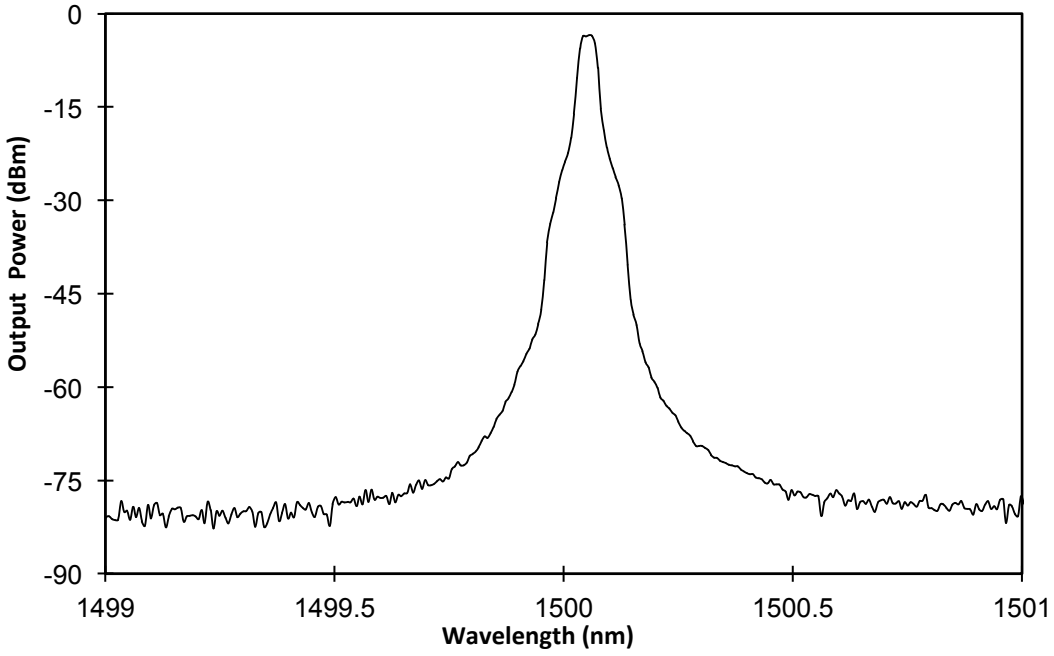

Figure 4.5: The output spectrum of the S-band EDFL using FBG with 2nm span

4.3.2 Tunability of S-band Silica EDFL

According to ITU conventions, the S-band region covers a wavelength range of between 1460 nm to 1520 nm. Based on these requirements, the proposed setup must be able to tune the lasing output within the wavelength range. As was previously discussed, the TBF exhibits high loss in S-band region, thereby limiting the lasing wavelength to shorter wavelengths of below 1515 nm. For DWDM optical systems, the tunable fiber laser is highly advantageous due to its low maintenance requirements and low cost per wavelength. The tunability of the fiber laser can be achieved by integrating a tuning element into the FBG. This can be done due to the fundamental operating principal of FBGs, where the expansion or compression of the FBG will result in a corresponding change in the wavelength [24 - 27]. The expansion or compression of the FBG can be achieved by a multitude of techniques, such as temperature, pressure and strain. Of these approaches, the induction of stress and strain onto an FBG is the best approach, as other methods, such as temperature changes are not effective due to the insensitivity of the fiber to temperature changes, of about 0.01 nm/^{o}C [28, 29]. The strain and stress effect on the other hand can be manipulated for a wide tuning range if the hybrid material is used together with the FBG [30, 31]. The next section is will discuss about the tuning package design of the proposed wavelength TFBG.

4.3.3 Design of the S-band Tunable Fiber Bragg Grating

Figure 4.6 shows the schematic of the TFBG's tuning mechanism using an FBG with a center wavelength of 1500 nm that has been glued onto a rectangular piece of Perspex with low Young modulus. This assembly is then glued onto a longer rectangular spring steel plate with high Young modulus. The spring steel plate is aligned to the grooves of

two steel blocks at both ends of the plate, with one of the steel blocks fixed in position whilst the other steel block can be moved using a thumb-screw to adjust and create movement relative to the fixed steel block. The movement of the steel block will flex the steel blade in either the upward or downward directions, causing the FBG to extend (tensile stress) or compress. This provides wavelength tunability to the fiber laser.

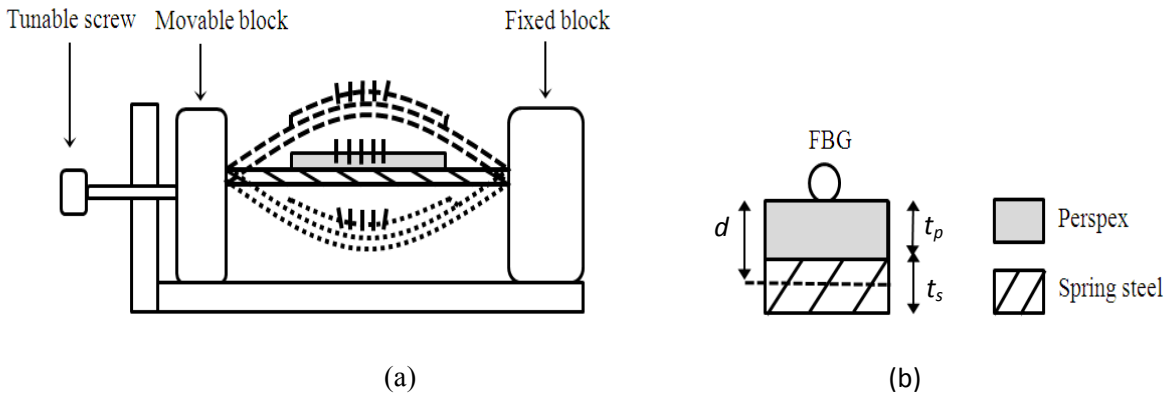

Figure 4.6: Schematic of (a) lateral beam bending technique with compression mode (dashed-line) and tensile mode (dotted-line) and (b) hybrid material with FBG mounted on top of the Perspex

Mechanical stress applied to the FBG will result in a shift of the Bragg resonance wavelength. Under ideal conditions, the relationship between the wavelength shift and the applied strain can be described by Equation 4.1 below [32]:

$$\lambda = (1 - \rho_e)\varepsilon_z \lambda_B \tag{4.1}$$

where the photo-elastic coefficient of silica fiber, $\rho_e = 0.22$, ε_z is the applied strain in the z-direction and λ_B is the Bragg resonance wavelength. The induced strain, $\varepsilon_z(R)$ as experienced by the FBG can be estimated by the strain-displacement as:

$$\varepsilon_z(R) = \pm\frac{d}{R} \tag{4.2}$$

where R denotes the bending radius of the beam. The positive and negative signs indicate the tensile and compressive mode respectively. The d factor of the hybrid sample can be given as

$$d = t_p + \frac{E_s t_s^2 - E_p t_p^2}{2(E_s t_s + E_p t_p)} \tag{4.3}$$

where E_p and E_s, are the Young's modulus of the Perspex and spring steel and also t_p and t_s are the thickness of the Perspex and spring steel respectively. In this case, $E_p = 3.2$ GPa, $E_s = 200$ GPa, $t_p = 3$ mm and $t_s = 1$ mm. The relationship between the wavelength shift of FBG and the bending radius is calculated and this is shown in Figure 4.7 below, making use of equations 4.1, 4.2 and 4.3.

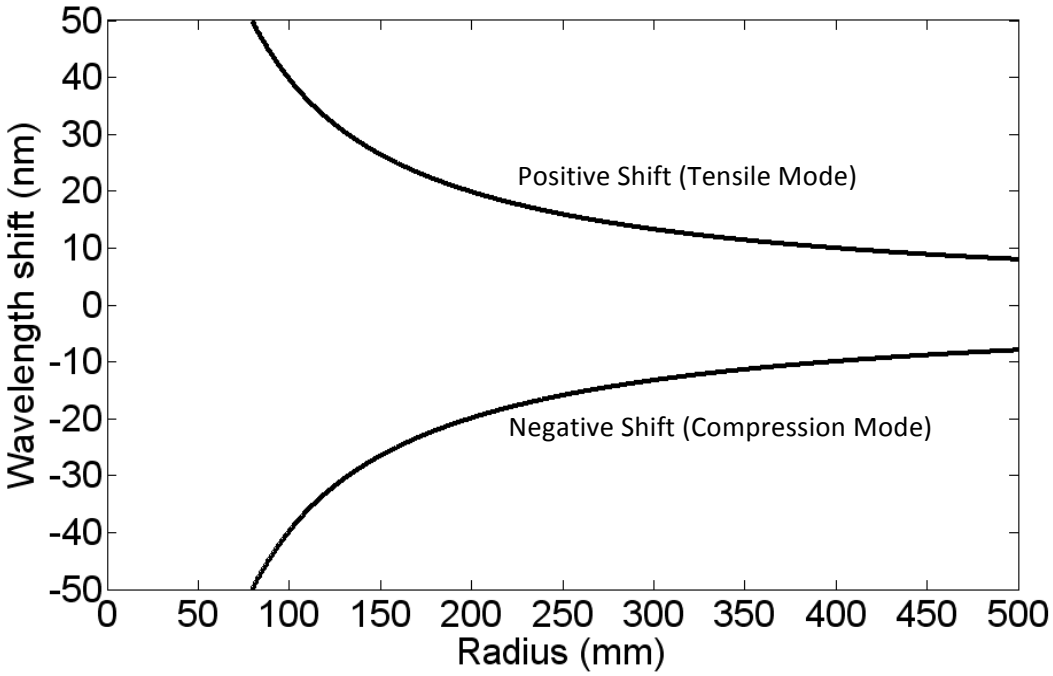

Figure 4.7: Calculated values of wavelength shift against bending radius for the hybrid material such as Perspex and Spring Steel plates with the FBG placed on top of them

From the calculation and as shown in Figure 4.7, a wavelength shift of $\pm$50 nm can be realized with the proper design of the tuning device. In reality, the limiting parameter is the bending radius, which in turn depends of the flexibility of the material.

4.3.4 Wavelength Tuning Range

The wavelength tuning range of S-band silica EDFL is shown in the Figure 4.8. The TFBG wavelength starts from 1500.07 nm and can be tuned to shorter wavelength when we apply lateral beam bending in tensile mode and to longer wavelength in compression mode. From Figure 4.8 the shortest wavelength that S-band silica EDFL can achieve is 1496.18 nm. Below this wavelength laser is not observed due to low population inversion of the silica EDF at shorter S-band wavelength, resulting in insufficient gain at these wavelengths. The longer wavelength can be achieved using TFBG is about 1507.05 nm. The wavelength tuning for longer wavelength is limited by the beam's bending radius which in turn depends on the flexibility of the material. For this setup the tuning range cover about 10.87 nm starting from 1496.18 nm to 1507.05 nm. The wavelength tuning can be extended towards the C-and L-band regions if the design issues as stated above have been resolved. There have been reports on wide tuning range FBG [30]. The wavelength selection can be done via fine tuning of tunable screw.

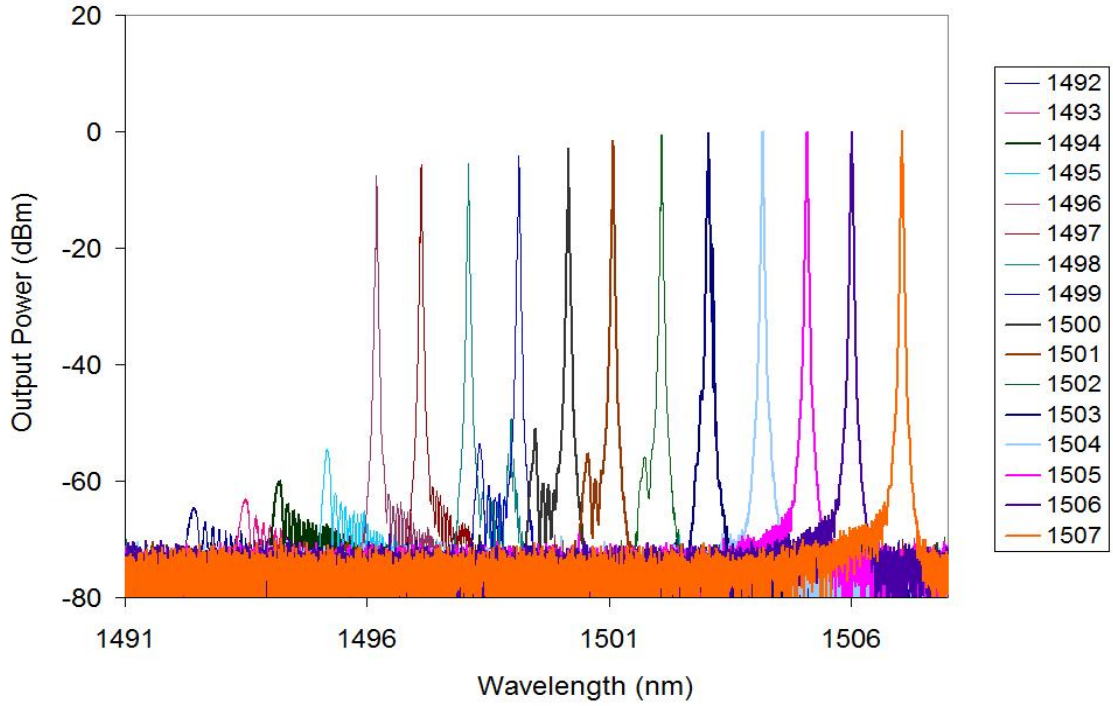

Figure 4.8: The tunable S-band multi-wavelength fiber laser spectrum by using tunable FBG

4.3.5 Output Power and Signal Mode Suppression Noise Ratio

Figure 4.9 shows the output powers from the selected wavelength. The output power increases linearly toward the longer wavelength from 1496.18 nm to 1502.07 nm and flattens from 1503.05 nm onwards with amplitude fluctuation of about 0.37 dB.

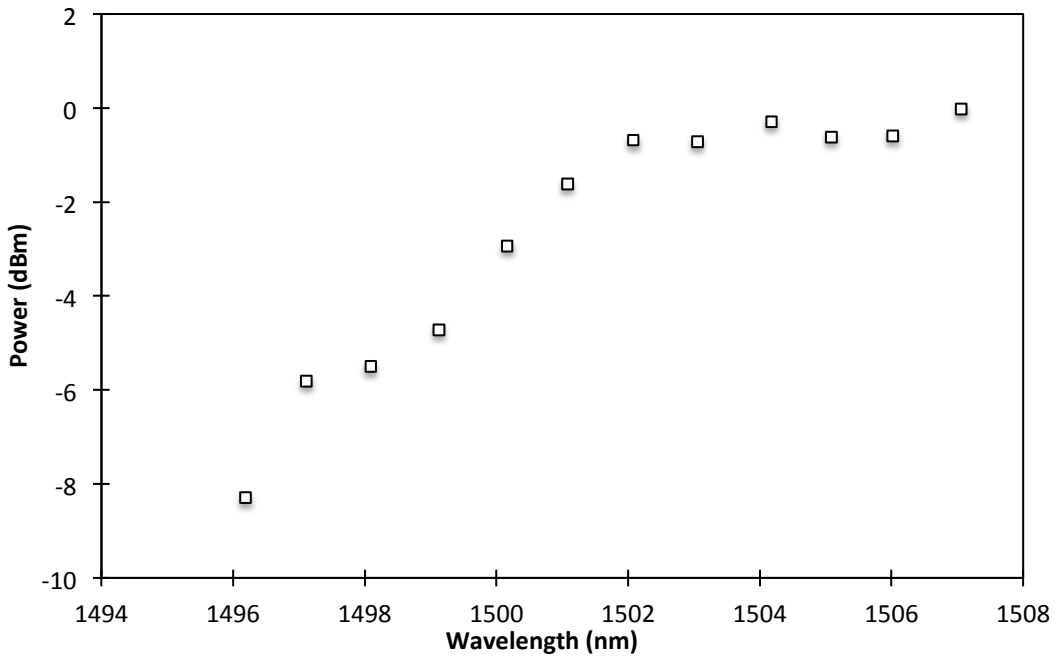

Figure 4.9: The output power of the tunable multi-wavelength S-band silica EDFL

As shown in Figure 4.10, the Side Mode Suppression Ratio (SMSR) is lower at shorter wavelength with the minimum SMSR at wavelength 1496.18 nm of about 66.19 dB. The SMSR increases linearly towards longer wavelength from 1496.18 nm to 1502.07 nm and becomes flat from 1503.05 nm to 1507.05 nm with maximum SMSR is recorded at wavelength 1507.05nm of about 74.46 dB.

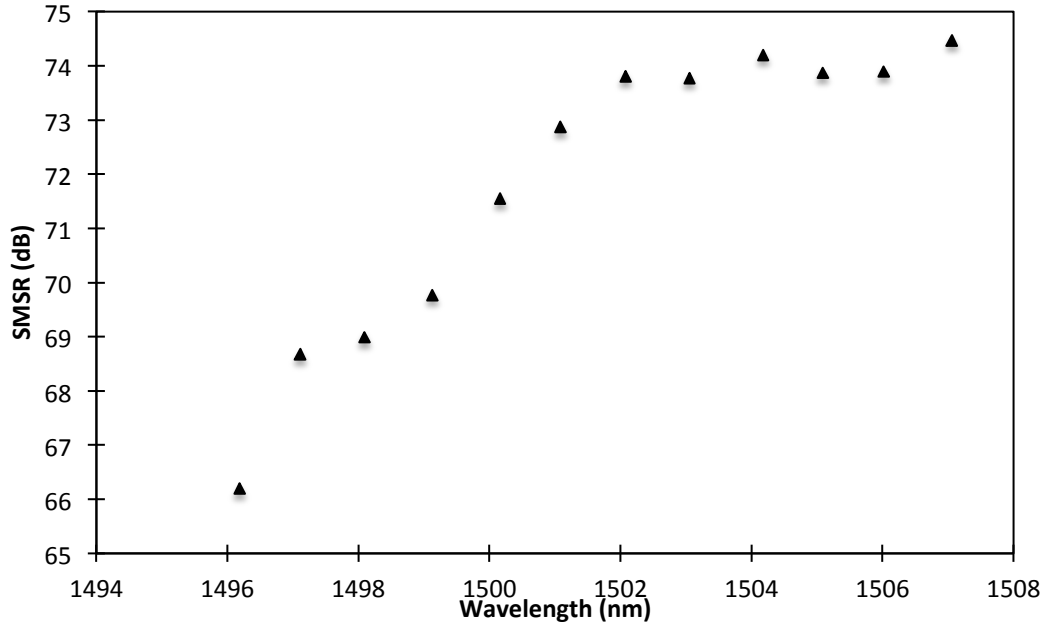

Figure 4.10: The SMSR of tunable S-band using silica EDF

4.3.6 Single Longitudinal Mode

SLM fiber lasers with wavelength tunable operation is also one of the important characteristic of a fiber laser. Tunable SLM fiber laser can be generated using many techniques such as multi-ring cavity with band pass filter [33,34], TFBG Fabry-Perot etalon [35] and saturation absorber [36,37]. Since silica EDFs have limited emission in S-band while providing good amplification for signal in the C-band and L-band region, other complex configuration can make the setup to experience loss. To avoid this problem a mechanism has to be designed for a low loss cavity and at the same time allows lasing in S-band. The saturable absorber method is suitable for this setup due to the shorter length required. The same setup as shown in Figure 4.3 is used. Two saturable absorbers are used in different location, namely location 1 and location 2 as shown in the Figure 4.11. The two locations are proposed such that they can optimize the power and achieve SLM operation. The operation of S-band SLM is as follows. Emission occurs when the 980 nm LD with 90.00mW power is pumped into the 3m silica EDF. Spontaneous emission is created and propagate in all directions. Some of the spontaneous emission is guided in the fiber and propagates to the optical isolator and to port 1 of optical circulator. The ASE is now incident to the 0.15 saturation absorber (SA1) which consists of un-pump EDF at location 1.A small portion of the ASE is absorbed inside the saturation absorber. After traveling through the SA1, the ASE is being filtered to a single wavelength of 1500 nm via 99% of TFBG. The reflected wavelength of 1500 nm carries multi-mode beating. When the selected wavelength passes through SA 1 at location 1, mode hoping is reduced. To make sure mode beating is further suppressed, SA 2 is inserted at location 2.

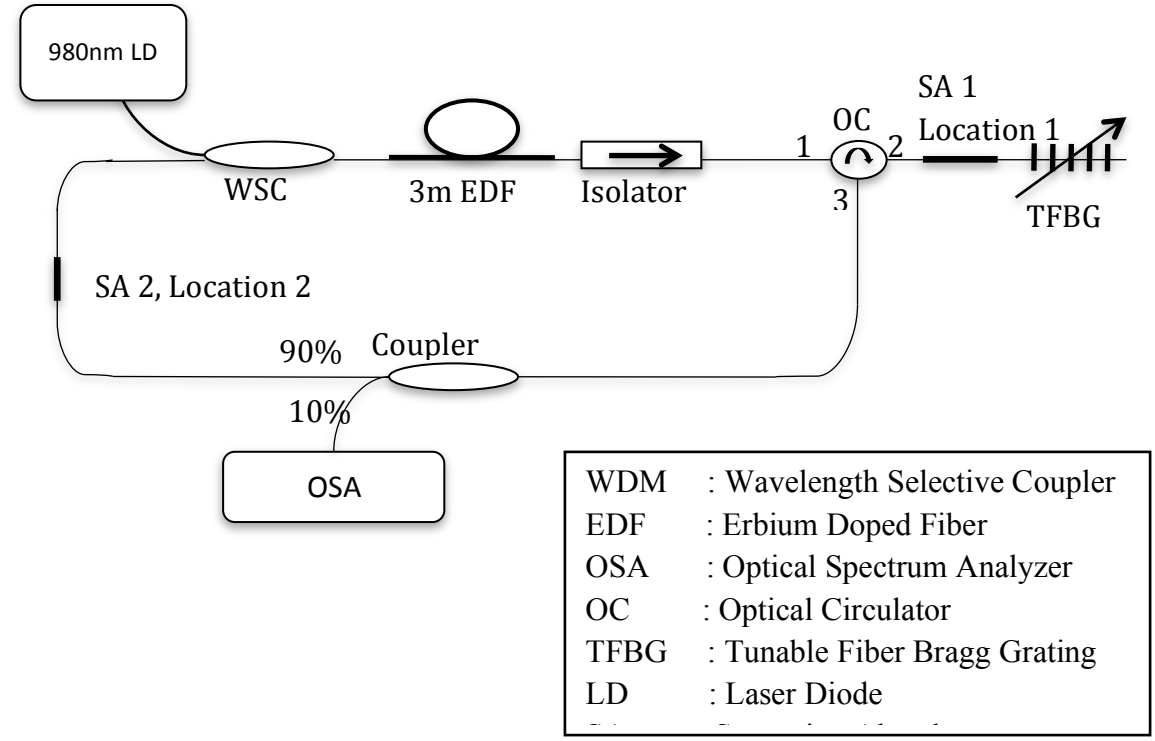

Figure 4.11 The experimental setup of S-band single longitidul mode operation.

The spectrum of S-band SLM fiber laser with different pump power is shown in Figure 4.12. The threshold of the SLM S-band laser is above 54mW and the highest power obtained is about -3dBm when pumped by 90mW of pump power at 980 nm.

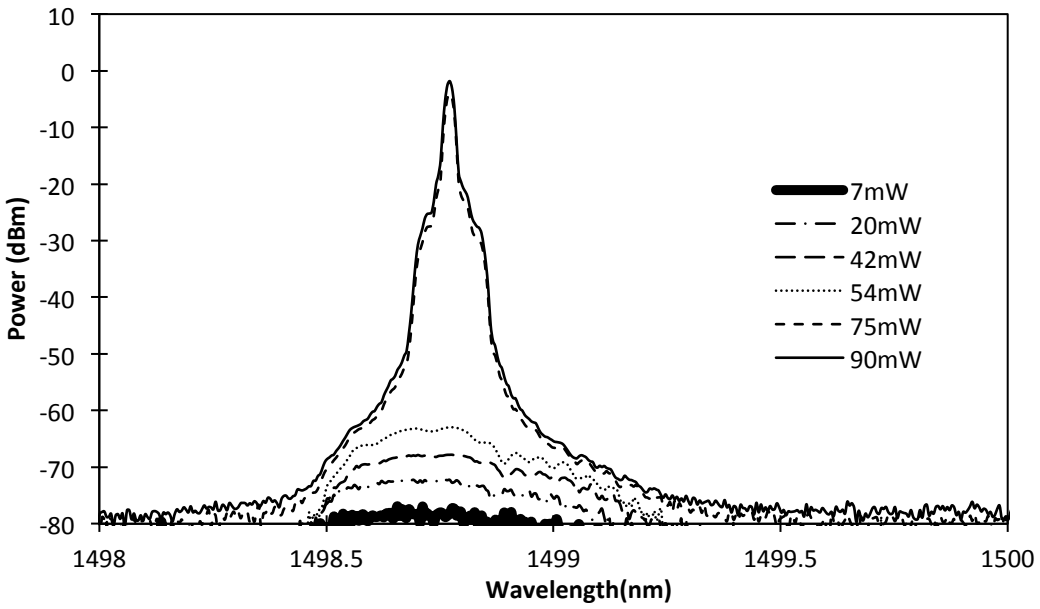

Figure 4.12: The laser spectrum of SLM operation

The mode beating of the laser output can be measured using the radio frequency spectrum analyzer (RSFA) and a high-speed photo detector**.** As shown in Figure 4.13 (a), multiple beat frequency occurs in the ring cavity without SA. The spectrum without SA is noisy and unstable due to mode hopping and beating frequency from longitudinal modes. This effect can be eliminated by inserting the two SAs inside the cavity. As shown in the Figure 4.13 (b) and Figure 4.13 (c) only one beating mode is observed which is at 93MHz when only SA 1 is inserted and a stable SLM operation can be achieved when both SAs are inserted in the cavity.

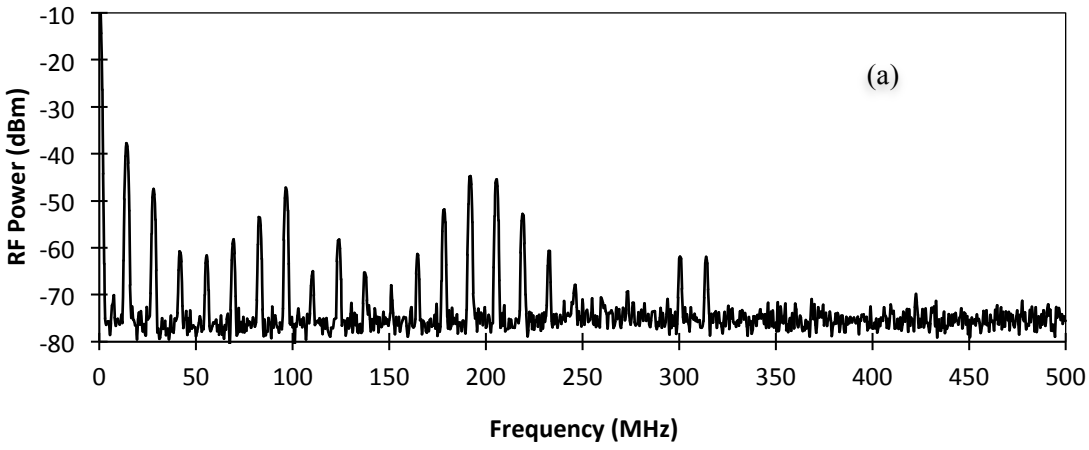

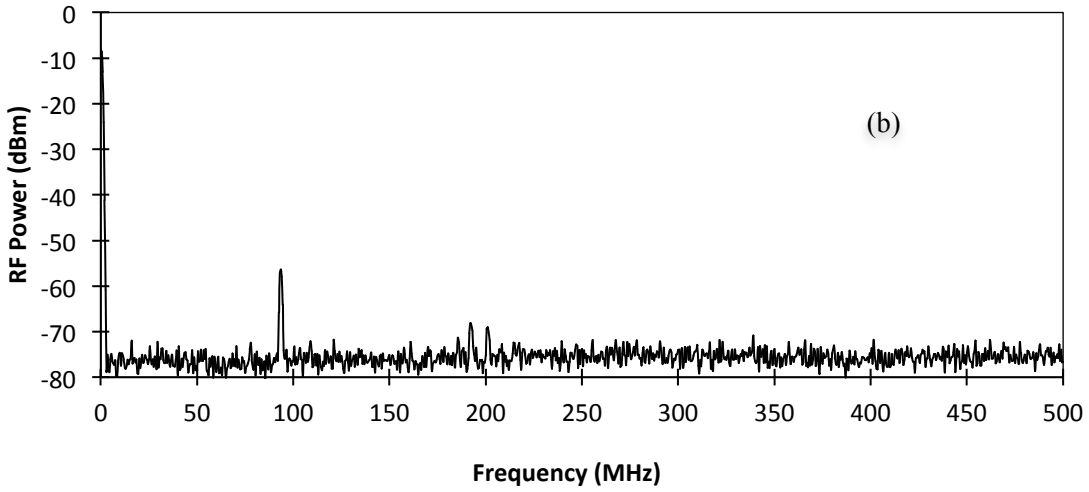

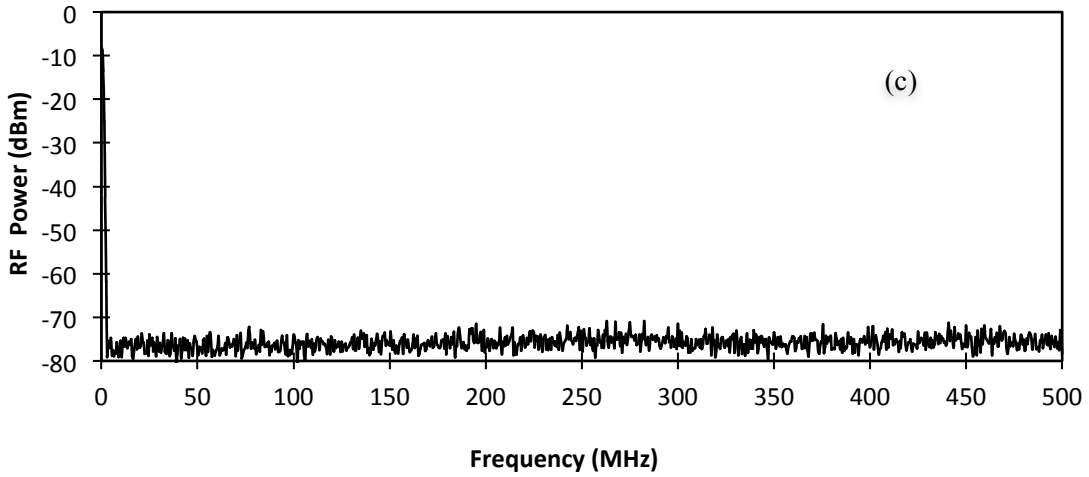

Figure 4.13: RF spectrum of output laser (a) without SA (b) with one SA at location 1 (c) with 2 SAs

4.3.7 Linewidth

The laser linewidth can be defined as the full-width half-maximum (FWHM) of the optical field of power spectrum. The linewidth can be measured using optical heterodyne method, delayed self-heterodyne method, the delayed self-homodyne method and optical discriminator technique [38].

The linewidth measurement technique used in this thesis is the delayed self-heterodyne technique as this technique provides a simple way to perform linewidth measurement without requiring a local oscillator laser like the heterodyne method. Figure 4.14 shows the delayed self-heterodyne technique experimental setup. By taking advantage of the large optical delay in optical fiber, Okashi etc. the width measurement could be performed with a simple optical interferometer [39]. The delayed self-heterodyne concept is as follow; the incident light from the laser under test is split into two path by the 3dB optical coupler. The optical frequency of one arm is offset with respect to the other. If the fiber delay line τ_0 of one path exceeds the coherent time τ_c of the laser under test, the combining beams interfere as if they originate from two independent

laser offset in frequency by δv as show in Figure 4.14. The beat tone produced is displaced from 0Hz by the frequency shift by δv in our experiment δv is 80 MHz. A spectrum from RFSA is displays the beat tone which is broadened by laser linewidth [38]. The translation of linewidth information from optical frequency to low frequency where RF SA operates is show in Figure 4.14. The requirement for incoherent mixing set a minimum delay requirement of the interferometer with respect to the laser linewidth:

$$\tau_0 \geq 1/\Delta v \tag{4.4}$$

when this condition is satisfied, the mixing becomes independent of the phases of interfering light, leading to more stable measurement.

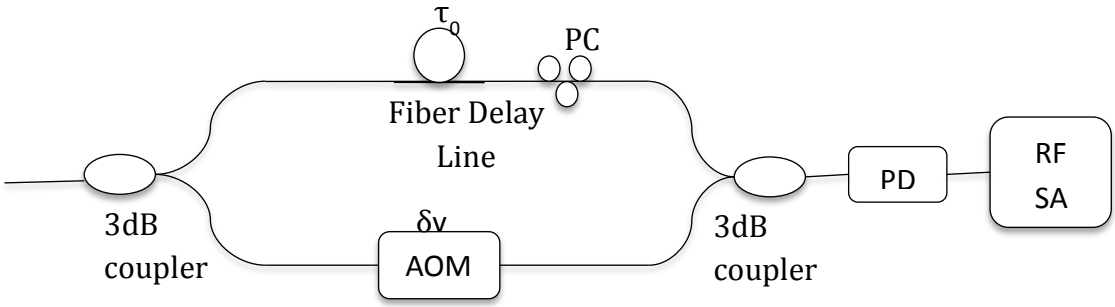

AOM	: Acousto Optic Modulator
PD	: Photodetector
RF SA	: Radio Frequency Spectrum Analyzer
PC	: Polarization Controller

Figure 4.14: The delayed self-heterodyne technique for line width measurement

Figure 4.15 shows a delayed self-heterodyne RF spectrum of the laser output that is used to measure the spectral linewidth of laser output.

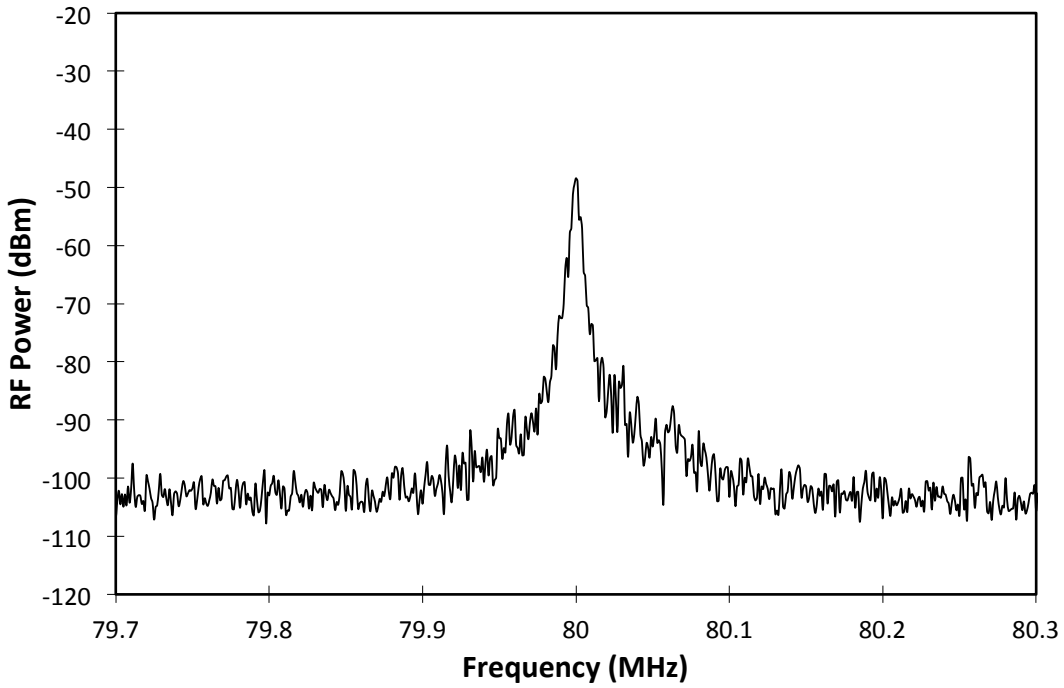

Figure 4.15: RF spectrum of delayed self-heterodyne signal.

The setup used for line width measurement consists of a 500m long single mode fiber used as the delay line and an acoustic optic modulator operating at 80MHz in one arm of the delayed self-heterodyne set-up to shift the beat frequency away from Direct Current (DC). The RF spectrum was plotted and the measured spectra linewidth of the SLM S-band fiber laser is about 0.14 MHz.

4.4 Depressed Cladding Erbium Doped Fiber Laser

The DC-EDF is purely designed for signal amplification in S-band. In this section we demonstrate the ring cavity fiber laser using DC-EDF as gain medium to obtain laser in the S-band. Characteristics such as output power and SMSR with different pumping configuration has been studied in this section. The depressed cladding erbium doped fiber laser (DC-EDFL) is constructed using a ring cavity.

The experimental setup to characterize the DC-EDFL is shown in the Figure 4.16. Two pumping direction are used, namely clockwise and anticlockwise pumping. The difference between the two setups is the direction of isolator that allows only directional propagation of the light. The clockwise direction can also be defined as forward pumping while the anticlockwise direction can be defined as backward pumping The DC-EDF length used in this setup is the same with the length that is been discussed in Chapter 3 which is is about 30m with spooling diameter of about 8cm. the pump power used is 307mW from 980nm laser diode. Different ratios of optical fused coupler which are 90/10, 80/20, 70/30 and 50/50 are used to study the efficiency of the laser. The output signal is measured and analyzed with OSA and optical power meter.

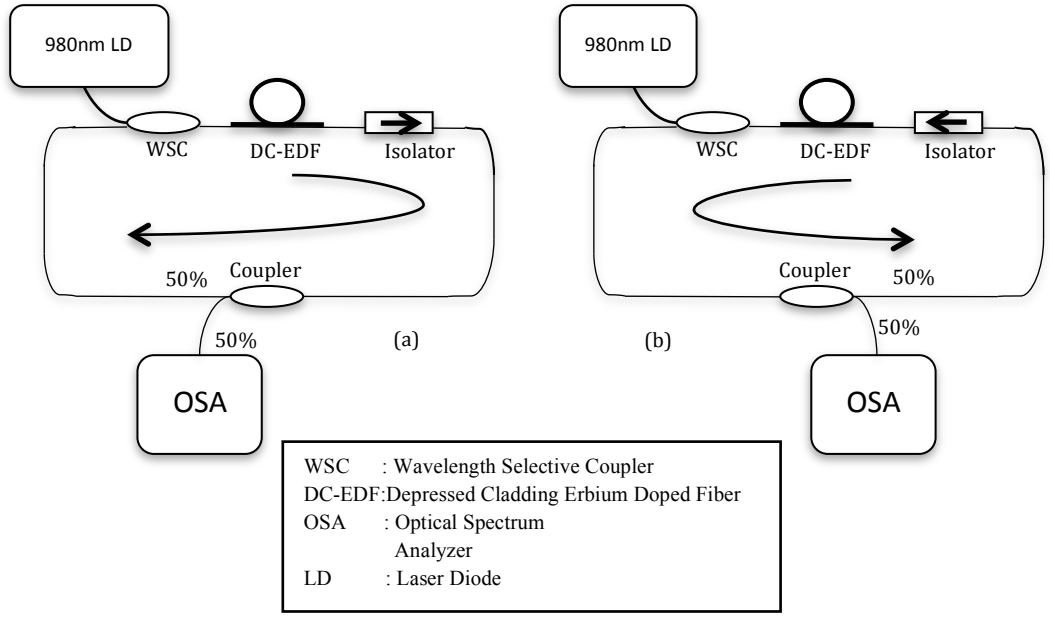

Figure 4.16 The experimental setup of ring cavity DC-EDFL (a) clockwise direction (b) anticlockwise direction

Figure 4.17 shows the output spectrum of the ring cavity DC-EDFL of both forward and backward pumping. The laser spectrum has a peak wavelength of 1498.03 nm for both pumping configurations. The output power for backward pumping is about 7.78dBm, which is higher than that of the forward pumping configuration, only about 2.40dBm.

ASE suppression occurs higher for forward pumping compared to the backward pumping.

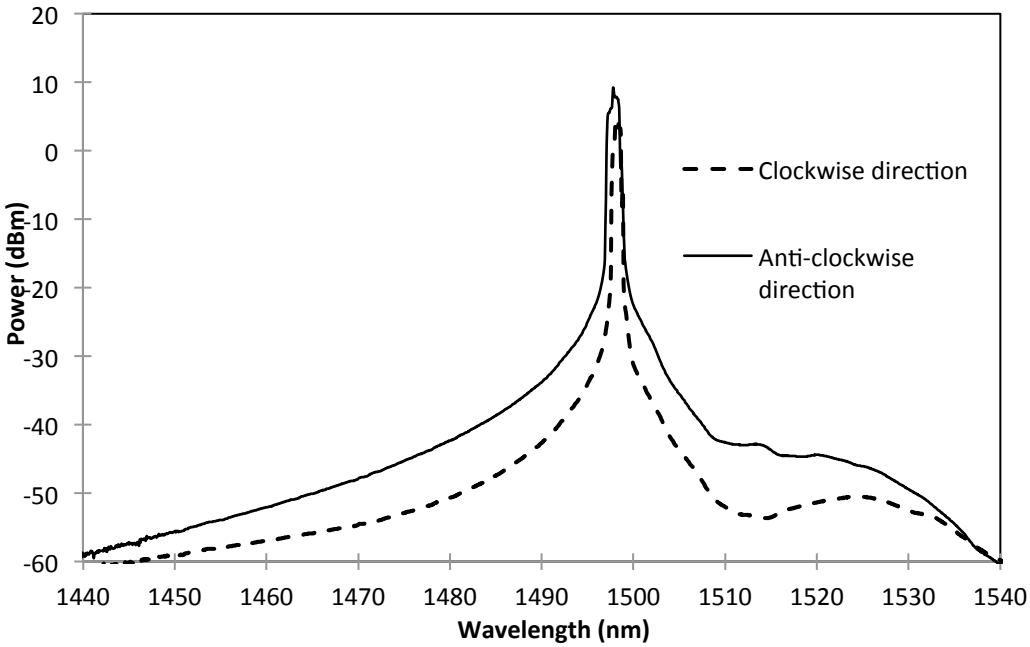

Figure 4.17 The output spectrum of the ring cavity DC-EDFL

4.4.1 Output Power Efficiency

Figure 4.18 (a) shows the output power with different pump power and coupling ratio for forward pumping. The coupling ratio are 90/10, 80/20 70/30 and 50/50 with the smaller portion of coupling ratio connected to the power meter. From figure 4.18(a) the power efficiency increases when a higher value of feedback is selected. The highest efficiency is recorded by using 50/50 coupler whereby half of the power is tapered out and the other half is being fed back into the cavity. The efficiency is about 1.49%. Figure 4.18 (b) shows the output power with different pump power and coupling ratio for backward pumping. Similar to forward pumping, the slope efficiency is the highest when 50/50 coupler is used. The maximum output power is about 13.8dBm with slope efficiency of about 5%. Figure 4.18 shows the comparison of output power with

different pumping configurations using the 50/50 coupler. As a comparison backward pumping is superior over forward pumping in terms of output power and slope efficiency with their corresponding difference are of about 9.7 and 3.51%, respectively

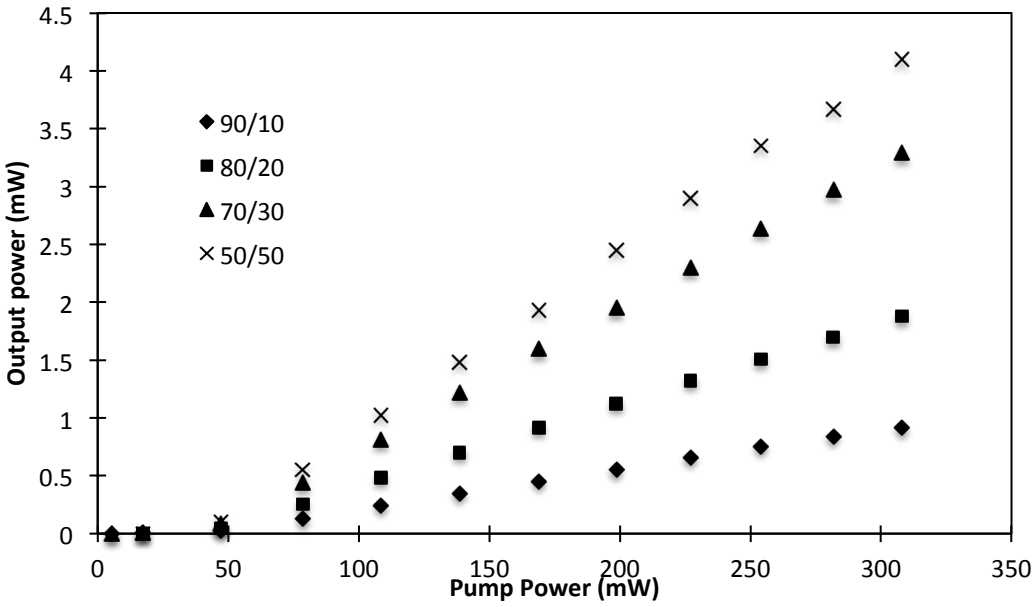

(a)

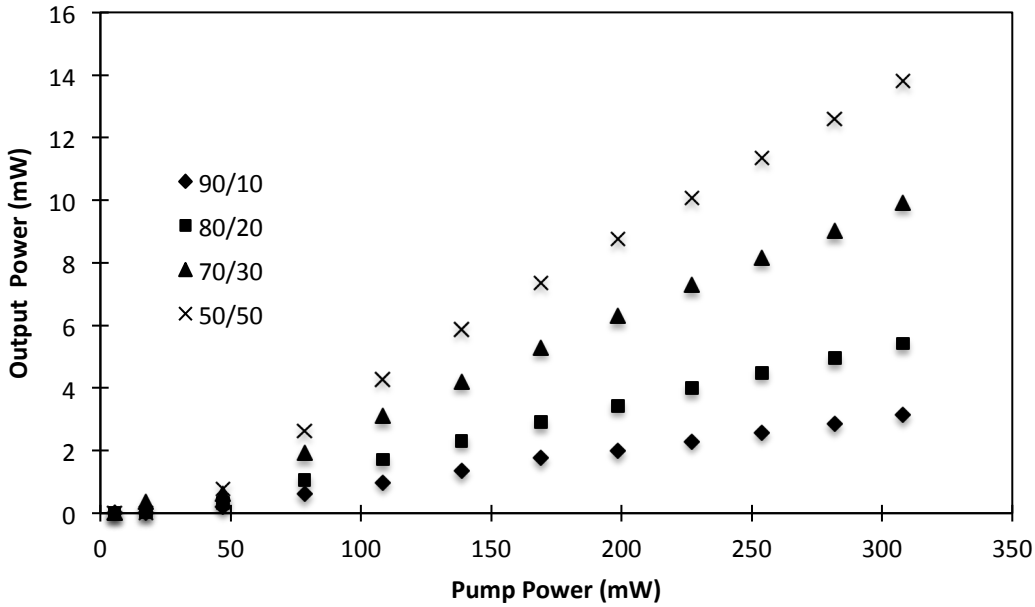

(b)

Figure 4.18 The output power efficiency of (a) clockwise direction and (b) anticlockwise direction with different pump power and coupler reflectivity

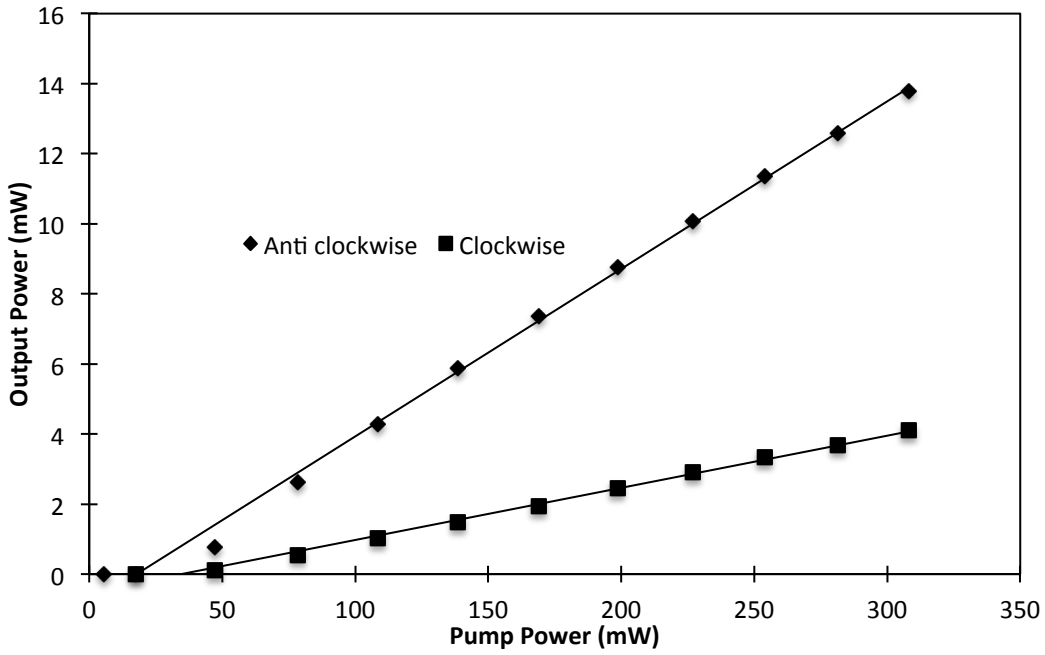

Figure 4.19 The performance of output power clockwise and anticlockwise direction with 3dB output coupler

Figure 4.20 shows the comparison of 3 dB spectra width by using 0.02 nm resolution OSA. The 3dB spectra width of forward and backward pumping of DC-EDFL is about 0.91 nm and 1.03 nm. This is due the relatively longer suppression of ASE in the forward pumped DC-EDFL

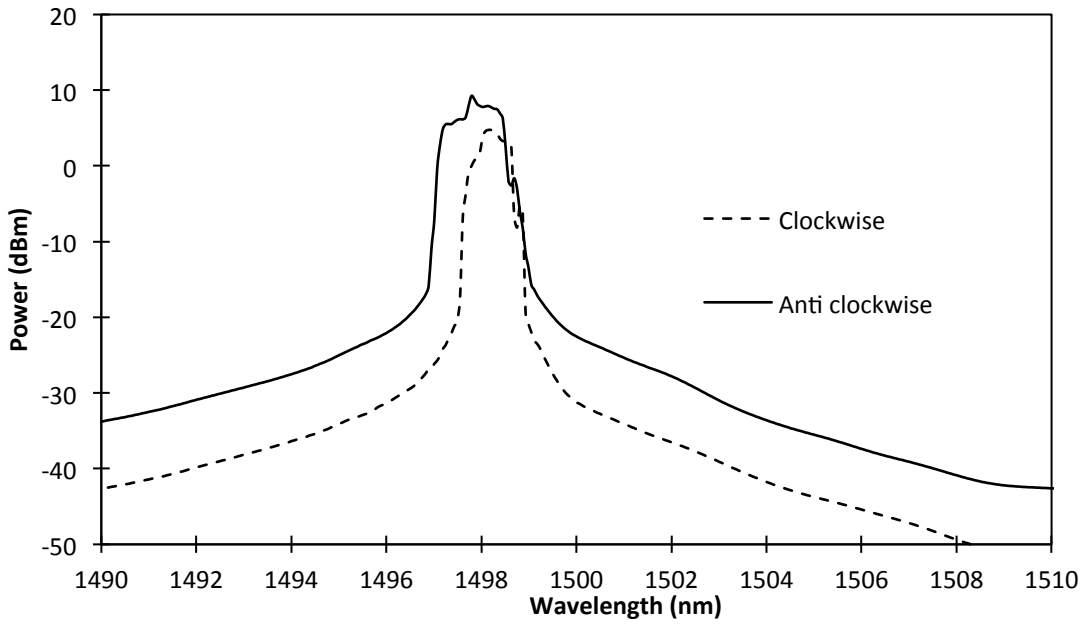

Figure 4.20 The comparison of 3 dB spectrawidth by using 0.02 nm resolution OSA

4.4.2 Tunable and Switchable S-band Depressed Cladding Erbium Doped Fiber Laser

4.4.2.1 Array Waveguide Grating

The use of AWG as a wavelength slicing mechanism has renewed interest in the development of multi-wavelength fiber lasers (MWFLs) operating at 50 GHz, 100 GHz and 200 GHz channel spacing which complies with current DWDM network standard. Therefore, an AWG can be used in conjunction with an ASE source such as an EDFA or a SOA to obtain a sliced ASE multi-wavelength spectrum, which is then rerouted onto itself to form MWFL [40-42]. Tunable fiber lasers using AWGs have also been explored whereby special input/ output mechanisms or integrated planar lightwave circuit (PLC) switches [43,44] are used to obtain switchable wavelengths, although these systems can proved to be very complex to develop.

Figure 4.21 shows the configuration of the tunable S-band DC-EDFL using AWG with (a) forward (b) backward pumping configuration. The setup consists of a 980/1550 WSC and a 30 m long DC-EDF pumped by a 980 nm laser diode. The DC-EDF provides the initial ASE spectrum as well as acting as the gain medium for the proposed laser. The WSC is used to combine pump signal with lasing signal that will be generated from the DC- EDF and AWG. An optical channel selector (OCS) provides tunability while a 1X16 AWG is used as spectrum slicing mechanism for the proposed setup.

The operation of the tunable S-band DC-EDFL using AWG in forward pumping configuration is as follow; the ASE generated from the DC-EDFA travels through the optical isolator. The ASE will then travel along the AWG to be sliced into 16 wavelengths. The 16 channels output of AWG are connected to 16 channels of OCS.

Only one selected wavelength is allowed to travel through the OCS. This wavelength will then oscillates in the setup and begin lasing once the threshold has been exceeded. A 50/50 coupler is used to extract a portion of the laser for analysis. The selected lasing wavelength can be changed using different OCS outputs that correspond to the different AWG channels, therefore allowing the proposed fiber laser to be tuned.

The OCS used in this experiment is a 2X16 motor driven optical switch with a maximum switching time of 500ms between each subsequent channel. However, for the purpose of this experiment, only one input channel is used, thus in effect making the OCS a 1X16 switch. The OCS has an operating wavelength range of 1200 nm-1650 nm, giving it a bandwidth of 450 nm. This makes the OCS suitable for this experiment, as the bandwidth of the AWG used falls well within the bandwidth of the OCS. The loss per channel is above 4.5 dB, while all channels have a minimum return loss of approximately 40 dB and a cross-talk of -65 dB. This is the same for the case of backward pumping except in the aspect of pumping direction.

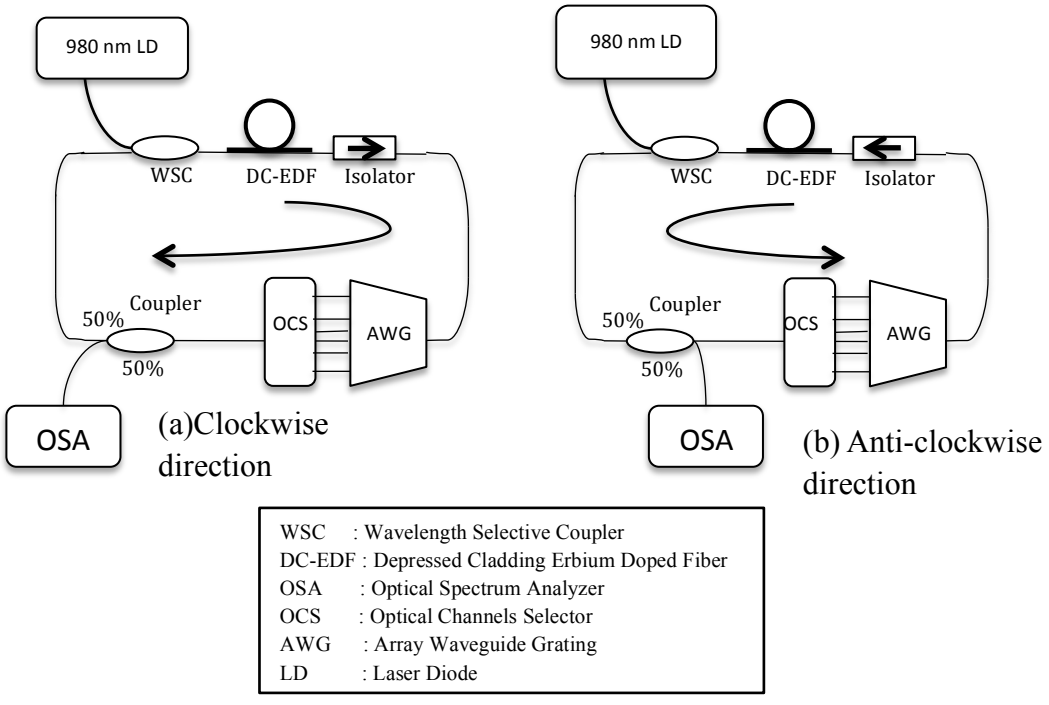

Figure 4.21 The experimental setup for tunable S-band DC-EDFL fiber laser using AWG

Figure 4.22 (a) and (b) show the tuning range of tunable S-band DC-EDFL operating in clockwise and anticlockwise direction. As can be seen in Figure 4.22 (a) and (b), the 16 channels have a spacing of 0.75 nm between each lasing wavelength and an overall wavelength tuning range of 11.3 nm from 1478.6 nm to 1490.1 nm. These values comply with the requirements of the ITU grid standards. The ASE level for the clockwise direction is lower compared to the anticlockwise direction. However the output power for the clockwise direction is lower than that of the anticlockwise direction with the average power with the average power of about 0.8 and -8.4dBm for the clockwise and anticlockwise directions respectively.

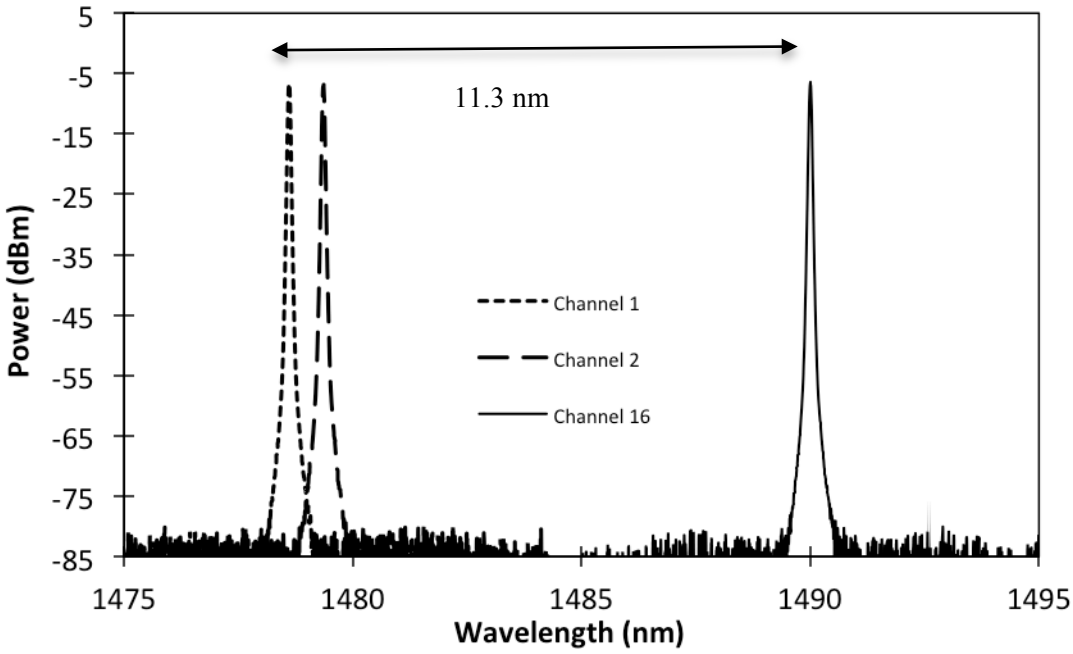

(a)

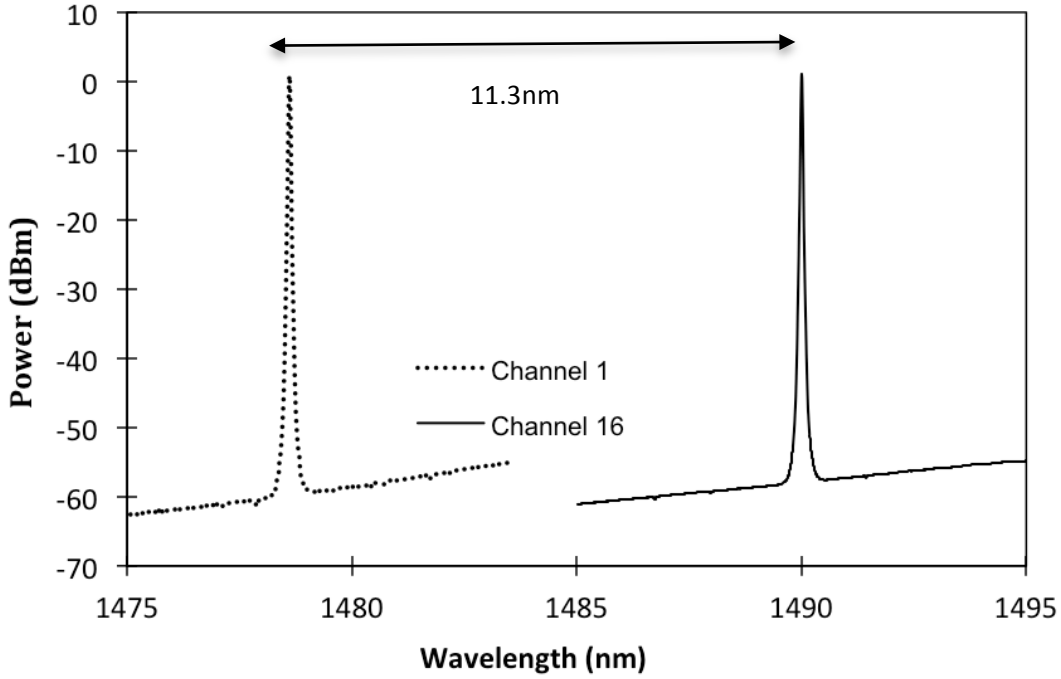

(b)

Figure 4.22 The tuning range spectrum of (a) clockwise (b) anticlockwise direction.

Figure 4.23shows the output power level for laser operation in forward pumping and backward pumping configuration for all 16 channels of AWG. The average output power of backward pumping operation is higher than that of the forward pumping with the output power of backward pumping is about 5.14dBm. The power difference is due to saturation power effect resulting from the pumping scheme where backward pumping has higher saturation power compared to forward pumping therefore it leads to the generation of higher output power.

However the SMSR of backward pumping operation is lower than that the forward pumping. As shown in Figure 4.24, the SMSR for forward pumping operation is higher than that of the backward pumping which their difference is13.72 dB. The average SMSR for forward pumping operation is about 72.82 dB whereas for backward pumping is about 77.7dB. The difference in SMSR quality is due to the ASE suppressions in which forward pumping operation has a higher suppressed ASE level compared to that of backward pumping operation.

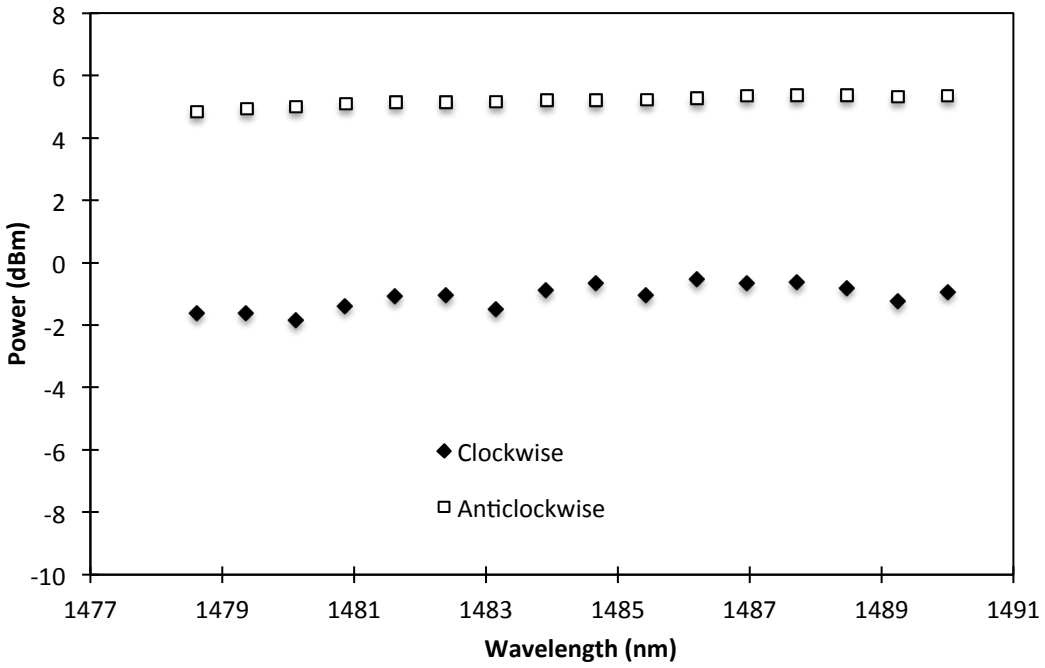

Figure 4.23: The output power of clockwise and anticlockwise direction for the entire channel

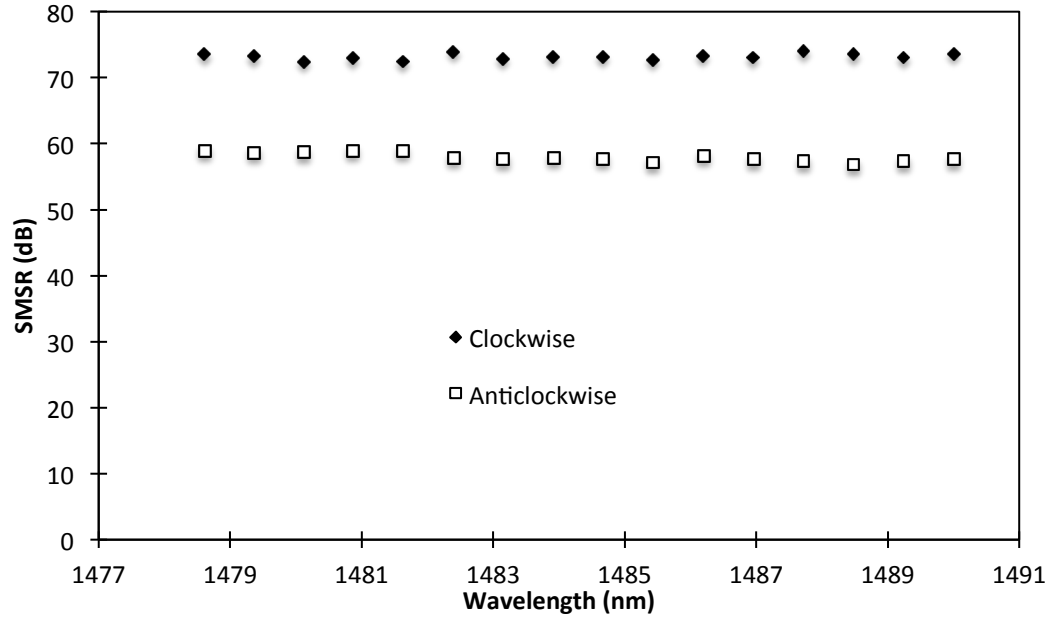

Figure 4.24 The SMSR of clockwise and anticlockwise direction for the entire channel

4.5 S-band Raman Fiber Laser

Raman fiber Laser (RFL) is one of the promising techniques to produce laser in the S-band because RFL lasing region depends on the pump wavelength. RFL has the advantage of producing high output power due to its ability to operate at high saturation [45-47]. The RFL also has the advantage to extending the bandwidth of the laser by combining Raman Pump (RP) of different wavelengths. However, the RFL also has some drawbacks. RFL normally operates in high threshold which needs high power RP which is cost intensive. To solve the issue of high threshold RFL, many techniques to have been proposed such as using microsphere tapered fiber [48], where only 86μW of RP power is needed to obtain RFL. In this section we demonstrate the S-band RFL (S-RFL) and study its characteristics in terms of laser bandwidth, output power as well as SMSR and the threshold of S-band RFL

The S-band Raman Fiber Laser (S-RFL) studied is configured as a ring cavity. The Raman gain medium used is a Dispersion Compensation Fiber (DCF) with a length of about 7.7km. The DCF is pumped by bidirectional pumping setup with total RP power and RP wavelength of about 370 mW and 1425 nm respectively. The Raman gain characteristic of this fiber is discussed in Chapter 3. To achieve lasing a TBF is inserted inside the cavity as shown in Figure 4.25. The TBF has an optimized tuning range in the C-band but still can filter down to S-band. The 3 dB spectra width of the TBF is about 0.1 nm. The proposed setup of S-RFL is in the formed of a ring cavity. It consists of an isolator to ensure unidirectional light propagation in the cavity. The 50/50 optical fused couple is used to tap out the output power of the S-RFL. OSA and optical power meter (OPM) are used to measure the output spectrum and output power respectively. The OSA resolution is set to be 0.02 nm.

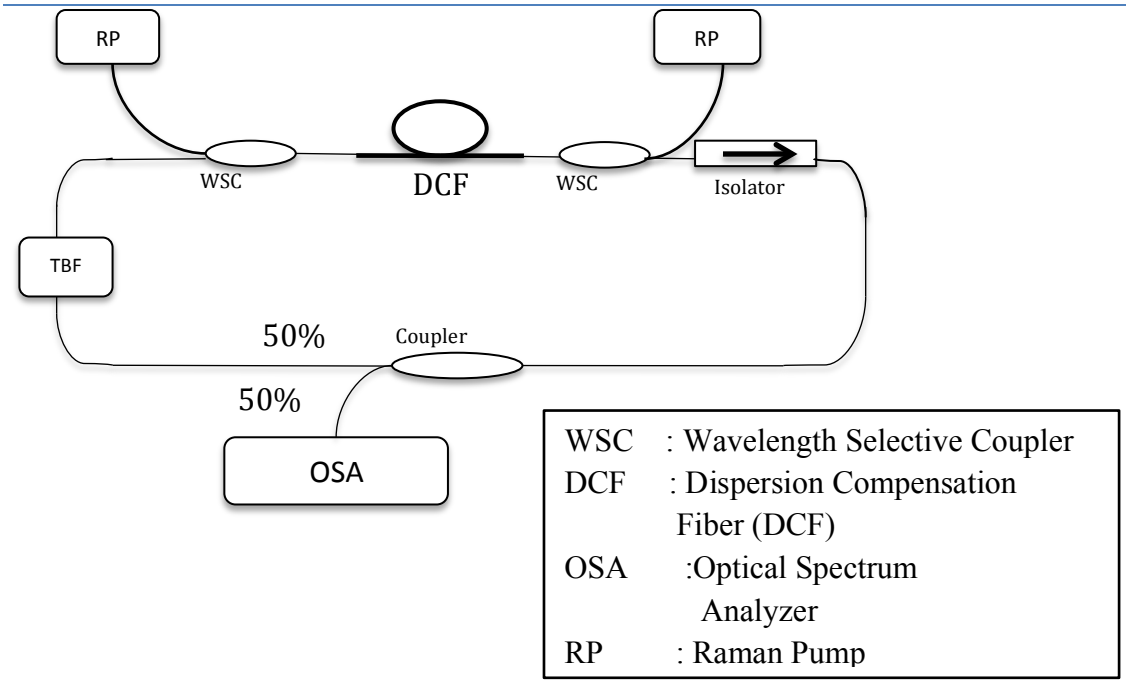

Figure 4.25 The experimental setup of S-band Raman fiber laser

As discussed in the Chapter 3, the bandwidth of the Raman amplifier depends on the RP wavelength. With the RP wavelength set at about 1425 nm for both RP, the tuning range of S-RFL is measured and shown in Figure 4.26. The tunablity is obtained by tuning the micrometer head of TBF. The tunabilty spacing is fixed around 2 nm. As shown in Figure 4.25 the superposition of wavelengths is from 1508.4nm to the 1534.2 nm with a bandwidth of about 25.8 nm. Wavelength shorter than 1508.4 nm and longer than 1534.2 nm cannot lase due to the limitation of Raman gain bandwidth. To make sure that the bandwidth limitation is purely caused by Raman gain bandwidth, we replace the TBF with 1500 nm FBG into the similar setup as shown in Figure 4.3 and the result shows that no laser is obtained at this wavelength. The average output power of S-RFL is about -11.5 dBm. The output power and the bandwidth can be improved if a different combination of RP is used.

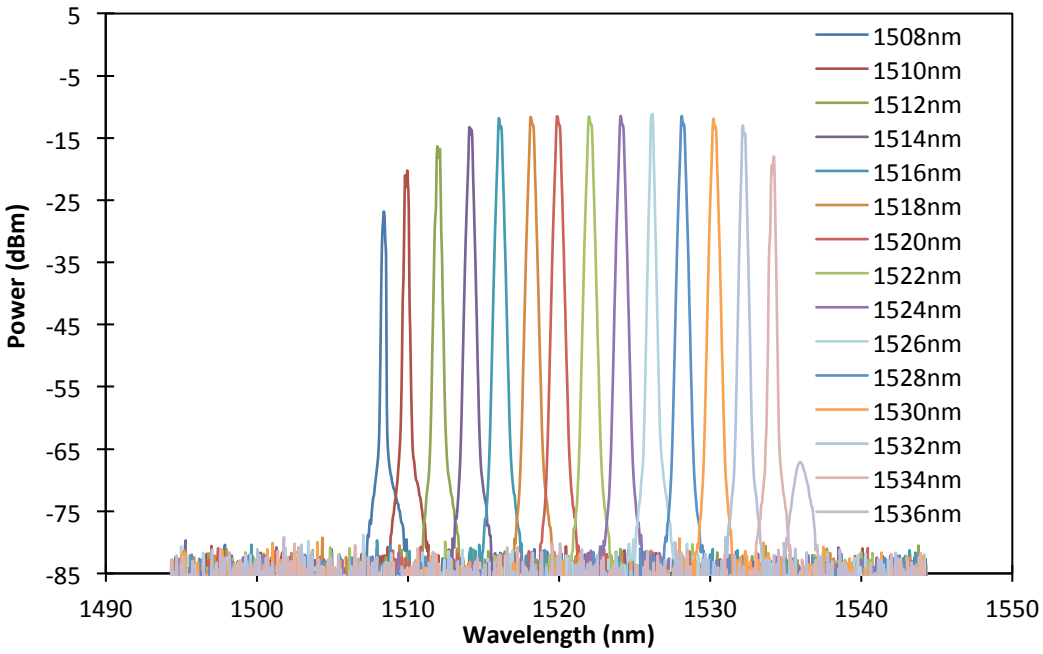

Figure 4.26 The tuning range of the S-band Raman fiber laser

Figure 4.27 shows the output power and SMSR of the tunable S-RFL. It can be seen that the output power of the laser reduces before and after the Raman optimum gain at 1525 nm. The Raman optimum gain occurs when RP wavelength is 100 nm shorter than Raman optimum gain. The output power of the S-RFL is reduces when the laser wavelength is 1525 nm. The average output power is about -11.5 dBm and the lowest output power is -28.49 dBm at 1508.3 nm. The same trend is observed for SMSR, with the highest SMSR is obtained 1526 nm is about 70.69 dB while the lowest SMSR is recorded at 1508 nm, at about 55.2 dB. In addition, the output power curve follows the same profile as of the gain curve as discussed in the Chapter 3. If the gain medium has the flat curve, the output profile of the S-RFL is also expected to be flat.

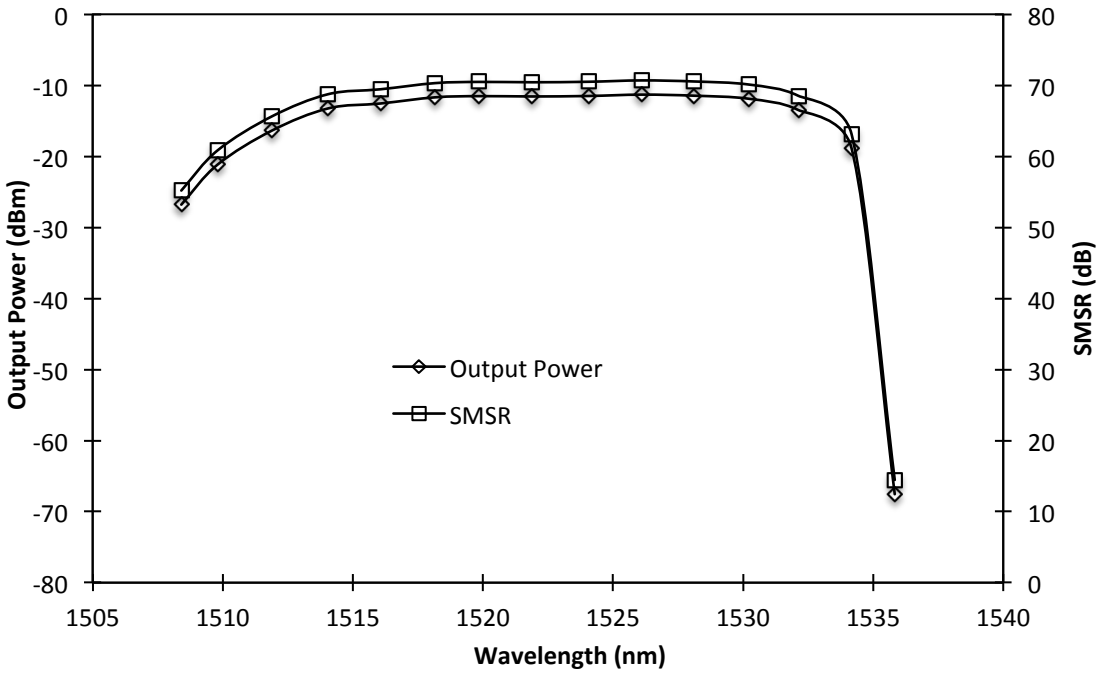

Figure 4.27 The output power and SMSR of the S-band Raman fiber laser with different tuning wavelength

As mentioned earlier the drawback of RFL is the high lasing threshold operation. The study of lasing threshold operation of S-RFL is done whereby the output power with different RP power is plotted in Figure 4.28. As shown in Figure 4.28 the lasing threshold of the S-RFL at 1515 nm is higher compared to the other type of the S-band gain medium in this study. The S-RFL lasing threshold is about 348mW of RP power. This value is higher compared to the threshold value achieved by using EDF, DC-EDF and the SOA. We also believe that high output power will be generated if we apply higher pump power to the gain medium. However due to the limitation of RP power in our facility we are unable to probe the output saturation of the current S-RFL setup. As conclusion, the S-RFL has the advantage of wide bandwidth selection and is also able to produce flat output power over the bandwidth. However one of the disadvantages of S-RFL is that it has high lasing threshold operation which requires the use of high power of RP.

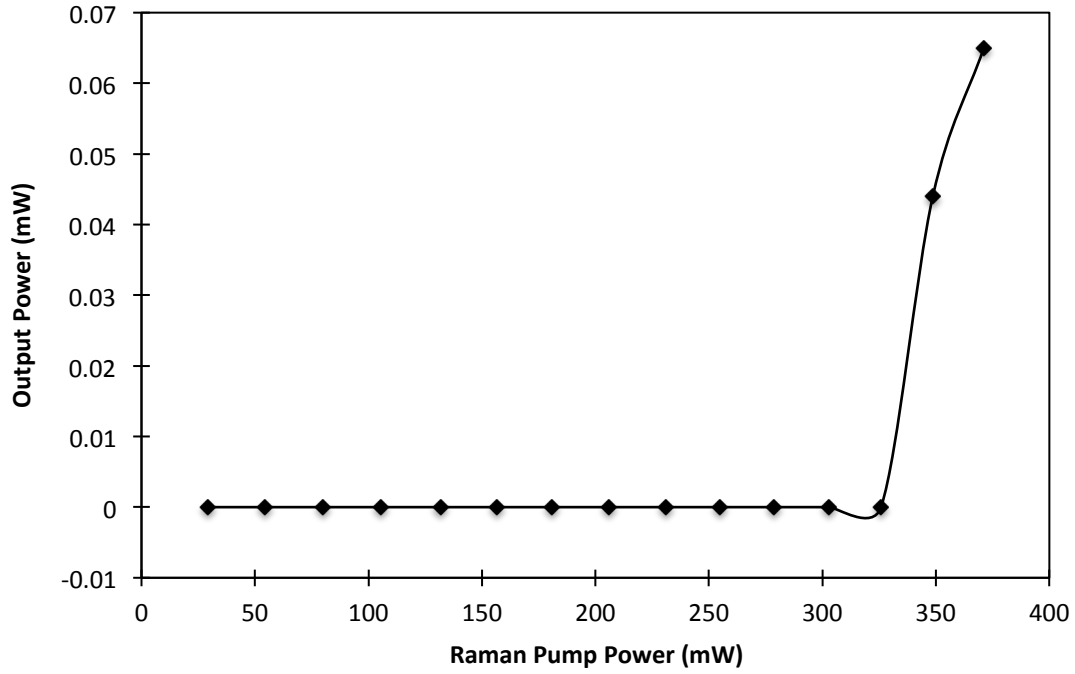

Figure 4.28 The output power with different Raman pump power at wavelength 1515 nm

4.6 S-band Semiconductor Optical Amplifier based Fiber Laser

As discussed in Chapter 3, a semiconductor optical amplifier (SOA) can provide a wide gain including in S-band. Experiment study of S-band SOA fiber laser (SOAFL) is not only focused on the laser characteristics at S-band as we also take the advantage to look into the laser operation at C-band and L-band to create an ultra wide band laser source.

4.6.1 Wide Band Ring Cavity SOA Fiber Laser

4.6.1.1 Array Waveguide Characteristics

Taking the advantages of the working principle of AWG and the ASE output of SOA, which covers the S-, C- and L-bands, each channel of the AWG will 3 laser output with wavelength from S-, C- and L-bands. In AWG each individual wavelength will be diffracted and focused at different angles at the AWG output plane according to equation (4.5) below [49],

$$\theta_m \approx \frac{N_{eff}}{N_f}\frac{\Delta L - m\lambda_g}{d_a} \tag{4.5}$$

where θ_m is the tilt angle, ΔL is the optical path difference, $\lambda_s = \frac{\lambda}{N_{eff}}$, m is an integer (diffraction order), d_a is the pitch between the array waveguide, and N_{eff} and N_f are the effective refractive indices in the waveguide array and in the free propagation region respectively. The AWG used is optimized for C-band operation from wavelength of 1530.56 nm to 1542.34 nm. However, when a broadband source (S-, C- and L-bands) is passed through the AWG, each channel will have 3 components, each one for S-, C- and L-bands. This is due to the various diffraction order which now includes *m-1*, *m* and *m+1* which satisfies the condition $\theta_{m-1}=\theta_m=\theta_{m+1}$ for different wavelengths.θ_{m-1} is for L-band, θ_m is for C-band, and θ_{m+1} is for S-band. Since they are focused at the same spot at the end of the free propagation region, they will be reproduced simultaneously in a single output although the AWG is designed to operate in C-band only. These output channels are connected to the 16 outputs of the 1X16 optical switch, which is referred

as the optical channel selector (OCS1). For instance, channel 1 contains outputs in S-, C- and L-bands at wavelengths that satisfy the equation (4.5).

The experimental setup, as shown in Figure 4.28, consists of a SOA, an AWG and two OCSs connected in a ring configuration. The SOA is from Alphion (SAS26P) with output characteristic that covers a wavelength range from 1400 nm to 1650 nm which acts as the gain medium. The Amplified Spontaneous Emission (ASE) emitted from the SOA is connected to the 1x16 AWG which slices the ASE output spectrum into 16 different wavelength outputs which are directed to 16 different channels.

The optical switch is a commercial unit (ANDO AQ3540) with a switching speed between channels of 500 ms and a transmission bandwidth ranging from 1200 nm to 1650 nm. This bandwidth is large enough to cover the experimental bandwidth of this work.

The output of channel 1 (similar for the other channels) is then connected to a S/C+L bands WSC that splits the S- and C+L bands through two different output ports. The C+L band is further split into C- and L- band outputs using a similar fused WSC coupler as shown in Figure 4.29. Each individual output for S-, C- and L- band, is then connected to channel 1, 2 and 3 of the second OCS (OCS 2). From OCS 2, the individual output, S, C or L, can be chosen as a mean to provide tunability. For instance, if the S output of channel 1 from OCS 1 is chosen (λ_{s1}=1478.6 nm), this signal will be injected into the ring cavity via channel 1 of OCS 2 to be amplified by the SOA. Similarly, selection of different channels of the AWG provides the tunability within the S-band region. A similar approach is also applicable for the C- and L-bands by choosing channel 2 and 3 of OCS 2. The injected light will travel in the ring cavity in an anticlockwise direction set upon by the optical isolator. The output signal is taken from a 90/10 broadband fused biconical tapered coupler with the 10% port connected to the optical spectrum analyzer (ANDO 6317 C) with a resolution of 0.02 nm. The tunability

spans over the S-, C- and L-bands providing a very well controlled and simple design, laser source that can be utilized for WDM, CWDM network and also for application in optical sensors, optical spectroscopy and many others.

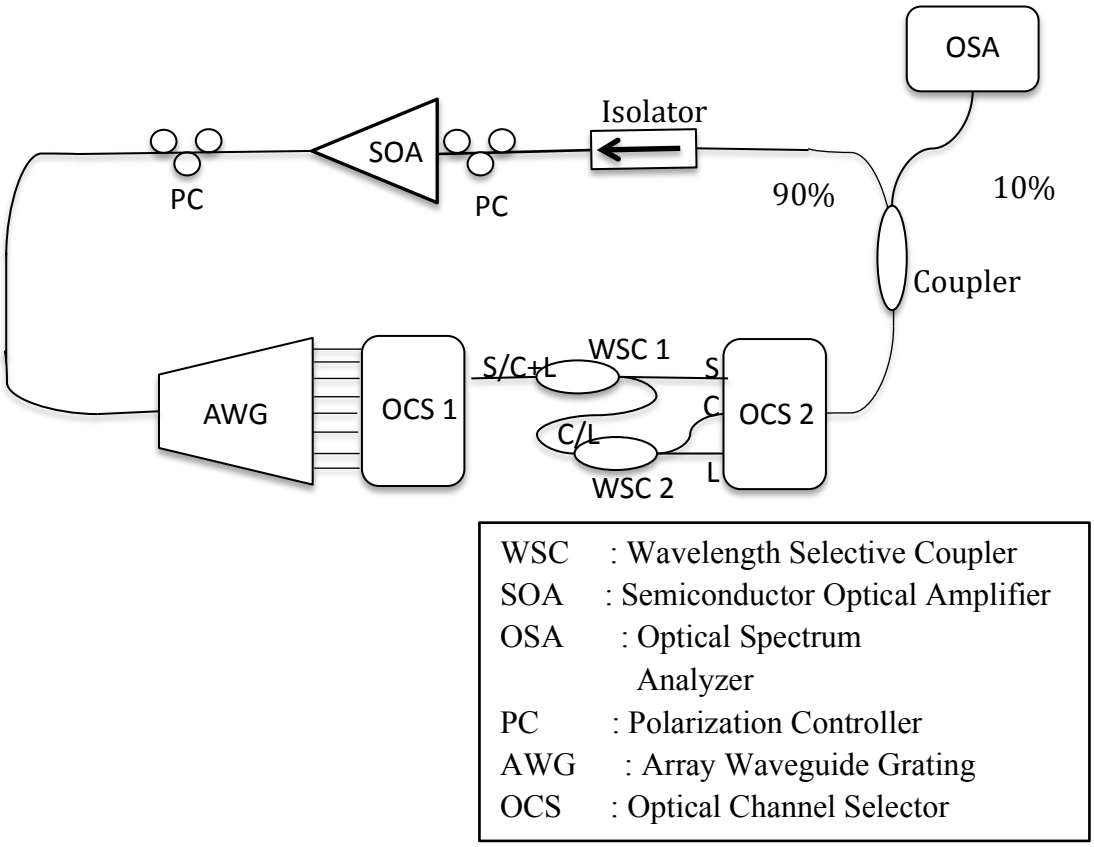

Figure 4.29 The experimental setup of wide band SOAFL [49]

Figure 4.30 shows the superimposed spectrum that consists of outputs in the three bands that are taken sequentially by selecting the channels at OCS2 which is measured by OSA from the 10% output port of the SOAFL. These peaks are the oscillating signals in the ring cavity, and the peak that will oscillate depends on the channels being selected. As illustrated in the figure, the measured peak powers are -9.92 dBm, -6.03 dBm and -7.57 dBm for 1478.69 nm(S-band), 1530.56 nm (C-band) and 1586.26 nm (L-band), respectively. The peak powers have power variation within 4 dB and they can be equalized by proper cleaning of the connectors and also by having an AWG with equal response at these wavelengths. For channel 2 and the rest of the channels the output will

be similar, representing the various bands, but shifted by 0.8 nm (100GHz) which originates from the interchannel spacing of the AWG.

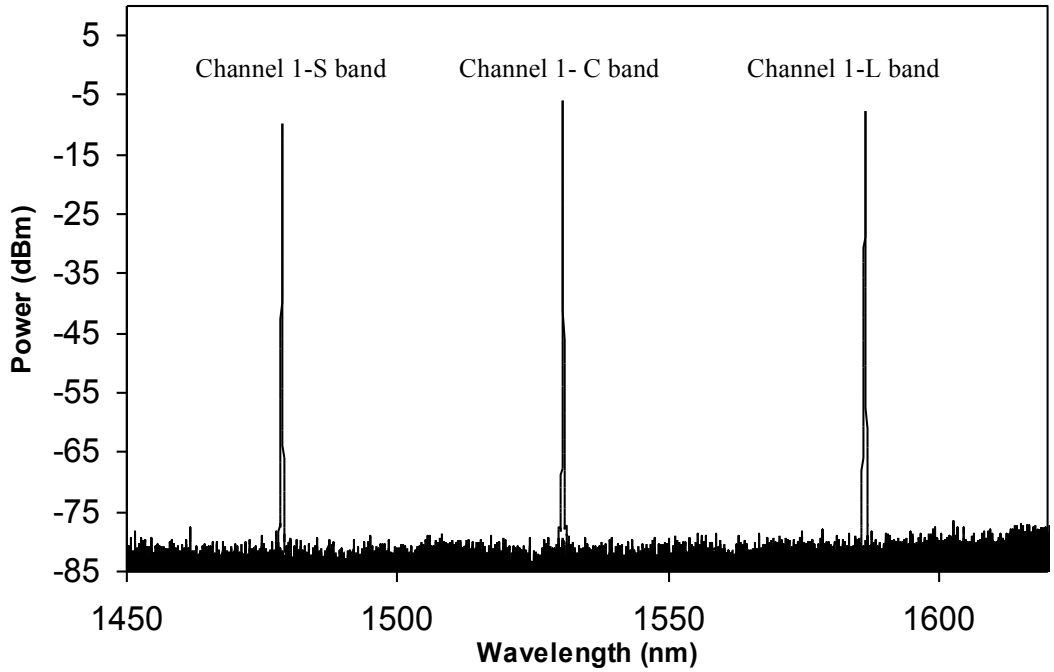

Figure 4.30 Spectrum of the output wavelength from channel 1 before it is split into three different bands by the S/C+L and C/L splitter

The tuning range of the single wavelength laser is shown in Figure 4.31. It shows that the widest tuning range can be realized for the S-, C- and L-bands by superimposing the output wavelengths coming from Channels 1 to 16 of the AWG. The tuning range for S-band is 11.7 nm stretching from 1478.3 nm to 1490.0 nm, for C- band is 11.8 nm from 1530.5nm to 1542.3 and for L band is 12.2 nm from 1586.2nm to 1598.4nm. The measured spectra width of the outputs in the S-, C- and L-bands are about 0.05 nm, 0.035 nm and 0.035 nm respectively. A wider tuning range can be achieved by using an AWG with more channel outputs. In the case of 1X16 AWG with 100GHz (0.8 nm) interchannel spacing, the maximum tuning range that can be realized in the C-band is 15 x 0.8 nm which equals to 12 nm. This value corresponds well with the measured

value of 11.8 nm. The tunability is similar for S- and L-band. For a higher channel count, such as 1X64 AWG, the tuning range can be as wider as 50.4 nm. This shows that the experimental approach can be extended a wider tuning range by having a larger number of channel outputs**.**

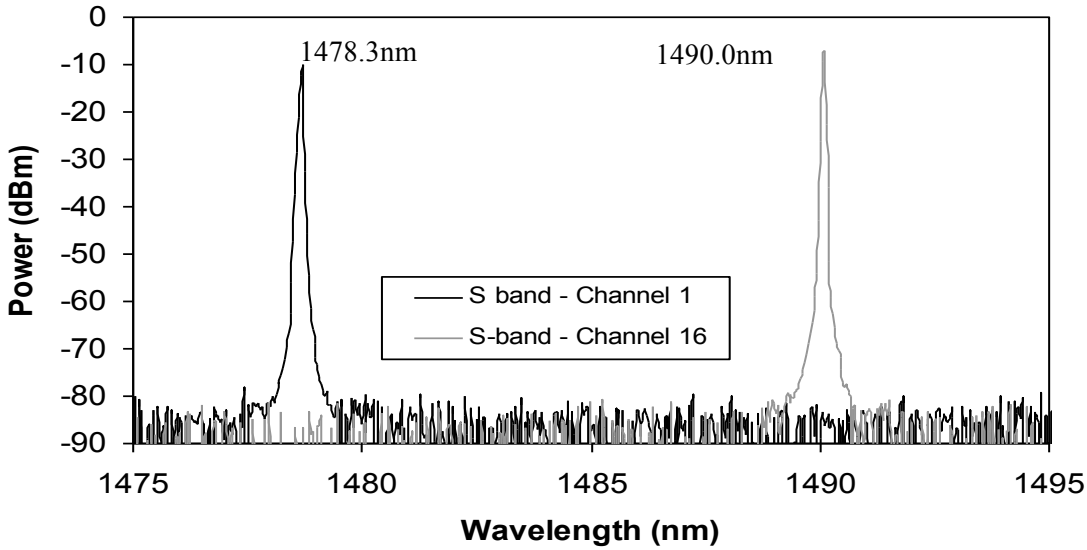

(a) S-band

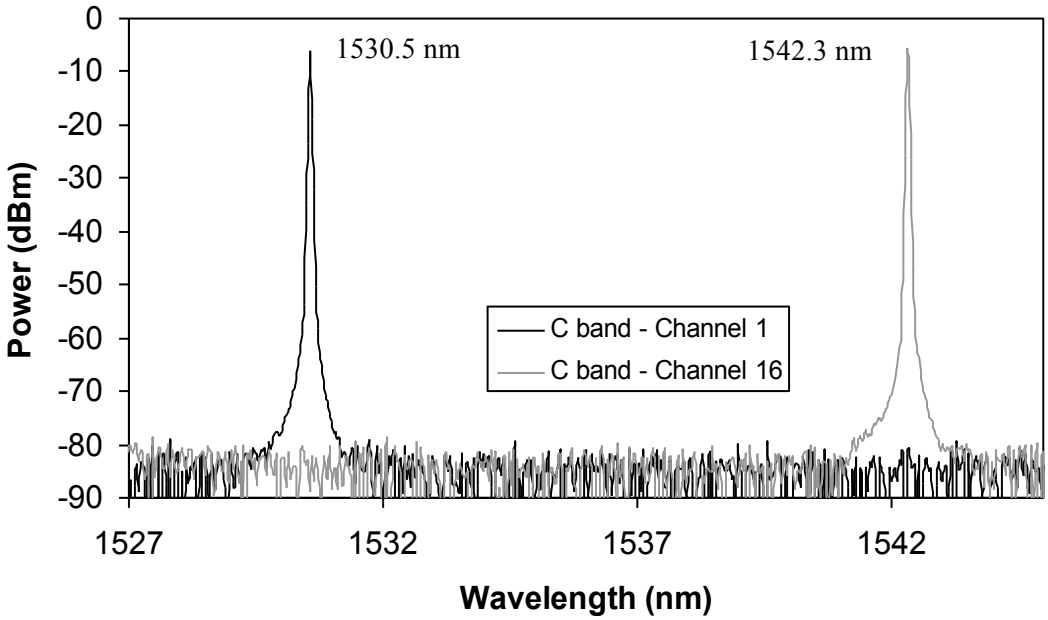

(b) C-band

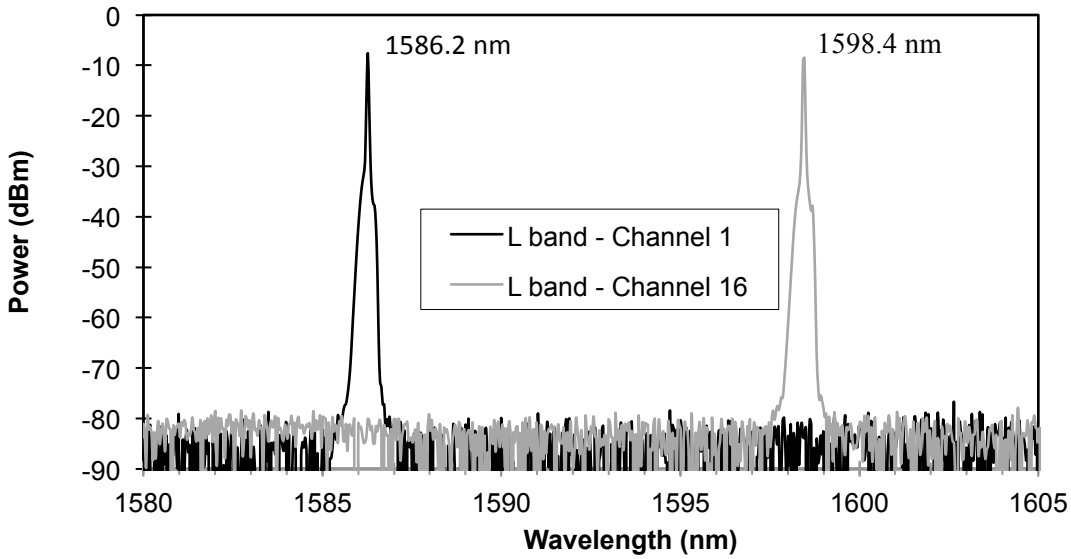

(c) L band

Figure 4.31 Widest tuning range for (a) S-band (b) C-band (c) L-band

Figure 4.32 shows the narrowest channel spacing achievable for the various bands with 0.8 nm interchannel spacing that can be attained by the AWG used in this experiment. Other important characteristics of the optical source such as power variations at different output wavelengths and the Side Mode Suppression Ration (SMSR) are presented in Figure 4.33.

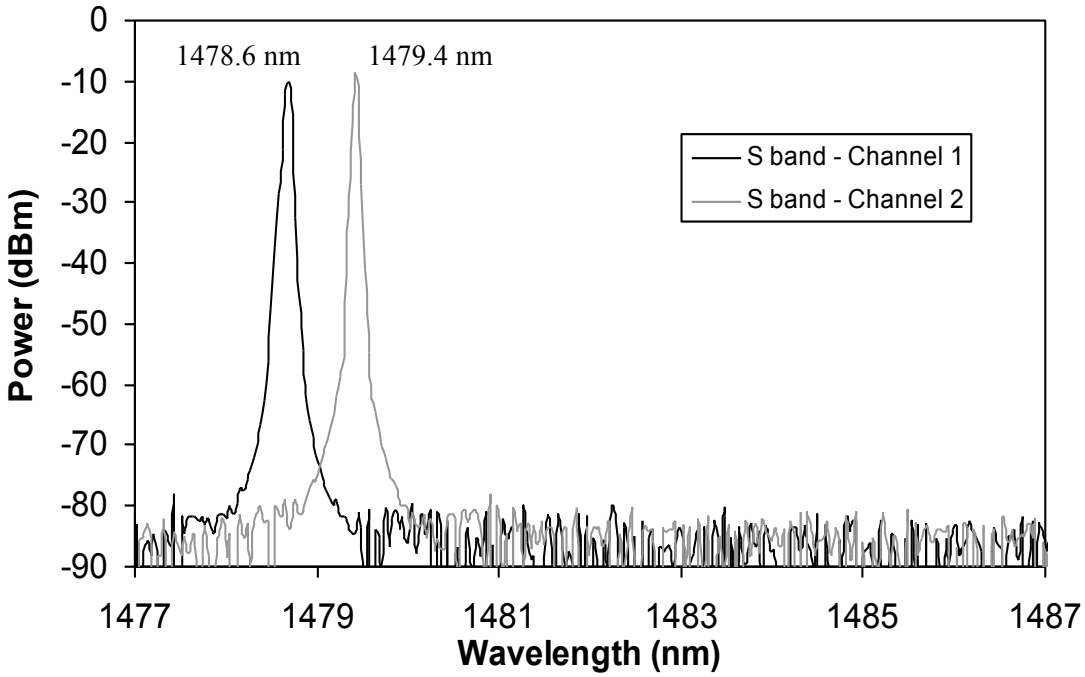

(a) S-band

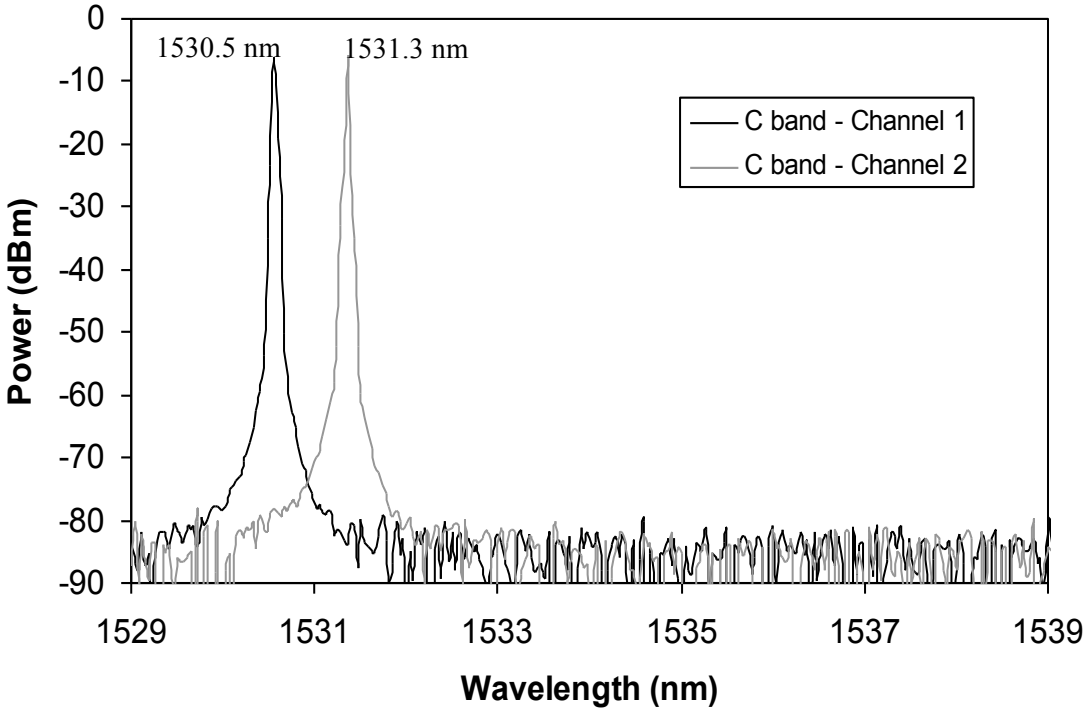

(b) C-band

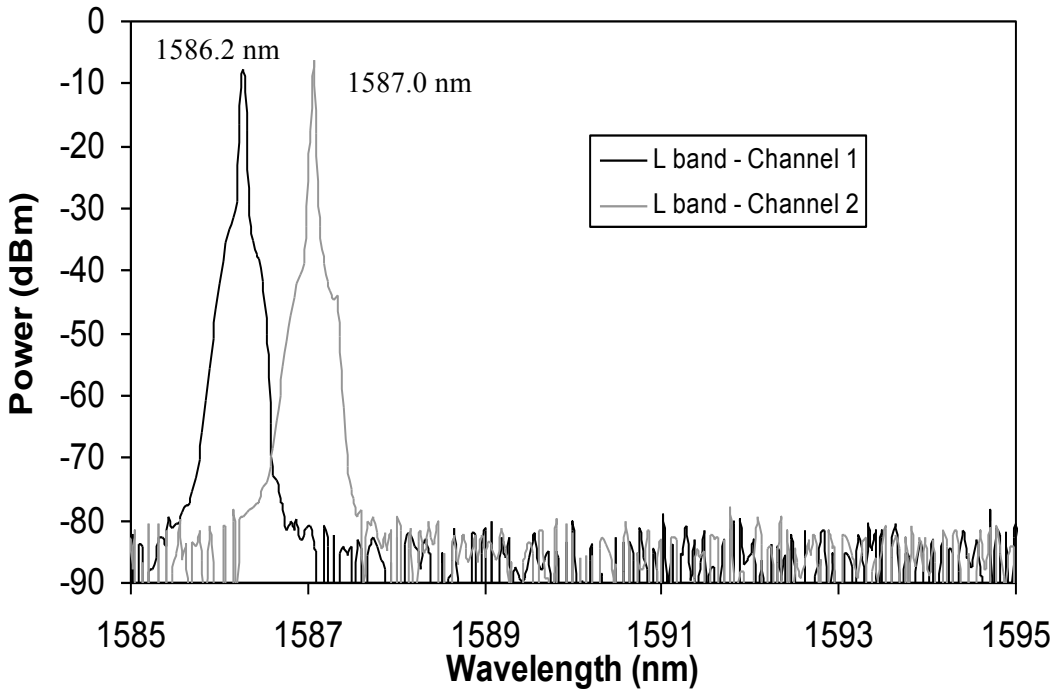

(c) L-band

Figure 4.32 Narrowest tuning ranges for (a) S-band (b) C-band and (c) L-band

Figure 4.33(a) shows the output power variations for the S-band with the lowest power value of -9.04 dBm at 1485.4 nm and the highest power value of -5.31 dBm for 1488.53 nm. The power variation is about 3.73 dB which can be improved by optimizing the connection and also by having an SOA with flat ASE output. The SMSR varies by about 69.95dB for wavelengths of between 1478.6 nm (Channel 1) to 1490.0 nm (Channel 16). In average, the SMSR is about 72 dB with the maximum and miniumm SMSR is about 74.5 dB and 69.1 dB.

Figure 4.33(b) shows a better result obtained in the C-band with small power variations at different wavelengths except for the wavelength of 1537.6 nm which has a peak power of -7.37 dBm. Similarly for SMSR, the variation is about 4 dB with an average value of 72 dB except for the wavelength of 1537.6 nm (Channel 10) which has an

SMSR of 70.7dB. This could be due to higher loss at channel 10 compared to the other channels in the AWG.

For the L-band region as shown in Figure 4.33(c), the peak power fluctuation is about 1.5dB for the 16 wavelengths outputs. The SMSR varies by about 2.5dB with an average value of 71.5dB. Large values of SMSR are observed for the three bands indicating that the output signals are of high quality.

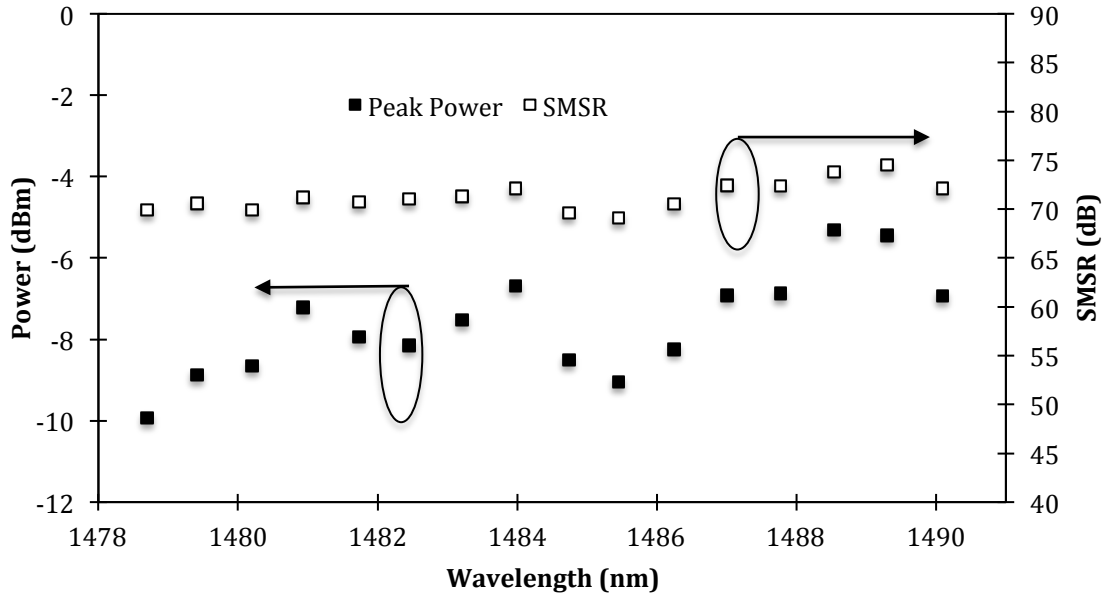

(a)S-band

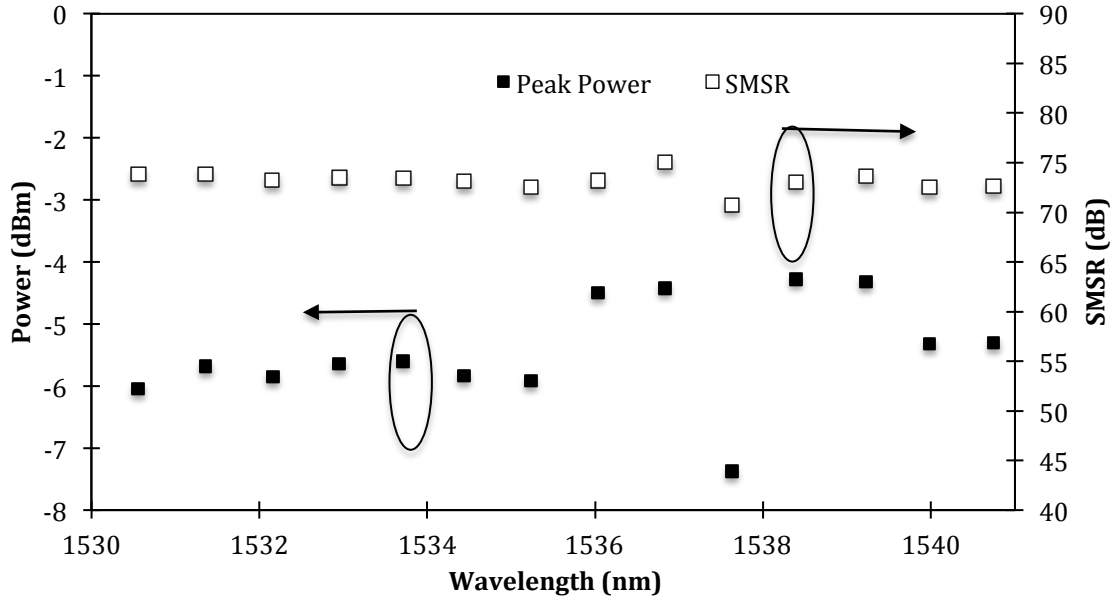

(b) C-band

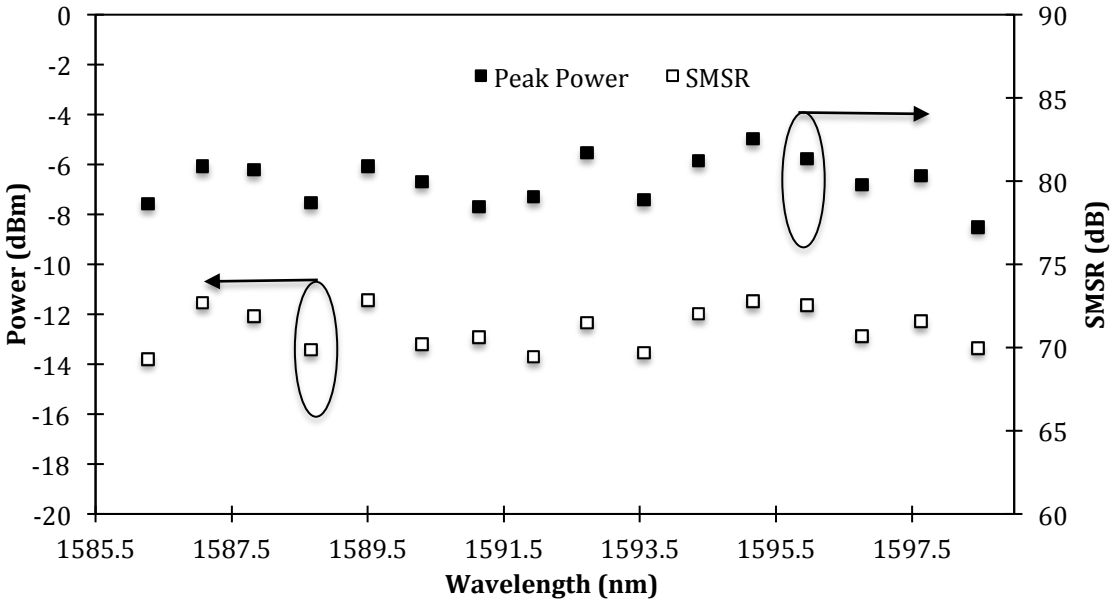

(c) L-band

Figure 4.33. Peak powers and SMSR for all channels of the entire bands, (a) S-band, (b) C-band and (c) L-band.

The bandwidth of the switchable output from 1478.7 nm to 1598.4 nm is shown in Figure 4.34 with a possible tunable bandwidth of 120 nm. The switching process is very stable and repeatable thus providing a wide selection of outputs within the S-, C- and L-bands. As shown in the figure, the spacing between the last channel (channel 16) of S-band and the first channel (channel 1) of the C-band (similarly between the C- and L-bands) is about 40 nm with no outputs, which is largely due to the usage of 1x16 AWG. The usable tuning range in each individual band is about 12 nm. This can be rectified by having an AWG with higher channel count, giving a continuous tunability that covers most of the S-, C- and L-bands. For instance, in a 1x64 AWG, the possible tuning range for each band would be about 51.2 nm. On the whole, this proposed design provides a novel way of generating switchable output that covers a wide tuning range.

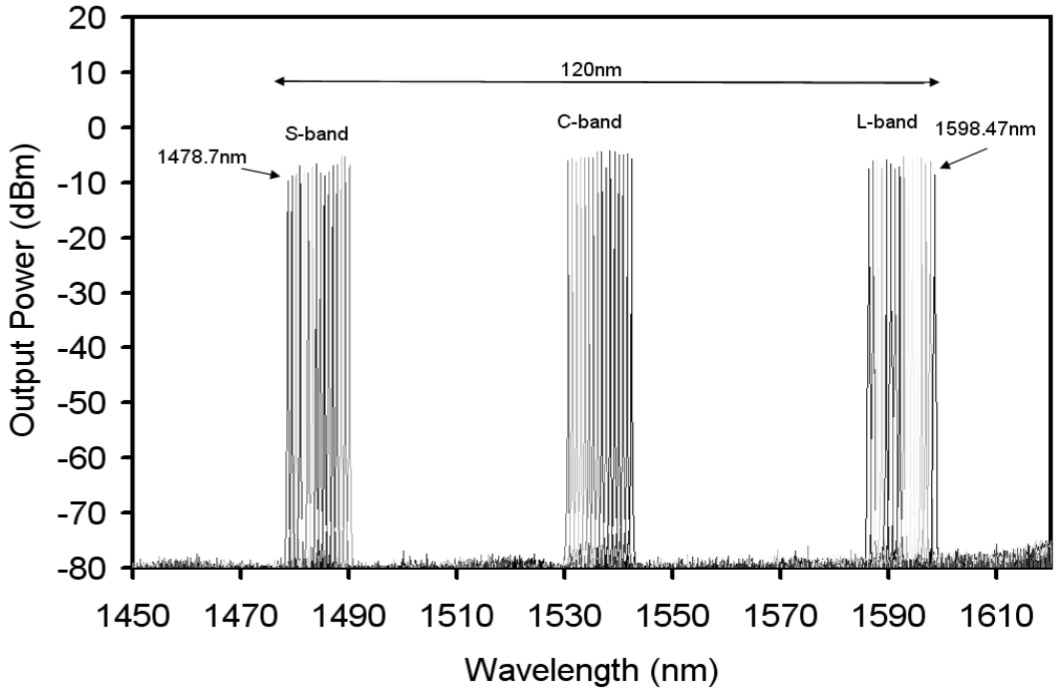

Figure 4.34. Spectrum of Output lasers for S-,C- and L-bands with 120 nm bandwidth.

4.7 Summary

In chapter 4, the application of the developed S-band optical amplifiers are explored. Two fiber laser configurations are discussed as the basis of this work, the linear cavity and ring cavity. In this chapter, various S-band fiber lasers based on the ring cavity are demonstrated by using the different S-band amplifiers characterized in Chapter 3. The design is based on the characteristics performance of each S-band optical amplifier.

The S-band EDFL is first demonstrated with the EDFL set up in a ring cavity and a TBF used as a selective mechanism. However due to the limitations of the TBF's bandwidth, the S-band laser can only be tuned to a wavelength 1515 nm. To resolve this issue, the S-band fiber laser is constructed using a standard step index 3 m EDF in the S-band region with a 1500 nm FBG as its selective tuning mechanism. The tunability of the FBG is designed to provide tunability for the EDFL. The measured tuning range is from 1496 nm to 1507 nm, with the peak power increasing from -5.8 to -0.7 dBm. The

measured SMSR is 66.2 dB at the shorter wavelength region and reaches a maximum value of 74 dB at the longer wavelength range. SLM operation is demonstrated by utilizing two SAs to compress the multi-mode beating. No mode beating is observed by the RFSA when the SA is inserted into the cavity. To make sure that the EDFL is operating as a SLM, the line-width of the laser is measured, and is found to be 140 kHz. The is the first time an S-band EDFL with SLM operation is demonstrated

Subsequently, the DC-EDF based fiber laser was characterized and designed. The characterization of DC-EDFL is done by testing of the performance of the output power and efficiency in both the forward and backward pumping setups. The backward pumping setup is shows the higher output power and higher efficiency compared to the forward pumping setup at a coupling ratio of 50/50. The maximum output power of forward and backward pumping setup is 4.1 mW and 13.8 mW respectively. The 3 dB linewidth for forward pumping is also bigger than that of the backward pumping setup, with a value of 1.03nm and 0.93nm respectively

The tunability of S-band DC-EDFL is achieved by using an AWG and OCS. The tuning range is about 11.3 nm ranging from 1478.6 nm to 1490.1 nm for both forward pumping and backward pumping setup. The output power for the backward pumping setup is higher than that of the forward pumping with a value of 0.1 dB and 8.1 dB for the backward and forward pumping configurations respectively. The output power also has a flat spectrum for both pumping setups. However the backward pumping setup exhibits lower quality of SMSR as compared to the forward pumping setup, with the average SMSR for both forward and backward pumping being 72 and 57 dB respectively. The proposed technique demonstrated is to show that the system is tunable and can be used to setup novel design for tunable fiber laser in other bands such as conventional band (C-band) and original band (O-band).[50-55]

The S-band Raman fiber laser (RFL) is also characterized and designed in Chapter 4. The tunability is provided by the TBF, and the tuning range for the S-RFL is about 25.8 nm from 1508.4 nm to 1535.8nm with an average output power is -11.5dBm. The average SMSR of S-RFL is about 70.2dB. The S-RFL also requires high Raman pump power to exceed the threshold of the fiber laser setup. The threshold value of the S-RFL is about 325mW. However the advantage of the S-band RFL is that it can produce high output power due to the gain medium dependent on the saturation gain effect.

The wide gain bandwidth of the SOA provides the opportunity to design an ultra-wideband tunable laser. In developing the S-band fiber laser, the design of the tunable laser with a wide band tuning range in single devise is an advantage. The wideband tuning range of the SOA provided by the AWG has its own advantage in term of wide wavelength range operation. Therefore, a design of a wide band switchable fiber laser with a tunability span of 120 nm is successfully demonstrated. It consists of an SOA that provides the ASE output which is then sliced into 16 individual outputs using a 1×16 AWG. The individual output is then amplified by the SOA to generate a stable switchable output that covers the S-, C- and L-bands. The switchable output can be tuned 11.7nm from 1478.3 nm to 1490.0 nm for S-band, from 1530.5 nm to 1542.34 nm for C-band, and from 1586.2 nm to 1598.4 nm for L- band. The average output powers for each of the S-, C- and L-bands are -7 dBm, -6 dBm and -6.5 dBm, respectively. The SMSR for the various bands is about 72 dB indicating a good signal-to-noise ratio. The output wavelengths are stable over time which has been tested for 2 hours with negligible power change. Although the usable tuning range is about 12 nm, this range can be increased by using a higher number of output channels in the AWG such as 1×64. Nevertheless, this work demonstrates an important technique in realizing a tunable switchable output that can span the entire S-, C- and L-bands.

The various configurations of S-band fiber laser by using EDF, DC-EDF, RA and SOA have been demonstrated in this chapter. The advantages and disadvantage of different type of fiber laser by using there gain mediums are evaluated. The characteristics of EDFL, DC-EDFL, SOA FL and RFL are shown in Table 4.1. The EDFL has the advantage of lower pump power required compared to the DC-EDFL and RFL. In term of tunability at S-band, the SOA fiber laser provides the best performance with gain tunability that can extent up to 120 nm. The RFL also has the advantage in term of tunability which depends on the RP wavelength. The EDFL and DC-EDFL S-band tunabilty is limited and largely depends on the ASE spectrum of the gain medium. The output power for the DC-EDFL is the highest compared to the other designs with its maximum output power of 5.14dBm. However, from the literature, we believe that the RFL can produce higher output power by having higher power of the Raman pump which is currently limited in our present set-up. For the SMSR, all types of S-band fiber laser have a similar characteristic with an average SMSR of 74 dB.

Table 4.1: The characteristics comparison for different type of S-band fiber laser

	EDFL	**DC-EDFL**	**SOA FL**	**RFL**
Pump power	90mW	300mW	NA	390mW
Wavelength Tunability at S-band	10.8nm	11.3nm	11.7nm	25.8 nm, depend on the RP wavelength
Maximum output power	-4.76dBm	5.14dBm	-5.31 dBm	-11.5dBm, depend on RP power
SMSR	74.4 dB	77.7 dB	74.5 dB	70.6 dB
Types	Homogeneous	Homogeneous	inhomogeneous	inhomogeneous
Stability	Good	Good	Good	Good

EDFL : Erbium Doped Fiber Laser
DC-EDFL : Depressed Cladding Erbium Doped Fiber Laser
SOA FL : Semiconductor Optical Amplifier Fiber Laser
RFL: Raman Fiber Laser
NA: Not Applicable

References

[1] A.M. Odlyzko, I. Kaminov and T. Li, Optical Fiber Telecommunications IVB Components ,Academic Press, San Diego, pp. 17–56, 2002.

[2] Mohd Zamani Zulkifli, "S-band Multiwavelength Fiber laser" Master of Science Thesis, University of Malaya, 2008.

[3] SYamashita, T. Baba, K. Kashiwagi, "Frequency-shifted multiwavelength FBG laser sensor" Optical Fiber Sensors Conference Technical Digest, 2002. OFS 2002, 15th , vol., no., pp. 285- 288 vol.1, 2002.

[4] P.C Peng; H.Y Tseng and S. Chi; , "A novel fiber-laser-based sensor network with self-healing function", IEEE Photonics Technology Letters, vol.15, no.2, pp.275-277, 2003.

[5] S. Pradhan, G.E Town and K.J Grant, "Microwave frequency generation using a dual-wavelength DBR fiber laser" Optical Fibre Technology/Australian Optical Society, 2006. ACOFT/AOS 2006. Australian Conference on , vol., no., pp.104-105, 10-13 July 2006.

[6] Y.J Kim, Y.Kim, B. J. Chun, S. Hyun and S.W. Kim, "All-fiber-based optical frequency generation from an Er-doped fiber femtosecond laser", Optics. Express, vol. 17, pp.10939-10945, 2009.

[7] Y.Yao; X.FChen; Y.T Dai and S.Z. Xie, "Dual-wavelength erbium-doped fiber laser with a simple linear cavity and its application in microwave generation" IEEE Photonics Technology Letters, vol.18, no.1, pp.187-189,2006.

[8] G. A. Ball and W. W. Morey, "Continuously tunable single-mode erbium fiber laser", Optics Letters, vol 17, pp. 420-422, 1992.

[9] S.Yamashita and K. Hotata, "Multiwavelength erbium-doped fiber laser using

intracavity etalon and cooled by liquid nitrogen," Electronics Letters, vol. 32, no. 14, pp. 1298–1299, 1996.

[10] N. Park and and P. F. Wysocki, "24-line multiwavelength operation of er- bium doped fiber-ring laser," IEEE Photonics TechnologyLetters, vol.8, no. 11, pp. 1459–1461,1996.

[11] J.Liu, J. Yao, J. Yao, and T. H. Yeap, "Single-longitudinal-mode multiwavelength fiber ring laser," IEEE Photonics Technology Letters, vol 16, issue 4, pp 1020-1022, 2004.

[12] S. Feng, O. Xu, S. Lu, X. Mao, T. Ning, and S. Jian, "Single-polarization, switchable dual-wavelength erbium- doped fiber laser with two polarization-maintaining fiber Bragg gratings", Optics Express, vol 16, issue 16, pp 11830-11835, 2008.

[13] S. L. Pan, X. F. Zhao, and C. Y. Lou, "Switchable single-longitudinal-mode dual-wavelength erbium-doped fiber ring laser incorporating a semiconductor optical amplifier", Optics Letters, vol 33, issue 8, pp 764–766, 2008.

[14] H. Ahmad, S. F. Norizan, M. Z. Zulkifli, S. W. Harun, "Dual-Wavelength Erbium Fiber Laser in a Simple Ring Cavity",Fiber and Integrated Optics, vol 28, issue 6, pp 430-439, 2009.

[15] H. Ahmad, M.Z. Zulkifli, A.A. Latif and S.W. Harun, "Tunable dual wavelength fiber laser incorporating AWG and optical channel selector by controlling the cavity loss" ,Optics Communications, vol 282, issue 24, pp 4771-4775, 2009.

[16] X.H. Feng, H.Y Tam, C. Lu C, P.K.A Wai, B.O Guan, "Multiwavelength Erbium-Doped Fiber Laser Employing Cavity Loss Modulation", IEEE Photonics Technology Letter, volume 21, issue 18, pp 1314-1316, 2009

[17] M. A. Ummy, N. Madamopoulos, A. Joyo, M. Kouar, and R. Dorsinville, "Tunable multi-wavelength SOA based linear cavity dual-output port fiber laser using Lyot-Sagnac loop mirror", Optics Express, vol 19, pp 3202-3211,2011.

[18] J. Yao, J.P Yao; Z.C Deng and J.Liu, "Multiwavelength erbium-doped fiber ring laser incorporating an SOA-based phase Modulator" IEEE Photonics Technology Letters, vol.17, no.4, pp756-758, 2005.

[19] B.A Yu, J.Kwon, S.Chung, S.W Seo and B.Lee, "Multiwavelength-switchable SOA-fibre ring laser using sampled Hi-Bi fibre grating," Electronics Letters , vol.39, no.8, pp. 649- 650, 2003.

[20] H.X Chen, "Multiwavelength fiber ring lasing by use of a semiconductor optical amplifier," Optics Letter, vol 30, issue 6, pp 619-621,2005

[21] A.M.R Pinto, O. Frazão, J.L. Santos, M. Lopez-Amo, "Multiwavelength Raman Fiber Lasers Using Hi-Bi Photonic Crystal Fiber Loop Mirrors Combined With Random Cavities", Jounal of Lightwave Technology, vol.29, no.10, pp.1482-1488, 2011.

[22] X.Y. Dong, P. Shum, N. Q. Ngo, and C. C. Chan, "Multiwavelength Raman fiber laser with a continuously-tunable spacing", Optics Express, vol 14, pp 3288-3293, 2006.

[23] J.R. Qian, J. Su, X.X Wang, and B.Zhu, "Er-doped fiber ring laser gyroscopes operating in continuous waves", Chinese Optics Letters, vol 5, pp 229-231, 2007.

[24] J.Jung, H.Nam, B. Lee, J.O Byun, and N.S Kim, "Fiber Bragg Grating Temperature Sensor with Controllable Sensitivity", Applied Optics, vol 38, issue 13, pp 2752-2754, 1999.

[25] Y.J Rao, D.J Webb, D.A. Jackson, L. Zhang, I Bennion, "In-fiber Bragg-grating temperature sensor system for medical applications", Jounal of Lightwave Technology, vol.15, no.5, pp.779-785, 1997.

[26] F.M Haran, J. K. Rew and PD Foote, "A strain-isolated fibre Bragg grating sensor for temperature compensation of fibre Bragg grating strain sensors", Measurement Science and Technology, vol 9, issue 8, pp 1163-1166, 1998.

[27] A. D. Kersey, T. A. Berkoff, and W. W. Morey, "Multiplexed fiber Bragg grating strain-sensor system with a fiber Fabry-Perot wavelength filter" Optics Letters, vol 18, issue 16, pp 1370-1372, 1993.

[28] S Ju, P.R Watekar and W.T Han, "Enhanced Sensitivity of the FBG Temperature Sensor Based on the PbO-GeO-SiO Glass Optical Fiber", Journal of Lightwave Technology, vol.28, no.18, pp.2697-2700, 2010.

[29] G.C. Lin, L. Wang, C.C Yang, M.C Shih and T.J Chuang, "Thermal performance of metal-clad fiber Bragg grating sensors", IEEE Photonics Technology Letters, , vol.10, no.3, pp.406-408, 1998.

[30] M.R.Mokhtar, C.S. Goh, S.A. Butler, S.Y. Set, K. Kikuchi, D.J Richardson, and M.Ibsen, "Fibre Bragg grating compression-tuned over 110 nm", Electronics Letters , vol.39, no.6, pp. 509- 511, 2003.

[31] C.Goh, S.Set, K. Kikuchi, M.Mokhtar, S. Butler and Ibsen, "Greater than 90 nm continuously wavelength-tunable fibre Bragg gratings" Optical Fiber Communications Conference, 2003. OFC 2003 , vol., no., pp. 643- 644 vol.2, 23-28 March 2003.

[32] C. S. Goh, S. Y. Set, and K.Kikuchi, "Widely Tunable optical filters based on fiber Bragg gratings", IEEE Photonics Technology Letters, vol. 14, no. 9, pp.1306-1308, 2002.

[33] K Zhang and J.U Kang, "C-band wavelength-swept single-longitudinalmode erbium-doped fiber ring laser, Optics Express, vol 16, issue 8, pp 14173-14179 , 2008.

[34] C. H. Yeh, T. T. Huang, H. C. Chien, C. H. Ko, and S. Chi, "Tunable S-band erbium-doped triple-ring laser with single-longitudinal-mode operation", Optics Express, vol 15, issue 2, pp 382-386, 2007.

[35] X. P. Cheng, P. Shum, C. H. Tse, J. L. Zhou, M. Tang, W. C. Tan, R. F. Wu, and J. Zhang, "Single-longitudinal-mode erbium-doped fiber laser based on high finesse , vol 20 pp 976-978, 2008.

[36] J. Yang, R. Qu, G. Sun, J. Geng, H. Cai, and Z.Fang, "Suppression of mode competition in fiber lasers by using a saturable absorber and a fiber ring", Chinese Optics Letters, vol 4, pp 410-412, 2006.

[37] C.H. Yeh, C.W. Chow, "Broadband wavelength-tunable single-longitudinalmode erbium-doped fiber ring laser using saturable-absorber filter", Laser Physics Letters Volume 7, Issue 2, pages 158–163, February 2010

[38] Dennis Derickson, "Fiber Optic Test and Measurement", Prentice Hall, pp 185-188, 1998.

[39] T. Okoshi, K. Kikuchi, A. Nakayama, "Novel method for high resolution measurement of laser output spectrum", Electronics Letters, vol 16, no.16, pp 630-631, 1980.

[40] M.Z. Zulkifli, N. Tamchek, A.A. Latif, S.W. Harun and H. Ahmad, "Flat output and switchable fiber laser using AWG and broadband FBG", Optics Communications,vol 282, issue 13, pp 2576-2579, 2009.

[41] H. Ahmad, K. Thambiratnam, A.H. Sulaiman, N. Tamchek and S.W. Harun, "SOA-based quad-wavelength ring laser" Laser Physics Letter, vol 5, no. 10, pp 726–729, 2008.

[42] Y. Tachikawa and K. Okamoto, "Arrayed-waveguide grating lasers and their applications to tuning-free wavelength routing", IEEE Proceedings: Optoelectronics, vol 143, issue 5, pp. 322-328, 1996.

[43] Y. Tachikawa and K. Okamoto, "32 wavelength tunable arrayed-waveguide grating laser based on special input/output arrangement", Electronics Letters, volume 31, no 19, pp. 1665-1666, 1995.

[44] R. Kasahara, M. Ishii, Y. Inoue, S. Sohma, H. Takahashi, S. Suzuki, T. Shibata, and T. Kitagawa "Integrated 32 ch dynamic wavelength channel selector using AWG and 32 × 1 PLC switch", in: Optical Fiber Communication Conference OFC, vol. 1, pp 600- 2602. 2004.

[45] S. Babin, D. Churkin, S. Kablukov, and E. Podivilov, "Raman gain saturation at high pump and Stokes powers", Optics Express, vol 13, pp 6079-6084, 2005.

[46] R. Vallee, E. Belanger, B. Dery, M. Bernier andD. Faucher, "Highly Efficient and High-Power Raman Fiber Laser Based on Broadband Chirped Fiber Bragg Gratings", Jounal of Lightwave Technology, vol.24, no.12, pp.5039-5043, 2006.

[47] A.K. Abeeluck, C. Headley, and C. G. Jørgensen, "High-power supercontinuum generation in highly nonlinear, dispersion-shifted fibers by use of a continuous-wave Raman fiber laser", Optics Letters, vol 29, pp 2163-2165, 2004.

[48] S. M. Spillane, T. J. Kippenberg and K. J. Vahala, "Ultralow-threshold Raman laser using a spherical dielectric microcavity", Nature, vol 415, 621-623, 2002.

[49] H. Ahmad, M.Z. Zulkifli, A.A. Latif, N.A. Hassan, Z.A. Ghani and S.W. Harun, "120 nm wide band switchable fiber laser" Optics Communications vol 283, issue 21, pp 4333-4337, 2010.

[50] A.A Latif, H Ahmad, N.A Awang, M.Z Zulkifli, C.H Pua, Z.A Ghani andS.W Harun, "Tunable high power fiber laser using an AWG as the tuning element", Laser Physics, vol 21, issue 4, pp 712-717, 2011.

[51] H. Ahmad, A.A. Latif, S.F. Norizan, M.Z. Zulkifli, and S.W. Harun, "Flat and compact switchable dual wavelength output at 1060 nm from ytterbium doped fiber laser with an AWG as a wavelength selector", Optics & Laser Technology, vol 43, issue 3, pp 550-554, 2011,

[52] A A Latif, N A Awang, M Z Zulkifli, S W Harun, Z A Ghani and H Ahmad, "Dual-wavelength tunable fibre laser with a 15-dBm peak power", Quantum Electronics, vol 41, no 8, pp 709, 2011.

[53] A. A. Latif, M. Z. Zulkifli, N. A. Awang, S. W. Harun and H. Ahmad, "A simple linear cavity dual-wavelength fiber laser using AWG as wavelength selective mechanism", Laser Physics, vol 20, no 11, pp 2006-2010, 2010.

[54] A.A.Latif, M.Z Zulkifli, N.A Hassan, S.W Harun, Z Ghani, and H Ahmad, "A compact O-plus C-band switchable quad-wavelength fiber laser using arrayed waveguide grating", Laser Physics Letters, vol 7, issue 8, pp 597-602, 2010.

[55] H. Ahmad, M.Z. Zulkifli, A.A. Latif, S.W. Harun, "Novel O-band tunable fiber laser using an array waveguide grating", Laser Physics Letters, vol 7, issue 2, pp 164–167, 2010.

Chapter 5
S-band Multi-Wavelength Fiber Laser

5.1 Introduction

The recent deployment of high capacity DWDM systems has allowed for a significant increase in data traffic globally. DWDM systems allow for the transmission of multiple data streams simultaneously on a single channel, thereby increasing the data carrying capabilities of the system significantly while not causing a drastic increase in the complexity and cost of the system. However, to fully exploit the benefits of DWDM systems, multiple signal sources must also be deployed, and this can be a costly and complex endeavor. For instance, a 16 channel DWDM system will require 16 discrete laser sources in order to fully exploit the potential of the DWDM system and this can be very expensive to implement. Another concern would be the availability of spare signal sources in the event one or more sources fails; this effectively doubles the cost of the system but does not provide any returns. Therefore, to fully deploy a 16 channel DWDM system, 32 wavelength sources will be needed, with 16 sources being used as active sources and another 16 sources kept spare.

A viable solution to this problem is the Multi-Wavelength Fiber Laser (MWFL). MWFLs are able to generate many closely spaced laser wavelengths from a single system while at the same time maintaining a simple and inexpensive design, thereby giving a good cost-per-wavelength ratio. MWFLs can be generated by a number of approaches; ASE generated from a linear gain medium such as an EDFA or an SOA can be sliced [1] or by employing Sagnac Loop Mirrors to generate a multiple wavelength output from EDF, SOA or other rare-earth based fiber lasers [2–4]. Non-linear effects in

fibers such as Four-Wave Mixing (FWM), Stimulated Brillouin Scattering (SBS) and Stimulated Raman Scattering (SRS) [5–8] can also be employed to develop MWFLs. Brillouin/Erbium fiber lasers (BEFLs) in particular have very high potential for deployment in DWDM systems due to its ability to generate a multi-wavelength output spectrum with a narrow spacing of 10 GHz, vital for increasing the capacity of current optical communication networks.

Current BEFL systems are designed for operation in the C- ad L-bands, but as demands for capacity continue to increase, efforts must now be made to develop BEFLs capable of operating in the S-band region. As discussed in the previous chapters however, this task is made difficult due to certain factors that limit the S-band amplification that can be obtained from silica based EDFs in the S-band region. The recent introduction of the DC-EDF provides a suitable material for the development of BEFLs and because they are still conventional silica transmission fibers, they require only a low pump power and thus becomes a very attractive option for commercial networks.

The first part of this chapter will focus on the generation of the SBS effect in Single-Mode Fibers (SMFs) of multiple lengths. The generation of the SBS effect in fibers with different effective areas, A_{eff} such as Dispersion Compensating Fibers (DCFs) are also studied. The cavity design of the S-band BEFL is also studied, particularly the ring and linear cavity configurations. The generation of a Birllouin multi-wavelength source in the S-band region is also studied, with the output spectrum between the two different cavities studied. The Multi-Wavelength Brillouin/Erbium Doped Fiber Laser (MWBEFL) is difficult to generate the multiple channel due to the limitation comes from the gain of the fiber.

In this chapter also the Multi-Wavelength Brillouin/Raman Fiber Laser (MWBRFL) will be explained. Its characteristic such as the number of wavelengths created, the

influence of the wavelength pump and other such behaviors is discussed. Moreover the discussion of different channel spacings compared to conventional S-band MWBRFL will also be discussed. Finally, an S-band Multi-Wavelength Brillouin/SOA fiber laser (MWBSOAFL) also will be explained in this chapter. SOA is being chosen due to its ability to emit wide gain bandwidth and the detail about this gain medium will be explained in this chapter.

With the identification of the strength and weaknesses of each S-band gain medium such as DC-EDF, SOA and Raman Amplifier, the chapter is concluded by looking at the generation of S-band Multi-wavelength Brillouin/ Hybrid S-band Gain medium such as DC-EDF with RA and RA with SOA.

5.2 Generation of S-band Brillouin Fiber Laser

5.2.1 Effect of Length and Effective Area for Stimulated Brillouin Scattering

Brillouin fiber laser is a process of interaction between laser signal or Brillouin pump (BP) and acoustic wave which is generated from the fiber thus creating the Brillouin Stokes which travel in opposite direction of the pump. To analyze the Brillouin Stokes that are generated in the fiber, an optical circulator is used between the BP and the fiber under test. The usage of optical circulator is to prevent the backward Brillouin Stoke that can cause damage to the BP and also to prevent the BP backward reflection. The basic configuration setup to generate SBS is shown in Figure 5.1. It consists of tunable laser source (TLS) as the BP, an optical circulator, different length of SMF and optical spectrum analyzers (OSA). The BP power is injected into the SMF from port 1 to port 2

of the optical circulator and the SBS is created in the backward direction which travel back toward port 2

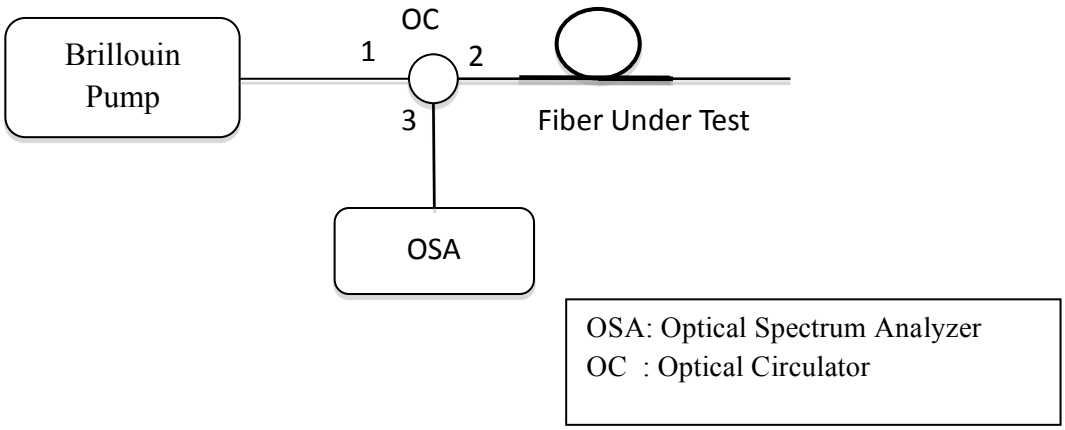

Figure 5.1 The setup to investigate SBS in the fiber

The SMF length tested are 0.5km, 10km and 50k. The selection of the lengths used are those currently available in the laboratories. The non-linear interaction depends on the length and cross section of the fiber [9,10]. The BP power is set to 12 dBm at 1500nm with a linewidth of about 15 MHz. As observed, the Brillouin Stokes power is higher for the longger length of SMF. This is shown in the Figure 5.2. The Brillouin Stokes only occurs for the 50 km SMF because there is enough non-linear interaction at this length. The similar expectation would be obtained if we use SMF longer than 50km but a higher BP power is probably needed. The Brillouin Stokes does not occur for the other shorter lengths of SMF due to the low non-linear medium. The Brillouin frequency shift is about 10 GHz or 0.09 nm which is given by the equation,

$$\nu_B = \frac{(2n v_A)}{\lambda_p} \tag{5.1}$$

where λ_p is the Brillouin pump wavelength, n is the refractive index of the fiber and v_A is acoustic velocity in the glass

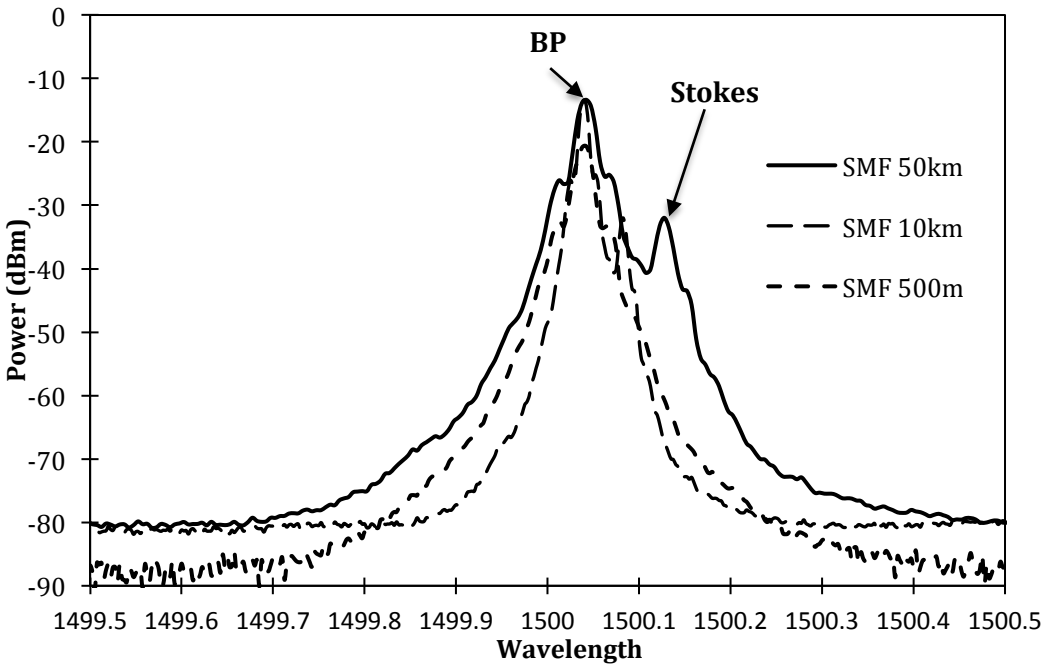

Figure 5.2. The Brilouin Stoke with different lengths of SMF

The Brillouin Stokes is generated at BP power of 12dBm and the Stokes power at different wavelength within the S-band range in a 50 km SMF is show in the Figure 5.3. The Stokes power linearly-increases with respect to the longer wavelength of the BP with a maximum Brilloiun Stokes power of -21.12 dBm at BP wavelength of 1520 nm. The lowest Brillouin Stokes power is at BP wavelength of 1490 nm with the measured power t of -36.54 dBm. The significance of this study is to characterize the optimum Stokes Power over the wavelength range in the SMF which is important in the generation of multi-wavelength Brillouin fiber laser.

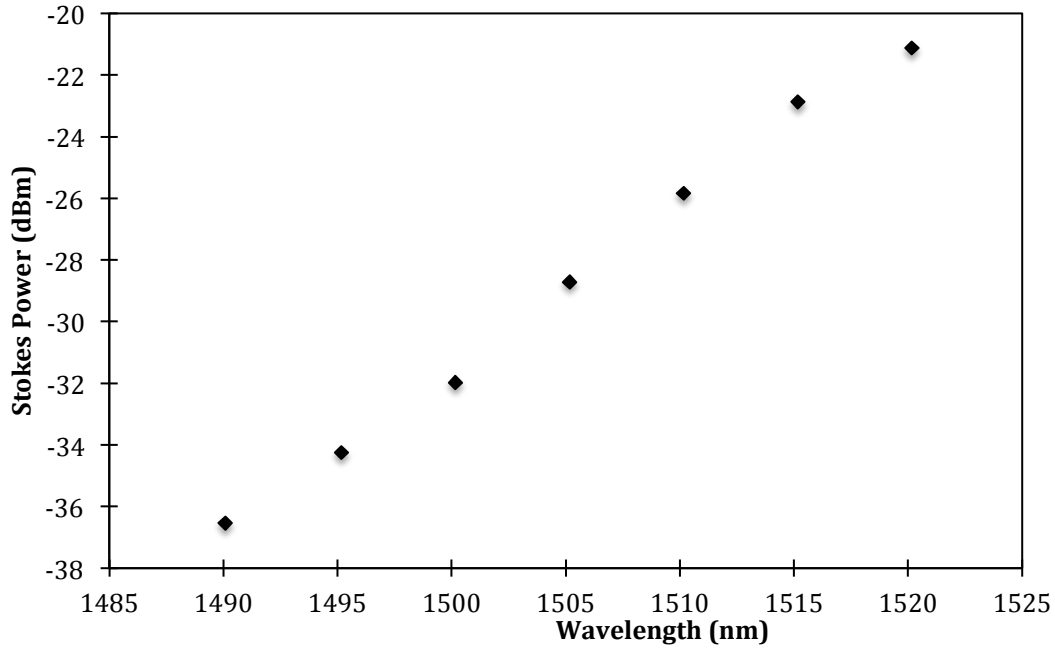

Figure 5.3 Measured Brillouin Stokes power at different BP wavelength with BP output power of 12dBm.

5.2.2 Stimulated Brillouin Scattering over Brillouin Pump Power

The generation of Brillouin also depends on the BP power. Figure 5.4 shows the effect of the generation of Brillouin Stokes at different BP power with output wavelength fixed at 1500 nm. The BP power is varied from 0 dBm to 12 dBm. As shown in Figure 5.4 the Brillouin Stokes power start to increases oonly when the BP power exceeds 4 dBm. This can be defined as the threshold of the Brillouin Stokes. Figure 5.5 shows the graph of the threshold of the Brillouin Stokes.

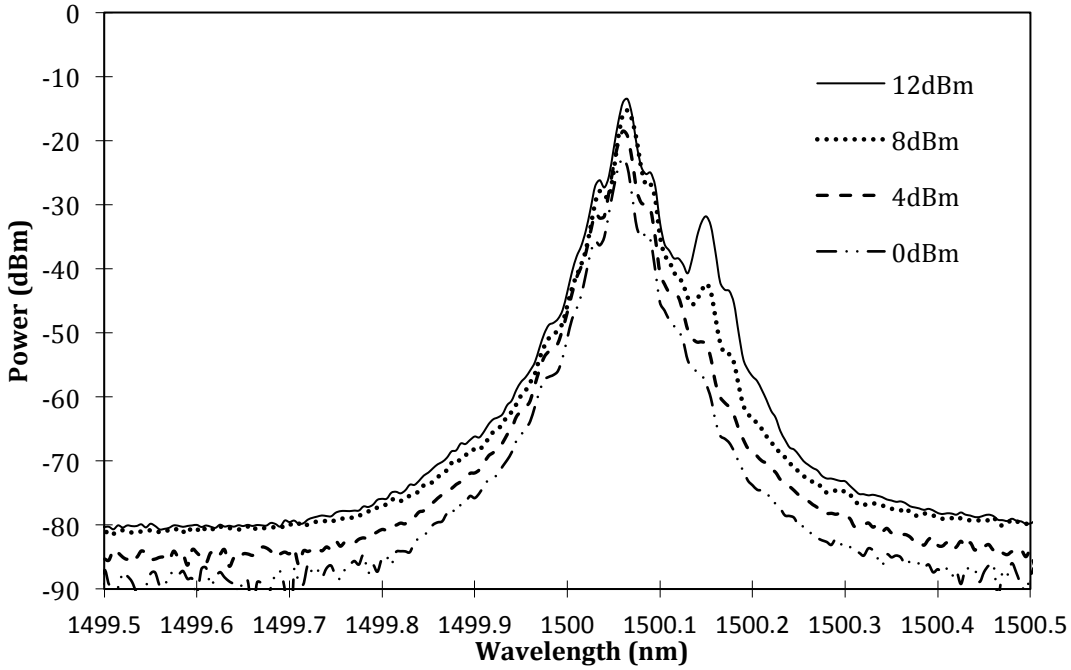

Figure 5.4 The output spectrum of Brillouin Stokes of 50km SMF with different BP power at BP wavelength 1500 nm

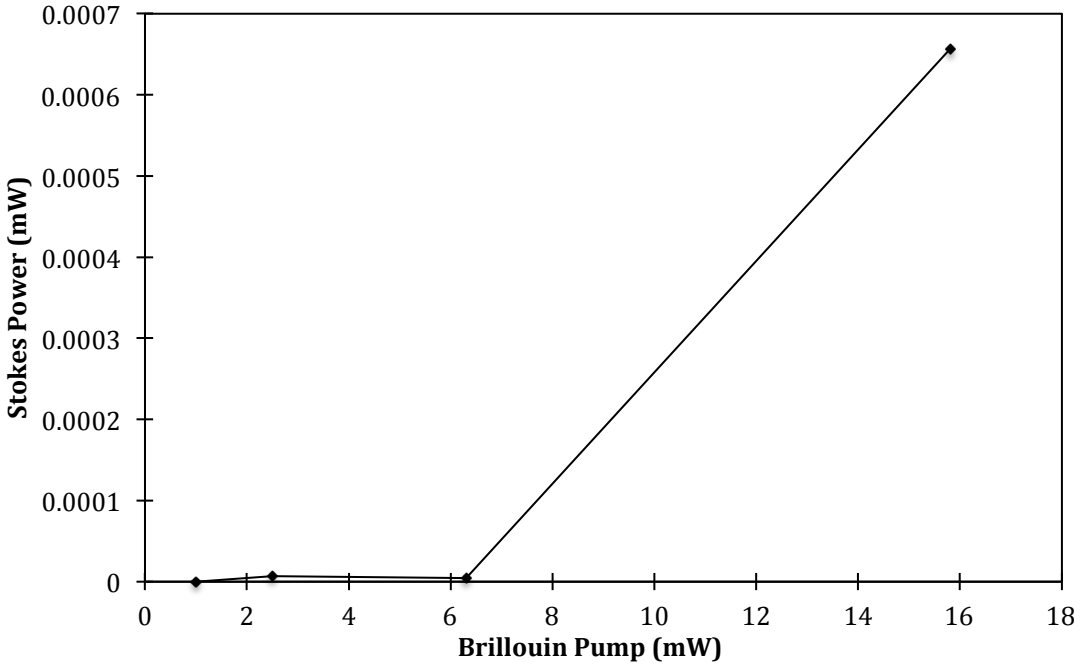

Figure 5.5 The Stokes power in the linear unit (mW) to determine the threshold of the Brillouin Stokes

5.2.3 Stimulated Brillouin Scattering in Dispersion Compensating Fiber

The problem associated with the long length of SMF is related to the loss as a result of optical absorption effect. To overcome this problem the Dispersion Compensating Fiber (DCF) can be an interesting alternative. The DCF has a shorter length compared to the SMF fiber. This will allow the construction of a compact device. The DCF has a smaller effective area of 55 μm^2. The comparison of the Brillouin spectrum between the DCF and 50 km SMF is shown in the Figure 5.6. The BP power and wavelength is about 12 dB and 1500 nm respectively. The Brillouin Stokes power of DCF is about -19.7 dBm which is 13.5 dB higher compared to the Brillouin Stokes of 50 km SMF with the power of about -32.7 dBm. The Brilloiun Stokes of DCF is also higher than the BP and this is called the Brillouin gain. The design of the Brillouin amplifier is useful in generating the Brillouin gain. However the Brillouin amplifier is not the subject of this study. The spectrum of DCF shows that the anti-Stokes is also created. The anti-stokes power is about -48.5 dBm.

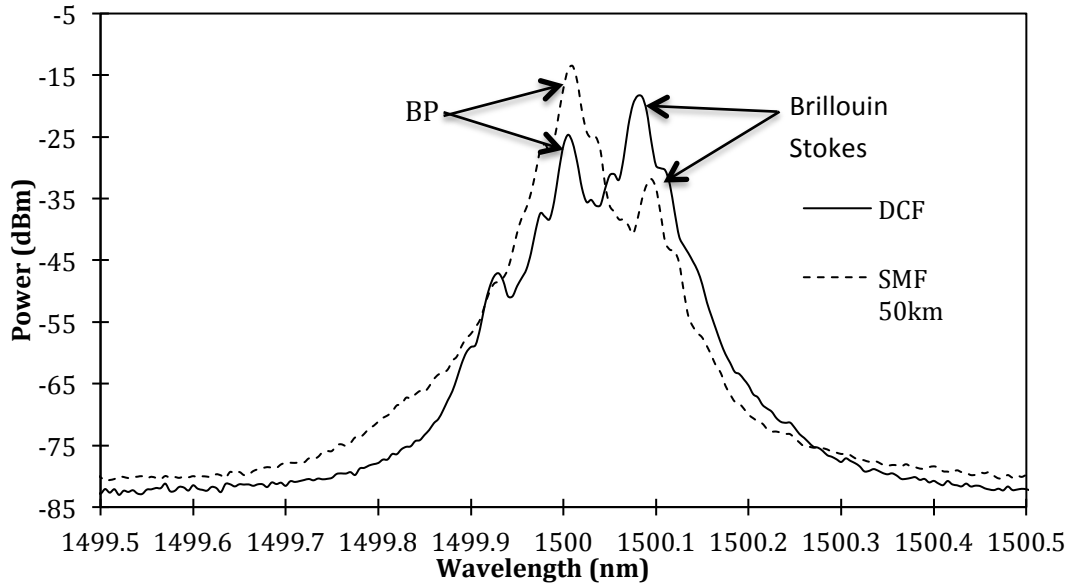

Figure 5.6 The comparison of Brilouin Spectrum between DCF and 50km SMF

The generation of Brillouin Stoke and anti Stokes with different BP power of DCF are shown in Figure 5.7 with the BP wavelength is about 1500 nm. From the figure it is clearly shown that the DCF has a lower threshold to create the Brilloiun Stoke compared to the SMF with the minimum BP power of about 0 dBm, creating SBS with -52.81 dBm of output power. The low threshold to generate SBS gives the design the an advantages in reducing the BP power needed in most applications [11].

As shown in Figure 5.8 the Stokes and anti-stokes power increases linearly when the BP is increased from 0 to 8 dBm with the lowest Stokes and anti-stokes power at -53.35 dBm and -54.4 dBm respectively at 0 dBm of BP power. When the BP is increased to above 8 dBm, the Stokes and anti-Stokes powers become flat with the maximum power of Stokes and anti–Stokes to be around -18.73 dBm and -47.58 dBm respectively. This condition is possibly due to gain saturation occurring in the medium.

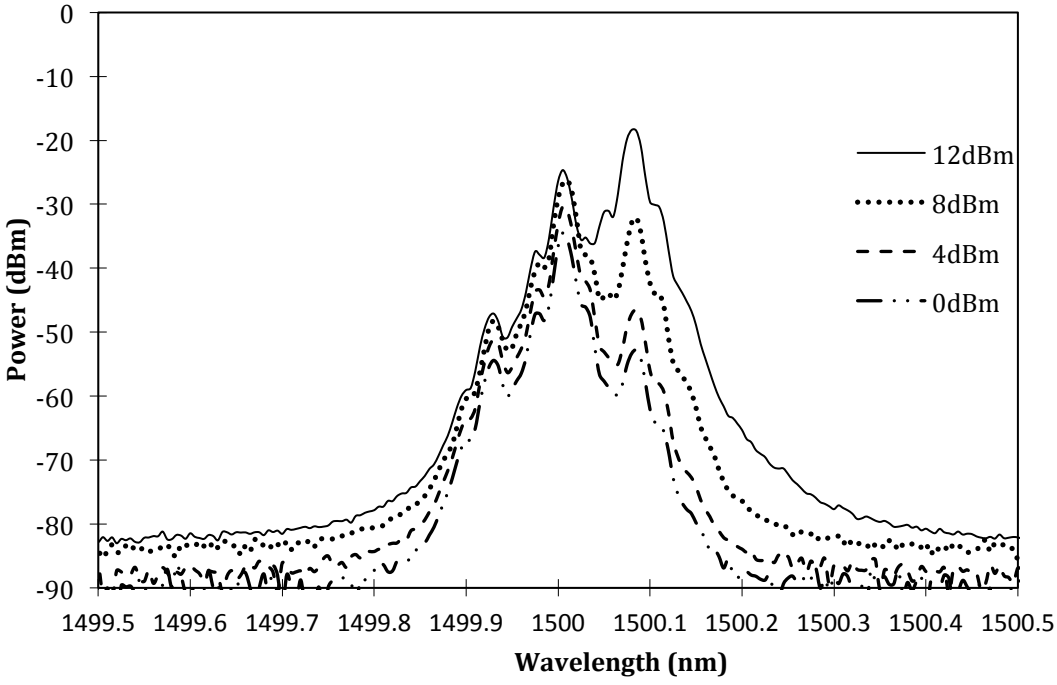

Figure 5.7 The Brillouin spectrum from DCF at BP wavelength 1500nm and at different BP powers

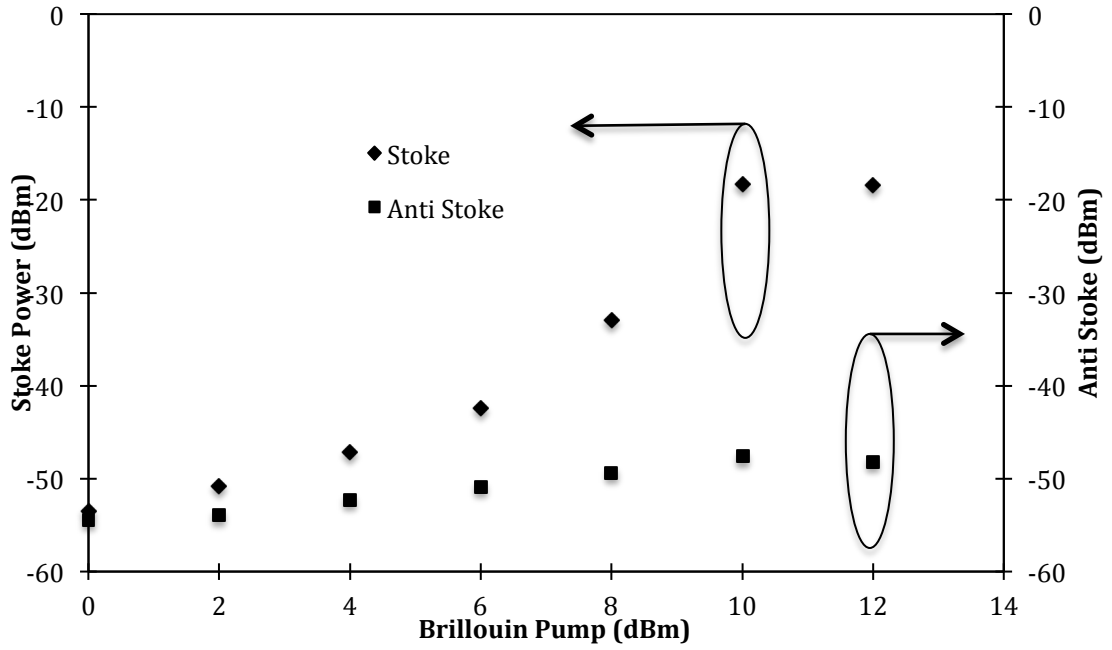

Figure 5.8 The Stokes and anti-Stokes power of the DCF at BP wavelength 1500nm and different BP power in dBm

To have a clear view to determine the Brillouin threshold in the DCF, the unit of the power must be changed in the linear scale and in this case it will be in mW. Figure 5.9 shows the Stokes power of the DCF. The threshold of SBS using the DCF is lower compared to that of the 50 km SMF. The SBS threshold of the DCF is about 6mW to observe the Brillouin Stokes. This is 10 times lower compared to the threshold of the 50 km SMF. A low threshold Brillouin Stokes is important to make multiple wavelength Brillouin fiber laser as will be discussed in section 5.5 onwards.

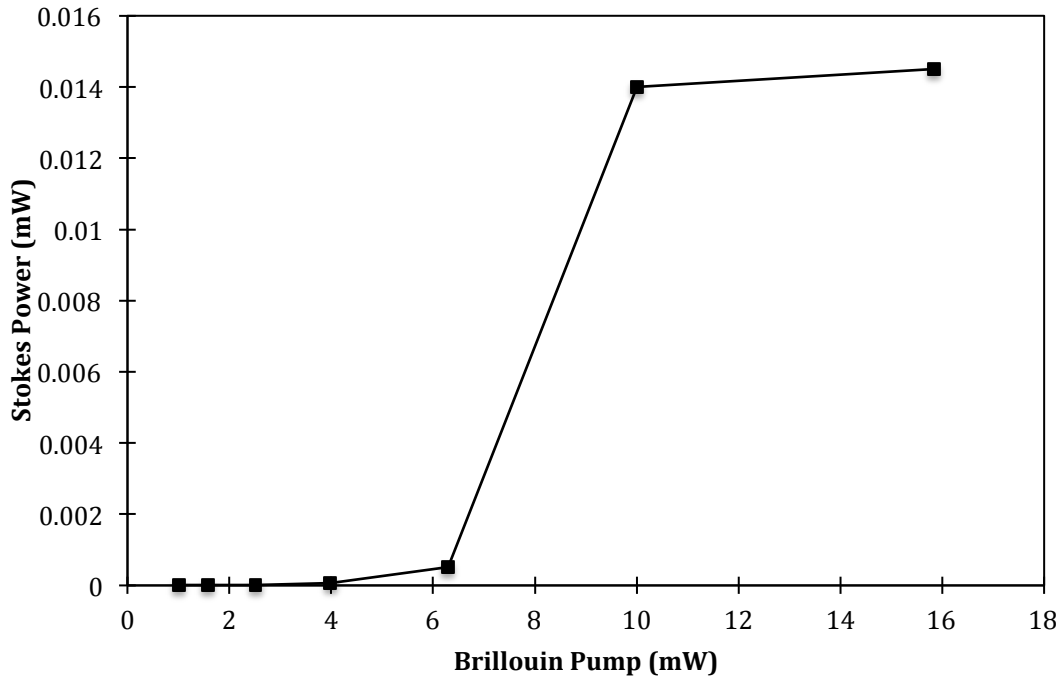

Figure 5.9 The Stokes power of the DCF at BP wavelength 1500 nm and different BP power in mW

The comparison of the Brillouin Stokes power between the DCF and 50 km SMF is shown in the Figure 5.10. It clearly shows that the Brillouin Stokes power of the DCF is higher than that of the 50km SMF with the average different of about 13.34dB. Meanwhile the output power pattern shows a similar characteristic for both fiber which increases linearly towards the longer wavelength from 1490 nm to 1520 nm.

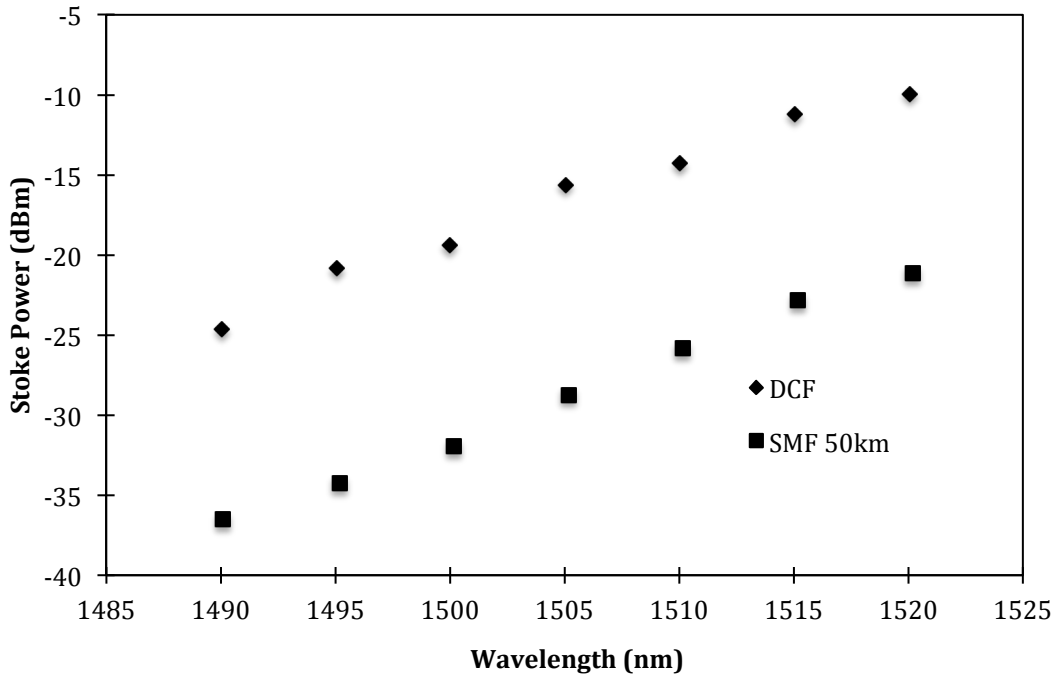

Figure 5.10 The comparison of the Stokes power between DCF and 50km SMF

5.3 Cavity Design of S-band Brillouin Fiber Laser

As has been discussed in Chapter 4, the fiber laser can be represented by two types of cavity, namely the ring cavity and Fabry-Perot cavity or linear cavity. In the Brillouin Fiber Laser (BFL) the design of the cavity is the same with the design of the conventional fiber laser except that the cavity has an external excess to allow the BP power to be inserted into the cavity. In ring cavity BFL, normally the BP is injected into the cavity through an optical circulator. The Brillouin Stokes generated oscillates inside the cavity and is tapped out by using the optical circulator as shown in Figure 5.11. The ring cavity BFL allows only a unidirectional propagation of the Brillouin Stokes.

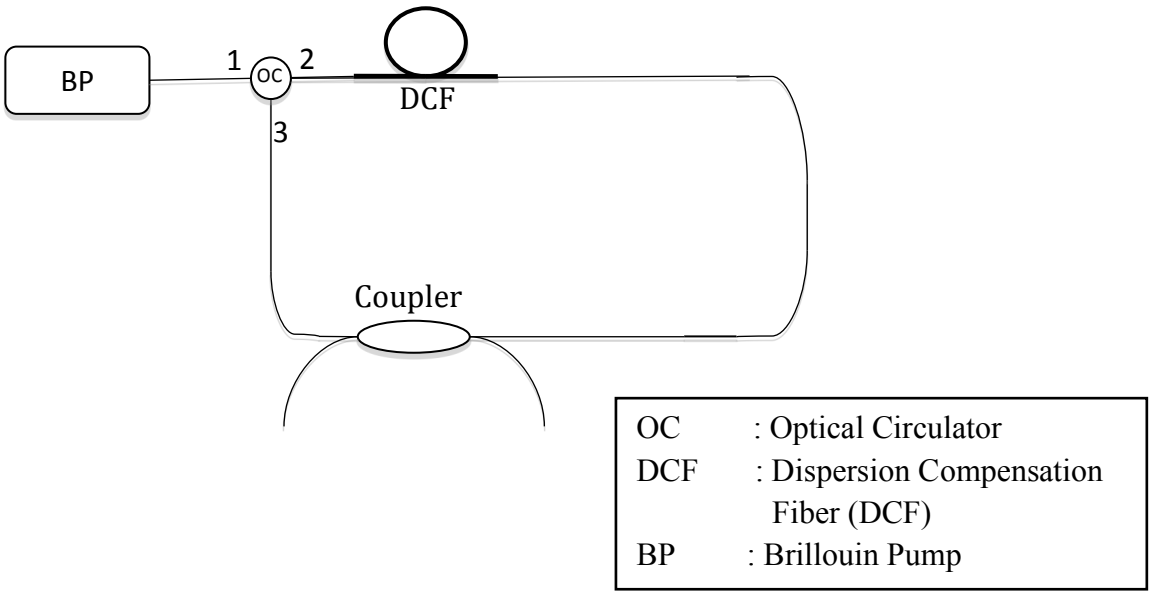

Figure 5.11 The ring cavity setup of Brillouin fiber laser

Other cavity type of BFL is the linear cavity BFL. The linear cavity BFL is almost the same with the ring cavity fiber laser. Linear cavity BFL has two mirrors or optical circulators to be used as the reflector mirror. Like the ring cavity, the linear cavity also needs external BP to be injected to the cavity and normally an optical isolator is used after the BP to protect the BP from the backward reflection that can damage the BP laser source. The linear cavity setup of BFL is shown in Figure 5.12. The difference between the linear cavity and the ring cavity is that the linear cavity allows multi-direction of the laser propagating inside the cavity thus giving an advantage in designing the Brillouin/S-band fiber laser and as well as studying the characteristics of the linear cavity BFL.

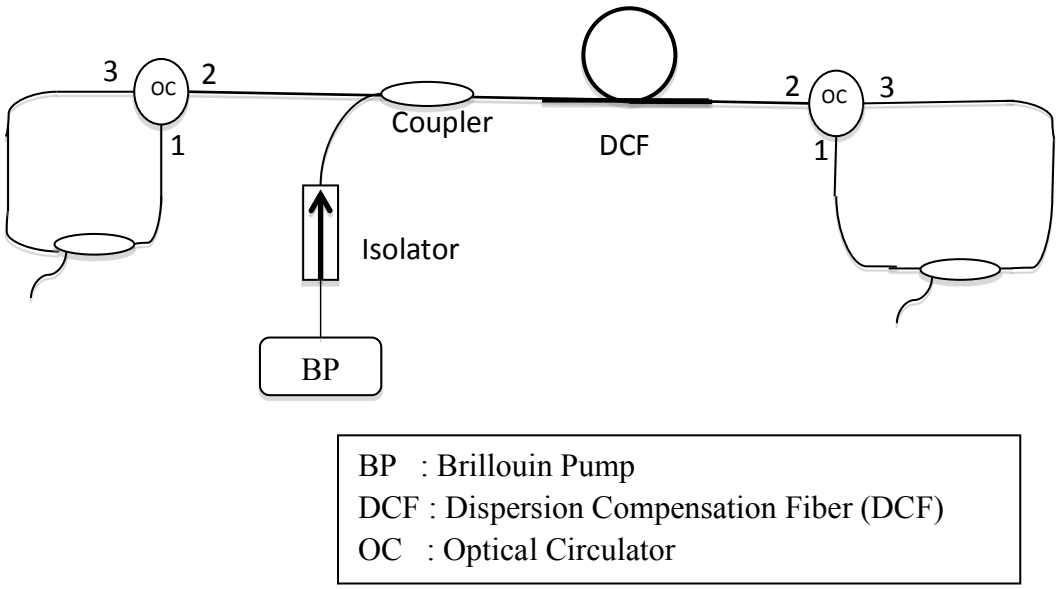

Figure 5.12 The linear cavity of a Brillouin Fiber Laser

5.4 S-band Hybrid Brillouin with Gain Medium

A hybrid Brillouin with EDF as the gain medium in generating fiber laser was first demonstrated by G. J. Cowle etc. al. [12-15] which integrated two gain media in the design of a laser cavity. The erbium-doped fiber amplifier (EDFA) offers a linear gain for high power generation to compensate the resonator loss. On the other hand, the Brillouin gain is provided by a section of optical fibers (DCF of SMF). In this case, the lasing wavelength generated at the Stokes-shifted frequency is determined by the injected Brillouin pump wavelength [14]. In the S-band region the first Brillouin fiber laser with hybrid gain medium is demonstrated by S.W.Harun and etc in 2006 [16]. In the report, the Brillouin laser cavity is hybrid with the Depressed Cladding Erbium Doped Fiber (DC-EDF) in a ring cavity which produces 4-output wavelength with a spacing of 0.08nm. However, only 4 to 5 wavelengths line can be produced [17]. As

stated in the objective at Chapter 1, one of the objectives is to enhance the number of Stokes generated in the previous report by S.W.Harun and etc [17].

5.5 S-band Multi-wavelength Brillouin/Depressed Cladding Erbium Doped Fiber Laser

S-band multi-wavelength Brillouin/depressed cladding erbium doped fiber laser (MWBDCEDFL) in linear cavity was demonstrated by S.W Harun etc in 2008[17].It consists of two optical circulators between the non-linear and linear gain medium. In this report the 500 m SMF is used as the non-linear gain medium. The number of wavelengths is only 4 with a spacing of 0.08 nm at wavelength of 1502.8 nm to 1503.2 nm. In this thesis, a design with numbers of channel and flatness improvement of the MWBDCEDFL's Stokes is demonstrated.

The improvement is done by using a 7.7km DCF with the same A_{eff} value as has been discussed earlier which is 55 μm^2. Figure 5.13 shows the set up which consists of a TLS as a BP source with its output injected into the cavity via the 3 dB optical coupler. The other port of the 3 dB optical fused coupler is connected to the DCF with a 30 m of DC-EDF ahead. The 30m DC-EDF is injected with a 300 mW pump power from a 980nm LD. The absorption of the DC-EDF is the same as discussed in Chapter 3 b. To complete the linear cavity setup, the optical circulators are inserted at both ends. The 90/10 optical fused coupler is connected into the cavity with 10 percent port to the OSA with a wavelength resolution of 0.02 nm.

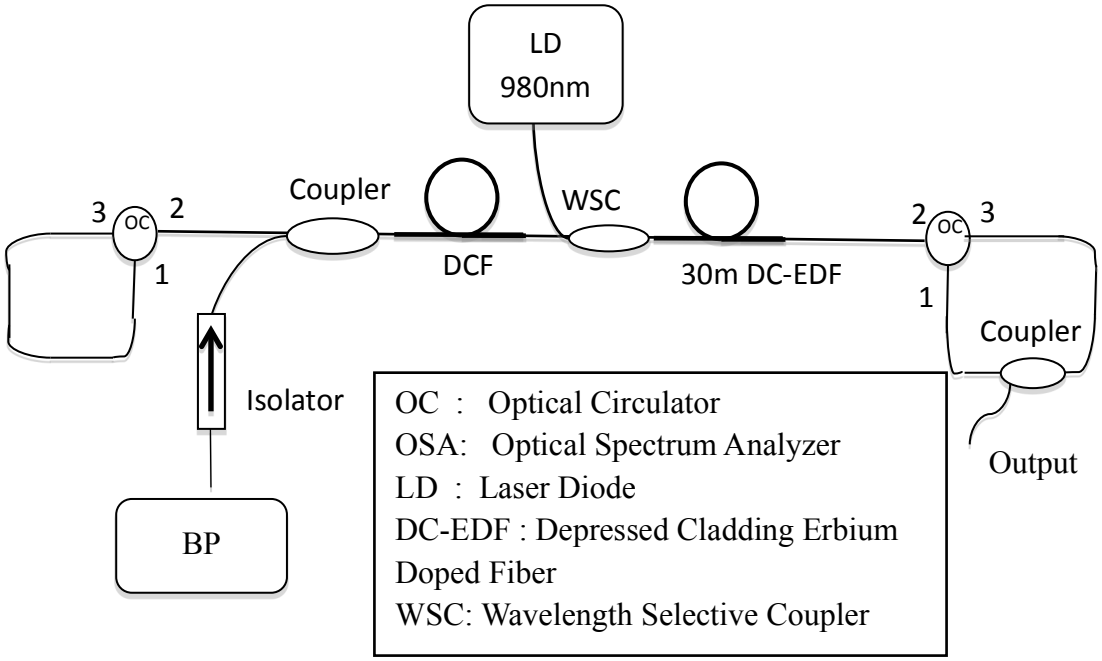

Figure 5.13 Experimental setup of S-band Multi-wavelength Brillouin/Depressed Cladding Erbium doped fiber laser in linear cavity

Figure 5.14 shows the operating range of the MWBDCEDFL obtained at different BP wavelengths, starting from 1485.08 nm to 1505.08 nm in 5 nm interval. At BP 1500.08nm 7 Stokes lines was obtain with average Stokes power is about –15.8 dBm dBm. From Figure 5.14 and 5.15(a), it can be inferred that the generated Stokes for a BP of 1485.08 nm is limited to only a single Stokes line (1st Stokes). This limited range is largely due to the gain profile of the DC-EDFA as discussed in Chapter 3. A BP wavelength at 1495.08 nm generates more Stokes lines, giving a total of 7 Stokes within the 3-dB region. On top of this, there are also 7 anti-Stokes generated at this BP wavelength as shown in Figure 5.15(b) as the BP wavelength increases, the number of Stokes and anti-Stokes wavelengths decreases due to the cut-off wavelength of the DC-EDF. The number of Stokes also decreases when the wavelength is increased towards the longer wavelength as shown in Figure 5.15 (c).

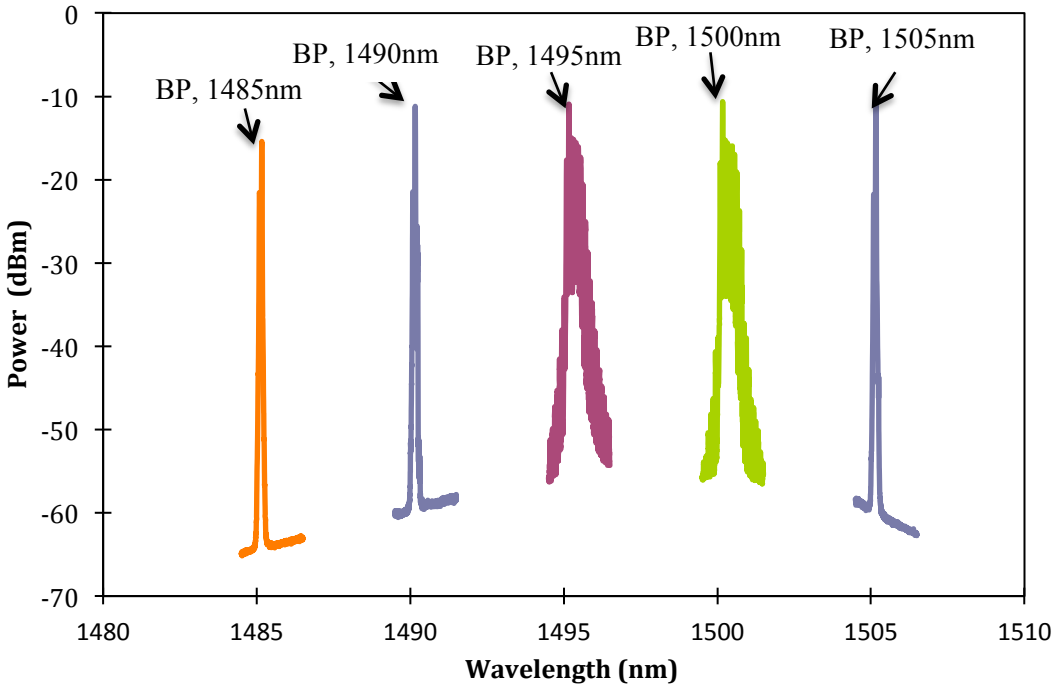

Figure 5.14 The operating range of the MWBDCEDFL obtained with different BP wavelengths

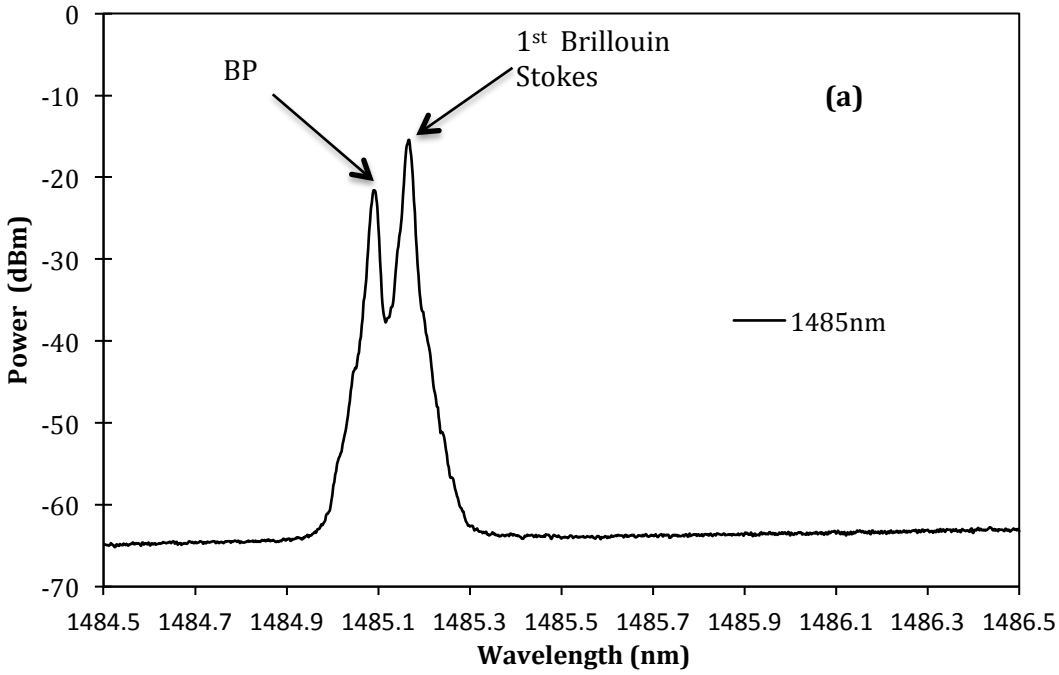

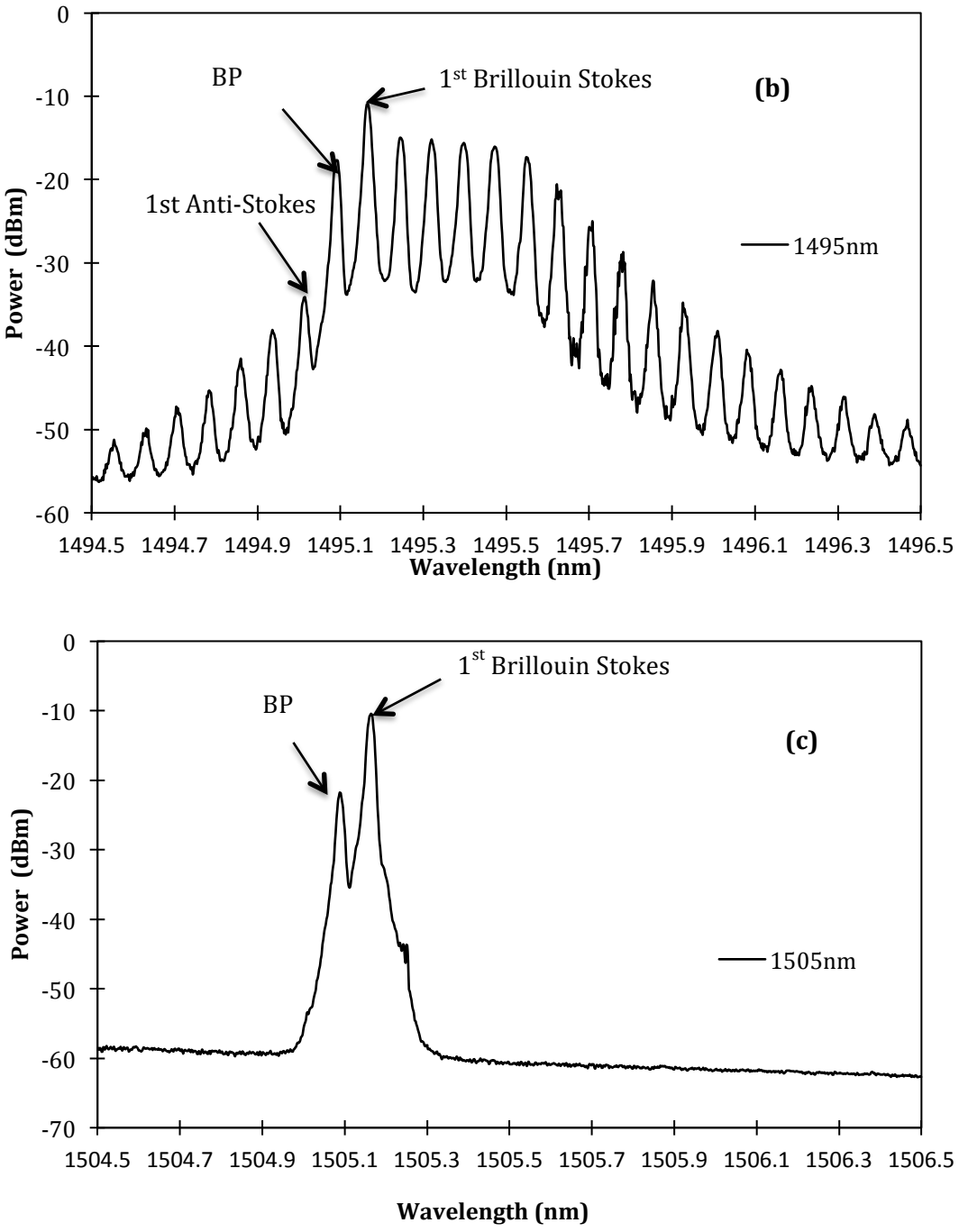

Figure 5.15 (a) Tuning range of the Stokes generated at different BP wavelengths, (a) 1485 nm (b) 1495 nm and (c) 1505 nm

Figure 5.16 shows the effect of changing the pump power of 980 nm LD which is injected into the DC-EDF to generation of multi-wavelength Brillouin Stokes. In this demonstration, the BP power is fixed at 12 dBm and the BP output wavelength is fixed at 1498.09 nm. At pump power of 980 nm at 9 mW and 41 mW, there is only one

Stokes line generated between 41 mW to 105 mW. The number of Brillouin Stokes increases linearly as the pump power increases, until saturation in the DC-EDF. This effect can be seen whereby no more Brillouin Stokes is generated when the pump power is increased further to 263 and 325 mW, for example. The number of Brillouin Stokes remains the same with 18 lines which start from wavelength of 1498.17 nm to 1499.47 nm. Within the 3 dB flat region of the proposed setup there are only 7 Brillouin Stokes with the average power of about-16.86 dBm. The use of the DCF fiber as a non-linear gain medium creates an anti-Stokes line which is not observed in the previous research reported [17]. This is due to the effect of four-wave mixing in the DCF fiber which is stronger compared to the SMF fiber. 7 anti-Stokes are created at maximum pump power of 325 mW with the wavelengths ranging from 1497.55 nm to 1498.02 nm.

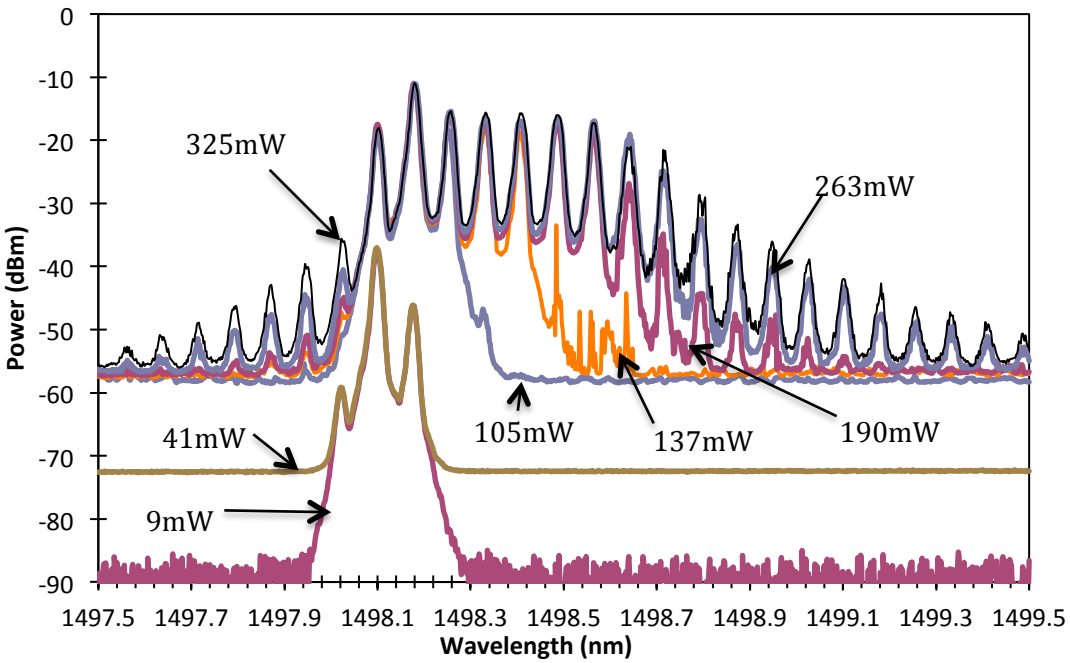

Figure 5.16 The multi-wavelength Brillouin spectrum with different 980 nm pump power of DC-EDF at BP power and wavelength of about 12dBm and 1498.07 nm respectively.

Figure 5.17 shows the MWBDCEDFL spectrum with different BP powers and fixed BP wavelength at 1498.09 nm and the pump power kept constant at 325 mW. The MWBDCEDFL spectrum depends on BP power. More Stokes line will be generated when the BP power is increased from -5dBm to 0dBm. The Stokes line power is almost constant with an average power of about -16.71dBm. However to generate more Brillouin Stokes line, higher BP power is required to produce Brillouin Stokes line above 16.

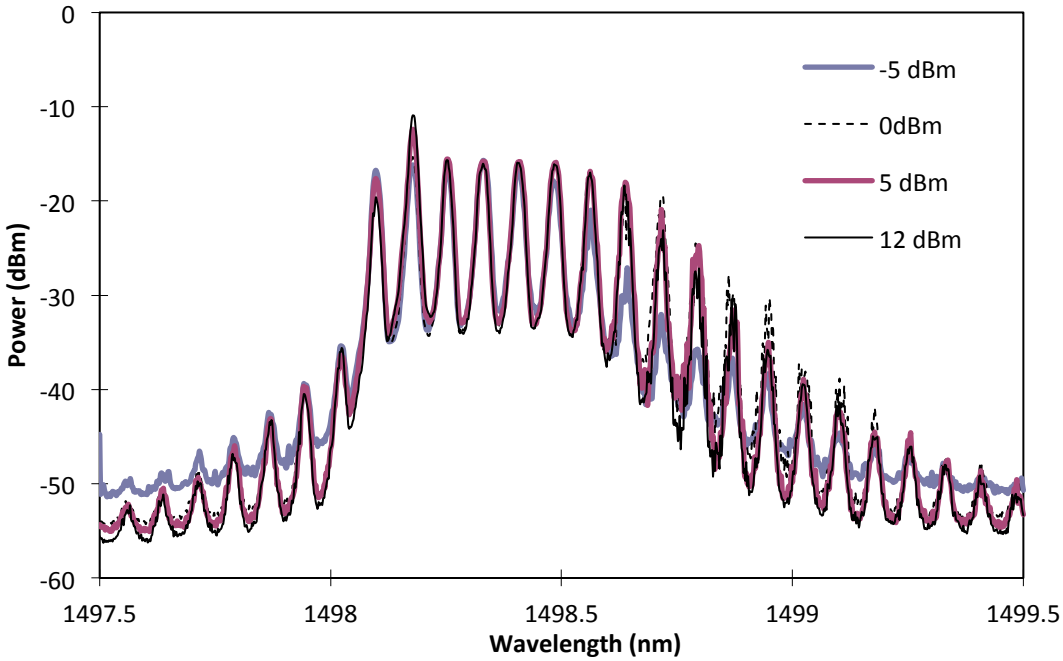

Figure 5.17 The MW-BDCEDFL spectrum with different BP powers with BP wavelength at 1498.09 nm and pump power of 325 mW

5.6 S-band Multi-wavelength Brillouin /Raman Fiber Laser

The configuration of the S-band Multi-wavelength Brillouin/ Raman fiber laser (MBRFL) is shown in Figure 5.18. It consists of DCF as the nonlinear medium having an effective core area of 55 μm^2 and a length of 7.7 km. TLS acts as the BP source, with a maximum optical power of 12.0 dBm and a linewidth of 15MHz which is connected

to the cavity via a 3dB fused coupler. Two Raman pump lasers (RP1) and (RP2) at wavelength of 1425nm, with pump power of 195mW each, are used to create the S-band Raman amplification in the DCF.A pair of wavelength selective coupler (WSC1, WSC2) is used to combine the 1425 nm RP with the S-band signal which is from 1460 nm to 1530 nm. Two optical circulators (C1, C2) are used as mirrors in the cavity. The optical couplers are placed at two positions namely Position A and B to study the optimum output of MWBRFL. The OSA is used to measure the output with the setting resolution of 0.02 nm.

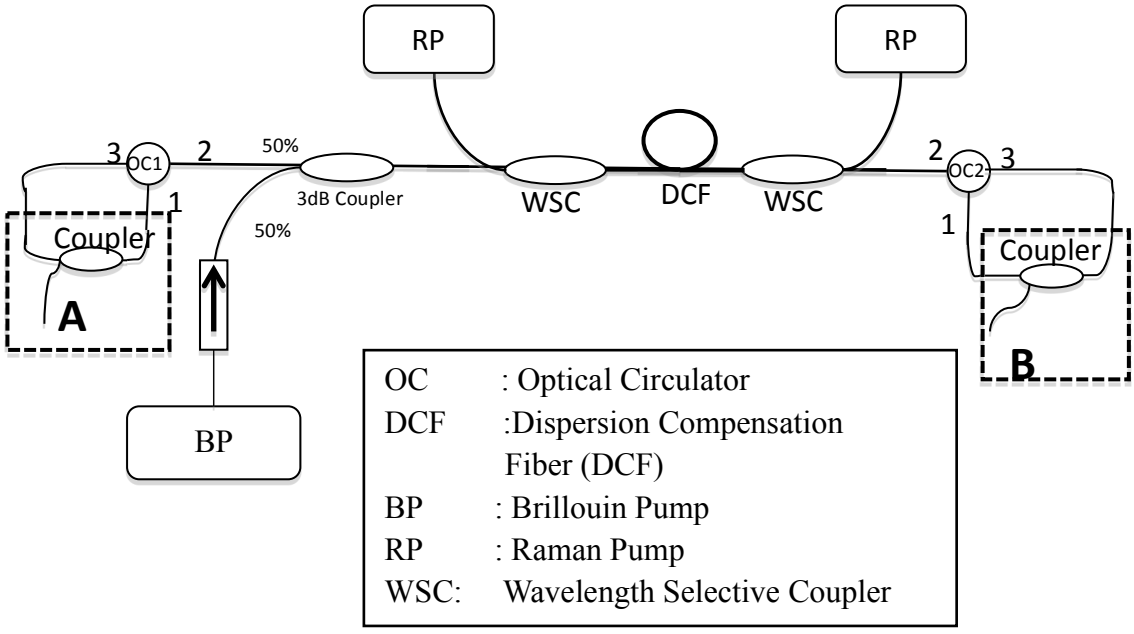

Figure 5.18 The experimental setup of MWBRFL

The MWBRFL is pumped by a BP power of 12dBm with a wavelength within the S-band range provide by the TLS which is injected into the linear cavity through the 3dB optical fused coupler, with the other 50% port is connected to port 2 of OC 1. BP enters into the cavity through a WSC coupler then travels to the nonlinear media DCF. Once the BP signal enters the DCF, it is then amplified by the S-band Raman gain medium which in this case is also provided by the DCF, which pump by two Raman pumps.

Amplified BP signal which exceeds the threshold power for Brillouin scattering will generate the 1stBrillouin Stokes which will propagate in the opposite direction of the BP. The 1stBrillouin Stokes will then be amplified by Raman amplifier along the fiber, and if its power exceeds that of the Brillouin threshold, 2nd Stokes will be generated, which has the same direction of BP. The same process repeats until the last Stokes is incapable of generating a new Stokes as the Stokes power does not reach the threshold value.

The positions, either A and B will be an important factor in determining the best characteristic of the Brillouin fiber laser in term ofStokes line number. Figure 5.19 shows the number of Stokes generated from the MWBRFL at different Brillouin Pump wavelengths and coupling ratios of coupler. The smaller ratio port is connected to the OSA at position A. As shown in the figure the number of Stokes increases when the BP wavelength increases within the maximum gain peak of Raman amplifier as discussed in Chapter 3. This is proves that the number of Stokes of MWBRFL is influenced by the Raman gain bandwidth. The highest number of Brillouin Stokes is at BP wavelength of 1520 nm with a coupling ratio of 70/30 giving 14 Brillouin Stokes generated, followed by coupling ratio of 80/20 and 90/10 with both having 13 Stokes lines. At BP wavelength of 1520 nm the coupling ratio of 50/50 shows the lowest number of Stokes which is about 9 Stokes lines. This is possibly due to the high loss of 1st Stokes power at the 50/50 coupler in Position A which is limits the Brillouin Stokes generation.

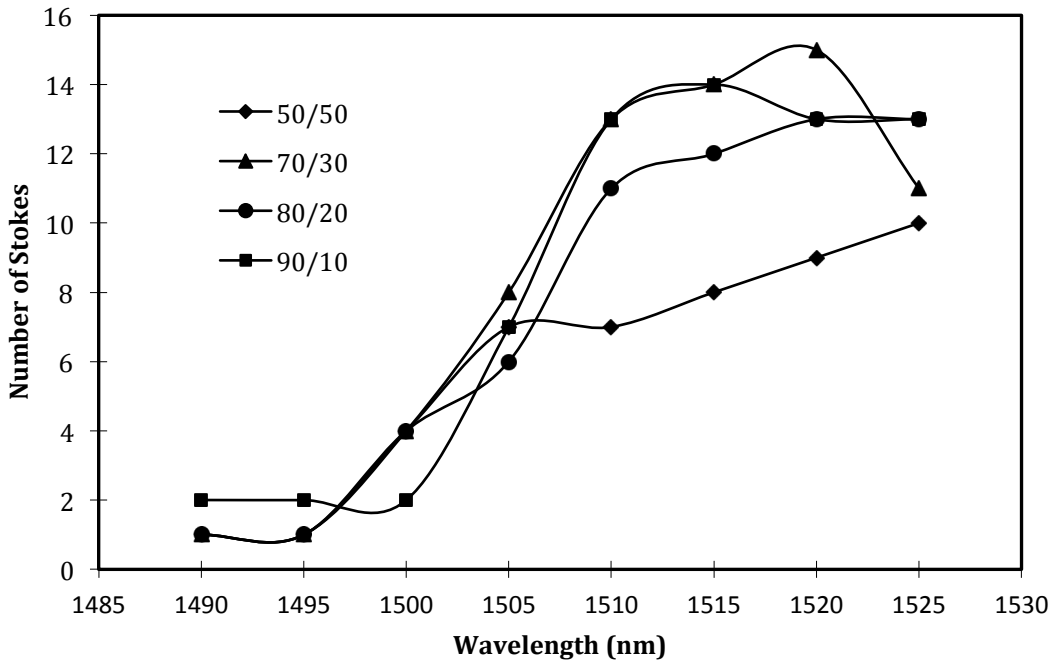

Figure 5.19 The number of Stokes with different BP wavelength and coupling ratio at position A

Figure 5.20 below shows the number of Stokes generated at different BP wavelengths with different coupling ratio at position B. As demonstrated in the experiment the Stokes lines generated have similar pattern for both position A and B except that in B the number of Stokes lines is higher compared to position A at any coupling ratio and BP wavelength. This is due to the extra loss experienced by the 1st Stokes when passing through the optical coupler at position A thus reducing the power to generate the 2nd Stokes line. The number of Stokes is also follows the pattern of Raman amplifier gain bandwidth. The highest number of Stokes is at BP wavelength of 1520 nm and 1525 nm with 23 channels are generated. At the same time, this Figure can be used to measure the tuning range for Stokes generation. By changing the BP wavelength from 1490 nm to 1525 nm a tuning range of 35 nm is obtained

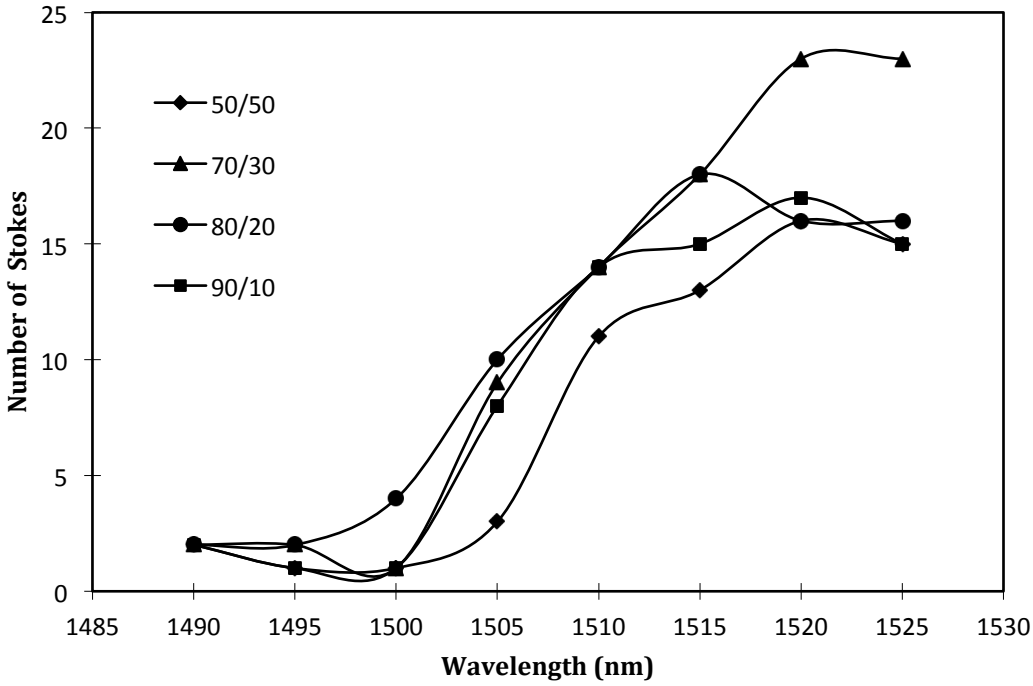

Figure 5.20 The number of Stokes at different BP wavelengths and also with coupling ratio at position B

5.6.1 Effect of the Brillouin Pump Power in the Multi-wavelength S-band Brillouin/Raman Fiber Laser in a Linear Cavity Configuration

In the MWBEFL, the number of Stokes is dependent of the BP pump power [18], and this normally occurs in the S-band MWBDCEDFL fiber laser as shown in Figure 5.17 above. However different behavior occurs in the S-band MWBRFL. The S-band MWBRFL is independent to the BP power. This is shown the Figure 5.21 below; with the decrement of the BP power, the Brillouin Stokes is almost the same especially within the 3dB region. The number of Stokes when the BP power is set at 12 dBm is 23 lines and it remains constant when the BP power is varied from 10dBm to the 2dBm. The number of Stokes dropped slightly when the BP power is about 0dBm with the number of lines generated is about 21. This is shown at Figure 5.22 below. This observation makes the S-band MWBRFL design to be an interesting option in the usage within the region of 12dBm to 2dBm of BP power

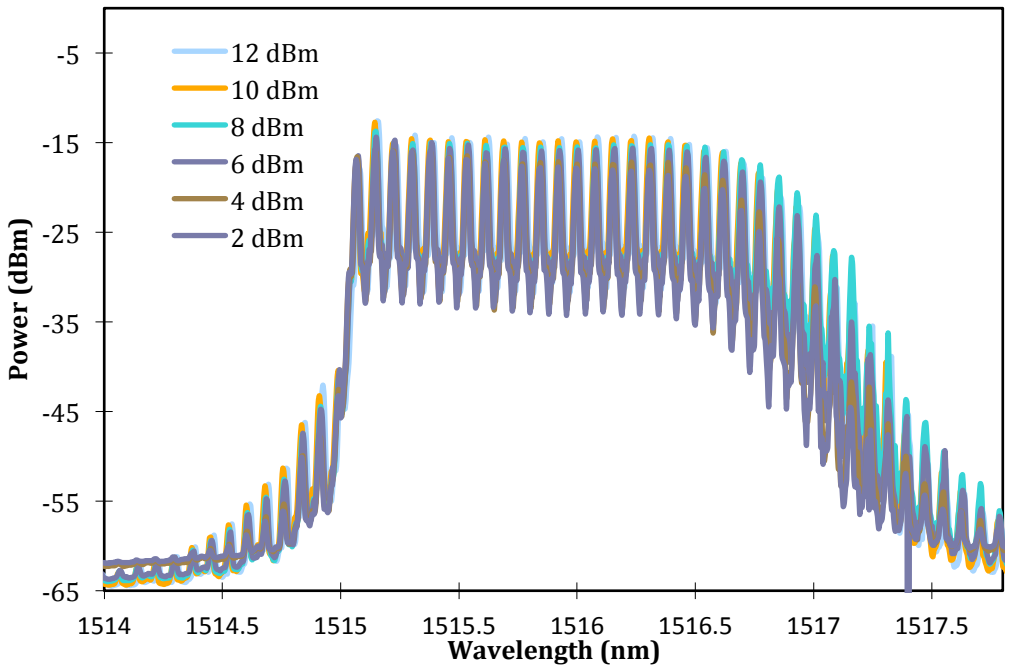

Figure 5.21 The output spectrum at the different BP powers

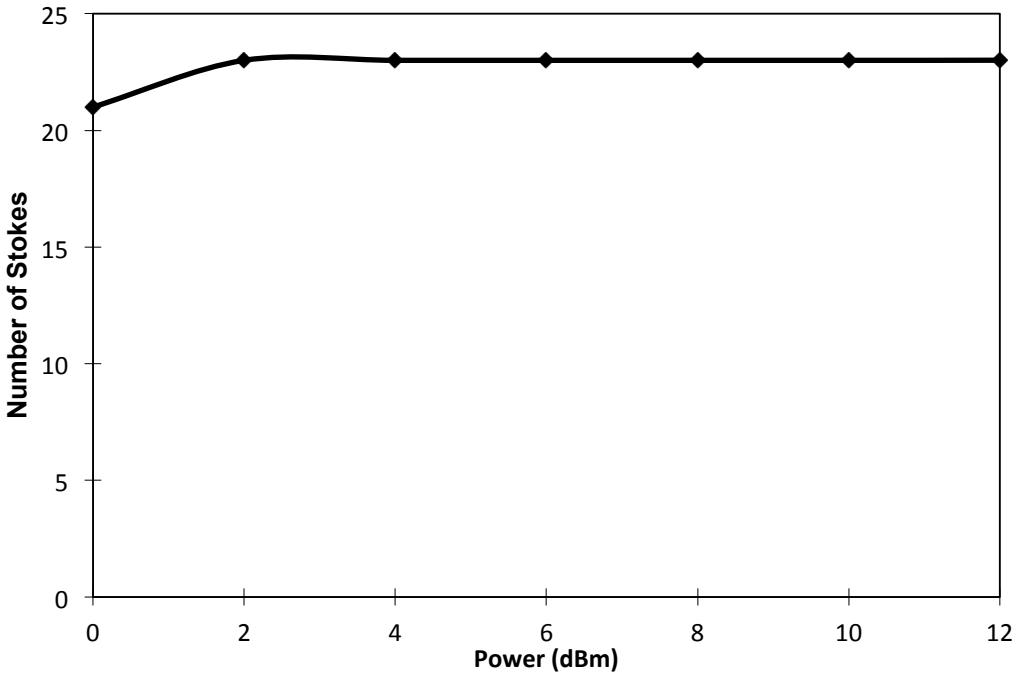

Figure 5.22 Number of Stokes generation with different BP power at BP wavelength of 1515 nm

5.6.2 Output Characteristics at Different Brillouin Pump Direction and Coupling Ratio

The generation of the Brillouin Stokes line depends on the BP, linewidth of the BP and also the non-linear gain medium. To get higher order Brillouin Stokes lines a high power BP has to be injected into the non-linear gain medium. Besisdes that, the position at which the BP is injected plays an important role to get high order Brillouin Stokes lines for the case of the linear cavity. The experimental setup of the S-band MWBRFL is shown in Figure 5.23 to investigate the position for BP to be inserted to give the maximum number of lines. It consists of Dispersion compensated fiber (DCF) as a nonlinear media with an effective core area of 55 μm^2 and a length of 7.7 km. Tunable laser source (TLS) acts as Brillouin pump (BP) source, with maximum optical power of 12.0 dBm and linewidth of 15 MHz. Two Raman pump lasers (RP1) and (RP2) at wavelength of 1425 nm, with power of 190 mW each are used to create S-band Raman fiber amplifier. A pair of optical circulator (OC1, OC2), wavelength selective coupler (WSC1, WSC2) and optical couplers (C1, C2) are used to create mirrors in the cavity. The first optical coupler (C1) has variable coupling ratio while the second optical coupler (C2) has a fix ratio of 10:90. An OSA is used to study the spectrum.

The BP power from TLS is injected into the linear cavity through the higher percentage port ratio of C1, example for coupling ratio 70/30, the 70% port power is connected to TLS while the 30% end is connected to port 3 of OC1. BP enters the OC1 from port 1 and exit at port 2, to be injected into nonlinear media DCF. If the BP signal exceeds the threshold power of Brillouin, it scattering will generate the 1st Brillouin Stokes that propagates in opposite direction of BP. The 1st Brillouin Stokes is also amplified by Raman amplifier along the fiber, and if its power exceeds the Brillouin threshold, 2nd

Stokes will be generated, that has the same direction of BP. The same process continues until the last Stokes is incapable of generating a new Stokes. The 1st Stokes continues to propagate in the opposite direction of BP and that it is recirculated back into the cavity by OC1 and C1 whereby the first Stokes enters port 2 of OC1 and goes out through its port 3 then it goes through C1 which recirculates it back into the linear cavity by port 1 of OC1. Meanwhile the transmitted BP and 2nd Stokes are recirculated back into linear cavity through OC2 and C2. The transmitted BP and 2nd Stokes will move towards port 2 of OC2 and will be emitted through port 3 and then 10% of its poweris tapped by C2 to be analyzed by the OSA with the rest of the power is feedback into the linear cavity by port 1. The experiment is repeated by changing the coupling ratio of C1 with 3 different values, 50/50, 70/30, and 80/20, in order to see the effect of BP power and the reflected Stokes power.

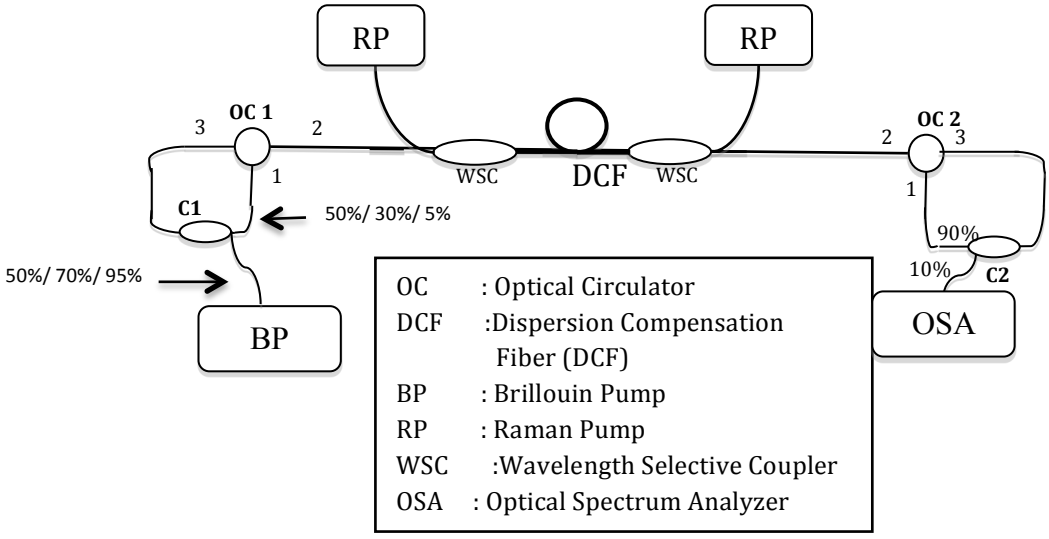

Figure 5.23 Experimental setup for S-band Multi-wavelength Brillouin Raman fiber laser with different BP location [19]

Figure 5.24 depicts the S-band MWBRFL spectrum for different C1 coupling ratio. The horizontal dashed lines represent the region of flat Stokes where the peak power difference between maximum the peak powers and the other Stokes falls within 3dB

region. These lines represent the Stokes that have flat peak power output. Coupler C1 with 50/50 coupling ratio generates 33 lines with flat Stokes output power. For C1 95/5, the number of flat lines are 29 and for 70/30 the number of flat lines are only 19. C1 with coupling ratio of 50/50 produces better Stokes number than the other two couplers. From the result, the optimization of the coupling ratio is important to produce maximum number of Stokes.

For C1 50/50, the BP power injected into the setup is small, but after it is amplified by Raman amplifier, it exceeds the Brillouin threshold and creates the first Stokes. With high reflectivity at left mirror (50%) it helps to generate more Stokes by allowing more power of 1st Stokes to be feedback into the cavity. As for C1 70/30, the BP power is higher compared to C1 50/50, but a small reflectivity at left mirror (30%) makes the cavity having less power to generate more Stokes. For C1 95/5, high power BP is enough to convert its power for generating new Stokes. Hence, from help of Raman amplifier, C1 95/5 can generate more lines compared to the setup using C1 70/30, even though the reflectivity of the left mirror is small (5%). The spacing between each channels or lines for all 3 different coupling ratios are the same which are all approximately 0.08 nm or 10.63GHz.

Beside the number of lines, the Stokes peak power is also an interest to the coupling ratio. From Figure 5.24 the average peak power for C1 50/50, 95/5, and 70/30 are at -18.83 dBm, -20.41dBm and -14.58 dBm respectively. The highest peak power obtained is for C1 with coupling ratio of 70/30. This is due to the amplification of S-band Raman fiber amplifier, where it only has to amplify few numbers of Stokes compared to those with different coupling ratios. From Figure 5.24, it can be inferred that for C1 70/30, a lot of anti-Stokes are generated. This condition is probably due to

the high output peak power of MWBRFL that stimulates the four wave mixing effect and creates an idler which results in creating an anti-Stokes. [20].

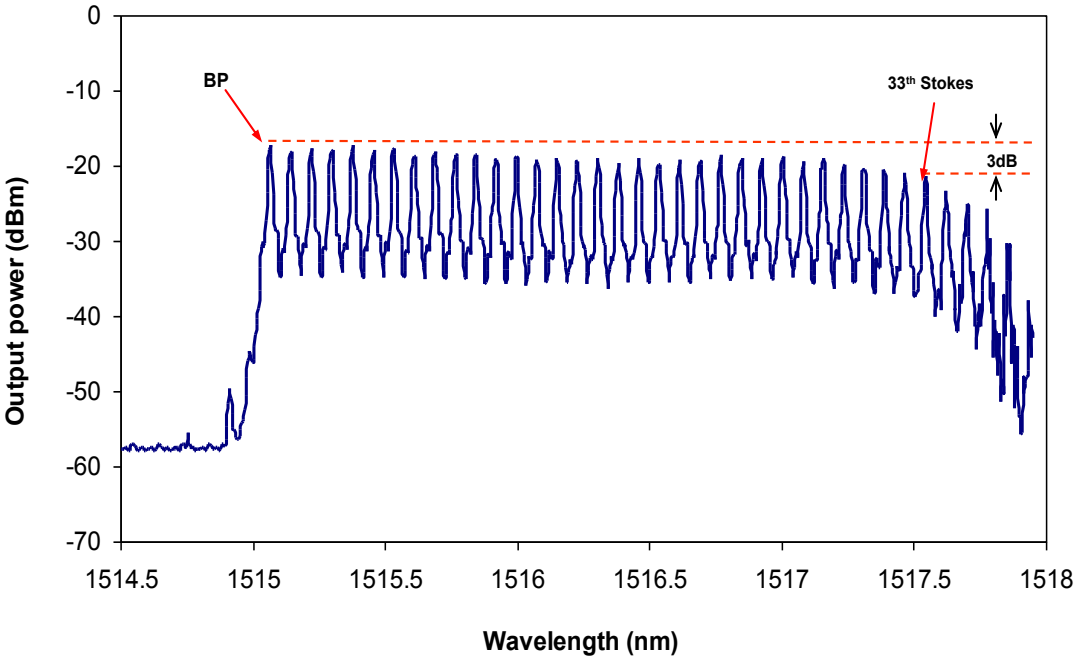

(a)

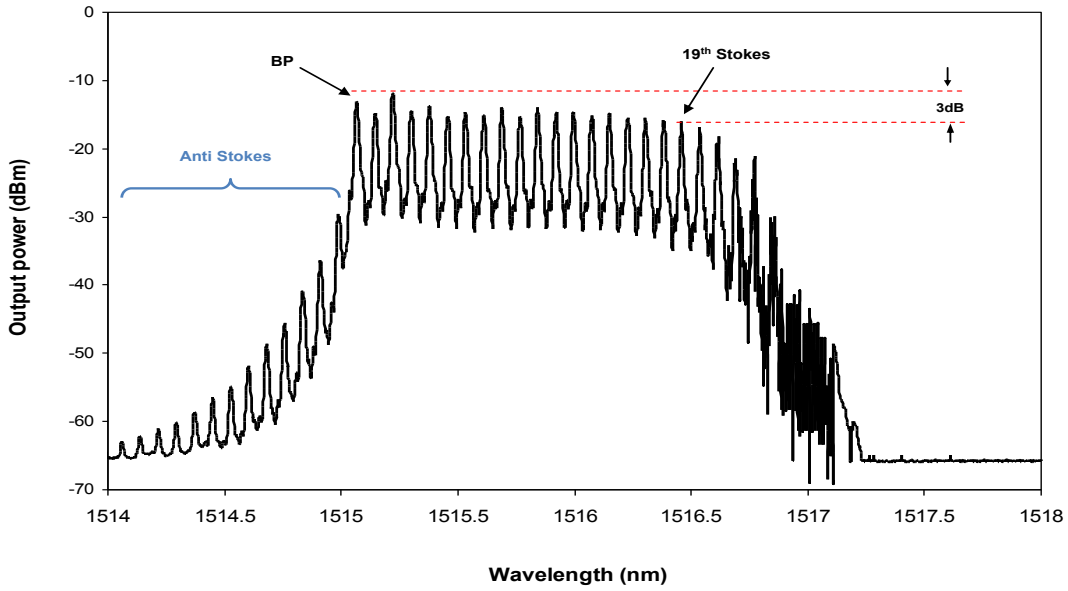

(b)

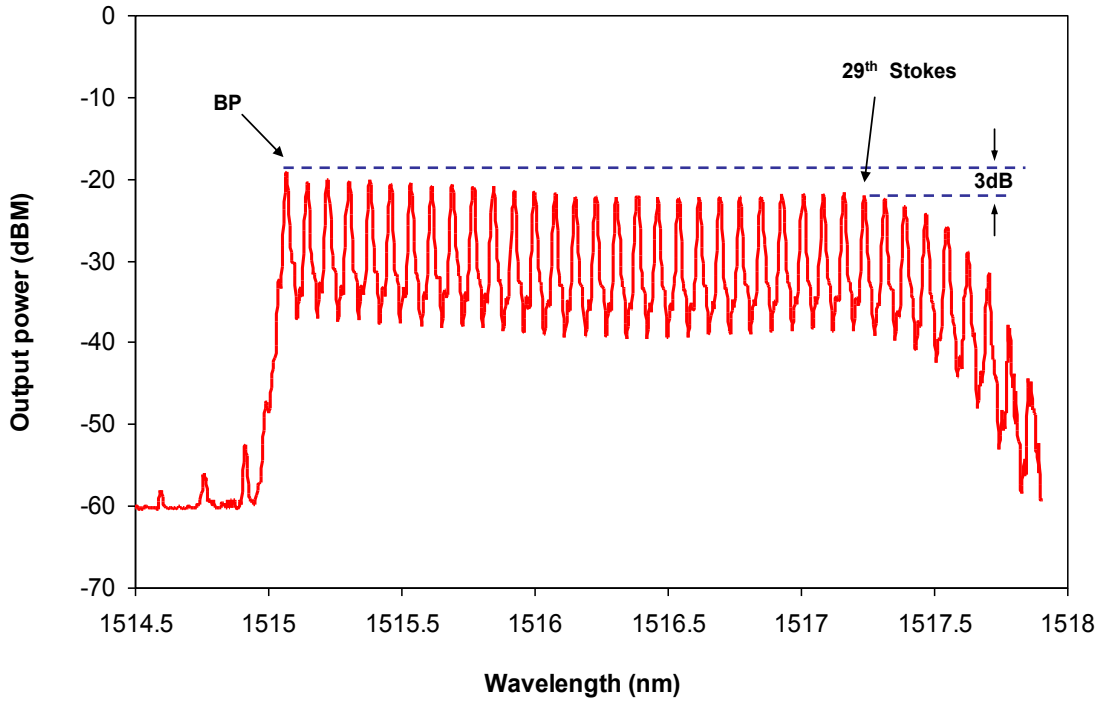

(c)

Figure 5.24 Spectrum of Brillouin Raman fiber laser with coupling ratio for C1; (a) 50/50, (b) 70/30 and (c) 95/5.

The enlargement of this anti Stokes is shown in Figure 5.25. The interaction between BP and 1st Stokes creates 1st anti Stokes, while 2nd anti Stokes is created as a result from interaction of BP and 2nd Stokes and so on until the Stokes power is insufficient to overcome the FWM threshold.

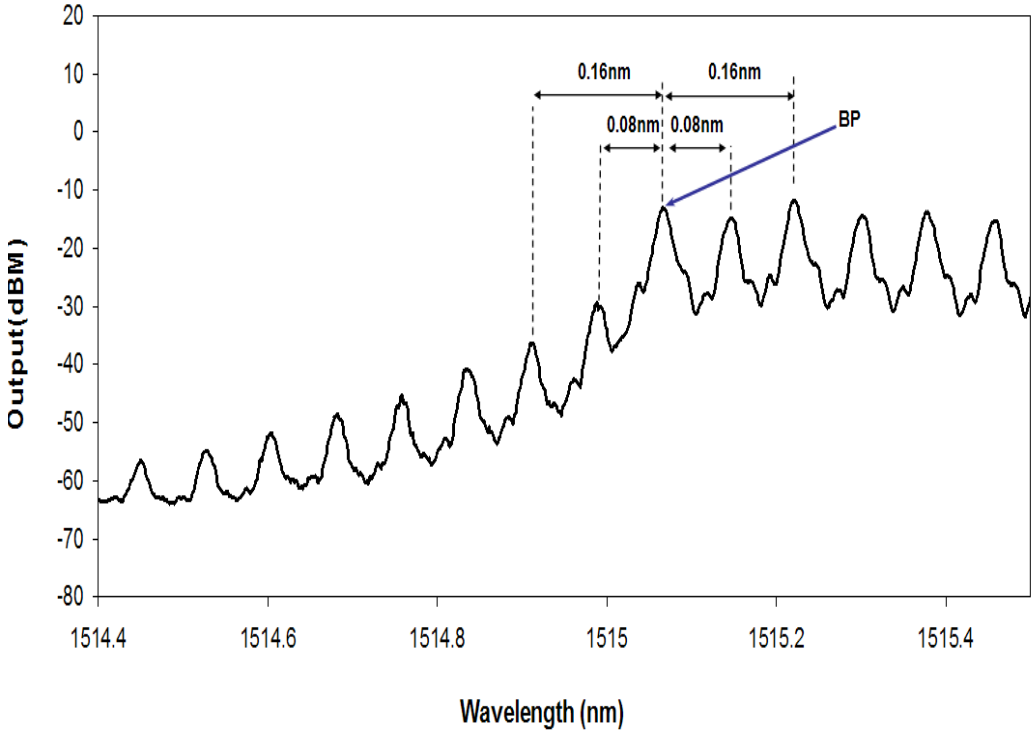

Figure 5.25 Enlarge scale on anti Stokes of S-band Brillouin Raman fiber laser at coupling ratio of C1, 70/30.

The effect of BP wavelength against the Stokes generation of Brillouin Raman fiber laser is shown in Figure 5.26. The number of Stokes plotted in the graph is the Stokes lines that has flat peak power output. It is important to have flat power to ensure that the output power of Brillouin Raman fiber laser can be used in multi-wavelength fiber laser applications [21]. The maximum number of flat Stokes lines is generated by using the optical coupler C1 with 50/50 coupling ratio and at BP wavelength of at 1515 nm. The number of Stokes line reduces when the BP wavelength is between 1508 nm and 1513 nm. For C1 with 70/30, the Stokes lines begins to be generated at BP wavelength of 1508 nm.

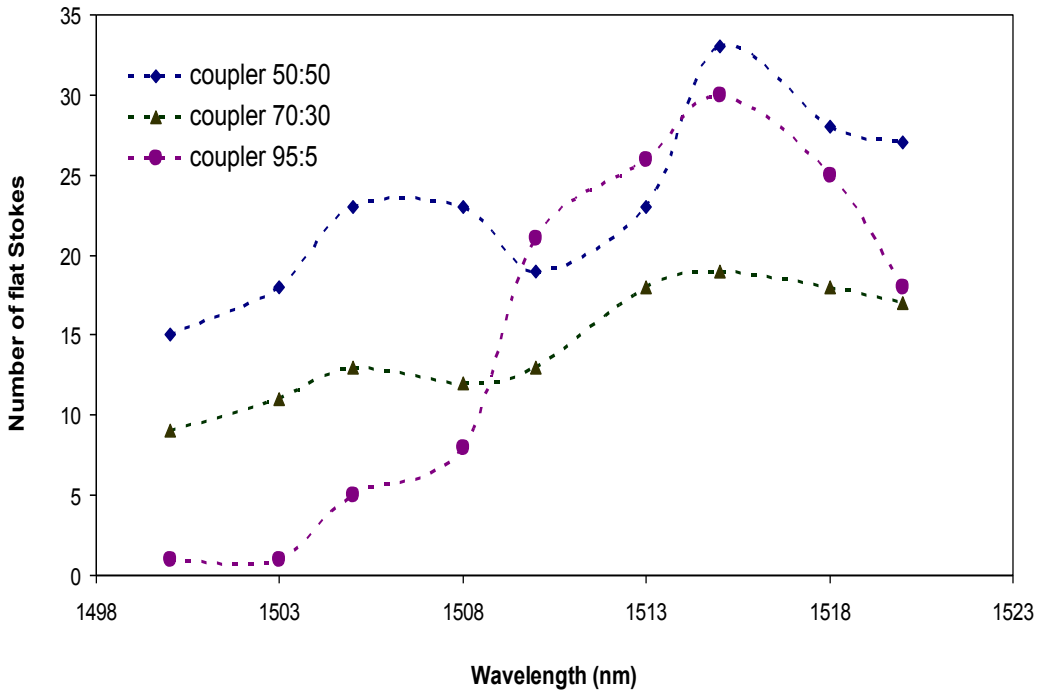

Figure 5.26 Number of flat Stokes at different wavelength.

Figure 5.27 shows effect of Raman pump power towards the generation of S-band BRFL. The spectrum is generated from the setup with C1 50/50 coupling ratio. It is chosen due to its ability to produce high number of Stokes. From this figure, it shows that the Raman pump power does not have any effect on the Stokes peak power but it has effect on the number of Stokes line generated.

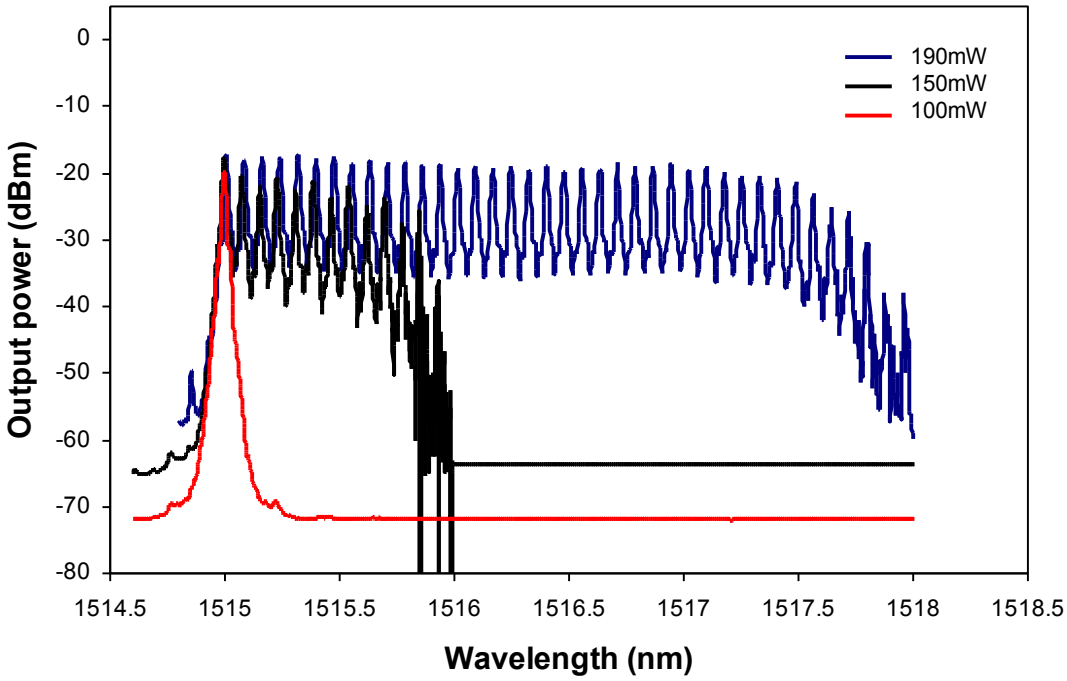

Figure 5.27 S-band Brillouin Raman fiber laser at different Raman pump power

5.6.3 Effect of Multiple Brillouin Pump to the Characteristics of S-band Multi-wavelength Brillouin/ Raman Fiber Laser

There are two types of gain medium, (i) homogenous and (ii) inhomogeneous. EDF is a good example of homogenous gain medium which limits the operation to only a single mode oscillation. The mode competition is an issue in Erbium doped fiber laser. As an alternative to this problem, the Raman gain medium is used to provide an inhomogeneous characteristic. The inhomogeneous effect can support dual or multiple wavelength emission. In this section we observe the effect of performance in S-band MWBRFL with two BP power injected spontaneously.

The experimental setup of this study is shown in Figure 5.28 It consists the same configuration of the Figure 5.28 except that we eject two BP power spontaneously into

the cavity. The 3dB coupler is used to combine two different wavelength and also into the cavity. The output of 70/30 coupling ratio is connected to the OSA with a resolution of 0.02nm to be analysed.

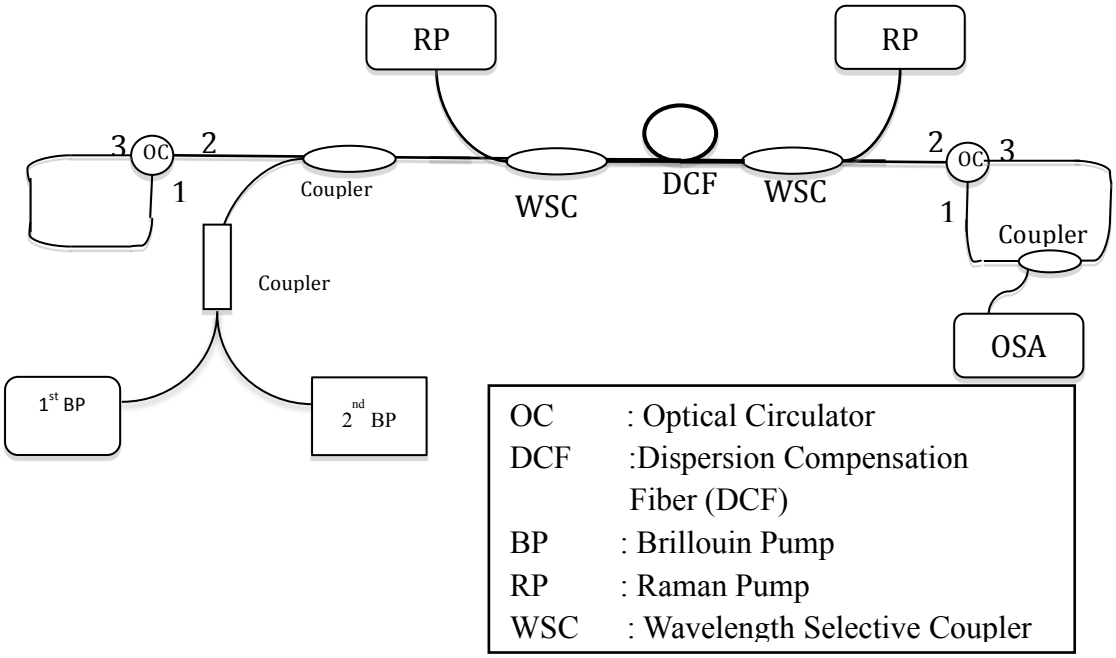

Figure 5.28 The experimental setup for studying the effect of inserting two BP of S-band Multi-wavelength Brillouin/Raman fiber laser in linear cavity

The output spectrum of the experimental setup to study the effect of inserting two BPs is shown in Figure 5.29. The output spectrum from the 1st BP is important to determine the wavelength of the 2nd BP. Form the Figure 5.29 the multi-wavelength fiber laser with 0.08 nm spacing is broad and has almost flat peak power from the BP wavelength 1517.03 nm to the 1519.2 5nm.The 3dB fluctuation is only observed until 1518.43 nm. The average power of the Brillouin peak is about -10dBm. From this result, the 2nd BP is injected with a wavelength of 1518.53 nm which is approximately 0.08 nm from the last Stokes line in 3 dB region.

The spectrum of the two BP is shown in Figure 5.30. The spectrum is extracted out from the cavity and analyzed by the OSA. Both of the BP powers are set equally to make sure the multi-wavelength output spectrum is exhibit the same effect. From the

figure the 1st BP is set at the wavelength of 1517.03 nm with injected power is about 12 dBm and 2nd BP is set to the wavelength 1518.53 nm with the same injected power of 12 dBm

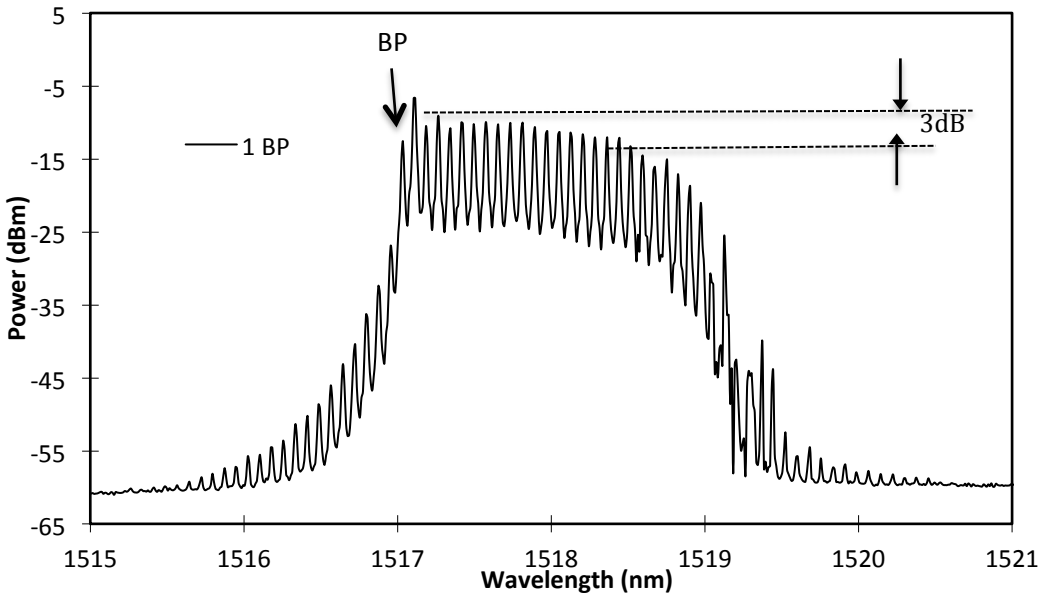

Figure 5.29 The output spectrum by using only one BP with wavelength 1517.03 nm

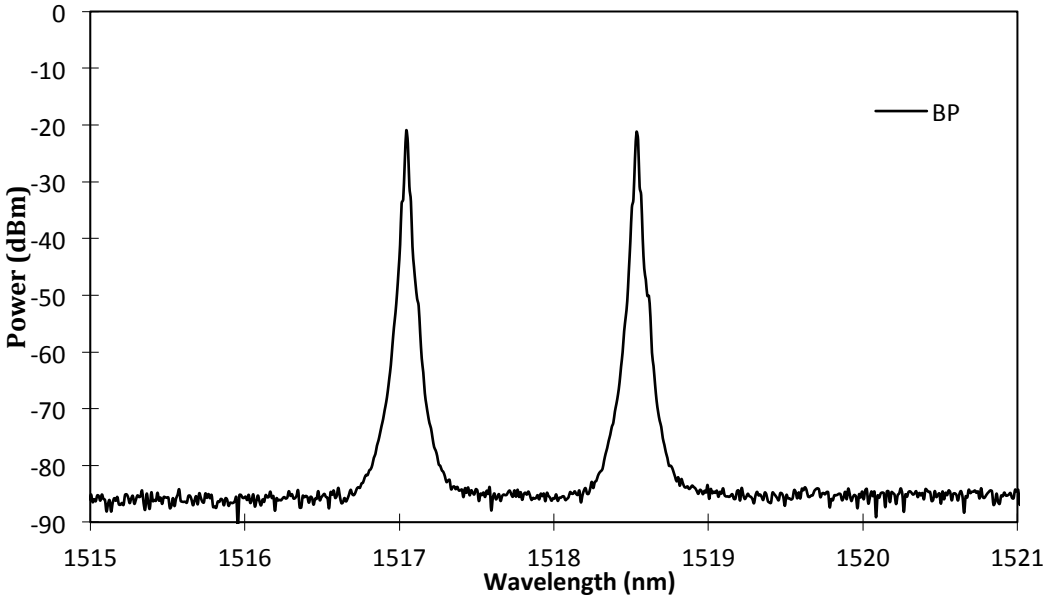

Figure 5.30 The spectrum of the two BP with wavelength is 1517.03 nm and 1518.53 nm with the Raman Pump is switched off.

After the 2nd BP wavelength has been determined, we injected both of the BP simultaneously into the cavity. The output spectrum of the S-band MWBRFL by using two BPs is shown in Figure 5.31. From the figure the influence of the 2nd BP is

observed in such a way that it expend the bandwidth, number of channel and the flatness of the S-band MWBRFL. The laser channel startes from 1517.12 nm to 1518.45 nm for the1st BP with a total channel count is about 31 Brillouin Stokes and then itexceeds from 1518.53 nm to 1519.61 nm with a total bandwidth is about 2.49 nm. The average output power for all the peak in the 3 dB region is about -12.4 dBm. There is a transition region between the 1st BP area and 2nd BP area. The transition region can obviously be seen with small output power at wavelength of 1518.45 nm, which is next to the 2nd BP. This effect is probably due to the interaction of two wavelengths from the last Stokes line of the 1st BP and 1st anti-Stokes line of the 2nd BP.

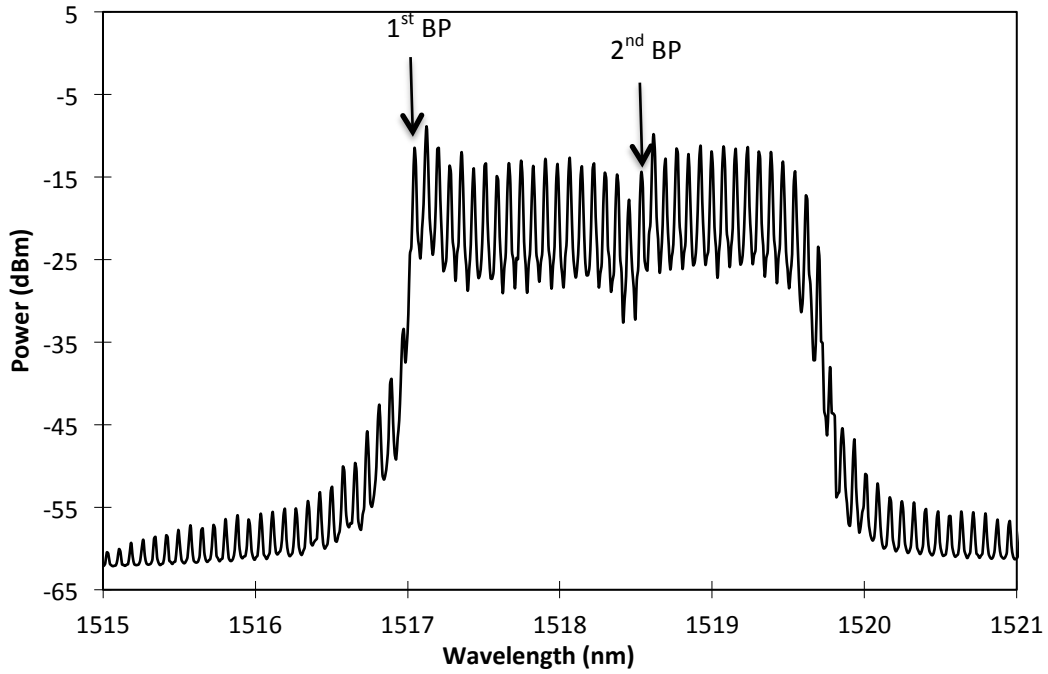

Figure 5.31 The output spectrum of S-band Multi-wavelength Brillouin/Raman fiber laser by injected 2 BP in the linear cavity

5.6.4 20GHz Spacing of S-band Multi-wavelength Brillouin/Raman Fiber Laser

There is an interest in expanding the channel spacing between the generated Stokes in MWBRFL. Early works have reported a tunable comb fiber laser with a channel

spacing of 10 and 20 GHz [22], with the oscillations of the Odd and Even Stokes separated into two different cavities and amplified by an EDFA. More recent works demonstrate similar results using a twin-cavity BEFL [23, 24] however these approaches are complicated and require the Odd and Even Stokes to oscillate in separate cavities, thus adding a fair level of complexity to the setup. Compact and tunable MBFLs have also been demonstrated using highly non-linear fibers such as photonic crystal fibers (PCFs), which are able to generate Stokes lines with channels spacings of 0.16 nm (20 GHz) [25]. These MBFLs have fairly simple configurations but as they are lack of linear gain medium, they are highly dependent on the Brillouin Pump (BP) power, requiring high BP powers to achieve the multi-wavelength comb.

The experimental setup of the 20 GHz channels spacing of simple ring cavity S-band MWBRFL with independent pump powers is shown in Figure 5.32. It consists of a Brillouin Pump (BP) from a Tunable Laser Source (TLS) which is capable of giving a maximum output power of 12 dBm. It is then connected to Port 1 of the 2x1 3 dB coupler, C1. The output of C1, Port 3 is then connected to Port 2 of the first WSC, WSC1 (1400-1430 nm, Port 1, Port 2 with transmission at 1480-1520 nm and Port 3 is common). Port 3 is then connected to a 7.7 km long Dispersion Compensating Fiber (DCF) which acts as linear and non-linear gain medium. The DCF has a dispersion of -584 ps/nm and an insertion loss of 6.66 x 10^3 dB/m. It is bi-directionally pumped by the usage of the second WSC, WSC2. The two Raman Pumps (RPs) used in this setup is operated at wavelengths of 1425 nm with combined powers that are adjusted from a total power of 156 mW to 371 mW.

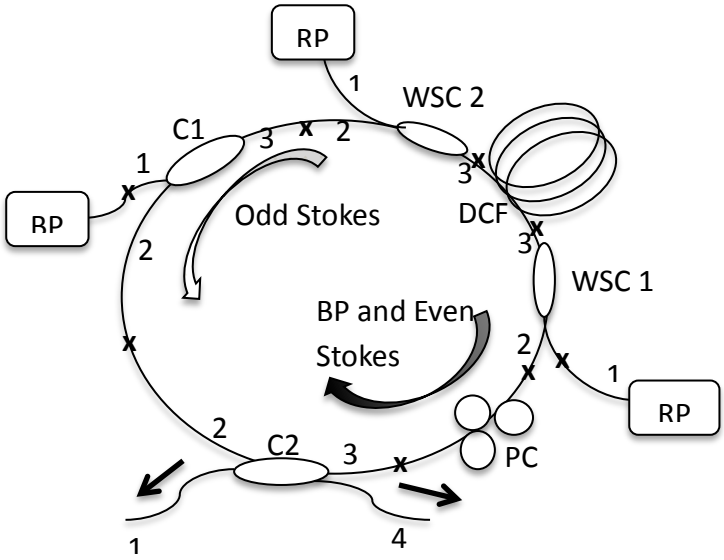

DCF	: Dispersion Compensating Fiber
PC	: Polarization Controller
BP	: Brillouin Pump
RP	: Raman Pump
WSC	: Wavelength Selective Coupler
C	: 3dB Fused Coupler

Figure 5.32 Experimental setup of 20GHz S-band multi-wavelength Raman fiber laser

The output port, Port 2 of WDM 2 is then connected to a Polarization Controller (PC) and the output from this PC is then connected to Port 3 of the 2x2 3 dB coupler, C2. Ports 1 and 4 of C2 are the output ports to detect the BP as well as the even Stokes and odd Stokes respectively. Port 2 of C2 is connected to Port 2 of C1 to close the ring cavity. The PC is used to control the polarization state of the signals oscillating in the cavity as to enhance the interaction.

When the DCF is pumped to provide the necessary gain, the BP signal that travels in the clockwise direction will generate the 1st Brillouin Stokes that will oscillate in the anti-clockwise direction. The 1st Brillouin Stokes will then travel in the anti-clockwise direction into the DCF, which then generates the 2nd Stokes which travels in the opposite direction. Then this 2nd Stokes will travel back into the DCF and generate the

3rd Stokes. This 3rd Stokes will travel in a similar direction as the 1st Stokes into the DCF to generate the 4th Stokes. This repeats until there is no more gain available for further Stokes generation. Besides providing the non-linear gain for the Brillouin effect, the DCF also acts as a linear gain medium, thus reducing the Brillouin threshold for Stokes generation. The odd Stokes is measured and observed at output Port 4 of coupler C2 whereas for the BP and even Stokes, are measured from output Port 1 using the same Optical Spectrum Analyzer (OSA) with a resolution of 0.02 nm (Ando AQ-6317C). The DCF provides the non-linear medium for generating the Stokes based on the Brillouin effect, and also acts as a Raman gain medium with an average net gain of 2 dB. It has a much higher gain based on the 'On-Off' gain measurement.

The Raman amplifier gain bandwidth plays an important role in obtaining the Brillouin generated Stokes at a lower threshold. The DCF fiber acts as the Raman gain medium as well as the non-linear medium for Brillouin Stokes generation. The Raman gain spectrum is shown in Figure 5.33.

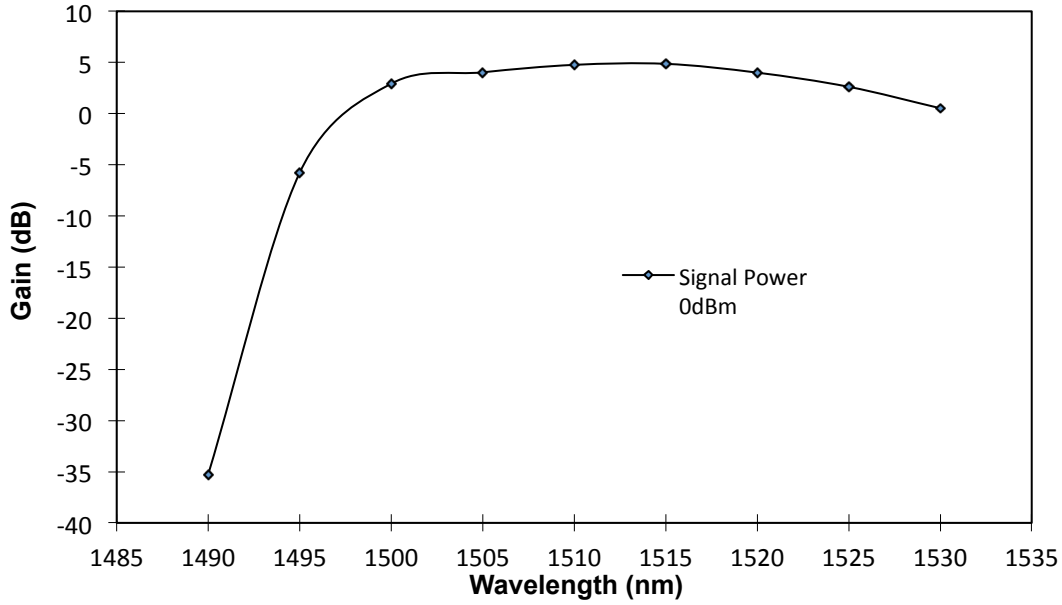

Figure 5.33 Raman gain spectrum of the DCF when pumped at 1425 nm with a combined power of 371 mW.

It has a flat gain profile from approximately 1500 nm to 1525 nm, with a gain of about 5 dB for an input signal at 0 dBm. It has a slope profile from 1490 nm to 1500 nm with gain ranging from -35 dB to about 3 dB.

The generated Stokes spectrum are taken at output ends 1 and 4 and are super-imposed as shown in Figure 5.34. It consists of the BP and the even Stokes which are shown in bold lines whereas the odd Stokes are shown in the broken lines. The peaks for the even Stokes averages to about -12 dBm and the odd Stokes average out at a slightly lower power , which is -14 dBm. The spacing between two even Stokes are approximately 0.16 nm (20 GHz), similarly for the odd Stokes. The first peak which is labeled as the BP is used as the reference point and the number of even Stokes peaks generated between the -12.6 dBm to -25.7 dBm are about 19 lines, which span from 1515.3 nm to 1518.1 nm. In the case of odd Stokes, there are also about 19 lines generated between the output power levels of -14.3 dBm to -35.5 dBm, spanning from 1515.2 nm to 1518.0 nm. Although there are a few more lines below this power level, the shape of the lines are undistinguishable.

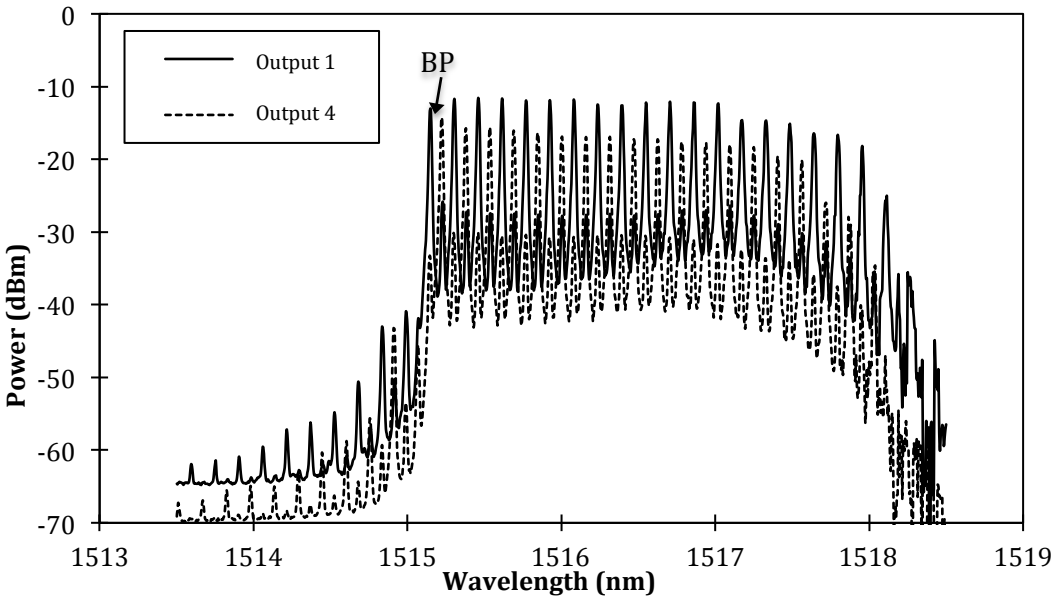

Figure 5.34 Super-Imposed Traces of Output 1 (BP and Even Stokes) and Output 4 (Odd Stokes).

On the left side of the BP, the observed peaks are the even and odd anti-Stokes whichare generated due to Four-Wave-Mixing (FWM). For instance, the first anti-Stokes for the even case, just before the BP, is generated due to the interaction between the BP and the first even Stokes. The second even anti-Stokes is generated due the interaction between first and the second even Stokes. For the odd anti-Stokes, a similar argument can be made. These generated anti-Stokes cover a range of 1513.6 nm to 1515.1 nm.

Figure 5.35 shows the Brillouin output of even Stokes at Port 1 at different RP powers for the simple ring cavity S-band multi-wavelength Brillouin / Raman fiber laser. As the RP power is set at 105 mW with a BP power of 12 dBm at 1515 nm, there are 2 Stokes peaks observed (1^{st} and 2^{nd}) which are indicated in the figure. Since Port 1 is the output port for the BP and even Stokes, but in the figure the 1^{st} Stokes has a higher output power as compared to the 2^{nd} Stokes. This is because at this RP power, the gain at the DCF is not enough to generate the 2^{nd} Stokes with significant power. The 1^{st} Stokes will be generated first as it has a lower threshold power compared to the higher-order Stokes. This output should only comprise of the BP and even Stokes, but due to the low isolation and return loss performance, the odd Stokes is reflected at the joints of the 2x2 fused coupler and appears at the output Port 1.

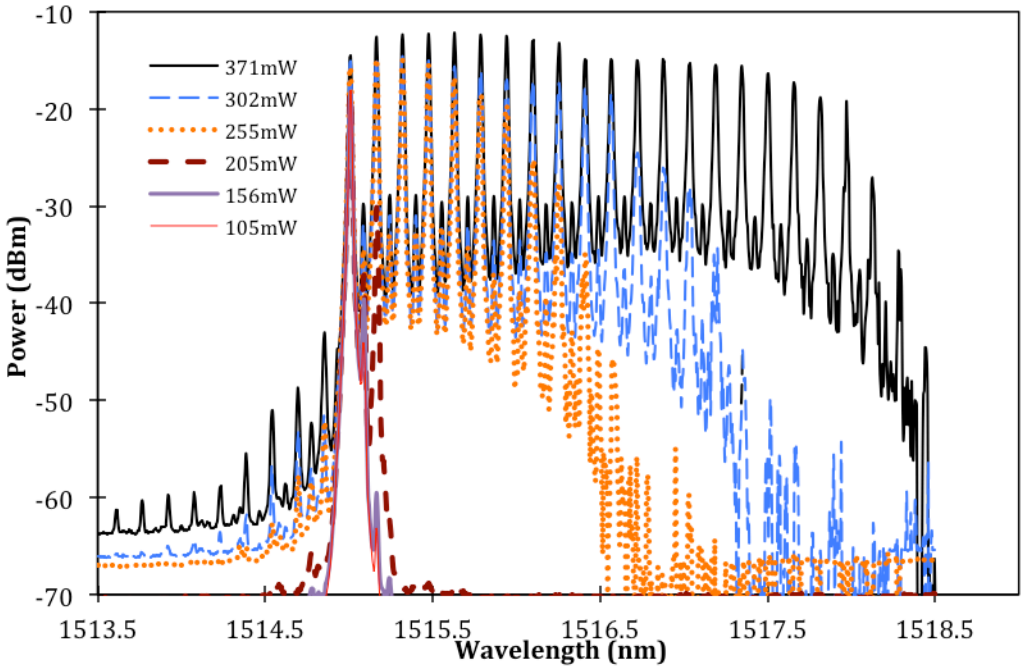

Figure 5.35 Output 1 with varying Raman pump power and fixed BP power.

As the RP power increases to 156 mW, a similar behavior is observed with the 1st, 2nd and 3rd Stokes are generated, although the 1st and 3rd Stokes that are due to the reflections at the fused coupler. At this RP power, the 1st anti-Stokes starts to appear with an output power of -70.3 dBm. Further increasing the RP power to 205 mW yields a similar pattern with Stokes at higher output powers. At a higher RP power of 255 mW, the even Stokes becomes dominant in comparison to that of the odd Stokes. This is a transition and this happens at a RP power of about 240mW. At RP power of 371 mW, the pattern of the even Stokes is more pronounced and distinctive, having sharp and high-powered peaks that range from -13.2 dBm to -19.4 dBm. The 1^{st} to 8^{th} even Stokes have relatively similar peak powers between -12.1 to -13.5 dBm. This is followed by the 9^{th} to 15^{th} even Stokes, which also has similar peak powers of between -15.4 to -15.6 dBm, whilst the power of the subsequent peaks drops as the wavelength increases.

The effect of different BP powers on the Stokes generation at a fixed RP power is measured and shown in Figure 5.36.

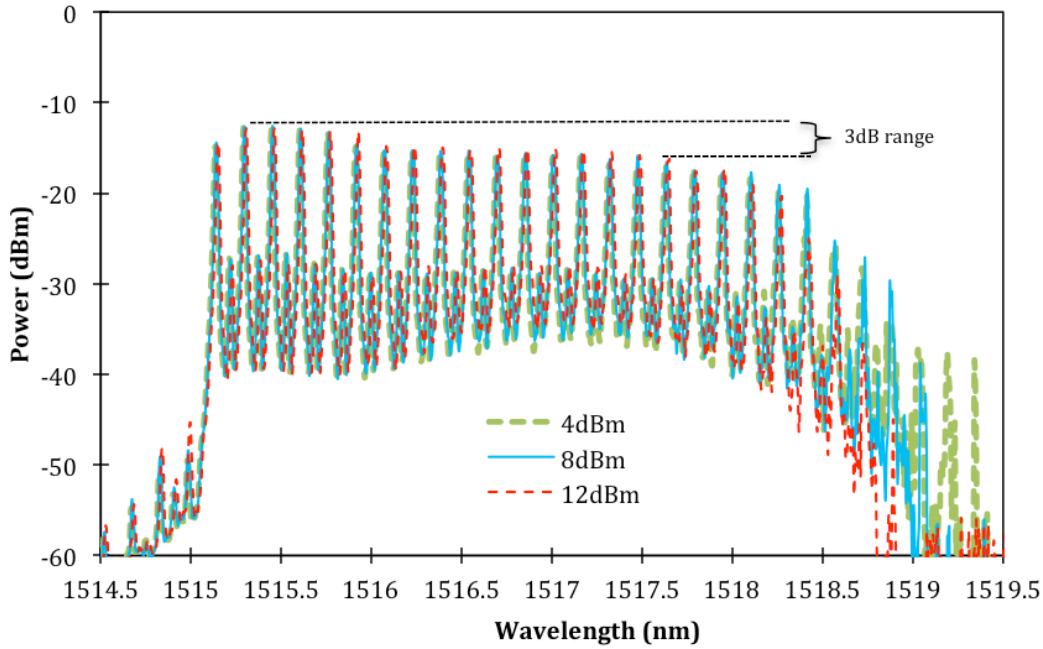

Figure 5.36 The dependence of Stokes output power at different BP power, fixing the Raman Pump (RP) at 371mW

It is observed that at different BP powers, the peak powers of the generated Stokes are similar, thus it can be inferred that there is no power dependence of the Stokes output powers against the BP. This is not similar for the case of Brillouin/Erbium [26], which has an output power dependence on the BP power. There are about 15 Stokes lines generated within the 3 dB region with power variations from -13.3 to -16.3 dBm for a wavelength range of 1515.3 to 1519.5 nm. All the above measurements are taken at a BP wavelength of 1515 nm. A similar observation can be made at other BP wavelengths.

Figure 5.37 (a) shows the operating range of the generated Stokes obtained with different BP wavelengths, starting from 1490 nm to 1530 nm at 5 nm intervals. From the figure, and as shown in Figure 5.37 (b), it can be inferred that the generated Stokes

at a BP of 1490 nm is limited to a range of 1490.1 to 1490.4 nm, giving only the 1st, 2nd, 3rd, 4th and 5th Stokes. This limited range is largely due to the gain profile of the Raman amplifier with the DCF as a gain medium as shown in Figure 5.33. A BP of 1495 nm generates more Stokes lines, giving a total of 7 even Stokes and 7 odd Stokes. On top of this, there are also 5 anti-Stokes generated at this BP wavelength. As the BP wavelength increases, the number of Stokes and anti-Stokes wavelengths also increases as has been discussed earlier in the case of the wavelength BP at 1515 nm. As the BP wavelength approaches the end of the S-band range, which is in this case taken at 1530 nm (the beginning of the C-band range), the number of Stokes and anti-Stokes lines reduces as shown in Figure 5.37 (b).

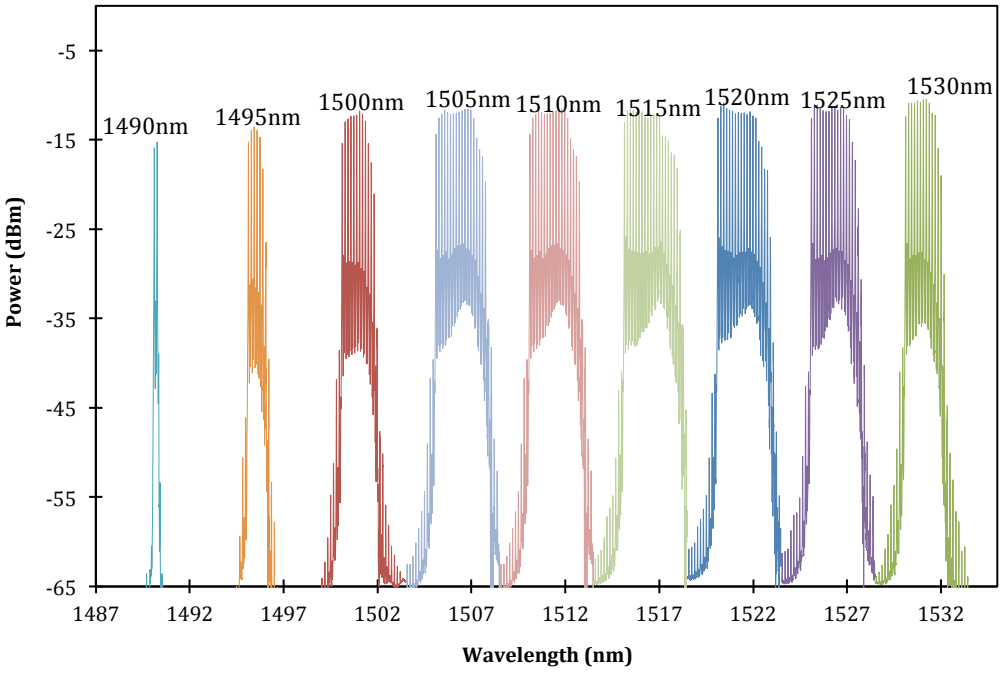

(a)

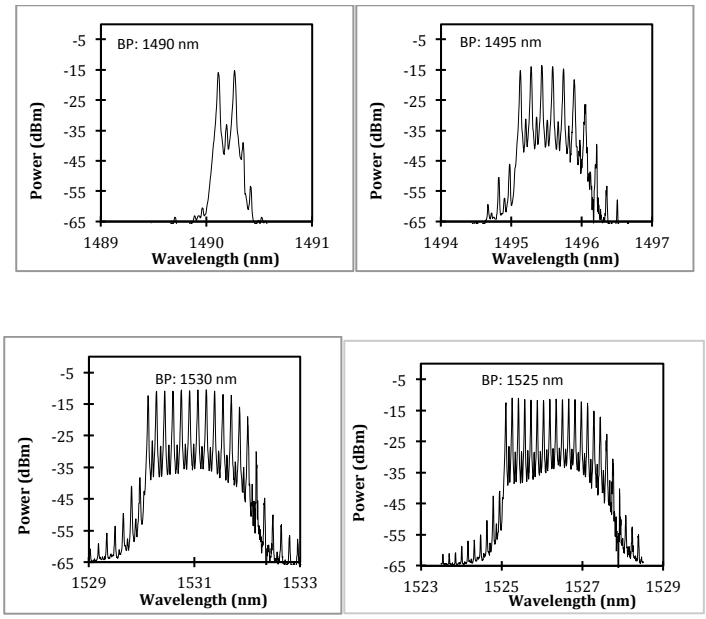

(b)

Figure 5.37 (a) Tuning range of the Stokes generated at different BP wavelengths, starting from 1490 to 1530 nm and (b) expanded trace at BP of 1490 nm, 1495 nm, 1525 nm and 1530 nm (Clockwise from top left)

5.7 S-band Multi-wavelength Brillouin/Semiconductor Optical Amplifier Fiber Laser

In the previous chapter, the SOA advantage is highlighted as means of providing a ultra wide band gain medium and wide band laser source. Based on these advantages, the S-band multi-wavelength Brillouin/SOA Fiber Laser (MWBSOAFL) is proposed to obtain the wide tuning range operation. Many reports imply the need of providing wide tuning range in Brillouin fiber laser. [27-29]

The proposed MWBSOAFL consists of a 7.7 km long dispersion compensating fiber (DCF) that acts as a non-linear gain medium. The DCF has a dispersion of -584 ps/nm and an insertion loss of approximately 6.66×10^{-3} dB/m as mentioned earlier in the text.

An ultra-wide bandwidth SOA is used as the linear gain medium to the MWBSOAFL system. A TLS (AQ8203 Yokogawa) acts as a Brillouin Pump (BP). The BP enters the system through one of the 50% ports of 50/50 fused coupler. After entering the 50/50 coupler, the TLS signal then travels to the DCF, which interacts with the non-linear gain medium and generates a multi-wavelength output comb through the SBS process. The multi-wavelength output comb exits the DCF and enters into the linear laser cavity (which is constructed using two Optical Circulators (OCs) with both ends connected to the BFL system designated as OC1 and OC2) as shown in Figure 5.38 The OCs are configured to act as "mirrors" by connecting Port 1 to Port 3 whilst Port 2 is connected to the input and output of the BFL system. The multi-wavelength signal is amplified by the SOA placed within the linear cavity as shown in Figure 5.38. The SOA is manufactured by Alphion and has an operational amplification bandwidth of 1460 nm to 1620 nm, which is able to cover the S-, C- and L-band regions. A 90/10 fused coupler is placed between Port 1 and Port 3 of OC2 as shown in Figure 5.38 to extract a 10% portion of the signal to be analysed by an OSA with a resolution of 0.02 nm

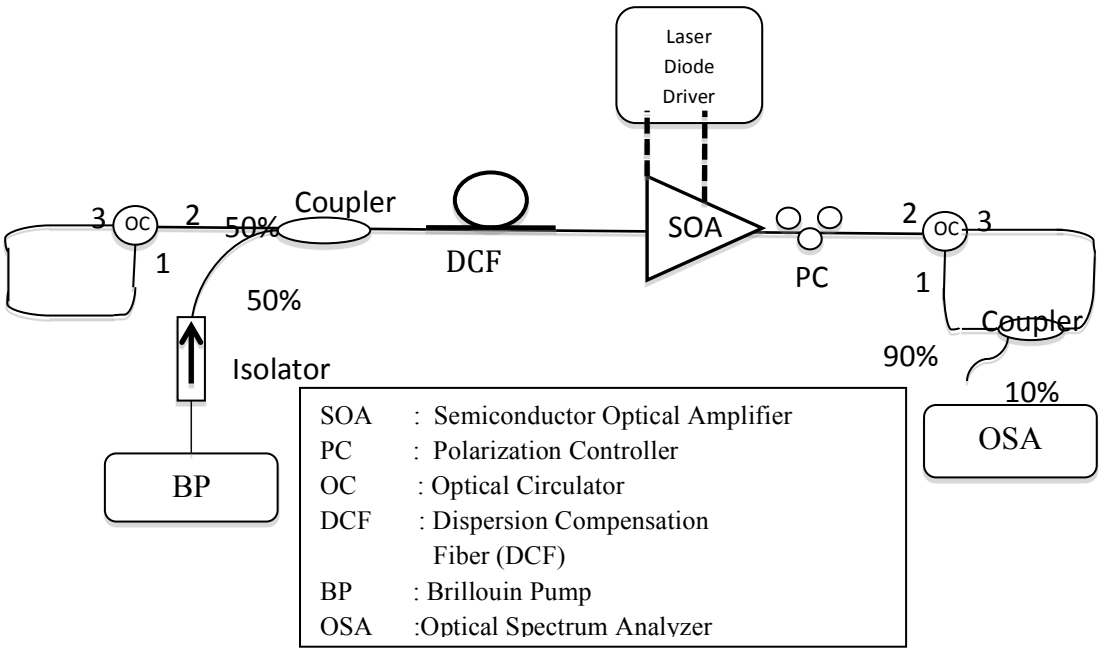

Figure 5.38 The experimental setup of Multi-wavelength Brillouin/SOA fiber laser in linear cavity [30]

5.7.1 Tuning Range Characteristics of Multi-wavelength Brillouin/SOA Fiber Laser

One of the important characteristics in the study of multi-wavelength Brillouin fiber laser is tuning range. Besides focusing on of the tuning range in the S-band, extra tuning range which reaches the C-band and L-band in a single device will be an advantage.

For the characteristic behavior measurement, the injection current of the SOA is set at 390 mA to provide the maximum linear amplification width as shown in Figure 5.39. At a BP wavelength of 1510 nm, it can be seen that 10 Brillouin Stokes are generated. The peak powers of the lasing wavelengths in the S-band region are observed to be in the range of -5.94 dBm to -0.41 dBm, with wavelength spacings of approximately 0.078 nm and a 3dB spectrawidth of approximately 0.017 nm obtained from the OSA. From Figure 5.39, the average peak power is about -1.03 dBm, by taking taking the first and fifth peaks.

Since the SOA has a wide ASE spectrum as discussed in Chapter 3, the multi-wavelength Brillouin generation is also tested for the C-band and L-band region. In the C-band region, 8 Brillouin Stokes with peak powers of -4.34 dBm to 0.02 dBm and wavelength spacings of approximately 0.080 nm with a 3 dB spectrawidth of approximately 0.016 nm are observed as shown in Figure 5.40. In the L-band region, 3 Brillouin Stokes with peak powers ranging from -2.19 dBm to 0.39 dBm are obtained with wavelength spacings between the consecutive Stokes line are observed to be approximately 0.081 nm and the 3 dB spectrawidth is observed to be approximately 0.014 nm as shown in Figure 5.41. The low number of Brillouin Stokes in Figure 5.42 is attributed to the low ASE output power (and henceforth low gain) in that region, as discuss earlier in Chapter 3, Figure 3.41. It can be seen that the number of Brillouin

Stokes generated is higher in the shorter wavelength region and reduces towards the longer wavelength region. This is attributed to the gain pattern of the ultra-wide band SOA, where the higher gain in the shorter wavelength region generates higher peak powers, and thus generates Stokes via the Brillouin's effect. Essentially, this shows that the higher the gain, the higher the peak power achieved in order to overcome the threshold power and generate more stokes via the Brillouin's effect. Further analysis of the output of the proposed MWBSFL shows that those generated multi-wavelength combs before the BP (anti-Stokes) are caused by the effect of four-wave mixing (FWM) as shown in the three cases. This is largely due to the high non-linearity properties of the SOA. The wavelength spacing between each adjacent wavelength is computed to be approximately 0.08 nm or approximately 10.7 GHz in the frequency domain. As a point to note, less anti-Stokes is generated using DC-EDFAs compared to the SOA

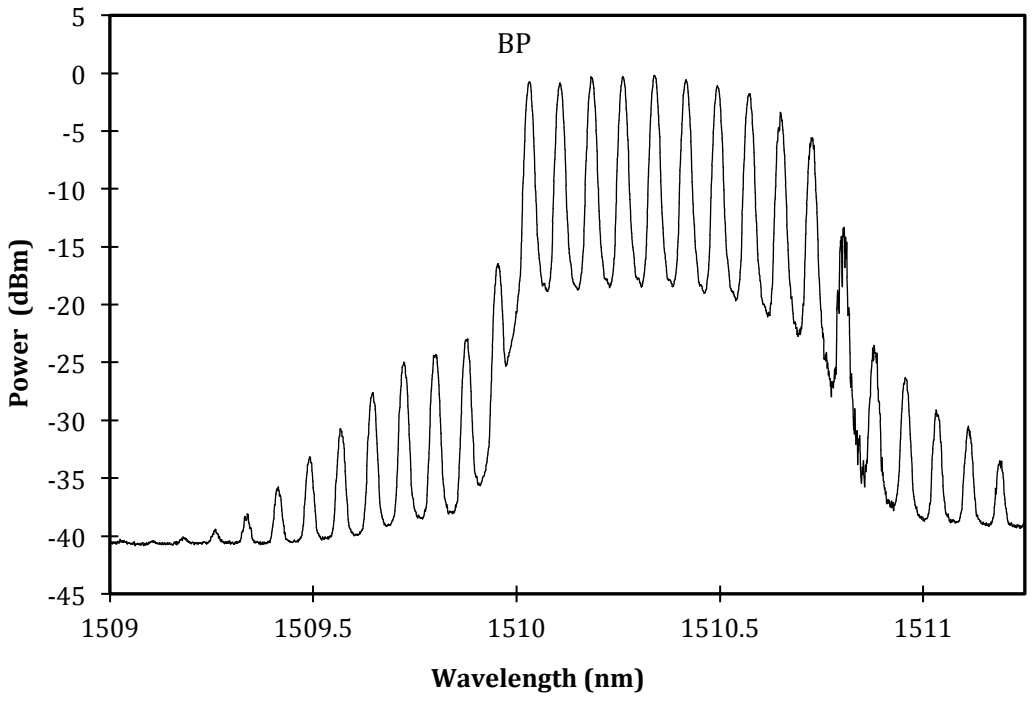

Figure 5.39 Lasing comb generated with 1510 nm BP (S-band) at 10.6 dBm

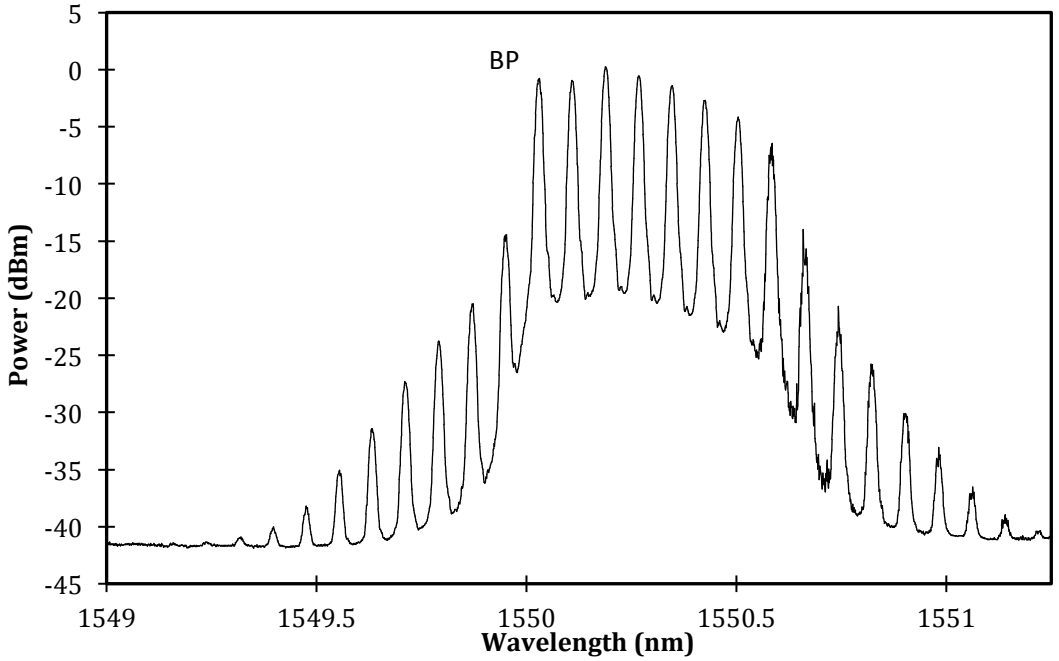

Figure 5.40 Lasing comb generated with 1550 nm BP (C-band) at 10.6 dBm

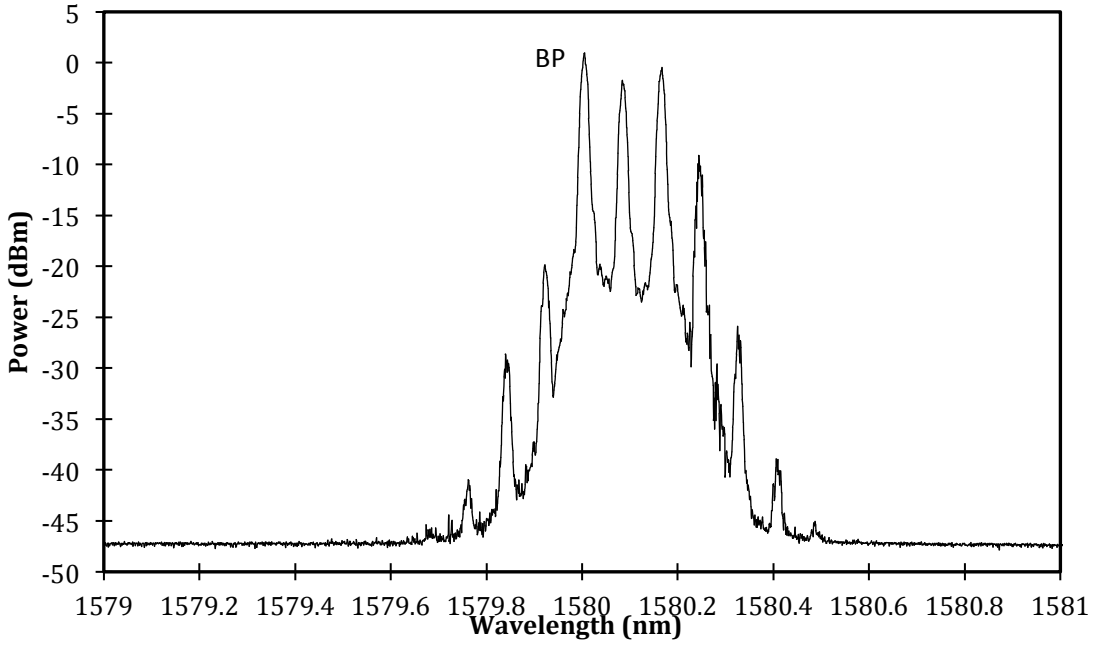

Figure 5.41 Lasing comb generated with 1580 nm BP (L-band) at 10.6 dBm

Figure 5.42 shows the number of lasing lines in the generated multi-wavelength comb for different BP wavelengths, and it can be inferred that the peak power of the lasing wavelengths from the generated multi-wavelength comb closely matches the ASE spectrum within the same wavelength range. Since the ultra-wide band SOA used in

this experiment covers a range of 1480 nm to 1610 nm, the Brillouin effect is also observed within this wavelength region, as the SOA can provide the necessary amplification for the SBS process to continue. The total number of Stokes lines for each BP wavelength is plotted as shown in Figure 5.42 and it can be inferred that the highest number of Stokes lines is generated at a wavelength range of 1500 nm to 1520 nm, which is approximately 10 Stokes lines.

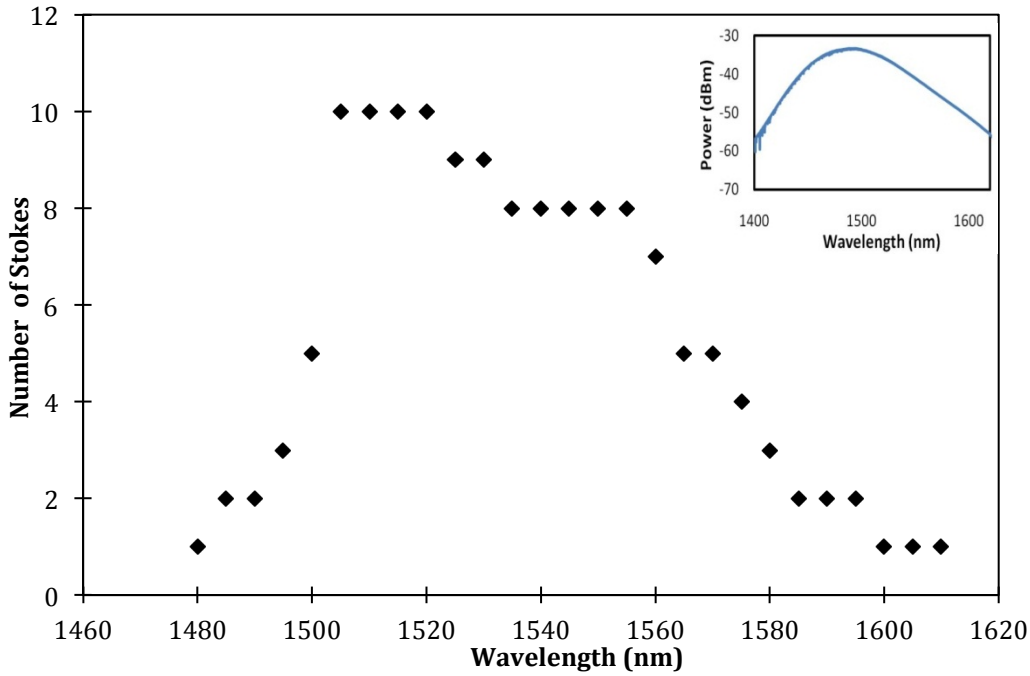

Figure 5.42 Total Stokes wavelengths observed within 1480 nm and 1610 nm at BP power of 10.6 dBm. The inset is the ASE spectrum of the ultra-wide band SOA with an injection current of 390 mA.

The MWBSOAFL system is tested at intervals of 10 minutes for a period of 70 minutes at room temperature to determine for its stability and reliability and the result is shown as in Figure 5.43 for different wavelength regions. In actual fact, this system is left running for a period of more than 10 hours for the total duration of this experiment

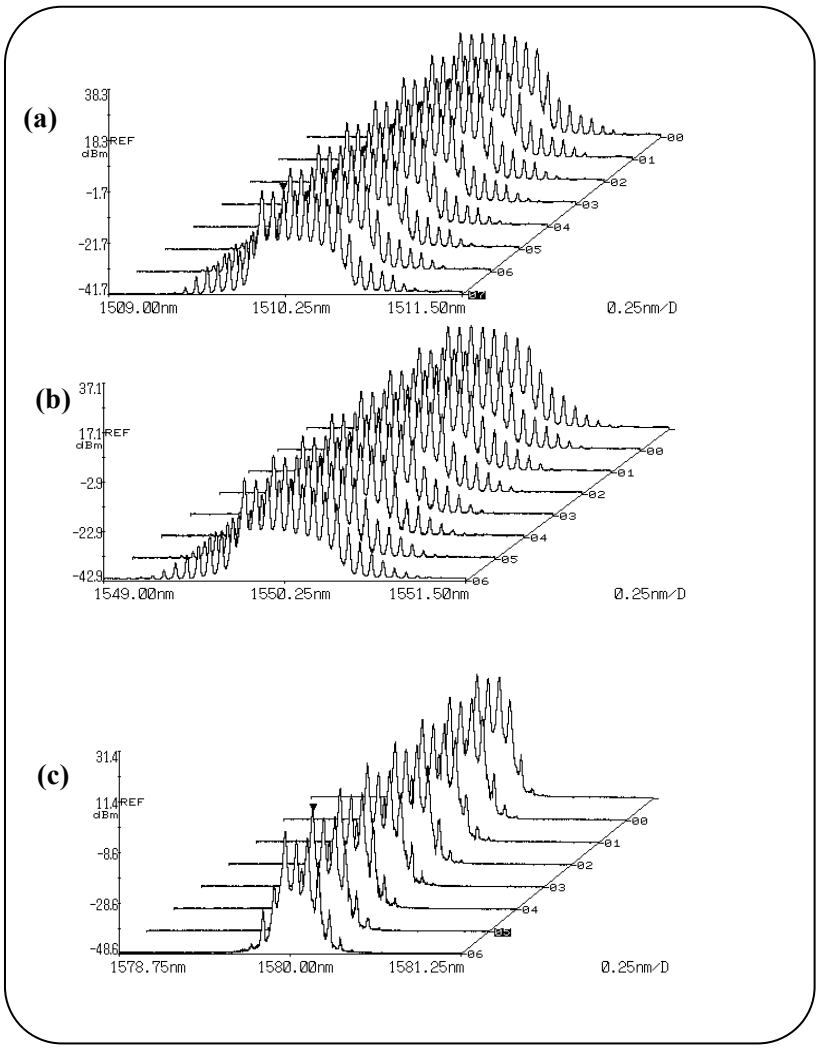

Figure 5.43 Spectrum of the proposed MBLF at 10 minute intervals over a testing period of 70 minutes for the (a) S-band, (b) C-band and (c) L-band region

From Figure 5.43 it can be seen that the output of the MWBSOAFL is stable, with almost no fluctuations or variations in the output power. This ensures that the system is stable and can be used for various applications

5.8 S-band Multi-wavelength Brillouin-Multi-Hybrid Gain Medium Fiber Laser

5.8.1 S-Band Multi-wavelength Brillouin/Depressed Cladding Erbium Doped – Raman Pump in Linear Cavity

The limitation of the S-band MWBDCEDFLis due to the reduced number of Brillouin Stokes generated. The number of Brillouin Stokes generated by the S-band MW-BDCEDFL can be enhanced by pumping the non-linear gain medium, DCF with a Raman pump to act as a Raman amplifier and also as the non-linear gain medium.

The proposed MWBDCEDFL with Raman Pump (FOL1405RTD Fitel) is shown in Figure 5.44 which consists of a Brillouin Pump (BP), a 7.7 km Dispersion Compensating Fibre (DCF) which acts as a non-linear gain medium and a 30 m long DC-EDF which acts as a linear gain medium. Two Optical Circulators (OCs) are placed at both ends of the setup which act as “mirrors”, thus forming a linear cavity. The BP comes from a narrow linewidth Tunable Light Source (TLS) which enters the linear cavity via the 20 per cent port of a 80/20 fused fiber coupler. This BP signal will generate the multi-wavelength spectrum via SBS in the 7.7 km DCF, which is also injected with a 1420 nm Raman Pump (RP) signal at 300 mW via a Wavelength Selective Coupler (WSC). The RP provides Raman amplification to the BP, thus reducing the BP loss and provides higher powered Stokes wavelengths (which will in turn help to generate more subsequent Stokes). The amplification of the generated Stokes wavelengths is accomplished by the use of the DC-EDF based amplifier. The 30 m long DC-EDF has an absorption ratio of 7.6 dB/m at 980 nm and is bi-directionally

pumped with two 980 nm LDs at a total pump power of 215 mW. This is to provide a high enough population inversion for significant amplification in the S-band region.

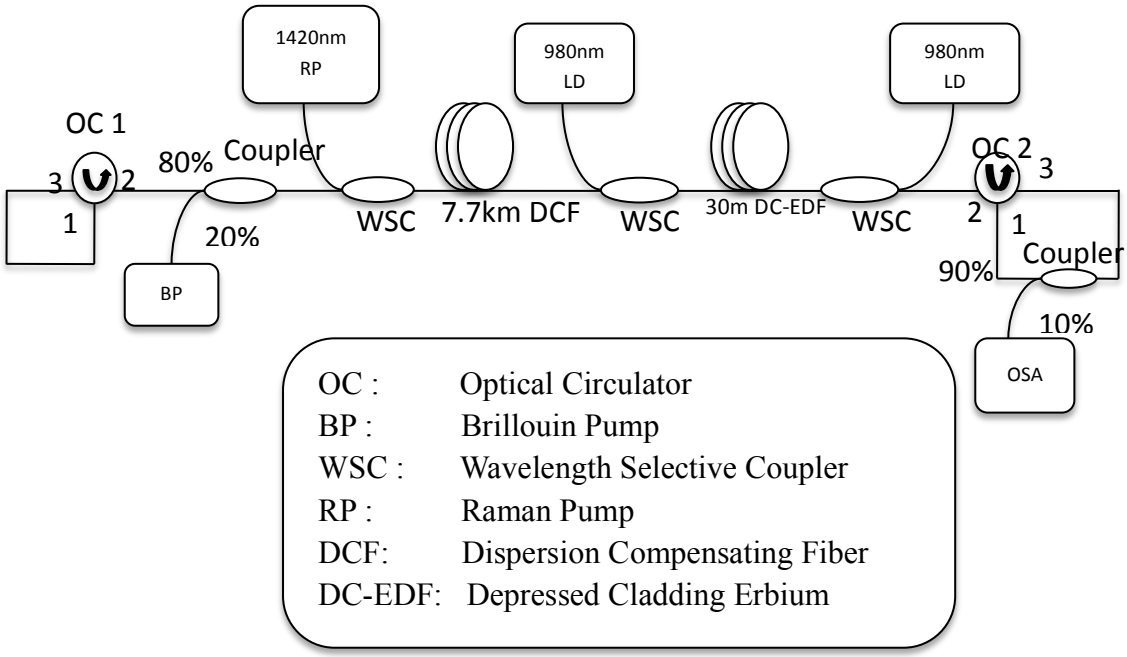

Figure 5.44 Experimental setup for the proposed S-band Multi-wavelength Brillouin / Depressed Cladding Erbium Doped Fiber with hybrid of Raman pump [31]

In order to obtain a multi-wavelength laser output, the generated Stokes is allowed to oscillate in a linear cavity with the two OCs placed at each end which act as reflector for optical feedback. For both the first and second OCs, designated as OC1 and OC2 in Figure 5.44, Port 1 and 3 of the OCs are connected together, while Port 2 is connected to the setup. In this manner, any signal entering the OC from Port 2 will be routed to Port 3 and onwards to Port 1 where it will be re-emitted Port 2 in the opposite direction, thus providing the optical feed back. A fused tap fiber coupler with ratio of 50/50, 80/20 and 90/10 is also added to the setup between Port 1 and 3 of OC2 to extract a portion (lower percent) of the signal to be analysed by an Optical Spectrum Analyzer (OSA) with a 0.02 nm resolution.

The operation of the proposed setup is as follows; the BP signal (generated by the TLS) enters the linear cavity via the 20 percent port of the 80/20 fused coupler, and passes through the coupler's common port to the port of the WSC and onwards to the DCF. Within the DCF, the BP will interact with the non-linear gain medium to form the 1st Brillouin Stokes. At this juncture, the BP will continue travelling in the linear cavity through the DC-EDF amplifier and to OC2. The 1st Stokes on the other hand will travel in the opposite direction towards OC1, passing through the WSC and the 80 percent port of the 80/20 fused fiber coupler, where it will encounter OC1 and will be reflected back towards the DCF where it will then interact and form the 2nd Stokes. This process continues to repeat itself as long as the Stokes wavelengths are above the threshold power for SBS. The many Stokes wavelengths generated now form the desired multi-wavelength spectrum and are amplified as it makes multiple passes through the DC-EDF gain medium until it forms the multi-wavelength lasing output. A portion of the obtained laser spectrum is extracted by the fused coupler placed within the loop created by OC2.

To obtain the optimum and highest Stokes power and numbers in one cavity. The fused coupler ratio are varied with different coupling ratio which are 50/50, 80/20 and 90/10 with the smaller percentage of each coupling ratio is connected to the OSA. The MWBDCEDFL with Raman Pump spectrum is shown in the Figure 5.45 with the BP wavelength and power of about 1499 nm and 5 dBm respectively. From the figure the coupling ratio of 80/20 shows the highest number of the Brillouin Stokes compared to other coupling ratio. This is probably because the 80/20 coupling ratio has an optimum cavity loss for BP and Stokes. Since the 80/20 coupling ratio is produces the highest number of Brillouin Stokes, all the measurement below is taken the 80/20 coupling ratio.

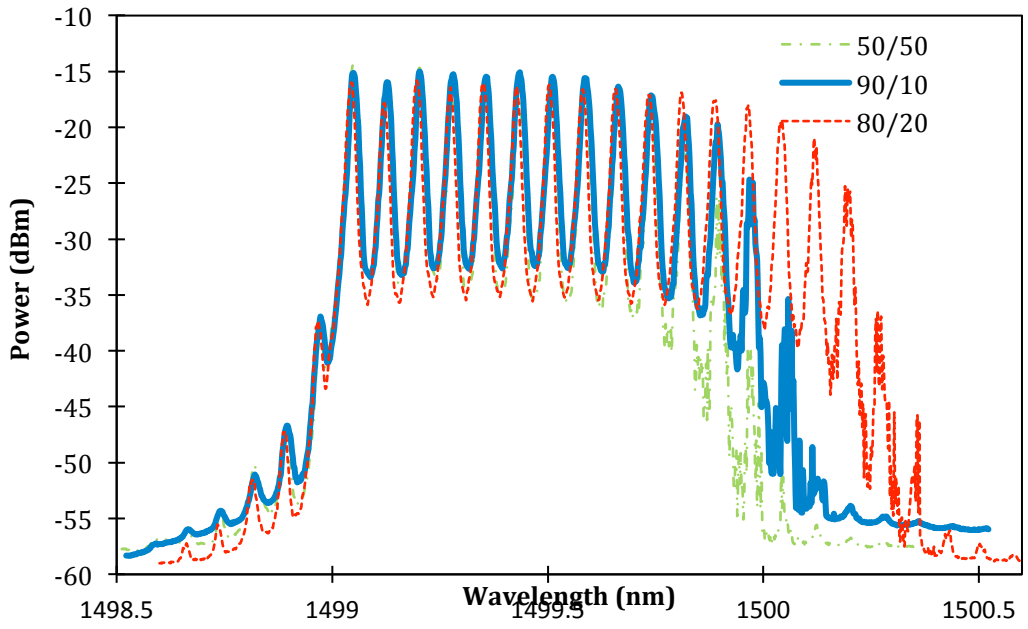

Figure 5.45 MWBDCEDFL with Raman Pump spectrum with different coupling ratios

To obtain the range for generating the optimum number of Stokes wavelengths and also to obtain the tuning range of the proposed MWBDCEDFL with Raman Pump, BP signals at different wavelengths are injected into the MWBDCEDFL with the Raman Pump cavity. Figure 5.46 shows the tuning range of the proposed S-band BEFL. As shown in Figure 5.46 the tuning range of the proposed MWBDCEDFL with Raman Pump is approximately 3 nm from 1499 nm to 1502 nm. Therefore, the higest number of Stokes wavelengths is obtained when the BP is set to fall within the tuning range of the MWBDCEDFL pumped by the Raman Pump and at a fixed BP power of 5 dBm. Should the BP signal's wavelength fall outside of the tuning range, much fewer Stokes wavelengths are observed. This is also shown in Figure 5.46 whereby after a wavelength of 1502 nm (at approximately 1503.1 nm) the injected BP only generates 5 Stokes wavelengths. On the other hand, the higest number of Stokes is observed at a BP signal of 1499 nm, which can be seen to generate up to 17 Stokes wavelengths.

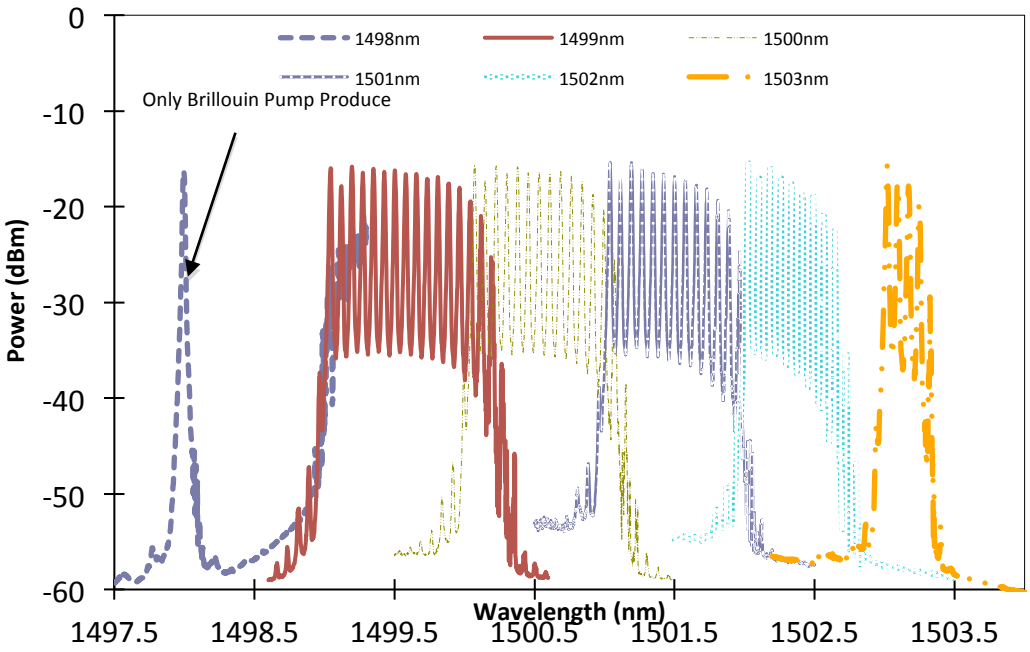

Figure 5.46 Tuning range of linear cavity S-band MBEFL

The spectrum of the MW-BDCEDFL with Raman Pump at a BP wavelength of 1499 nm is shown in Figure 5.47. As can be seen in the figure, the average Stokes power of the wavelengths generated is about -15.9 dBm and at a constant channel spacing of 0.08 nm (10GHz). The generation of the 17 Stokes occurs when the RP injected into the 7.7 km DCF is set to provide a maximum power of 300 mW. This is because the RP acts as a gain medium to overcome the high losses in the DCF, allowing the BP and Stokes wavelengths that are now oscillating within the MW-BDCEDFL with Raman Pump cavity encounters minimal loss and stays mostly above the Brillouin gain threshold level.

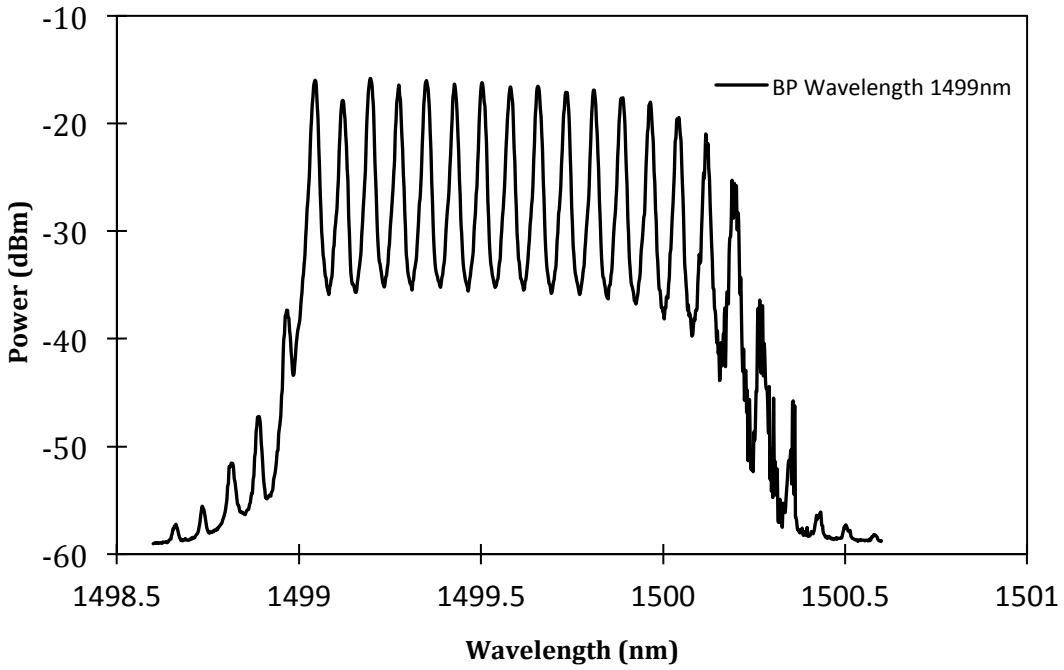

Figure 5.47 The maximum number of Stokes wavelengths is observed at a BP wavelength of 1499 nm

The effect of different RP powers can be seen in Figure 5.48 below. From the figure it can be seen that when the RP power is increased, the number of Stokes wavelengths generated also increase. Furthermore, the increase in the RP also provides a flatter output spectrum, i.e. only small variation in the peak power of the Stokes generated is observed from the figure. This effect can be seen more clearly in Figure 5.49 which shows the peak power of the Stokes wavelengths when the maximum RP of 300 mW is injected into the DCF.

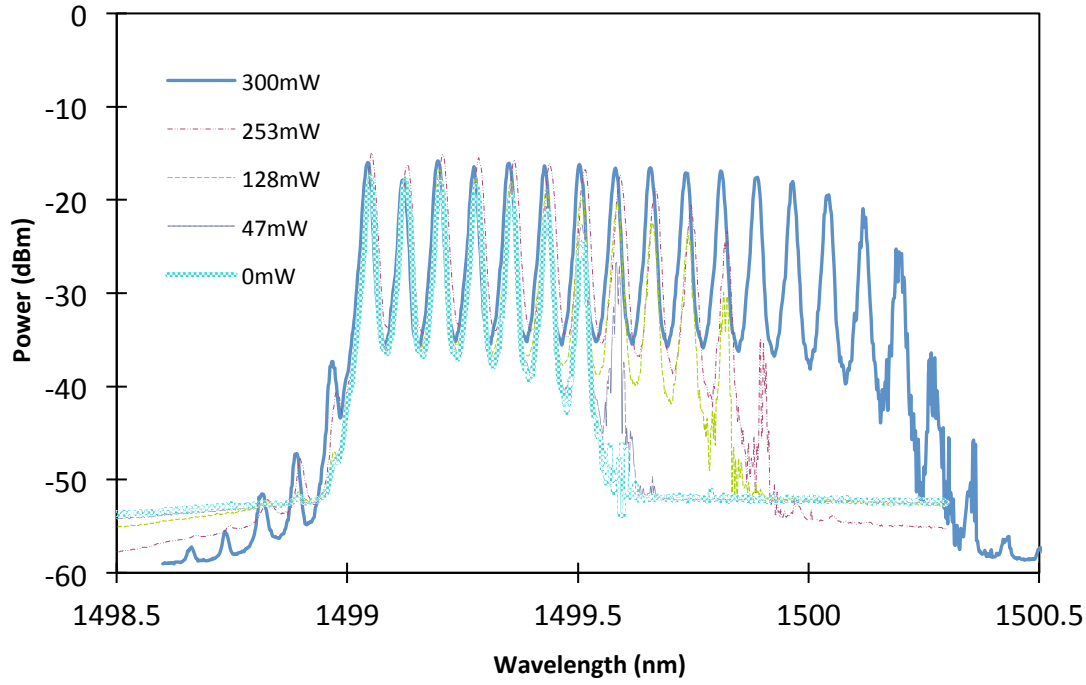

Figure 5.48 Stokes wavelengths generated with different RP powers at a constant BP wavelength of 1499 nm

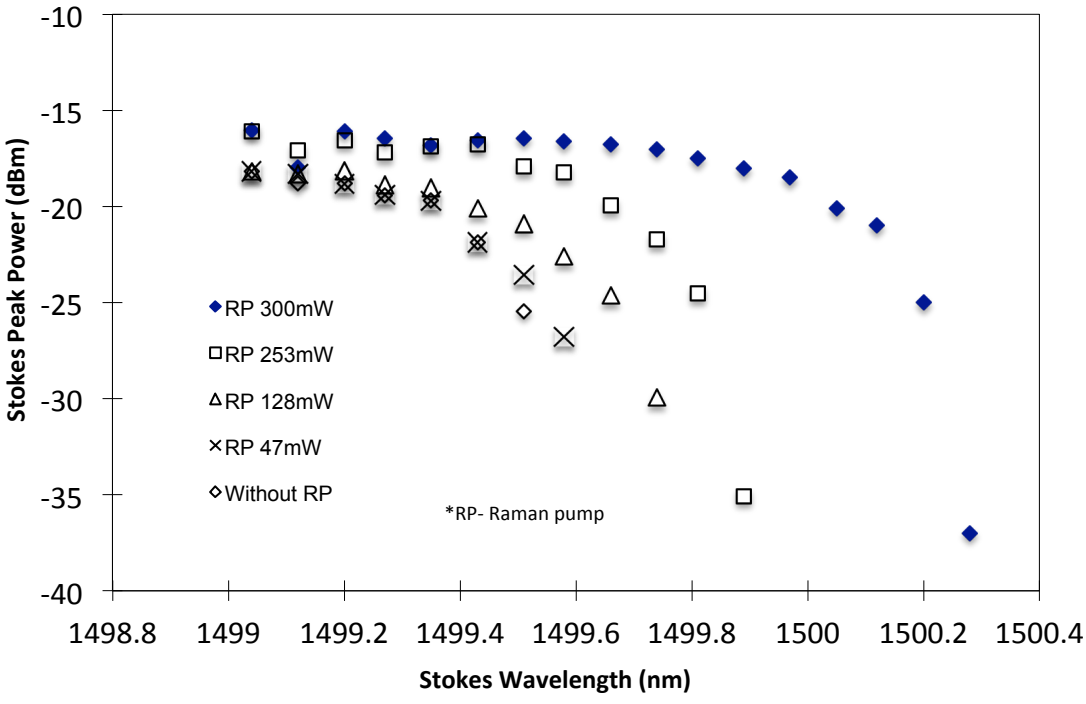

Figure 5.49 Stokes wavelengths observed at different RP powers

Therefore, it can be seen from the figure that at the maximum RP power, 17 Stokes wavelengths are generated with the variations in the peak power of less than 2 dB. The proposed setup is also for the stability of the system. Figure 5.50 shows the output spectrum of the MW-BDCEDFL with Raman Pump taken at 10 minute intervals over a period of one hour of operation at room temperature. As can be seen in Figure 5.50 the BEFL is highly stable and exhibits only minimal fluctuations in the peak power of the Stokes wavelengths even after an hour of operation. In addition the channel spacing of the BEFL does not alter over time, thus showing that the proposed BEFL is not affected by variations in the external conditions.

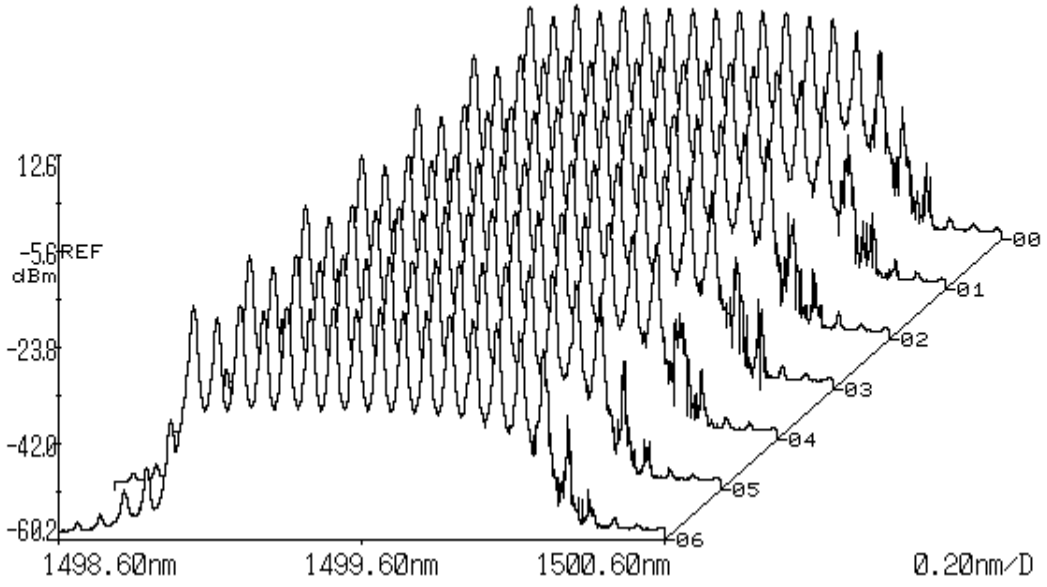

Figure 5.50 Output of the S-band BEFL over 1 hour of operation (at 10 minute intervals)

5.8.2 S-band Multi-Wavelength Brillouin/Semiconductor Optical Amplifier - Depressed Cladding Erbium Doped

The advantage of the multi-wavelength Brillouin fiber laser is that they allow multiple gain medium to be used inside the cavity. However the multiple gain medium is

restricted to have the same gain behavior in the same band. The DC-EDF and SOA have their own advantages as discussed in the chapter 3 which the DC-EDF has produce high gain while the SOA can operate in the wide band region. With our focus is still to enhance the number of Brillouin and the tuning range in the S-band region, we propose the hybrid gain medium DC-EDF and SOA in the linear cavity to produce and enhance the characteristics of the Brillouin spectrum in terms of number of Stokes and tuning range. The experimental setup is shown in Figure 5.51 The non-linear gain medium to produce Brillouin Stokes is supplied by 7.7 km DCF with the TLS is used as the BP. The BP is connected to the 3dB coupler after the output port of optical isolator to prevent the BP from any light comes from the cavity. The SOA and DC-EDF is connected after the DCF to act as the linear gain medium for the Brillouin fiber laser. Two optical circulator was connecter at both end to act as a reflective mirror and thus creating the linear cavity. The 90/10 fused coupler is used to tap out the Brillouin spectrum with 10% port was connecter to the OSA with 0.02 nm resolution.

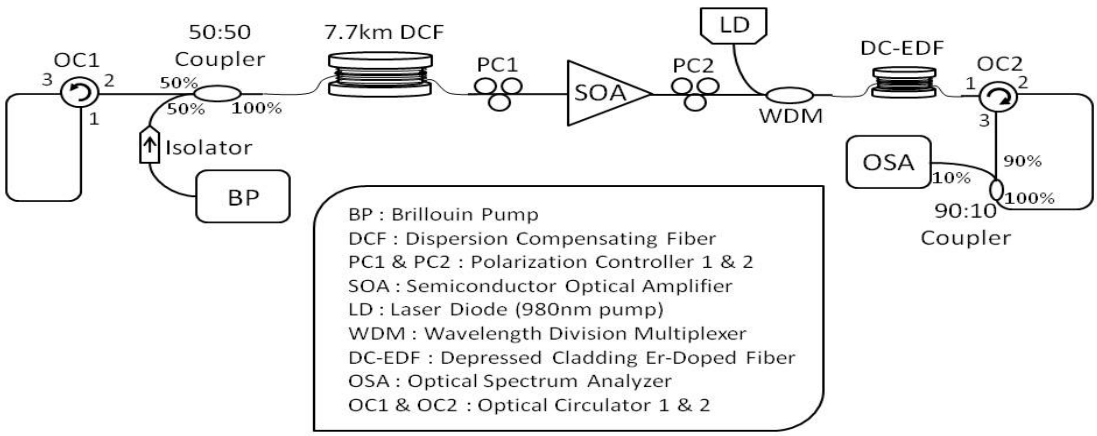

Figure 5.51 The experimental setup of S-band Multi-wavelength Brillouin and SOA/ DC-EDF fiber laser

Figure 5.52 below shows the comparison of output spectrum with three different setups with each of the setup uses either an SOA, or DC-EDF or hybrid of SOA and DC-EDF with the BP wavelength and power is fixed about 1500 nm and 12 dBm. From Figure 5.52, it is clearly shown that the setup with hybrid DC-EDF and SOA produces the highest number of Brillouin Stokes wavelength which is about 17 Brillouin Stokes starting from 1500.07 nm to 1501.32 nm with the average power is about -16.79 dBm. The number of Brillouin Stokes generated by using only the SOA and the DC-EDF is less than the hybrid setup, but in term of output power of Brillouin Stokes, the setup which uses only the SOA has the highest Brillouin Stokes power which is about -2.41 dBm. The is probably due to the SOA has more gain at this BP wavelength whereas the hybrid setup experiences more loss inside the cavity thus limiting the Brillouin output power.

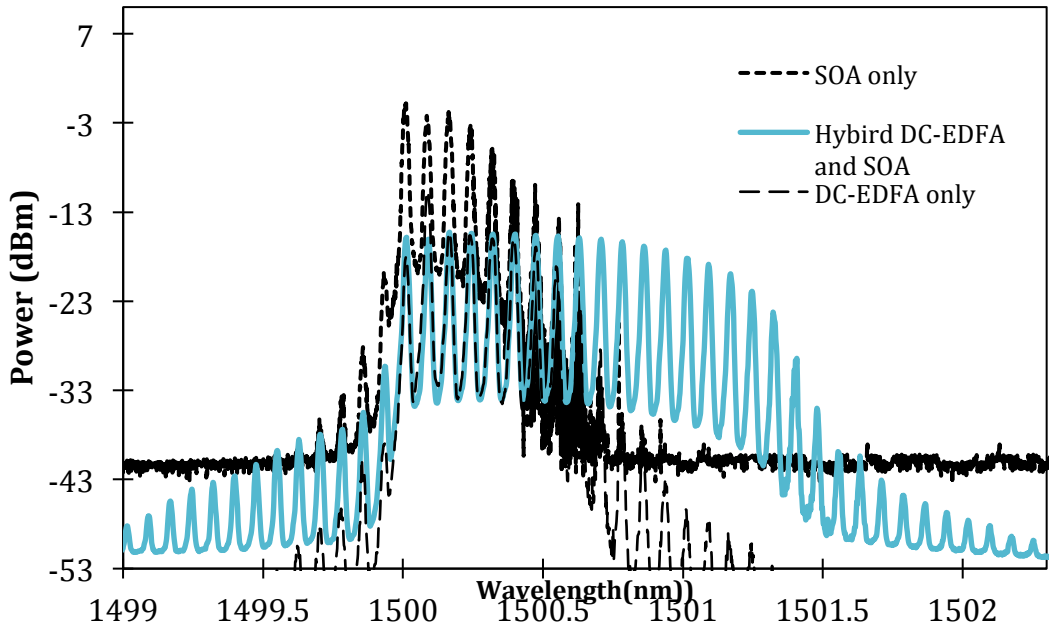

Figure 5.52 The comparison of the output spectrum with different linear gain medium

The number of Brillouin Stokes over the different BP wavelength for tuning range testing (The tuning range is defined as the BP range that can generate Stokes lines) are tasted with different setup is shown in Figure 5.53. From Figure 5.53, the hybrid DC-EDF and SOA setup show significant number of Stokes with better tuning range compared to the setup by using either using DC-EDF or an SOA only. The highest number of Brillouin Stokes is recorded at BP wavelength 1499.02 nm and 1500.28 nm with 28 Brillouin Stokes are created via hybrid SOA and DC-EDF setup with the tuning range of Brillouin Stokes is about 35 nm. For the case of S-band multi-wavelength Brillouin/ DC-EDF only, 17 Brillouin Stokes was crated at BP 1495.18nm with tuning range is about 30 nm. The setup of S-band multi-wavelength Brillouin/SOA only show wide tuning range of Brillouin Stoke of 45nm from 1480 nm to 1525 nm while the number of Brillouin Stokes for this hybrid SOA and DC-EDF setup produce the higher Brillouin Stokes which is about 28 with tuning range limit to 35 nm from BP wavelength 1490 nm to 1525 nm

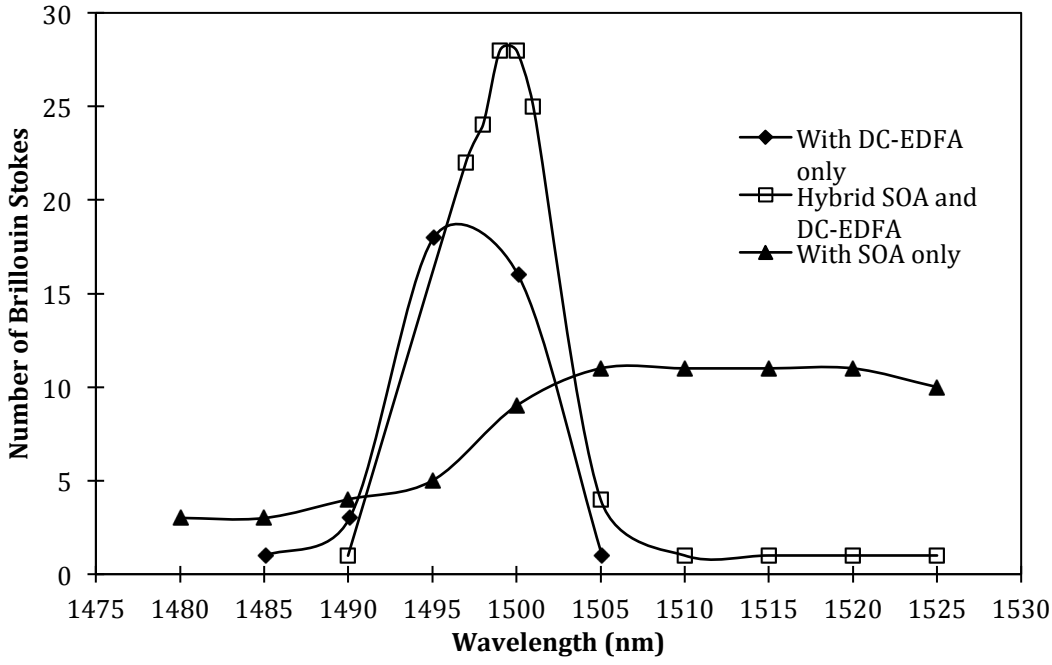

Figure 5.53 The number of Brillouin Stokes with different BP wavelength

The setup of S-band multi-wavelength Brillouin/ Hybrid SOA and DC-EDF shows the best output in terms of number of Stokes and tuning range achieved. Figure 5.54 shows the evolution of the Brillouin spectrum by changing the driven current and pump power of SOA and DC-EDF. The Brillouin Stokes increases from 3 Brillouin Stokes to 17 Brillouin Stokes (at 3dB region) with ithe increment ofthe current and pump of SOA and DC-EDFA

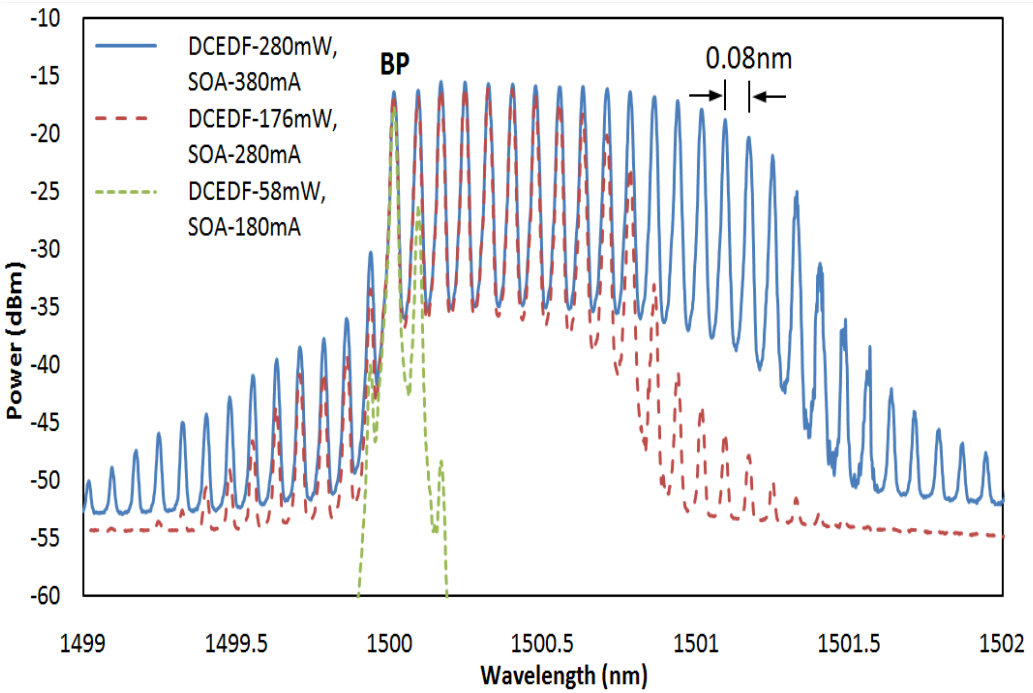

Figure 5.54 The Brillouin spectrum evolution with different pump powers and at different driver currents of DC-EDFA and SOA

The evolution of the Brillouin spectrum at different SOA drive current with DC-EDFA pumped fixed at 300mW is show in the Figure 5.55. From the figure, it can be inferred that on the drive current increased, the number of Brillouin Stokes generated also increased. This is largely due to the SOA having a high ASE output indicating also the gain spectrum.. From the Figure 5.55 the maximum Brillouin Stokes is archived at drive current of 580mA and 300mW pump power of DC-EDF is apply to the both gain

medium. The figure also show the SOA gain medium its very significant to improve the number of Brillouin Stoked in S-band region.

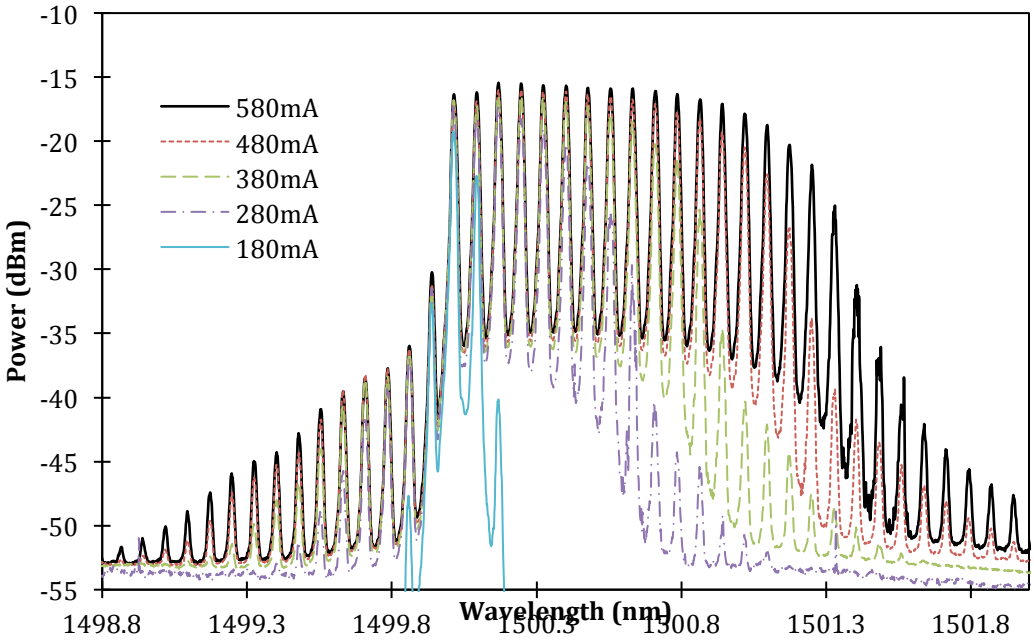

Figure 5.55 The evolution Brillouin spectrum of the S-band multi-wavelength Brillouin/ Hybrid SOA and DC-EDFA with different SOA driven current and DC-EDF pumped

5.9 Summary

In this chapter analyze the use of the S-band amplifier as a key component in the development of multi-wavelength sources for the S-band region. The chapter begins with the characterization of three different lengths of SMF, namely 500 m, 10 km and 50 km. From the characterization of the three fibers, the 50 km SMF can produce the highest Stokes powers as compared to the other lengths when injected with a BP power and wavelength of 12 dBm and 1500.0 nm respectively. The Brillouin Stokes obtained shows a shift of 0.08 nm from the BP wavelength with a power of about -33.97 dBm.

However, the use of long non-linear gain media results in high losses and the need for complex cavity designs. Alternatively, highly non-linear mediums, such as a 7.7 km DCF with the smaller A_{eff} size as compared to the SMF can be used, and have been proven to be able to generate more Brillouin Stokes power with the same power and wavelength BP injected. The Brilouin Stokes generated from DCF is about -19.7dBm. Anti-Brillouin Stokes is also produced at about - 48.79 dBm due to the four-wave mixing effect.

The S-band MWBDCEDFL is demonstrated earlier in this chapter, but with limited laser lines produced, as compared to the expected number of lines to be generated based on the characteristics and results of the S-band amplifier carried out in earlier works. In this work, the design of the MW-BDCEDFL is improved by changing the non-linear gain medium from an SMF to a DCF, obtaining 8 Stokes lines with wavelengths from 1498.17 nm to 1498.71 nm and the 3 dB output power of about -17.37 dBm. The SMSR of the laser lines generated are about 15.5 dB, although a higher SMSR could probably be obtained if a high resolution OSA was used.

A novel design S-band MWBRFL is also demonstrated in this chapter. The S-band MWBRFL is first characterized to determine the impact of the output coupler location and coupling ratio plays on the performance of the multi-wavelength source. Two locations are tested, namely position A and B and it was observed that the position B provides a much better performance than that of the first, generating 33 Brillouin Stokes with a coupling ration of 70/30, as compared to only 23 Stokes generated with the coupler placed at the first location. It was also observed that the BP power has no effect on the performance of the multi-wavelength laser, with the number of Brillouin Stokes is remains constant when the BP power is increased from 2 dBm to 12 dBm. This is an advantage of this design as compared to other Brillouin lasers with hybrid

gain media effect has an advantage compared to the other hybrid gain medium of Brillouin fiber laser. In this chapter also the effect of the number of BP signals injected into the cavity is also studied. The proposed S-band multi-wavelength Brillouin fiber laser is tested by using two BPs, with the wavelength of the second BP configured to be the same as the last Stokes generated from the first BP. The result of this is a new method capable of producing a fiber laser with a wider output bandwidth. In this work, a bandwidth of 2.48 nm is obtained. Furthermore, adjustments to the design of the S-band multi-wavelength laser also allow for the development of a simple multi-wavelength source with a channel spacing of 20 GHz (0.16 nm). From the work carried out in this chapter, proposed setup is able to produce 19 Brillouin Stokes from 1515.3 nm to 1518.1 nm.

In this chapter also a new design is proposed for an S-band MWBSOAFL. The proposed system takes advantage of the wide band characteristic of the SOA to provide a wide tuning range for the MWBSOAFL. This is the first time a tuning range of 130 nm, covering the region of 1480 nm to 1620 nm and also S, C- and L-bands has been demonstrated for this type of fiber laser. A laser comb with 10 Brillouin Stokes is achieved in the S-band with a wavelength spacing of 0.078 nm and 3-dB linewidth of 0.017 nm. The peak to peak output power is seen to vary from between -5.94 dBm to -0.41 dBm. In the C-band region, 8 Stokes lines are generated with a wavelength spacing of 0.08 nm and 3-dB linewidth of 0.016 nm. The peak to peak output power varies from -4.34dBm to 0.02dBm. In the L-band region, only 3 Stokes lines are observed as a result of the lower ASE output at this region, which is in turn due to the gain distribution of the SOA. The wavelength spacing between these lines is approximately 0.081 nm with 3-dB spectra width of 0.014 nm. The values of the output power are observed to be within the range of -2.19 dBm to 0.39 dBm. The system is allowed to

run continuously from between 70 minutes to more than 10 hours to observe the stability of the system and the consistency of its output, and it can be seen to be very stable, with only minor power fluctuations of less than 2 dB.

The S-MWBFL has also demonstrated using multiple S-band gain media which consist in two different setups, one of which is a hybrid of DC-EDF and SOA gain medium. The idea of the hybrid gain medium is to enhance the characteristics of the output Brillouin spectrum. The novel design of an S-band MWBDCEDFL and Raman amplifier aims to generate more Brillouin Stokes channel compared to the conventional S-band multi-wavelength Brillouiin/DC-EDFA. The Brillouin Stokes lines increases to 17 flat channels with the assistance of the Raman pump power. The hybrid S-band multi-wavelength Brillouin/ SOA and Raman amplifier also gives some enhancement in terms of flatness of the Brillouin Stokes and the tuning range of the output spectrum compared to the output Brillouin Stokes spectrum by using only SOA. The inclusion of the Raman amplifier increases the flatness of Brillouin spectrum as well as the maximum tuning range to about 35 nm as compared to the setup which uses only the SOA. However the output Brillouin Stokes spectrum of the setup with the hybrid SOA and Raman amplifier shows a reduction of power due to the increased cavity loss from these two gain mediums.

As a conclusion, a comparison is made between the setup of S-band MWBDCFL, S-band MWBSOAFL, S-band MWBRFL amplifier and it is tabulated in Table 5.1. The comparison made is based on the performance of Brillouin Stokes channel produced in the 3dB region, the average output spectrum for each setup and tuning range

Table 5.1 Comparison performance of S-band Multi-wavelength Brillouin/ S-band Amplifier in linear cavity fiber laser

	Brillouin/ DC-EDF	**Brillouin/ Raman Amplifier**	**Brillouin/ SOA**	**Brillouin/ DC-EDF and Raman Amplifier**	**Brillouin/ SOA and DC-EDF**
Number of Stokes (3dB region)at 1500nm BP	7	23	8	17	17
Average Output Power of Brillouin Spectrum	-15.8dBm	-14.3dBm	-1.03dBm	-15.9dBm	-16.7dBm
Tuning Range in the S-band Region	30 nm (1485 nm to 1515 nm)	35 nm (1490 nm to 1525 nm)	50 nm (1480 nm to 1530 nm)	4nm (1499 nm to 1503 nm)	35nm (1490 nm to 1525 nm)

Note: The tuning range is defined as the BP range that can generate Stokes lines.

Reference

[1] S.W. Harun, F.A. Rahman, K. Dimyati and H. Ahmad, "An efficient multiwavelength light source based on ASE slicing", Laser Physics Letters, vol 3, issue 10, pp 495–497, 2006.

[2] X. M. Liu, Y. Chung, A. Lin, W. Zhao, K. Q. Lu, Y. S. Wang, and T. Y. Zhang, "Tunable and switchable multi-wavelength erbium-doped fiber laser with highly nonlinear photonic crystal fiber and polarization controllers", Laser Physics Letters, vol 5, issue12, pp 904-907, 2008.

[3] A. P. Luo, Z. C. Luo, and W. C. Xu, "Channel-spacing switchable multi-wavelength fiber ring laser with one segment of polarization maintain fiber", Laser Physics Letters, vol 6, issue 8 pp 598-601, 2009.

[4] D. Chen, H. Ou, H. Fu, S. Qin, and S. Gao, "Wavelength-spacing tunable multi-wavelength erbium-doped fiber laser incorporating a semiconductor optical amplifier", Laser Physics Letters, volu 4, issue 4, pp 287-290, 2007.

[5] S. W. Harun, S. Shahi, and H. Ahmad,, "Bismuth erbium-doped fiber based multi-wavelength laser assisted by four-wave mixing process", IEICE Electronics Express, vol: 6, issue 1, pp: 40-43, 2009.

[6] X. S. Liu, L. Zhan, X. Hu, H. G. Li, Q. S. Shen, and Y. X. Xi, "Multiwavelength erbium-doped fiber laser based on nonlinear polarization rotation assisted by four-wave-mixing", Optics Communications, vol 282, Issue 14, pp 2913-2916, 2009.

[7] M.N.M. Nasir, Z. Yusoff, M. H. Al.Mansoori, H.A.A. Rashid, and P. K. Choudhury, "Broadly tunable multi-wavelength Brillouin-erbium fiber laser in a Fabry-Perot cavity", Laser Physics Letters, vol 5, issue11, pp 812-816, 2008.

[8] X.Dong, P. Shum, N. Q. Ngo, and C. C. Chan, "Multiwavelength Raman fiber laser with a continuously-tunable spacing", Optics Express, vol 14, pp 3288-3293, 2006.

[9] S. P. Smith, F. Zarinetchi, and S. Ezekiel, "Narrow-linewidth stimulated Brillouin fiber laser and applications", Optics. Letters, vol 16, pp 393-395, 1991.

[10] M. R. Shirazi, S. W. Harun, M. Biglary, and H. Ahmad, "Linear cavity Brillouin fiber laser with improved characteristics", Optics Letters, vol 33, pp 770-772 2008.

[11] M H.A. Mansoori, S.J Iqbal, M.K Abdullah, and M.A Mahdi, "Low threshold characteristics of an L-band Brillouin-erbium comb fiber laser in a linear cavity" Journal of the Optical Society of Amerika B, vol 23, pp 2281-2284, 2006.

[12] G. J. Cowle and D.Y. Stepanov, "Hybrid Brillouin/erbium fiber laser" Optics. Letters, vol 21, pp 1250-1252, 1996.

[13] G.J.Cowle and D.Y.Stepanov, "Multiple wavelength generation with Brillouin/erbium fiber lasers", IEEE Photonics Technology Letters, vol.8, no.11, pp.1465-1467, 1996

[14] D.Y. Stepanov and G.J Cowle, "Properties of Brillouin/erbium fiber lasers" IEEE Journal of Selected Topics in Quantum Electronics, vol.3, no.4, pp.1049-1057, 1997.

[15] G.J. Cowie, D. Yu and Y.T Chieng, "Brillouin/erbium fiber lasers", Journal of Lightwave Technology, vol.15, no.7, pp.1198-1204, 1997.

[16] S.W. Harun, X.S Cheng, N.K Saat, H. Ahmad, "S-band Brillouin erbium fibre laser,", Electronics Letters , vol.41, no.4, pp. 174- 176, 2005.

[17] S. W. Harun, M. Z. Zulkifli, H. Ahmad, "A linear cavity S-band Brillouin/Erbium fiber laser", Laser Physics Letters, vol 3, issue 7, pp 369-371, 2006.

[18] M.H Al-Mansoori, M.A Mahdi, M. Premaratne, "Novel Multiwavelength L-Band Brillouin–Erbium Fiber Laser Utilizing Double-Pass Brillouin Pump Preamplified Technique", IEEE Journal of Selected Topics in Quantum Electronics, vol.15, no.2, pp.415-421, 2009.

[19] H. Ahmad, M.Z. Zulkifli, S.F. Norizan, M.H. Jemangin, S.W. Harun, "S-band multiwavelength Brillouin Raman Fiber Laser", Optics Communications, vol 284, Issue 20, pp 4971-4974, 2011.

[20] Govind P. Agrawal, Nonlinear Fiber Optics, Third Edition (Optics and Photonics), pp 376, 2001.

[21] M.H. Al-Mansoori, M.K. Abdullah, B.M. Ali, M.A. Mahdi, "Hybrid Brillouin/Erbium fibre laser in a linear cavity for multi-wavelength communication systems", Optics & Laser Technology, vol 37, issue 5, pp 387-390, 2005.

[22] W. Y. Oh, J. S. Ko, D. S. Lim, and W. Seo, "10 and 20 GHz optical combs generation in Brillouin/erbium fiber laser with shared cavity of Sagnac reflector", Optics Communications, vol 201, pp 399-403, 2002.

[23] M. R. Shirazi, M. Biglary, S. W. Harun, K. Thambiratnam, and H. Ahmad, "Bidirectional multiwavelength Brillouin fiber laser generation in a ring cavity," Journal of Optics. A: Pure and Applied Optics, vol 10, pp 055101, 2008.

[24] Y. G. Shee, M. H. Al-Mansoori, A. Ismail, S. Hitam, and M. A. Mahdi, "Multiwavelength Brillouin-erbium fiber laser with double-Brillouin-frequency spacing" Optics Express, vol 19, pp 1699-1706, 2011.

[25] R. Parvizi, H. Arof, N.M. Ali, H. Ahmad and S.W. Harun, "0.16 nm spaced multi-wavelength Brillouin fiber laser in a figure-of-eight configuration" Optics & Laser Technology, vol 43, issue 4, pp 866-869, 2011.

[26] M.H Al-Mansoori, M.H Mahdi and M. Premaratne, "Novel Multiwavelength L-Band Brillouin–Erbium Fiber Laser Utilizing Double-Pass Brillouin Pump Preamplified Technique", IEEE Journal of Selected Topics in Quantum Electronics, , vol.15, no.2, pp 415-421, 2009.

[27] Y.J. Song, L. Zhan, S. Hu, Q.H. Ye and Y.X. Xia, "Tunable multiwavelength Brillouin-erbium fiber laser with a polarization-maintaining fiber Sagnac loop filter", IEEE Photonics Technology Letters, vol.16, no.9, pp.2015-2017,2004.

[28] M. H. Al-Mansoori, M. Kamil Abd-Rahman, F. R. Mahamd Adikan, and M. A. Mahdi, "Widely tunable linear cavity multiwavelength Brillouin-Erbium fiber lasers", Optics Express, vol 13, pp 3471-3476, 2005.

[29] M.N. Mohd Nasir, Z. Yusoff, M.H. Al-Mansoori, H.A. Abdul Rashid, P.K. Choudhury, "Broadly tunable multi-wavelength Brillouin-erbium fiber laser in a Fabry-Perot cavity", Laser Physics Letters Volume 5, Issue 11, pp 812-816, 2008

[30] M Z Zulkifli, H Ahmad, N A Hassan, M H Jemangin, S W Harun, "An ultra-wideband tunable multi-wavelength Brillouin fibre laser based on a semiconductor optical amplifier and dispersion compensating fibre in a linear cavity configuration", Quantum Electronics, vol 41, pp 602–605, 2011.

[31] H. Ahmad, M. Z. Zulkifli, A. A. Latif, K. Thambiratnam and S. W. Harun, “17-channels S band multiwavelength Brillouin/Erbium Fiber Laser co-pump with Raman source”, Laser Physics, vol 19, no 12, pp 2188-2193, 2009.

Chapter 6

Conclusion and Future Works

6.1 Conclusion

As a result of the current traffic increase, existing networks which utilize the C-band region (1530 nm to 1565 nm) have become over-utilized. Even the use of capacity increasing methods such as Time-Division Multiplexing (TDM) and subsequently WDM technology, the C-band is still not able to cope with this increase. The current networks have expanded their transmission band from the C-band to the C- + L-bands, covering a region from 1530 nm to 1625 nm. There has been interest to further extend this bandwidth to cover also the S-band region, thus giving a very wide-bandwidth to support future traffic flow.

The S-band region has been the motivation of this thesis that covers the region of 1460 to 1520 nm. Before going into the discussion, a brief summary of the thesis is given in this section. Chapter 1 provides an introduction, with Chapter 2 giving the theoretical background of this work, taking into account the basic principles of optical amplification in the S-band region. The thesis provides a good coverage of the various approaches of S-band amplification, from the conventional silica-based EDFA to the specially designed DC-EDFA as well as Raman Amplifiers and S-band SOAs. Additionally, this chapter also provides some theoretical background on S-band fiber lasers and S-band Brillouin multi-wavelength fiber lasers.

Chapter 3 provides an experimental overview on the S-band optical amplifier. This chapter studies the amplification of S-band signals using a conventional silica EDF,

covering the small signal and saturation gain, gain bandwidth and ASE and noise figure characteristics of the fiber. Subsequently, the DC-EDF is studied, focusing on the tuning of the cut-off wavelength by the spooling effect, and also the performance of the DC-EDF in terms of its small-signal and saturation gain, gain bandwidth and noise figure. In addition to the EDF, the amplification of S-band signals by Raman amplification and S-band SOAs are also analyzed, and their performance is compared to that of the EDF and DC-EDF.

In Chapter 4, the results from Chapter 3 are used as a basis in the design of the S-band fiber laser. This is further expanded into the study of the S-band EDFL, with the analysis focusing on selected performance characteristics such as cavity design, wavelength tuning range and single longitudinal mode operation. On top of this, the study of the S-band fiber lasers are also undertaken for the DC-EDF, Raman and SOA gain media.

Besides operating the gain medium as an S-band fiber laser, there are also interests to generate multi-wavelength outputs in the S-band region. Chapter 5 provides an in-depth study of generating a multi-wavelength output based on the findings of Chapter 4. Although there are many methods of generating multi-wavelength outputs, this work focuses specifically on the SBS effect. The study of the SBS effect is undertaken for the different gain media such as the DC-EDF, Raman and SOA as well as hybrid DC-EDF-Raman and DC-EDF-SOA gain media and their performances are compared.

The following section provides a more detailed summary of the findings obtained throughout this research.

S-band Amplifier

The S-band amplifier has been summarised in detail in Chapter 3. The key findings of the Chapter are given in Table 6.1.

Table 6.1: Comparison of S-band Optical Amplifier

	EDFA	**DC-EDFA**	**SOA**	**RA**
Pump power	90 mW	300 mW	NA	390 mW
Gain at lower input signal	8.2 dB	29.3 dB	23.2 dB	5.47 dB
Gain at highest input signal	5.6 dB	8.1 dB	5.4 dB	1.2 dB
Gain bandwidth	45 nm	55 nm	160 nm	Depends on the pump wavelength
Polarization Sensitivity	No	No	3 dB	1 dB
Noise Figure	4 dB	10 dB	6 dB	4 dB

EDFA : Erbium Doped Fiber Amplifier
DC-EDFA : Depressed Cladding Erbium Doped Fiber Amplifier
SOA: Semiconductor Optical Amplifier
RA: Raman Amplifier
NA: Not Applicable

Of the four amplifier types studied, the DC-EDFA shows the highest performance in terms of gain, achieving a small-signal gain of 29.3 dB and a large-signal gain of 8 dB. However, the DC-EDFA also shows the highest noise figure, approximately 10 dB. The conventional EDFA on the other hand does not perform as impressively, with a small-signal gain of only slightly higher than 8 dB and a large-signal gain of 5.6 dB. However, the noise figure of the conventional EDFA is much lower than that of the DC-EDFA. The low gain in the EDFA is expected because the erbium doped fibers used in this setup are used for C-band amplification. Normally, in the case of C-band

amplifier, the small-signal gain is about 30 dB or more at 1530 nm. In the S-band region, as measured in this thesis, it is only about 8.2 dB. The gain bandwidth of the EDFA is comparable to that of the DC-EDFA, which is also expected because the active gain medium are erbium ions.

The SOA provides the best gain bandwidth as given in Table 6.1, which at 160 nm is almost triple that of the DC-EDFA. It has a small signal gain of 23.2 dB with a noise figure of 6 dB. This is the actual value measured although most SOAs have a higher noise figure of about 8 to 10 dB. The disadvantage of the SOA is its sensitivity to the polarization state of the input signal, which is observed in this work. Besides this, the SOA can act as a good medium for S-band amplification.

Besides the EDF, DC-EDF and SOA, Raman Amplifiers can also be used as a gain medium for S-band amplification, which has been studied in this work. The advantage of the Raman Amplifier is the position of the gain, which depends on the pump wavelength. By having mulitple pump wavelenghts, a broad gain bandwidth can be obtained. However, it has a low small-signal gain of only 5.47 dB and noise figure of 4 dB. From these four different gain media, the Raman Amplifier has the lowest gain at high input signals, whilst the DC-EDFA has the highest gain. It is worthwhile to note that a higher Raman gain can be achieved with a higher Raman pump power, though this may not be a practical approach.

S-band Fiber Lasers

The S-band fiber lasers are designed on the various amplifying media that was characterised in Chapter 3. In the case of the EDF gain medium, the fiber laser is constructed using a 3 m long standard EDF with a step index and a 1500 nm FBG used as the wavelength selection mechanism, giving a tuning range of 11 nm, ranging from 1496 nm to 1507 nm. The generated fiber laser has a measured peak power of between -5.8 to - 0.7 dBm with an SMSR of 66.2 dB at the shorter wavelengths and reaching a maximum value of 74 dB at the long wavelengths. This is the first demonstration of an S-band EDF with Single Longitudinal Mode (SLM) operation, with a measured linewidth of 140 kHz.

In the case of the DC-EDF gain medium, the fiber laser has a similar design as above, but using a 1x16 Arrayed Waveguide Grating (AWG) as the tuning element. The tuning range is about 11.3 nm from 1478.6 nm to 1490.1 nm. The design is configured in both the backward and forward pumping configurations, with an SMSR of 57 dB and 72 dB respectively. For the S-band fiber laser using the Raman gain medium, a Dispersion Compensating Fiber (DCF) is used together with a Tunable Bandpass Filter (TBF), giving a tuning range of 25.8 nm from 1508.4 nm to 1534.2 nm. The average output power of the Raman based S-band fiber laser is - 11.5 dBm, but it can be made to give higher output power with the use of a higher pump power, which in this work is limited to 390 mW. The SMSR measured is 70.6 dB.

For the fiber laser using the SOA as the gain medium, which has a very wide gain bandwidth of 160 nm, the achievable tuning range is about 120 nm covering the S-, C- and L-bands. The detailed measurements are given in Chapter 4, and the for the case of the S-band a tuning range of 11.5 nm, stretching from 1478.7 nm to 1490.1 nm, which

is limited by the tuning element used - in this case the AWG. By having a proper AWG, a wider tuning range can be realised. The maximum output power is about – 5.31 dBm is the S-band region. The SMSR in the S-band region is about 74.5 dB, although a higher value is achieved for the other regions.

These findings are summarised in Table 6.2 below:

Table 6.2: Comparison for different type of S-band fiber laser

	EDFL	**DC-EDFL**	**SOA FL**	**RFL**
Pump power	90mW	300mW	NA	390mW
Wavelength Tunability at S-band	10.8nm	11.3nm	11.7nm	25.8nm, depend on the RP wavelength
Maximum output power	-4.76dBm	5.14dBm	-5.31 dBm	-11.5dBm, depend on RP power
SMSR	74.4dB	77.7dB	74.5dB	70.6dBm
Types	Homogeneous	Homogeneous	inhomogeneous	inhomogeneous
Stability	Good	Good	Good	Good

EDFL : Erbium Doped Fiber Laser
DC-EDFL : Depressed Cladding Erbium Doped Fiber Laser
SOA FL : Semiconductor Optical Amplifier Fiber Laser
RFL: Raman Fiber Laser
NA: Not Applicable

From the table, the S-band Raman Fiber Laser provides a wider tuning range as compared to the other gain medium, but requires a higher pump power. The DC-EDFL on the other hand has the advantage of a higher output power. In the case of the SOA gain medium, the tuning range is limited by the tuning element, which in this case is the 1x16 AWG. A wider tuning range can be achieved using a TBF or an AWG with the right frequency response. On the whole, all the different gain medium fiber lasers have nearly a similar value for their SMSR. The other advantage of the SOA and Raman Fiber Laser is the inhomogeneous broadening of the gain medium, which will allow

dual wavelength generation without any significant mode competition. In the case of homogeneously broadened gain media, only one mode tends to dominate and various methods are needed for simultaneous, multiple wavelength generation. All designs show good stability in terms of their output wavelength and power.

S-band Multi-Wavelength Fiber Laser

From the results of Chapter 4, the multi-wavelength fiber laser will be of great interest for possible applications as sources in DWDM communications networks as well as sources for fiber sensors and optical instrumentation systems. The various designs of multi-wavelenght fiber lasers are undertaken in this thesis, using the Stimulated Brillouin Scattering (SBS) effect in the fiber, although there are other methods.

In this work, the EDF cannot generate a multi-wavelength output by the SBS effect in the S-band region due to the limitations of the gain medium which has been clearly explained in Chapter 5. For SBS based multi-wavelength outputs, a 7.7 km DCF is used as a Brillouin gain medium together with the respective amplifying medium. The choice of DCF is due to its lower Brilluoin threshold power and also allows for the generation of more Stokes lines as compared to the Single-Mode Fibers (SMFs).

In the case of the S-band Multi-Wavelength Brillouin/Depressed Cladding Erbium Doped Fiber Laser (MWBDCEDFL), the DC-EDF is combined with the DCF to form the laser cavity. In this design, 7 Stokes lines are generated with wavelengths starting from 1498.17 nm to 1498.71 nm and a inter-Stokes spacings of 10 GHz. The Stokes output power at the 3dB point is about -17.37 dBm. By changing the BP wavelength,

the Stokes lines generated can be shifted, giving a tuning range of 30 nm from 1485 nm to 1515 nm.

The next design, which uses a Raman gain medium together with the DCF, generates more Stokes lines, amounting to 23 lines with also a large number of anti-Stokes lines which is taken at a BP wavelength of 1500 nm and with a similar inter-Stokes spacing of 10 GHz. The measured average output power is about -14.3 dBm, and in this design optimization is performed by placing the different coupling ratio output couplers at two separate locations in the cavity. In this design the BP power is also varied from 2 dBm to 12 dBm as a means to optimize the number of lines generated. The best BP wavelength for this design is 1515 nm, which generates up to 33 Stokes lines. In this design and inter-Stokes spacing of 20 GHz is also demonstrated, which in a way will be attractive as a source for DWDM networks. This design is able to produce 19 Brillouin Stokes ranging from 1515.3 nm to 1518.1 nm.

The next gain medium investigated for multi-wavelength generation is the SOA, which has a similar setup as the above designs, using the DCF as the Brillouin gain medium. S-band Multi-wavelength Brillouin/Semiconductor Optical Amplifier Fiber Laser (MWBSOAFL) has the advantage of wide operational bandwidth, which in turn allows for wide tuning range. For the S-band region, a laser comb with 8 Brillouin Stokes lines is achieved with a similar inter-Stokes spacing of 10 GHz. The average peak power is -1.03 dBm. The tuning range of the laser comb is 50 nm, from 1480 nm to 1530 nm, obtained by changing the BP wavelength.

From the table, the number of Stokes generated based on the Brillouin / DC-EDF is limited. Therefore, efforts have been taken to enhance the Stokes line generation in this design by Raman pumping the DCF (which is the non-linear medium for Brillouin generation) to also act as a Raman gain medium. This configuration, Brillouin / DC-

EDF / Raman is termed as the hybrid design. This design can increase the number of Stokes lines generated to 17 lines. In the case of the Brillouin / DC-EDF / Raman gain media, the average peak power of the Stokes lines generated is -15.9 dBm, similar to the Brillouin / DC-EDF gain medium. In this hybrid gain medium, the tuning range is reduced significantly to only 4 nm from 1499 nm to 1503 nm, compared to the much wider tuning range of the Brillouin / Raman Amplifier. The measured tuning range is taken by changing the BP wavelength, and in this case the BP wavelength change is done only from 1499 nm to 1503 nm due to the certain technical limitations of the equipment used at the time. The tuning range should be the same as the Brillouin / DC-EDF gain medium. Another advantage of the hybrid gain medium is the flattness of the spectra obtained, as can be seen in Figure 5.45.

Table 6.3: Comparison performance of S-band Multi-wavelength Brillouin/ S-band Amplifier in linear cavity fiber laser

	Brillouin/ DC-EDF	**Brillouin/ Raman Amplifier**	**Brillouin/ SOA**	**Brillouin/ DC-EDF and Raman Amplifier**	**Brillouin/ SOA and DC-EDF**
Number of Stokes (3dB region)at 1500nm BP	7	23	8	17	17
Average Output Power of Brillouin Spectrum	-15.8dBm	-14.3dBm	-1.03dBm	-15.9dBm	-16.7dBm
Tuning Range in the S-band Region	30nm (1485nm to 1515nm)	35nm (1490nm to 1525nm)	50nm (1480nm to 1530nm)	4nm (1499nm to 1503nm)	35nm (1490nm to 1525nm)

Note: The tuning range is defined as the BP range that can generate Stokes lines.

In addition, the Brillouin / SOA design also shows limited Stokes lines, which in this case is only 8 lines. The number of lines can be further enhanced by combining a 30 m

long DC-EDF to create a hybrid Brillouin / SOA / DC-EDF gain medium. In this configuration, the number of Stokes generated increases from 8 to 17 lines with a flat spectrum output. The average peak power of the Stokes lines is -16.7 dBm. The tuning range achieved in this design is about 35 nm stretching from 1490 nm to 1525 nm. The tuning range is defined as the BP wavelength range that can generate Stokes lines.

From the table, it can be inferred that the Brillouin / Raman configuration can generate the most number of Stokes lines, whilst the Brillouin / DC-EDF and Brillouin / SOA designs give the lowest number of Stokes lines. Even with the enhancement of these designs as discussed earlier, the number of lines generated is still lower than the Brillouin / Raman configuration.

The two best performing gain media are the DC-EDFA and the SOA. The DC-EDFA has the highest small-signal gain of about 29.3 dB and a noise figure of 10 dB. Although the noise figure is higher as compared to the normal EDF, proper optimization can reduce this noise figure. The DC-EDF is designed for S-band amplification, which is not the case for the normal EDF. In terms of bandwidth, the SOA provides the best gain bandwidth with a value of 160 nm but with a limitation towards the polarization of input signal. The other interesting aspect of the SOA is the high small-signal gain which has a value of 23.2 dB, comparable to that of the DC-EDFA. The noise figure measured in this work is about 6 dB, which has a better value than that of the DC-EDF. This makes the SOA an interesting gain medium for S-band amplification.

In the case of the fiber laser, among the four gain medium studied, the DC-EDF based fiber laser provides the best output power at a pump power of 300 mW. Among the gain medium, the Raman Fiber Laser and the SOA based fiber lasers can provide a wide tuning range in comparison to the EDF and DC-EDF based designs. Although in the

early part of the conclusion the SOA provides the widest gain bandwidth, with a small signal gain of 23.2 dB, as an S-band fiber laser source the SOA and Raman Fiber Lasers will be a better option as compared to the others.

In designing the S-band multi-wavelength fiber laser, three designs are initially investigated, namely the Brillouin / DC-EDF, Brillouin / Raman and Brillouin / SOA. The number of Stokes lines generated for the Brillouin / DC-EDF and Brillouin / SOA is only 7 and 8 lines respectively, while the Brillouin / Raman design is able to generate 23 lines. Efforts have been taken to try to increase the number of lines generated by the Brillouin / DC-EDF and Brillouin / SOA configurations by having Raman pumps for the DCF (which also acts as a Brillouin gain medium) and also adding a DC-EDF to the Brillouin / SOA configuration. After careful experimentation, the number of lines that can be generated is only 17 lines. This shows that the Brillouin / Raman medium is the best configuration for generating a multi-wavelength fiber laser in the S-band region.

6.2 Future Works

S-band optical amplifiers such as the EDFA, DC-EDFA, RA and SOA have high potential for applications such as fiber lasers and Brillouin fiber lasers. Based on these findings, several issues have been identified for future research works.

From the study, it is observed that the gain of the EDFA in the S-band region is low compared to the other amplifier types. This issue could be resolved in future designs of the EDF. The gain performance at the S-band region can be better if the high ASE output in the 1530 nm region can be eliminated. This is possible by flattening the ASE from the EDFA using several methods such as an FBG Gain Flattening Filter (FGFF).

The DC-EDFA has a higher NF compared to other type of S-band optical amplifiers. In this thesis the aim of the experiment is to improve the NF value of DC-EDFA. However, the proposed design causes a degradation of the gain value. Future works should look into improving the NF quality while at the same time not affecting the gain of the system. These improvements are possible by designing a low loss TMZF or by using other type of filter such as FBG and Sagnac loop mirror.

In this study it is also observed that the DC-EDFA has higher gain saturation and produces a high output power when pumped with backward pumping. This result shows new potential applications to design the high power S-band optical amplifier.

The limitation of the Raman pump power is one of the main focuses in this study. High RA gain can be demonstrated if this issue can be solved. The broad gain bandwidth can also be achieved if there are several Raman Pump wavelengths. For future work the high gain and broad gain bandwidth of RA can be designed and demonstrated when the high power Raman pump is available.

The SOA shows broad gain bandwidth as compared to the other type of amplifiers in this study, covering the S-to L-band region. The major issue of using the SOA is the high PDG. For the future work, reducing the PDG needs to be done. Reducing the PDG can be made by put the polarization controller at the input and the output of the SOA.

The S-band Fiber laser is demonstrated by using four types of gain medium in Chapter 4. Various types of fiber laser designs have been demonstrated in this Chapter. Based on this studied several issue and limitation need to be overcome in the future.

The novel design of S-band fiber laser by using silica EDF is a successful design in this chap ter. Even though lasing is obtained in the S-band by using 1500nm FBG, the tuning range of the fiber laser can be improved. The improvement of tuning range can

be made by two ways. One is improving the design of TFBG and used other type of EDF. Our design of TFBG also need to improve in future work by redesign the TFBG device to the better design such as change the spring material with the material more springer than this material.

The DC-EDFL has been demonstrated in the Chapter 4. The tunabilty of the DC-EDFL is done by using WCS and AWG. The spacing can be changed by selecting different channels of the AWG. From the result the output power can be obtained by pumping the DC-EDF in the backward direction. For the future work, a higher output power of DC-EDFL with backward pumping is needed to make the high power fiber laser especially in the S-band region.

The RFL has a lot of advantages in order to design the high power S-band fiber laser. However due to limitation of the Raman pump power; the output power achieved currently was only about -14dBm output power. The threshold of the RFL is also high compare to other type of fiber laser. In future work the threshold reduction is one of the challenges. One of the potential methods to reduce the threshold of the RFL is by using microsphere nanowire fiber.

The advantage of the SOA fiber laser is its ultra wide band tuning range characteristic. The ultra-wide band tunable fiber laser is designed in this chapter. For the future, the output power of the design need to be improved and also the stability of the laser spectrum also need to be improved. The stability of the laser can be enhanced by reducing the polarization effect of the SOA.

The improvement of the characteristics in term of number of Stokes is demonstrated. Compared to previous report by Harun [7], the new setup produces more Stokes line. For this type of setup, future improvements need to be made to enhance the quality of

laser. The flatness of the spectrum needs to be improved future. The number of anti-Stoke also need to be reduced.

MW-BRFL it shows better performance if compared to the other type of multi-wavelength fiber laser. The number of Brillouin Stokes can be enhanced if high Raman pump is injected into the cavity. For future work also, the MW-BRFL is a potential field to be studied and in designing the short cavity of MW-BRFL.

The novel design of MW-BSOAFL with ultra wide band tuning range is demonstrated in this thesis. In the future work, the enhancement of Brillouin Stokes over the S-band need to be improved and on par as the number of Stokes channel for C-and L- band region.The enchantment of MW-BDCEDFL is demonstrated in chapter 5 by pumping the DCF with the RP. 17 Stokes line was generated. The enhancement for future work can be improved in term of number and tuning range of the Brillouin Stokes. The number of Brillouin Stokes can be enhanced if we have Raman pump at 1500nm. This is because at 1500nm maximum ASE of DC-EDF is obtained. The tuning range also can be enhanced further if we used different Raman pump wavelength in the cavity.Other methods to enhance the MW-BDCEDFL is through the use of the SOA. This is demonstrated in this thesis. The hybrid MW-BDCEDFL with the SOA enhances the tuning range of the MW-BDCEDFL however the power of Stokes is dropped. Further enhancements in order to increase the Stokes line need to be done in the future works.

Appendix A:

Selected Papers Related to this Work